

NUMERICAL MODELING OF UNCERTAINTY AND
VARIABILITY IN THE TECHNOLOGY, MANUFACTURING,
AND ECONOMICS OF CRYSTALLINE SILICON
PHOTOVOLTAICS

A Thesis
Presented to
The Academic Faculty

By

Alan H. Ristow

In Partial Fulfillment
Of the Requirements for the Degree
Doctor of Philosophy in Electrical and Computer Engineering

Georgia Institute of Technology
August 2008

©2008 by Alan H. Ristow

NUMERICAL MODELING OF UNCERTAINTY AND
VARIABILITY IN THE TECHNOLOGY, MANUFACTURING,
AND ECONOMICS OF CRYSTALLINE SILICON
PHOTOVOLTAICS

Ajeet Rohatgi
School of Electrical and Computer
Engineering
Georgia Institute of Technology

Thomas Gaylord
School of Electrical and Computer
Engineering
Georgia Institute of Technology

Miroslav Begović
School of Electrical and Computer
Engineering
Georgia Institute of Technology

Ronald Harley
School of Electrical and Computer
Engineering
Georgia Institute of Technology

Bernard Kippelen
School of Electrical and Computer
Engineering
Georgia Institute of Technology

Christopher Jarrett
College of Architecture
Georgia Institute of Technology

Date Approved: April 29, 2008

UNLESS someone like you
cares a whole awful lot,
nothing is going to get better.
It's not.

DR. SEUSS, *The Lorax*

To the memory of my grandfather.

ACKNOWLEDGMENTS

There are many people I would like to acknowledge for their support, advice, encouragement, and help over the past several years. First and foremost I thank my family and friends for their love, encouragement, support, and patience over the many years I spent completing this work. Thanks especially to my wife Amanda for providing the strength, stability, and motivation to see me through to the end.

I would like to thank my committee members for their interest in my project and for their helpful and insightful comments and suggestions. In particular, I thank Dr. Thomas Gaylord for his helpful editorial comments and Dr. Bernard Kippelen for several enlightening discussions on organic solar cells and the state of the renewable energy industry. A special thanks goes to Dr. Christopher Jarrett not only for his instrumental role in bringing the Solar Decathlon project to Georgia Tech and his insight on energy-efficient building design, but for saving the day by providing a place to hold my defense after the original location was double-booked. Thanks also to Dr. Ronald Harley for his interest in my project. Finally, I would like to thank my advisor, Dr. Ajeet Rohatgi, and my co-advisor, Dr. Miroslav Begović, for all of their guidance and the effort they have invested in my education. I am truly grateful for the freedom they granted me and the wisdom they imparted along the way.

I owe a tremendous debt of gratitude to my colleagues at the University Center of Excellence for Photovoltaics (UCEP) at the Georgia Institute of Technology. Thanks to Vijay Yelundur, Aleksandar Pregelj, Mohamed Hilali, Kenta Nakayashiki, Ji-Weon Jeong, Ben Damiani, and Jed Brody for their friendship and support over the many years I have now known them. Thanks also to Manav Sheoran, Ajay and Vijaykumar Upadhyaya, Arnab Das, and Vichai Meemongkolkiat, particularly for their many hours of conversation about India and South Asia. I also give my thanks to Dr. Abasifreke Ebong and Dr. Dong Seop Kim for their insight into photovoltaics and the photovoltaics industry. Finally, I thank Denise Taylor, Sean Riordan, Brian Rounsaville, Dean Sutter, and Keith Tate for the advice, support, and conversation they have given me over the years.

During the course of my research I have had the opportunity to come into contact with numerous people in the photovoltaics industry, and a number of them have influenced my work and my decisions. Dr. Martin Green of the University of New South Wales was instrumental in kindling my interest in photovoltaics while I was a member of the University of Michigan Solar Car Team in my undergraduate years and has my eternal gratitude. I must also acknowledge Dr. Richard Swanson for influential advice he gave me during my undergraduate years, and for interesting and insightful conversations in the years since.

Thanks to Keith Matthei of GT Solar for sharing his insight into the process and economics of photovoltaics manufacturing, and for sharing the data that allowed me to validate my manufacturing cost model; to Paul Maycock of PV Energy Systems for several helpful conversations on the economics of photovoltaics manufacturing; and to Dr. Matthew Realf of the Georgia Tech School of Chemical and Biomolecular Engineering for helping me to greatly simplify what had become a terribly complicated PV module manufacturing cost model. Thanks also to Paul Basore and Rolf Brendel for their help and patience in answering my questions about PCID and Sunrays. I also thank Dave Mooney of the National Renewable Energy Laboratory for arranging for me to be a beta tester for SAM, which greatly improved my understanding of levelized cost analysis.

Finally, I would be remiss if I did not also acknowledge the entire University of Michigan Solar Car Team and the people at the Department of Energy, such as Richard King and Cecile Warner, who organize events like the North American Solar Challenge and the Solar Decathlon. These are the people who sparked my interest in photovoltaics and sent me on my present career path.

TABLE OF CONTENTS

ACKNOWLEDGEMENTS	v
LIST OF TABLES	xi
LIST OF FIGURES	xv
SUMMARY	xx
1 INTRODUCTION	1
1.1 Background and Motivation	1
1.1.1 Photovoltaic Energy Conversion: Current Status and Future Prospects . .	2
1.1.2 Fundamentals of Solar Cell Operation	5
1.1.3 PV System Components	9
1.2 Research Objectives	11
1.2.1 Task 1: Develop a Model to Assess the Impact of Power Conversion Efficiency on Photovoltaic Module Economics	13
1.2.2 Task 2: Use Numerical Device Modeling to Establish a Roadmap to High-Efficiency Solar Cells with the Potential for Low Manufacturing Cost . . .	13
1.2.3 Task 3: Develop a Model to Estimate Photovoltaic Module Manufacturing Cost	14
1.2.4 Task 4: Apply the Manufacturing Cost Model to the High-Efficiency Solar Cell Roadmap	14
1.2.5 Task 5: Model the Cost of Electricity from Grid-Connected Photovoltaic Systems in the Presence of System Failures	15
1.2.6 Task 6: Develop a Methodology for Predicting Inverter Failure Rates . . .	15
2 REVIEW OF LITERATURE	16
2.1 Photovoltaic Module Cost Analyses and Projections	16
2.2 Historical Development of Photovoltaic Device Models	21
2.3 Foundations of Photovoltaic Device, System, and Economic Modeling	22
2.3.1 Device Models	23
2.3.2 System Models	24
2.3.3 Economic Models	25
3 ANALYTICAL MODELING OF PV MODULE AND SYSTEM COST	27
3.1 Relationship between PV Module Manufacturing Cost and Efficiency	28
3.1.1 Nomenclature	28
3.1.2 Derivation of the Model	29
3.1.3 Assessing the Relative Importance of Efficiency and Manufacturing Cost	33
3.1.4 Preliminary Conclusions	35
3.2 Impact of Efficiency on PV System Cost	37

3.2.1	Nomenclature	37
3.2.2	Development of the System Cost Model	40
3.2.3	Analysis of the System Cost Model	43
3.2.4	Input Parameter Determination	51
3.2.5	Computation of Efficiency Premium	59
3.2.6	Application of the Model	59
3.2.7	Caveats and Limitations	73
3.3	Influence of System Service Life on Efficiency Premium	75
3.3.1	Computing the Levelized Cost of Electricity	76
3.3.2	Efficiency Premium for Systems with Unequal Service Lives	78
3.3.3	Analysis of the Levelized Cost Model	80
3.3.4	Limitations of the Financial Model	82
3.3.5	Grid Parity Cost for PV Modules with 20-Year Service Life	83
3.4	Using the Analytical Cost Model	83
3.4.1	Calculation of Efficiency Premium for Crystalline Silicon vs. Amorphous Silicon PV Modules	86
3.4.2	Calculation of Efficiency Premium for Crystalline Silicon vs. Cadmium Telluride PV Modules	88
3.5	Conclusions	90
4	DEVICE MODELING AND DESIGN OPTIMIZATION TO MITIGATE THE EFFECTS OF MATERIAL- AND PROCESS-INDUCED VARIABILITY IN SOLAR CELL PERFORMANCE	92
4.1	Device Modeling	93
4.2	Solar Cell Designs for Maximum Efficiency	99
4.3	Effect of Device Parameter Variability on Optimum Design	103
4.4	Modeling the Impact of Device Parameter Variability Using Monte Carlo Simulation	106
4.5	Roadmap for High-Efficiency Crystalline Silicon Solar Cells	110
4.6	Conclusions	113
5	MODELING PHOTOVOLTAIC MODULE MANUFACTURING COST	114
5.1	Overview of Manufacturing Cost Estimation	115
5.1.1	Capital Cost Estimation	115
5.1.2	Operating Costs and Computation of Manufacturing Cost	118
5.2	Model Structure	121
5.2.1	Process Specification	122
5.2.2	Throughput and Equipment Sizing	124
5.2.3	Manufacturing Cost Evaluation	129
5.3	Economies of Scale	137
5.3.1	Estimating Capital Costs	138
5.3.2	Estimating Material Costs	147
5.3.3	Estimating Labor Costs	149
5.4	Model Coding and Implementation	151
5.5	Model Validation	162
5.6	Generating a Manufacturing Cost Roadmap from the Technology Roadmap to 20% Efficiency	164

5.7	Conclusions	170
6	MODELING THE IMPACT OF SYSTEM RELIABILITY ON ENERGY PRODUCTION AND COST	172
6.1	Factors in Photovoltaic System Reliability	174
6.2	Modeling Reliability and Availability	176
6.2.1	The Exponential Distribution	178
6.2.2	The Weibull Distribution	179
6.3	Development of a Stochastic Reliability Model for PV System Simulation	180
6.3.1	Simulation Results	183
6.3.2	Sensitivity Analysis	186
6.4	Characteristics of Inverters for Photovoltaic Systems	190
6.5	Determination of Inverter Failure and Repair Rates	192
6.5.1	GTAC Inverter Experience	193
6.5.2	Estimating Failure Rates from a Prediction Standard	196
6.5.3	Estimating Repair Rates	200
6.6	Modeling Inverter Reliability and Availability	202
6.6.1	Simulating Inverter Failures	202
6.6.2	Improving Inverter Availability	204
6.6.3	Increasing Repair Rates	205
6.7	Discussion	208
6.8	Conclusions	210
7	GUIDELINES FOR FUTURE WORK	212
7.1	Improve Scale Estimates in Manufacturing Cost Model	212
7.2	Monte Carlo Simulation to Assess Uncertainty in Manufacturing Cost	213
7.3	Modeling the Manufacturing Cost of Organic and Other “Next Generation” Solar Cells	215
7.4	Develop an Inter-Operable Suite of Models to Simulate the Entire Photovoltaic Value Chain	216
A	ECONOMIC CALCULATIONS FOR PHOTOVOLTAIC SYSTEMS	218
A.1	Concepts in Financial Analysis	219
A.1.1	Cash Flow	219
A.1.2	Inflation	220
A.1.3	Discount Rate	221
A.1.4	Net Present Value	222
A.2	Calculating the Levelized Cost of Electricity	223
B	EXAMPLES USING THE ANALYTICAL COST MODEL	225
B.1	Example Efficiency Premium Calculation: Crystalline Silicon and Cadmium Telluride	225
B.2	Example Efficiency Premium Calculation: Crystalline Silicon and Cadmium Telluride with Unequal Service Lives	227

C	SCALE PARAMETERS FOR MODELING PHOTOVOLTAIC MODULE MANUFACTURING COSTS	230
C.1	Capital Equipment	230
C.1.1	Band Saws	231
C.1.2	Wire Saws	232
C.1.3	Wet Etching Equipment	234
C.1.4	Furnaces	237
C.1.5	PECVD Silicon Nitride Deposition Systems	240
C.1.6	Fully Automated Screen-Printing Lines	241
C.1.7	Solar Cell Testers and Sorters	242
C.1.8	Combined Tabber/Stringers	245
C.1.9	Laminators	247
C.1.10	Solar Simulators	248
C.2	Raw Materials	252
C.2.1	Ammonia	253
C.2.2	Argon	254
C.2.3	Carbon Tetrafluoride	254
C.2.4	Ethylene Glycol	255
C.2.5	Helium	256
C.2.6	Hydrochloric Acid	257
C.2.7	Hydrofluoric Acid	257
C.2.8	Nitric Acid	258
C.2.9	Nitrogen	259
C.2.10	Oxygen	259
C.2.11	Phosphorus Oxychloride	260
C.2.12	Silane	261
C.2.13	Silicon Carbide	262
C.2.14	Sodium Hydroxide	263
	REFERENCES	266
	VITA	280

LIST OF TABLES

Table 1.1	Contribution to domestic and global electricity production by source (percentage of total, 2004).	4
Table 2.1	Manufacturing cost estimates for crystalline silicon PV module production capacities of 1 MW _p /yr to 500 MW _p /yr.	19
Table 3.1	Band gap energies (E_g) and typical temperature coefficients (α_T) for four commercially important terrestrial PV materials.	52
Table 3.2	Coefficients used in determining solar cell operating temperatures for open-rack-mounted PV modules of various constructions.	53
Table 3.3	Computed AWOCT (°C) for selected U.S. cities and PV module constructions for south-facing open-rack-mounted PV arrays at latitude tilt and 22.6° tilt.	54
Table 3.4	MYPP benchmarks for residential, commercial, and utility PV system costs in 2005, and reference systems for 2011 and 2015.	56
Table 3.5	Derived values of A_{var} and A_{fix} (\$/m ²) MYPP reference systems.	57
Table 3.6	PV module assumptions for model calculations using 2005 MYPP benchmarks.	60
Table 3.7	Size, installed cost, and efficiency premium for residential PV systems using c-Si and thin-film module technologies to produce 6000 kW·h/yr at equal installed cost in Phoenix using 2005 BOS costs.	63
Table 3.8	Model calculations for c-Si and thin-film PV modules using 2005 MYPP benchmarks for commercial and utility systems.	64
Table 3.9	Retail module prices required for grid parity in 2015 for current and record PV cell and module efficiencies.	72
Table 3.10	Retail module prices required for grid parity in 2015 for CIGS and CdTe PV modules with current and record PV module efficiencies, assuming 20-yr service life.	83
Table 3.11	Input data for efficiency premium calculations on c-Si PV modules with efficiencies of 13.0% (System 1) against 6.3%-efficient a-Si PV modules (System 2).	87

Table 3.12	Results of efficiency premium computation comparing a PV system using typical c-Si PV module technology to that using typical a-Si technology.	88
Table 3.13	Results of efficiency premium computation comparing a PV system using typical c-Si PV module technology to that using typical a-Si technology.	89
Table 3.14	Efficiency premium calculations on a residential PV system using 2015 BOS costs comparing c-Si modules with 20% efficiency at \$1.50/W _p (System 1) to CdTe modules with 16.5% (System 2).	90
Table 4.1	Optimum solar cell thickness and efficiency associated with different bulk lifetime values for the device modeled in section 4.1 with BSRV of 10 cm/s.	99
Table 4.2	PCID inputs for modeling incremental improvements to base multicrystalline silicon solar cell technology.	112
Table 5.1	Classifications of capital cost estimates.	117
Table 5.2	Classification of PV module manufacturing plant operating costs used by the model.	120
Table 5.3	Illustrative income statement example for a PV module manufacturer (all figures in thousands of dollars).	121
Table 5.4	Typical values used for calculating the number of hours a machine operates each year.	126
Table 5.5	Typical values used for calculating the shift multiplier.	129
Table 5.6	Operating cost factors for computation of PV module manufacturing cost.	137
Table 5.7	Nominal throughput and equipment cost for PECVD deposition systems.	141
Table 5.8	Regression coefficients for computing representative capital equipment costs.	143
Table 5.9	Capital requirements C_{tot} for multicrystalline silicon PV module manufacturing plants using turnkey production lines from Spire.	146
Table 5.10	Capital equipment cost for Spire process with total capital cost estimate and resulting value for κ	147

Table 5.11	Price quotations for phosphorus oxychloride (POCl ₃) as a function of volume.	149
Table 5.12	Regression coefficients for computing unit material prices as a function of required volume.	150
Table 5.13	Input assumptions, including prices for commodity materials, assumed in validating the PV module manufacturing cost model against GT Solar calculations for a 25 MW _p turnkey production line.	163
Table 5.14	Comparison of GT Solar manufacturing cost calculations to modeled manufacturing cost for the same process.	165
Table 5.15	Changes to manufacturing process at each step of the technology road-map described in section 4.5.	167
Table 6.1	Failure history of the GTAC PV system.	194
Table 6.2	Weibull parameters and sample repair times for GTAC inverter repair distributions.	201
Table 6.3	Failure rates (per million hours) used for Monte Carlo simulation of GTAC inverter.	203
Table 6.4	Mean (standard deviation) number of failures and overall mean availability in 30-year inverter life for 10,000 simulations.	206
Table 6.5	Required repair rates to achieve 98.9% availability with consumer-grade components.	208
Table B.1	Input data for efficiency premium calculation comparing Sunpower c-Si module with 17% efficiency to First Solar CdTe module with 11.1% efficiency.	226
Table B.2	Input data for efficiency premium calculation comparing Sunpower c-Si module with 17% efficiency to First Solar CdTe module with 11.1% efficiency.	227
Table C.1	Nominal throughput and equipment cost for band saws.	231
Table C.2	Nominal throughput and equipment cost for wire saws.	233
Table C.3	Nominal throughput and equipment cost for saw-damage removal equipment.	234

Table C.4	Nominal throughput and equipment cost for phosphorus glass removal equipment.	236
Table C.5	Nominal throughput and equipment cost for texture etching equipment.	236
Table C.6	Nominal throughput and equipment cost for tube-type diffusion furnaces.	239
Table C.7	Nominal throughput and equipment cost for inline furnaces.	239
Table C.8	Nominal throughput and equipment cost for PECVD deposition systems.	241
Table C.9	Nominal throughput and equipment cost for fully automated screen-printing lines.	243
Table C.10	Nominal throughput and equipment cost for solar cell tester/sorters. .	244
Table C.11	Nominal throughput and equipment cost for combined tabber/stringers.	246
Table C.12	Nominal throughput and equipment cost for PV module laminators. .	249
Table C.13	Nominal throughput and equipment cost for solar simulators.	251
Table C.14	Price quotations for ammonia as a function of volume.	253
Table C.15	Price quotations for argon as a function of volume.	254
Table C.16	Price quotations for carbon tetrafluoride as a function of volume. . . .	255
Table C.17	Price quotations for ethylene glycol as a function of volume.	255
Table C.18	Price quotations for helium as a function of volume.	256
Table C.19	Price quotations for hydrochloric acid as a function of volume.	257
Table C.20	Price quotations for hydrofluoric acid as a function of volume.	258
Table C.21	Price quotations for nitrogen as a function of volume.	259
Table C.22	Price quotations for oxygen as a function of volume.	260
Table C.23	Price quotations for phosphorus oxychloride (POCl ₃) as a function of volume.	260
Table C.24	Price quotations for silane as a function of volume.	262
Table C.25	Price quotations for 400– mesh silicon carbide as a function of volume.	263
Table C.26	Price quotations for sodium hydroxide (NaOH) as a function of volume.	265

LIST OF FIGURES

Figure 1.1	Growth in annual worldwide PV module shipments, 1988–2007.	5
Figure 1.2	Crystalline silicon PV value chain.	6
Figure 1.3	Structure of a simple silicon solar cell.	6
Figure 1.4	Solar cell DC equivalent circuit and I-V curve.	7
Figure 2.1	Learning curve for photovoltaic modules.	17
Figure 3.1	Power-related module cost as a function of efficiency. Each line represents a different area-related module cost and follows the relationship given by equation (3.1).	30
Figure 3.2	Relative impacts of efficiency and direct manufacturing cost on power-related module cost. Note top and bottom x -axes — moving left-to-right along either axis represents <i>improvement</i> in the associated characteristic.	35
Figure 3.3	Contour plot displaying change in power-related module manufacturing cost, ΔC , as a function of relative changes in area-related manufacturing cost, $\Delta A/A$, and module efficiency, $\Delta\eta/\eta$	36
Figure 3.4	Comparison of cost components for two grid-connected PV systems of equal cost and capacity.	39
Figure 3.5	Schematic representation of the area-related energy outputs and cost parameters of systems one and two and the relationships resulting in the dimensionless quantities r , ν , and ω	42
Figure 3.6	Contours of $(A_{m,2}/A_{m,1})_{eq}$ as a function of ν and ω . The values of $(A_{m,2}/A_{m,1})_{eq}$ and ω are expressed as multiples of r . In the hatched region, system one is always the more economical system.	45
Figure 3.7	Qualitative assessment of Figure 3.6 showing the relationships between BOS costs that most strongly favor low- and high-efficiency PV modules.	47
Figure 3.8	Relative impacts of changes in module efficiency and area-related cost on installed system cost when $\nu > 0$. For the same relative improvement, efficiency has a greater impact than area-related cost when the magnitude of the improvement is between zero and ν	50

Figure 3.9	Efficiency premium as a function of AWOCT using 2005 MYPP benchmarks for c-Si PV modules with 13.5% efficiency relative to CIGS, CdTe, and CIGS PV modules with efficiencies of 9.0%, 8.0%, and 6.0%, respectively.	66
Figure 3.10	PV module cost to achieve parity with 2011 MYPP c-Si reference system as a function of module technology, efficiency, and market sector for PV systems located in Phoenix.	69
Figure 3.11	PV module cost to achieve grid parity according to the 2015 MYPP reference scenario as a function of module technology, efficiency, and market sector for PV systems located in Phoenix.	70
Figure 3.12	Effect of PV system service life on LCOE for 2005 MYPP residential benchmark system.	76
Figure 3.13	Financial parameters affecting the LCOE ratio L_2/L_1 as a function of inflation, discount rate, and inflation.	80
Figure 3.14	Contours of $(A_{m,2}/A_{m,1})_{eq}$ as a function of ν and ω for UCRF ratios of (a) 0.9 and (b) 1.1. The values of $(A_{m,2}/A_{m,1})_{eq}$ and ω are expressed as multiples of r . Compare with Figure 3.6, for which the UCRF ratio is implicitly unity.	81
Figure 4.1	Simulated solar cell efficiency as a function of thickness, bulk lifetime, and back-surface recombination velocity.	94
Figure 4.2	Effect of back surface recombination velocity on optimum L/W ratio and efficiency for $1.3\ \Omega\text{-cm}$ base resistivity.	95
Figure 4.3	Determination of τ_{crit} , the value of bulk lifetime at which further improvement has no appreciable effect on efficiency.	97
Figure 4.4	Solar cell efficiency as a function of τ_b for substrate thickness less than $400\ \mu\text{m}$ and S_b equal to $10\ \text{cm/s}$	100
Figure 4.5	Solar cell efficiencies and PV module manufacturing costs for solar cells having optimized, $100\text{-}\mu\text{m}$, and $300\text{-}\mu\text{m}$ thicknesses ($S_b = 10\ \text{cm/s}$). . .	102
Figure 4.6	Derivative of device efficiency with respect to L/W	104
Figure 4.7	Effect of varying base resistivity from 0.5 to $2.0\ \Omega\text{-cm}$ and BSRV from 10 to $10^6\ \text{cm/s}$ on $(L/W)_{opt}$ and optimum efficiency for τ_b of $30\ \mu\text{s}$. . .	107
Figure 4.8	Results of Monte Carlo simulation of variability in bulk lifetime and base resistivity with and without correlation between the variables. . .	109

Figure 4.9	Improvements in base commercial multicrystalline silicon solar cell efficiency obtained by incremental progress in device design as described in Table 4.2.	112
Figure 5.1	Elements of manufacturing and selling price of a manufactured product.	119
Figure 5.2	Cost of PECVD deposition equipment as a function of nominal throughput for 156-mm wafers.	142
Figure 5.3	Results of power regression analysis for determination of κ	148
Figure 5.4	Cost of phosphorus oxychloride as a function of purchase volume. . . .	150
Figure 5.5	Example of plant specification file.	153
Figure 5.6	Flow diagram showing the operation of the manufacturing cost model.	154
Figure 5.7	Example of workstation specification file.	155
Figure 5.8	Flow diagram showing the workstation loading process.	156
Figure 5.9	Flow diagram showing the plant initialization process.	158
Figure 5.10	Flow diagram showing the workstation initialization process.	159
Figure 5.11	Sample output from the manufacturing cost model directly after plant initialization.	160
Figure 5.12	Sample income statement generated from the cost sheet of Figure 5.11 on page 160.	161
Figure 5.13	Process flow diagram for base industrial solar cell (step A in the technology roadmap).	166
Figure 5.14	Results of manufacturing cost modeling of the solar cell technology roadmap of Figure 4.9 on page 112 for 100 MW _p annual production capacity.	168
Figure 5.15	Levelized cost roadmap for residential PV systems using the estimated retail prices from the cost roadmap in Figure 5.14 on page 168 and 2015 BOS costs from the MYPP reference system shown in Table 3.4 on page 56.	169
Figure 5.16	Estimated retail price of a PV module (displayed on contour lines in \$/W _p) made from 20%-efficient solar cells from the roadmap as a function of feedstock cost and cell thickness.	170

Figure 6.1	Flow diagram of reliability model for a PV system with a service life of T hours.	182
Figure 6.2	Typical modeled annual energy output for the sample PV system over its 30-year life span.	184
Figure 6.3	Input distributions for system component costs and financial parameters.	185
Figure 6.4	Probability density function for the cost of energy produced by the system over its 30-year lifetime. (a) Mean 34.7 ¢/kW·h, 90% confidence interval 29.8 ¢/kW·h to 39.8 ¢/kW·h. (b) Mean 10.4 ¢/kW·h, 90% confidence interval 9.2 ¢/kW·h to 11.8 ¢/kW·h.	185
Figure 6.5	Sensitivity of energy cost to the input parameters. Black bars show model sensitivity, the change in energy cost per 1% change in the input parameter. Gray bars show the standardized regression coefficient, the change in energy cost resulting from a change of one standard deviation in a given input.	188
Figure 6.6	GTAC PV system availability (through March 2006). The solid black line represents average system availability since system activation in July 1996.	194
Figure 6.7	Histograms showing distributions of failures per inverter subsystem modeled over 30-year service life using failure rates from Table 6.3 and 10 000 samples.	203
Figure 6.8	Capacitor failure rate modeled as a function of temperature.	204
Figure 6.9	Histograms showing Distribution of failures per inverter subsystem modeled over 30-year service life using failure rate for military-grade capacitors (0.30 per million hours) with rates for other components from Table 6.3 and 10 000 samples.	206
Figure A.1	Sample cash flow diagrams representing gross and the equivalent net cash flows (arbitrary units).	220
Figure C.1	Band saw cost as a function of nominal throughput for 156-mm bricks.	232
Figure C.2	Wire saw cost as a function of nominal throughput for 156-mm bricks.	233
Figure C.3	Saw-damage removal equipment cost as a function of nominal throughput for 156-mm wafers.	235

Figure C.4	Phosphorus glass removal equipment cost as a function of nominal throughput for 156-mm wafers.	237
Figure C.5	Texture-etching equipment cost as a function of nominal throughput for 156-mm wafers.	238
Figure C.6	Tube furnace cost as a function of nominal throughput for 156-mm wafers.	239
Figure C.7	Inline furnace cost as a function of nominal throughput for 156-mm wafers.	240
Figure C.8	Cost of PECVD deposition equipment as a function of nominal throughput for 156-mm wafers.	242
Figure C.9	Fully automated screen-printing line cost as a function of nominal throughput for 156-mm wafers.	243
Figure C.10	Solar cell tester/sorter cost as a function of nominal throughput for 156-mm wafers.	245
Figure C.11	Combined tabber/stringer cost as a function of nominal throughput for 156-mm wafers.	247
Figure C.12	Laminator cost as a function of nominal throughput for standard-cure and fast-cure EVAs.	250
Figure C.13	Solar simulator cost as a function of nominal throughput.	252
Figure C.14	Price of ethylene glycol as a function of purchase volume.	256
Figure C.15	Price of phosphorus oxychloride as a function of purchase volume.	261
Figure C.16	Price of silane as a function of purchase volume.	263
Figure C.17	Price of 400– mesh silicon carbide as a function of purchase volume.	264
Figure C.18	Price of sodium hydroxide as a function of purchase volume.	265

SUMMARY

Electricity generated from photovoltaics (PV) promises to satisfy the world's ever-growing thirst for energy without significant pollution and greenhouse gas emissions. At present, however, PV is several times too expensive to compete economically with conventional sources of electricity delivered via the power grid. To encourage market acceptance, a number of state and national governments around the world provide subsidies to defray the cost of using this environmentally friendly energy source, but for PV to succeed in the long term it must break free from the need for subsidies and achieve cost parity with electricity from the grid.

The United States Department of Energy (DOE) estimates that for this to happen, the retail cost of high-efficiency crystalline silicon PV modules must drop from its current level around $\$4.00/W_p$ to a range of $\$1.00/W_p$ to $\$1.50/W_p$. At this price, combined with DOE's projected future inverter and balance-of-system (BOS) costs, the levelized cost of electricity (LCOE) generated by crystalline-silicon PV systems will drop to 8 ¢/kW·h to 10 ¢/kW·h for residential PV systems and less for commercial and utility systems. This is competitive with rates for electricity from conventional sources.

Competing photovoltaic module technologies are also trying to reach this goal. Currently, the most commercially important solar cells using these technologies are comprised of thin layers of amorphous silicon (a-Si), cadmium telluride (CdTe), or copper indium gallium selenide (CIGS). Because they are produced from thin layers of semiconductor film they are often referred to collectively as "thin film" solar cells. From an economic standpoint, the major difference between these technologies and crystalline silicon is in consumption of raw materials. Where a silicon solar cell may be as much as 300 μm thick, thin film solar cells are typically only a few micrometers thick. As a result, these cells are much less expensive to manufacture than wafer-based silicon cells and hold the promise of producing energy from the sun at very low cost. However, thin-film PV modules tend to convert sunlight to electricity with lower efficiency than crystalline silicon modules and may also be less durable.

The goal of this work was to develop and use a series of analytical and numerical models to assess how crystalline silicon solar cells can achieve the grid parity goals set forth by DOE. To do this, a systems approach to modeling was undertaken to simulate every aspect of the silicon PV value chain, from purified silicon to solar cell fabrication to field deployment in an energy-producing PV system. This was accomplished by using and developing, when necessary, four types of models in conjunction with one another: devices, systems, manufacturing cost, and PV energy cost.

An additional goal of this work was to assess thin film PV technologies to determine what will be required of them, with their lower efficiencies, to also achieve grid parity and remain competitive with crystalline silicon. To this end, Task 1 of this thesis was to develop a model to assess the impact of power conversion efficiency of PV module economics. This task is addressed in Chapter 3, where an analytical model is derived to explain the effect of PV module efficiency on balance-of-systems (BOS) costs and the implications that this effect has for module costs. There it is shown that low-efficiency PV modules incur higher BOS costs which must then be offset by reduced module prices. This difference in the required module price is described as the “efficiency premium.” As a result, thin-film PV module technologies must either increase efficiency to at least 16% to achieve grid parity according to the DOE goals, or they must significantly undercut the goals (and hence high-efficiency crystalline silicon) on price. This is shown to be especially true for PV technologies that cannot match crystalline silicon in service life.

The objective of Task 2 is to use numerical device modeling to establish a roadmap to high-efficiency solar cells with the potential for low manufacturing cost. A series of device simulations using a typical commercial solar cell design is presented in Chapter 4. Using these simulation results in conjunction with fundamentals of semiconductor device physics, a set of guidelines is proposed to steer crystalline silicon solar cell development toward low cost with little sacrifice in efficiency. These guidelines suggest: (1) reducing back surface recombination velocity below a threshold value S_{crit} that is dependent upon bulk lifetime; (2) increasing bulk lifetime to a threshold value τ_{crit} that is dependent upon wafer thickness; and (3) minimizing wafer thickness to reduce manufacturing cost. A roadmap is developed based

on these principles to push solar cell efficiency from 14.4% to 20.0% in a manner intended to minimize manufacturing cost.

In Task 3, a numerical model was developed to estimate the manufacturing cost of crystalline silicon PV modules. The development of the model is described in Chapter 5. It is a highly general and flexible model implemented as an object-oriented program in Matlab. The goal of the model is simply to estimate manufacturing cost for arbitrary solar cell and module fabrication processes with relative accuracy. To enhance its utility, it also accounts for economies of scale so manufacturing costs may be estimated for high-volume production. The model was tuned and validated against cost calculations obtained from two different providers of turnkey PV module production lines.

Task 4 was to apply the manufacturing cost model to the technology roadmap developed in Task 2 to see if it succeeded in meeting the DOE cost targets for 2015. At the end of Chapter 5 it is shown that at current silicon feedstock prices of \$70/kg the proposed roadmap falls a bit short of the \$1.50/W_p retail module price target. The model is then used to evaluate several alternative ways in which the cost targets can be met through relatively simple changes to plant economics or the manufacturing process itself. It is also shown that if feedstock costs drop to \$38/kg or less the target can be achieved without having to consider these changes.

The goal of Task 5 was to develop a model for quantifying the impact of PV system reliability on its levelized cost of energy (LCOE). In Chapter 6 a Monte Carlo simulation is developed to predict the incidence and duration of system failures. The results of the simulation were applied to the output of a deterministic PV system model to quantify the energy lost during downtime over an assumed 30-yr service life. These results were then used to calculate LCOE and assess the economic impact of the system failures. With the assumed probability distributions for failure and repair times, it was found that the mean increase in LCOE that resulted from system failures was 3.7%.

The problem of establishing inverter failure probabilities was tackled in the final task of this thesis, where a methodology was proposed to estimate these probabilities based on inverter topology. The purpose of the proposed methodology, described in the second half of Chapter 6, is to adapt traditional reliability assessment procedures, which have massive data

requirements and are updated slowly, to keep up with fast-moving PV inverter technology. The methodology is exemplified through application based on the topology of the inverter used in the PV system at the Georgia Tech Aquatic Center (GTAC). Monte Carlo simulations are performed to illustrate the nature and rate of failures of various inverter subsystems. It is shown that the inverter's capacitors are primarily responsible for failures. Two methods are proposed to reduce system downtime: (1) improved reliability and (2) accelerated repair time. In the near term, inverter production volume is likely to remain too small for capacitor manufacturers to address the unique requirements of PV inverters, so methods are suggested to effect repairs more quickly.

CHAPTER 1

INTRODUCTION

The principal objective of this thesis is to use and develop a collection of technical and economic models of the photovoltaic (PV) industry supply chain to estimate the impact of technological progress on the cost of PV modules, systems, and the electricity they generate. Section 1.1 describes the motivation for this research. It also reviews the current technological and economic status of the PV industry and its role in the global energy market. Section 1.2 explains in detail the objectives and contributions of this research.

1.1 BACKGROUND AND MOTIVATION

Worldwide consumption of electricity was 16 695 TW·h in 2005 [2] and is expected to increase to 28 093 TW·h by 2030 [3], a near doubling over the next two-and-a-half decades. The International Energy Agency (IEA) predicts that meeting this demand for power will require 5087 GW of new electricity generating capacity (including replacement capacity) at a cost of \$5.2 trillion. The new plants will require an additional \$6.1 trillion worth of transmission and distribution networks, making electric power an \$11.3 trillion market over the next 25 years. This represents more than half of expected global investment in energy-supply infrastructure between 2005 and 2030 [3] and constitutes an enormous opportunity for all electricity-generating technologies.

While developed nations such as the United States will continue to demand electricity at a steadily increasing rate, rapid economic expansion in the developing world, where an estimated 1.6 billion people are without electricity, will account for a majority of the anticipated growth [3]. Electrification is widely regarded as a prerequisite for economic growth in developing nations and is strongly correlated with public health and quality of life indicators [4–7]. On the other hand, atmospheric emissions from electricity-generating power plants are implicated in climate change [8] and a host of illnesses [9]. A significant

challenge lies in building sufficient electrical generation capacity to meet the predicted demand growth without undermining public health and global ecology.

PV converts light directly to electricity via solar cells, solid-state semiconductor devices free of moving parts, costly fuel requirements, and harmful emissions. Solar-electric technology is extremely modular, allowing it to be quickly deployed at or near the point of consumption, minimizing transmission losses and even providing electricity in regions that lack centralized power stations and their requisite distribution systems. This modularity makes PV attractive in industrialized and developing nations alike. Furthermore, the cleanliness and environmental friendliness of PV make it an attractive technology for meeting the challenges of global electricity demand growth while simultaneously satisfying requirements for reduced emissions.

1.1.1 PHOTOVOLTAIC ENERGY CONVERSION: CURRENT STATUS AND FUTURE PROSPECTS

The commercial terrestrial PV power industry was born in the 1970s, roughly 20 years after the invention of the modern silicon solar cell in 1954 [10, 11]. Its birth was a response not just to the rapidly developing field of climate science and the resulting environmental movement that had blossomed over the preceding two decades, but to the energy crises that had destabilized energy markets in the United States and around the world in 1973 and 1979 [12]. Because it produces electricity directly from sunlight, photovoltaic technology was promoted as an emissions-free method of power generation that could replace existing fossil fuel-based power plants and their toxic by-products. After the partial meltdown of one reactor at the Three Mile Island Nuclear Generating Station in 1979 it also came to be seen as a safe alternative to nuclear power. Furthermore, since sunlight falls freely over the entire planet, solar energy was touted as independent from the politics that frequently encumber other sources of energy.

It was largely on the basis of these characteristics that solar energy research enjoyed immense public support and significant government research funding in the United States in the 1970s. By 1979, a plurality of Americans believed solar would be the nation's primary

energy source by the year 2000 [13]. However, despite a three-fold improvement in the price of PV modules between 1976 and 1980 [14], energy from PV remained far too expensive to compete with conventional sources of electricity. Political changes in the United States in the early 1980s ended substantial funding for solar energy research and, since the nation represented nearly 80% of the global market for solar energy at that time, virtually halted solar energy development around the world [12].

More recently, global awareness of climate change, the approval of the Kyoto Protocol by most of the world's nations, and a further decline in PV prices between 1980 and the mid-1990s (by about a factor of six [14]) have led to a resurgence of interest in photovoltaics over the past decade. PV is widely regarded as a potentially significant contributor to the global and national energy portfolio by virtue of its potential to sate the world's appetite for electricity without the continual release of harmful pollutants into the atmosphere.

In 2004, the most recent year for which detailed global energy statistics are available, renewable energy sources accounted for 9.6% of the electricity generated in the United States and 18.6% worldwide, as shown in Table 1.1(a). Table 1.1(b) shows that of this, just 0.001% was due to photovoltaic technologies in the United States and 0.03% worldwide. However, PV is one of the most rapidly growing energy technologies in world. As shown in Figure 1.1, PV module shipments have grown at an average annual rate of 40% since 1996, up from 13% over the period 1988 to 1996, reaching 2520.8 MW_p in 2006 [15].¹ A significant fraction of the 5087 GW in new demand anticipated by 2030 will be met by PV if the high growth rates of the past decade can be sustained, potentially transforming PV into a \$100-billion industry.

The key to sustaining these growth rates and achieving this transformation successfully is a substantial reduction in the cost of both PV modules and other PV system components. Currently, electricity from PV systems is a factor of two to five times more expensive than retail electricity in the United States [22], depending on system construction, geometry, and geography. Only by becoming more economically competitive with conventional energy technologies can PV achieve significant market penetration.

¹A peak watt (W_p) is defined by convention as one watt of power produced under an incident light intensity of 1000 W/m², which is the intensity of sunlight available at solar noon on a clear day at average latitude in the United States [16].

Table 1.1: Contribution to domestic and global electricity production by source (2004) [17, 18].

(a) Percentage of total.			(b) Percentage of renewables.		
Source	United States	World	Source	United States	World
Coal	50.1	39.6	Hydroelectric	74.5	88.6
Petroleum	3.3	6.7	Biomass	11.8	4.6
Gas	17.5	19.5	Waste	6.1	2.4
Nuclear	19.5	15.6	Geothermal	3.9	1.7
Renewables	9.6	18.6	Solar PV	0.001	0.03
			Solar thermal	0.1	0.05
			Other sources	3.6	2.6

The PV value chain, illustrated in Figure 1.2, maps the way to the most expedient means by which to reach cost parity with conventional energy sources. Silicon cost and quality strongly influences ingot cost and quality; in turn, ingot cost and quality strongly influences wafer cost and quality. This relationship continues as one travels left-to-right through the chain, each segment imposing its own qualities on the next with limited capacity to influence the segments that precede it. This is true for all segments but one: solar cells. Increased solar cell efficiency propagates forward through the value chain, of course, by increasing the power produced by a single PV module. This reduces the number of modules that a consumer will require to produce a desired output power, which minimizes the cost of installation and other BOS, ultimately reducing the total cost of the PV system. However, the solar cell efficiency increase can also propagate *backward* through the value chain by reducing the number of wafers required per peak watt of output, thereby minimizing the number of ingots and volume of silicon consumed. These economic benefits of these savings, of course, also propagate back *forward* through the value chain and reduce the total system cost even further. Other improvements at the solar cell segment, such as reduced device thickness, can have a similar effect. No other segment has such great effect on all of the other segments, regardless of their positions within the chain; for this reason, the solar cell is often seen as the linchpin of the PV value chain.

This linchpin may be exploited to gain an economic advantage by two broadly categorized approaches: (1) reducing PV module manufacturing cost, and (2) increasing power conversion

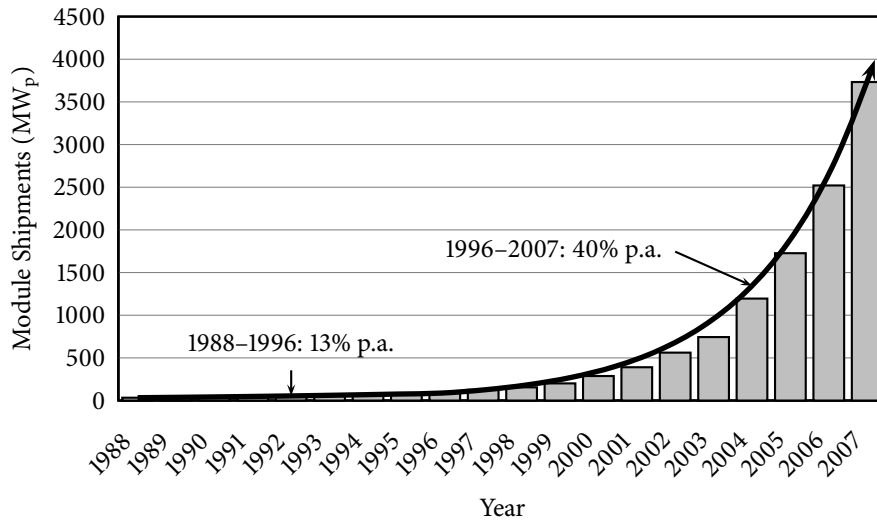


Figure 1.1: Growth in annual worldwide PV module shipments, 1988–2007 [14, 15, 19–21].

efficiency. In reality, it is difficult to reduce the manufacturing cost without affecting the efficiency, and vice versa. Furthermore, the efficiencies of many commercially produced crystalline silicon solar cells are already more than half of the theoretical maximum of 29% [23]. Since a doubling of power output cannot, by itself, overcome a factor of two to five, PV modules based on crystalline silicon technology will clearly require a combination of both approaches if they are to remain a viable technology for the future.

1.1.2 FUNDAMENTALS OF SOLAR CELL OPERATION

A solar cell is fundamentally nothing more than a p-n junction diode. When exposed to light, the substrate absorbs incident photons and excites electron-hole pairs, which are separated by the electric field present at the p-n junction. The structure of a simple silicon solar cell is shown schematically in Figure 1.3. It consists of a modestly doped substrate, a heavily doped emitter, an ohmic rear contact that covers the entire back side of the device, and an ohmic front contact applied as a grid to allow light to enter. In commercial silicon solar cells, the substrate is usually doped p-type and the emitter n-type. More advanced designs may include heavier doping at the rear surface to minimize the effects of surface recombination, texturing the front surface to enhance light trapping, or placement of both sets of contacts

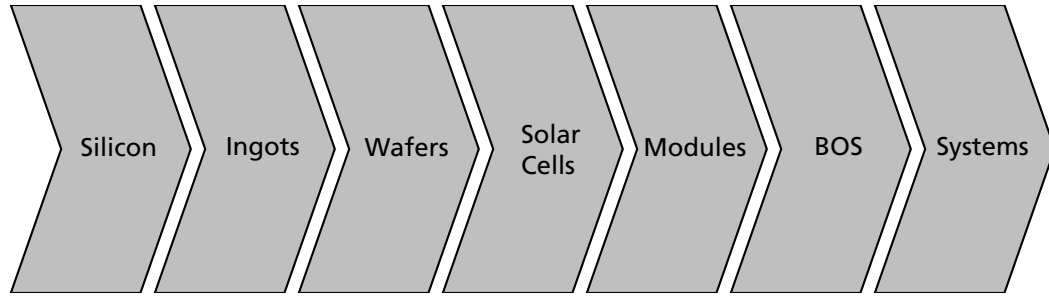


Figure 1.2: Crystalline silicon PV value chain.

on the rear to maximize light absorption, among other features. Some of these will be discussed in-depth in later chapters.

Given the basic device structure of Figure 1.3, the DC equivalent circuit of a solar cell is not difficult to derive. Generation of free electron-hole pairs is proportional to light intensity and corresponds to a current source. The p-n junction implies a diode in parallel with the current source, accompanied by a shunt resistor representing ohmic leakage currents. Finally, any normally conducting medium will present a non-zero resistance to the flow of current, represented by a series resistor at the output terminal of the solar cell. The circuit resulting from this analysis is shown in Figure 1.4(a).

In the equivalent circuit diagram, the photocurrent generated by the absorption of photons is represented by I_L . The cell's output current I is equal to this photocurrent, minus the currents diverted through the diode and the shunt resistor, represented by I_D and I_{SH} .

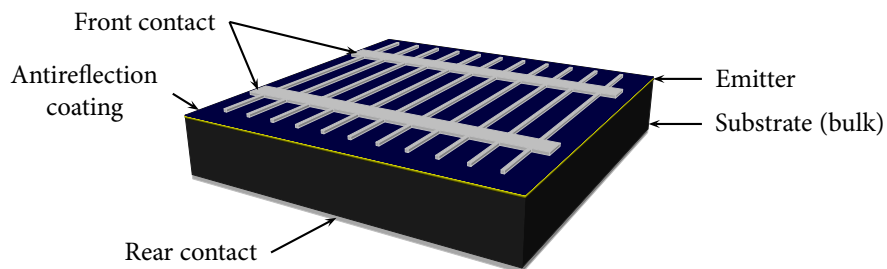


Figure 1.3: Structure of a simple silicon solar cell.

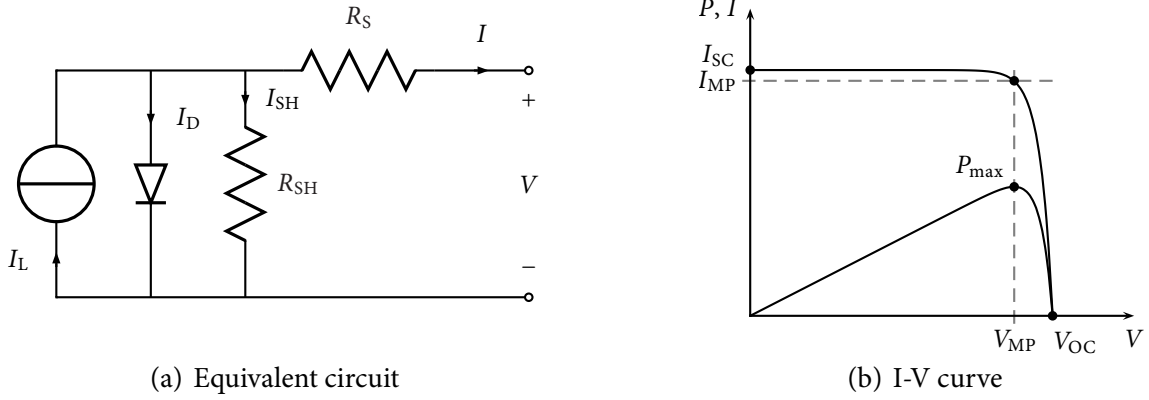


Figure 1.4: Solar cell (a) DC equivalent circuit and (b) I-V curve [23].

respectively. Mathematically, this is simply:

$$I = I_L - I_D - I_{SH}. \quad (1.1)$$

Replacing I_D and I_{SH} with expressions written in terms of I and the output voltage V yields [23]:

$$I = I_L - I_0 \left\{ \exp \left[\frac{q(V + IR_S)}{nkT} \right] - 1 \right\} - \frac{V + IR_S}{R_{SH}}, \quad (1.2)$$

where I_0 and n are the dark saturation current and ideality factor of the diode, respectively, k is Boltzmann's constant, T is temperature, and R_S and R_{SH} are the series and shunt resistances, respectively.

Plotting I as a function of V yields the characteristic I-V curve of the solar cell. By multiplying I by V at each point along the I-V curve, the output power P may also be plotted as a function of V . These curves are shown in Figure 1.4(b). When $V = 0$ the cell is, by definition, short-circuited, and the current produced is the short-circuit current I_{SC} . From equation (1.2) it may be seen that $I_{SC} \approx I_L$. As V increases from zero, I remains relatively steady at first, causing P to rise. However, I eventually begins to drop rapidly and, consequently, P reaches a maximum value P_{max} , then declines with further increases in V . This point is the *maximum power point*, and the accompanying voltage and current are designated V_{MP} and

I_{MP} , respectively. Finally, I drops to zero and the cell is, by definition, open-circuited; the value of V at this point is the open-circuit voltage V_{OC} .

The power conversion efficiency η of the solar cell is defined as the ratio of P_{max} to the power input to the cell:

$$\eta = \frac{P_{max}}{GA}, \quad (1.3)$$

where G is the insolation per unit area received by the cell and A is the surface area of the cell. Efficiency is generally measured under standard test conditions (STC), which specify $G = 1000 \text{ W/m}^2$ and a measurement temperature of $25 \text{ }^\circ\text{C}$. The efficiencies of commercially produced crystalline silicon solar cells tend to be in the range of 12–17%, with the best cells exceeding 20%. The highest efficiency achieved in the laboratory is 24.7% [24].

Another important solar cell metric is the *fill factor*:

$$FF = \frac{V_{MP}I_{MP}}{V_{OC}I_{SC}}, \quad (1.4)$$

which characterizes the loss mechanisms represented in Figure 1.4(a), particularly the series and shunt resistances. It is often described as a measure of the “squareness” of the I-V curve, since high fill factors tend to produce a very square-looking I-V curve. Values range from 0.72–0.77 in commercial devices, but can exceed 0.80 in laboratory devices. When the fill factor is known, equation (1.3) may be rewritten:

$$\eta = \frac{V_{OC}I_{SC}FF}{GA}. \quad (1.5)$$

The current produced by a solar cell is proportional to the cell’s surface area A : The larger the solar cell, the higher the output current. This characteristic can complicate comparison of test data and output parameters, so current is often scaled by dividing it by A to transform it into a current density. After this transformation, equation (1.2) becomes:

$$J = J_L - J_0 \left\{ \exp \left[\frac{q(V + J\rho_s)}{nkT} \right] - 1 \right\} - \frac{V + J\rho_s}{\rho_{SH}}, \quad (1.6)$$

where J is output current density, J_L is photocurrent density, J_0 is dark saturation current density, and:

$$\rho_S = R_S A \quad (1.7)$$

$$\rho_{SH} = R_{SH} A, \quad (1.8)$$

giving ρ_S and ρ_{SH} units of specific contact resistance (e.g., $\Omega \cdot \text{cm}^2$). The short-circuit and maximum-power-point current densities are denoted by J_{SC} and J_{MP} , respectively.

The voltage and current density a solar cell can produce under STC is primarily a function of the band gap energy of the underlying semiconductor material. For crystalline silicon solar cells, typical values of V_{OC} are 0.57 V to 0.63 V, with V_{MP} generally equal to 80–90% of V_{OC} . Typical values of J_{SC} are 32 mA/cm² to 38 mA/cm², with J_{MP} equal to 85–90% of J_{SC} . While these voltages and currents appear rather low to provide meaningful amounts of power, individual solar cells can be connected in series to increase voltage and in parallel to increase current. PV modules generally contain series-connected strings of solar cells with voltages of 20 V to 60 V; often, these strings are connected in parallel with one another increase module output current. These ideas will be revisited in Chapter 4, where the results of numerical modeling will be used to estimate the power output of a PV module consisting of multiple solar cells.

1.1.3 PV SYSTEM COMPONENTS

Once deployed in the field, PV modules are but one component of a solar-electric system. Usually, modules are combined with additional equipment for power conditioning and, sometimes, energy storage in order to ensure proper voltage and current supply. Furthermore, PV systems, like any other system, sometimes fail, resulting in downtime while the failure is corrected. Thus, in addition to the direct monetary costs due to system hardware and installation, the reduced energy production resulting from downtime must be factored into any calculation of a PV system's final energy cost.

The cost of the PV system is simply the sum of the costs of its components, amortized over the expected lifetime of the system. The cost of capital in a residential system is typically

taken to be equal to the interest rate on the loan used to finance the system. The major costs in a PV system are:

PV Modules: Retail price of the PV modules.

Inverter: Retail price of the inverter.

Hardware: Retail price of the equipment and wiring required to mount and interconnect the modules, along with any additional permanent equipment required to complete installation.

Installation: Fee for the physical labor, supervision, and equipment required to install the PV modules, inverter, and hardware.

Indirect Costs: All costs not directly related to items in the other categories. These costs typically include engineering, permitting, grid interconnection fees, and similar costs.

The sum of inverter, hardware, installation, and indirect costs is the *balance-of-systems*, or BOS, cost. The sum of all five cost components is the *installed cost* of the PV system and encompasses all of the capital costs due at the time of system construction. Each component must include all relevant distribution and shipping costs and all applicable taxes.

Specific component prices are determined by the markets for each component and vary with vendor, geographical location, quantity purchased, and supply and demand. In addition, prices can change over time. Thus, no single price is the correct one to use in all calculations and considerable price uncertainty can exist up until the time of purchase. For example, PV modules rated for high power (e.g., 150 W_p) tend to be cheaper per peak watt than similar modules with low power ratings (e.g., 50 W_p), so two different consumers using two different-sized modules might conceivably pay different amounts for PV systems that are, in the end, equal in size. Similarly, volume discounting can cause the same type of PV module to be sold for different prices to different customers.

While in previous decades most of the cost of a PV system was attributable to the PV modules, their prices have dropped significantly enough in recent years that they are now responsible for only about half of the total installed system cost. As a result, pressure has

increased on BOS providers to reduce their costs. This is particularly true of inverters, which are not only about a factor of three too expensive for PV to be cost-competitive, but which suffer from reliability problems and must be replaced several times over the course of a PV system's life [25].

The cost-effectiveness of a PV system may be judged by a number of measures, and no single measure can be considered the best for every circumstance [26]. However, a widely applicable, easily interpreted measure that has gained wide acceptance for policy analysis and generalized cost comparisons is the *levelized cost of energy* (LCOE). The appeal of LCOE is that it is effectively the cost of a PV system per unit of energy it generates over its lifetime and can be expressed in units that are directly comparable to rate paid for electricity from the local utility (e.g., ¢/kW·h). Thus, a simple way to assess the cost-effectiveness of a PV system is to compare its LCOE to the rate charged by the local utility.² LCOE will play an important role in later chapters and is rigorously defined in Appendix A.

1.2 RESEARCH OBJECTIVES

Completely modeling every single aspect of the value chain and tying all of the models together is an extremely ambitious undertaking. To make the research more manageable it is necessary to limit its scope. Accordingly, it focuses on aspects of the PV value chain that (a) directly impact LCOE and (b) can be readily simulated using physical models. The latter condition primarily eliminates direct modeling of BOS costs from consideration, as components like installation and hardware costs are determined largely by local economics and site-specific considerations. Therefore, this research focuses on establishing and tying together models of solar cell performance, PV module manufacturing cost, inverter reliability, and PV system performance and economics.

Setting the stage for this research is the DOE retail module price target of $\$1.00/W_p$ to $\$1.50/W_p$ for PV modules of 20% efficiency to achieve grid parity by 2015. As c-Si is increasingly challenged by thin-film PV module technologies it is important to understand

²Such a comparison implicitly assumes the rate charged by the utility will increase at the rate of general price inflation assumed in the LCOE calculation.

the conditions under which c-Si and thin films will be economically competitive with one another. Assessing these conditions plays a major role in motivating this research.

As discussed in the previous section, tools for estimating the impact of solar cell design on efficiency are well established and widely used in PV device research. However, there are currently no standard tools available for estimating the manufacturing cost of a PV module. As a result, changes to solar cell designs that enhance PV module efficiency can be readily modeled, but the economic cost of making the changes cannot. Clearly, a need exists for a set of tools that can guide PV module development on the basis of cost and efficiency improvements simultaneously. Developing these tools is the major task of this research.

Furthermore, PV manufacturers are forced to adopt broad tolerances on material parameters in order to maximize resource utilization and minimize production costs. As a result, solar cell design improvements resulting from laboratory research on a small number of samples can be affected in unexpected ways by the wide range of material parameters encountered on a typical production line. Tools to model the effects of this variability have the potential to help maximize technology transfer from the laboratory to the production line. In addition, the electrical mismatch between solar cells that results from this variability affects PV module performance and, therefore, cost. Developing tools to model these impacts are important to the assessment that is developed in this work.

Finally, accurate estimates of the cost of electricity produced by a PV system require accurate estimates of the amount of electricity produced. System downtime resulting from the failure of system components reduces the amount of energy produced and increases maintenance and capital costs. While many software tools exist for modeling PV system performance, none take into account the random nature of failures and downtime; therefore, they fail to reveal the full range of economic impacts that might result from the failures. This motivates the development of a model to account for the impact of system reliability on energy production over the life of the PV system.

This research addresses these challenges systematically through the application of numerical modeling and statistical analysis to each step of the photovoltaic power generation process.

1.2.1 TASK 1: DEVELOP A MODEL TO ASSESS THE IMPACT OF POWER CONVERSION EFFICIENCY ON PHOTOVOLTAIC MODULE ECONOMICS

The object of this task is to develop an analytical model to explain the effect of PV module efficiency on balance-of-systems (BOS) costs and the implications that this effect has for module costs. PV systems incorporating low-efficiency modules require more modules to produce the same amount of energy than high-efficiency systems do. As a result, low-efficiency systems tend to incur higher BOS costs than those using high-efficiency modules. This difference results from differences in installation, hardware, and other variable costs that scale with the number of modules in the system. Because of this, it is possible to define an “efficiency premium,” or an amount by which the price of high-efficiency modules may exceed that of low-efficiency modules without increasing the cost of energy produced by the PV system. In this task, an expression for computing the efficiency premium is derived. It is then used to assess the efficiency premium for current module designs, and to establish thin film module cost targets for 2015 based on the \$1.00/W_p to \$1.50/W_p range targeted for 20%-efficient c-Si.

1.2.2 TASK 2: USE NUMERICAL DEVICE MODELING TO ESTABLISH A ROADMAP TO HIGH-EFFICIENCY SOLAR CELLS WITH THE POTENTIAL FOR LOW MANUFACTURING COST

The goal of this task is to demonstrate the use of numerical modeling to establish a technology roadmap leading to a solar cell design optimized for low cost with minimal sacrifice in efficiency. The commercially available quasi-one-dimensional device simulator PC1D [27] will be used in this task to perform the required device simulations. PC1D has been validated with great success using solar cells fabricated in a laboratory setting. As a result, PC1D has also been used successfully to predict the results of design changes and maximize efficiency by optimizing the values of one or more device parameters. In this task, it is used to perform an extensive series of device simulations based on a typical commercial solar cell design. Using these simulation results in conjunction with fundamentals of semiconductor device physics, a set of guidelines is proposed to steer crystalline silicon solar cell development toward low cost with little sacrifice in efficiency. Finally, the guidelines are applied to a modern

commercial solar cell design to establish a roadmap that improves solar cell efficiency while simultaneously reducing manufacturing cost.

1.2.3 TASK 3: DEVELOP A MODEL TO ESTIMATE PHOTOVOLTAIC MODULE MANUFACTURING COST

The 8 ¢/kW·h to 10 ¢/kW·h goal set by DOE cannot be met by high efficiency alone because module manufacturing cost plays a very important role in determining the cost of electricity generated from PV. Through a combination of improvements in cell and module design, fabrication processes, and economies of scale, manufacturing costs must be reduced significantly. However, the marginal cost attributable to a particular design feature or production process is difficult to evaluate because no widely available tool exists for assessing manufacturing costs and comparing competing processes. As a result, individual manufacturers rely on proprietary models of their own processes while non-industrial research groups often base their claims of “low-cost” and “manufacturable” processes on ill-defined qualitative measures. The object of this task is to develop a modern manufacturing cost model for the purpose of evaluating the impact of changes in solar cell and module design on the direct module manufacturing cost. The model will account for alterations in the production process required to accommodate the design changes and economies of scale associated with increased production volumes.

1.2.4 TASK 4: APPLY THE MANUFACTURING COST MODEL TO THE HIGH-EFFICIENCY SOLAR CELL ROADMAP

The goal of this task is to apply the manufacturing cost model developed in Task 3 to the technology roadmap established in Task 2 to generate a complementary cost roadmap. The cost roadmap is used to assess whether the solar cell design guidelines developed as part of Task 2 succeed in reducing manufacturing cost to levels compatible with the DOE goals for 2015. It is also used to suggest adjustments to the roadmap and to plant economic requirements that can help achieve the goal.

1.2.5 TASK 5: MODEL THE COST OF ELECTRICITY FROM GRID-CONNECTED PHOTOVOLTAIC SYSTEMS IN THE PRESENCE OF SYSTEM FAILURES

The underlying reason to use PV modules is, of course, to generate electricity, and the cost of electricity produced by a PV system is ultimately its most important characteristic. The components of a PV system, like the components of any type of electrical or mechanical system, are subject to failure from time to time, which can lead to system shutdown and reduced energy output. This effectively increases the cost of the energy produced by the system. However, accurate models of PV system failures and their effects on system performance do not exist. The object of this subtask is to develop a model to predict these effects and calculate their impact on the cost of energy. Because failures cannot be planned and inherently have an element of chance, they must necessarily be modeled stochastically. The model uses probability distributions to determine the time between failures and the duration of each failure that occurs.

1.2.6 TASK 6: DEVELOP A METHODOLOGY FOR PREDICTING INVERTER FAILURE RATES

In this task, the problem of establishing inverter failure probabilities is tackled. A methodology is proposed to estimate these probabilities based on inverter topology. The purpose of the proposed methodology is to adapt traditional reliability assessment procedures, which have massive data requirements and are updated slowly, to keep up with fast-moving PV inverter technology. The methodology is exemplified through application based on the topology of the inverter used in the PV system at the Georgia Tech Aquatic Center (GTAC). Monte Carlo simulations are performed to illustrate the nature and rate of failures of various inverter subsystems. Finally, methods of increasing reliability and speeding up system repairs are discussed.

CHAPTER 2

REVIEW OF LITERATURE

Modeling of photovoltaic devices, systems, and economics has a long history within the PV community. Indeed, this research draws heavily on prior work, particularly where photovoltaic device and system modeling are concerned. As a result, it is vital to place the present research into context with its predecessors in order to understand its contributions to the field. This chapter attempts to do this by reviewing the models currently in use by the photovoltaic industry.

2.1 PHOTOVOLTAIC MODULE COST ANALYSES AND PROJECTIONS

PV growth has been “driven by market introduction programmes, but also by progress in materials and manufacturing technology, resulting in a significant cost reduction” [28]. Japan and Europe, in particular, have introduced aggressive subsidies in recent years with the intention of spurring investment in PV. Japan’s NEDO Sunshine Programme reversed five years of stagnant growth and shrinking market share for Japan’s PV industry, which is now the largest in the world [29, 30]. European subsidy programs were successful in accelerating the rate of adoption of PV systems, particularly in Germany, but European investment in PV manufacturing has lagged that of Japan or has been displaced to sites outside of Europe. The United States has been considerably less aggressive in subsidizing PV power, but has been the beneficiary of European investment in manufacturing capacity. In part as a result of this, since 1987 more than half of all PV cells and modules produced in the United States have been exported [31].

PV module prices have fallen consistently since solar cells were first commercialized. A number of investigators have characterized these price fluctuations using learning curves, which describe price as a function of cumulative production [32]. The learning curve for photovoltaic modules is shown in Figure 2.1 and plots PV module price against cumulative

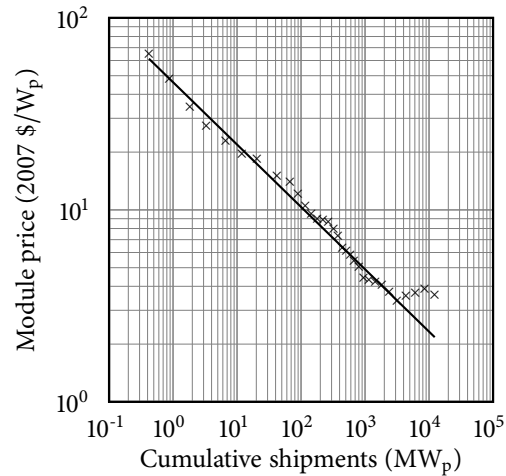


Figure 2.1: Learning curve for photovoltaic modules [14, 15, 20, 21, 36–38].

production over the history of the PV industry. For PV module production from approximately the mid-1970s to the mid-1990s, these studies have produced industry-wide learning rates ranging from 0.16 to 0.32, with most settling on a value near 0.20 [32–35]. This corresponds to a decrease in PV module price of 20% for each doubling of cumulative module production. However, in recent years this trend has been interrupted as the supply of PV modules has not been able to keep up with demand, resulting in the inflated module prices illustrated in Figure 2.1.

Cost reduction via the economies of scale offered by high-volume production has been the subject of considerable study in recent years [39–55]. Table 2.1 on pages 19–21 summarizes manufacturing cost analyses for plant capacities in the range of 1 MW_p to 500 MW_p per annum. The studies cited vary considerably in their assumptions. Studies conducted in the 1970s [39–41] tend to be more speculative, assuming that certain technological goals of the era would be realized in short order. In hindsight, these studies appear overly optimistic. Studies conducted in the early 1990s tend to assume thicker substrates, lower cell efficiencies, or lower production volumes than those conducted later [42–45, 50]. The latest studies tend to combine incremental technological improvements with the improved economics of large-scale production. The most optimistic of these consider solar cell designs with high efficiencies and high manufacturing yields on thin substrates [46–48, 54, 55]. Such

designs have been demonstrated on pilot production lines [56, 57], but have yet to move into commercial production.

In 1995, Alonso et al. published preliminary data from the cost analysis that was later incorporated into a European Commission study dubbed MUSIC FM. It indicated that the cost of PV modules from a 25 MW_p production facility could be reduced by 14% by scaling the plant up to 250 MW_p, provided the plant performed wafer fabrication in-house. A plant outsourcing its wafer production showed a higher production cost than one producing wafers in-house, and no significant savings from scaling up. By 1997, the methods used to estimate manufacturing costs had been updated, though new calculations for the 25 MW_p to 250 MW_p scale-up were not provided [46]. The release of this update coincided with that of the final MUSIC FM report [47, 48], which applied these cost estimation methods to seven different crystalline silicon technologies at a scale of 500 MW_p/yr, and three thin-film technologies at a scale of 60 MW_p/yr. This study concluded that costs of less than €1.00/W_p were possible through modest efficiency improvements and substantial scaling up of manufacturing capacity. A follow-up study released in 2002 further revised this figure to €0.77/W_p and predicted that the first 500 MW_p plants would be built by 2010 [54]. Selected results from the MUSIC FM study and its followup are summarized in Table 2.1(h).

A number of studies have analyzed costs for 10 MW_p to 25 MW_p plants [39, 40, 42–45, 49, 51–53, 55]. However, information on plants between 25 MW_p and 500 MW_p is limited. Frantzis et al. [51] estimate that increasing production line capacity from 10 MW_p to 100 MW_p would result in a manufacturing cost reduction of 21% for Cz-Si and 25% for mc-Si. Rohatgi [55] uses this information to estimate manufacturing costs of \$0.79/W_p to \$0.91/W_p at an annual production volume of 100 MW_p, based on calculations performed for a 25 MW_p plant. The MUSIC FM study looked indirectly at the scale effects for a 100 MW_p plant, estimating the price of a PV module at €1.50/W_p to €2.00/W_p [47]. Maycock [53] estimates that retail prices for PV modules will decline 22% to 42% for Cz-Si and 33% to 50% for mc- and ribbon Si between 2000 and 2010, assuming expansion from 10 MW_p to 100 MW_p in that span. Maycock does not provide estimates of manufacturing costs for 2000, but expects a 30% reduction in manufacturing cost for all crystalline Si technologies for scale up from 10 MW_p

Table 2.1: Manufacturing cost estimates for crystalline silicon PV module production capacities of 1 MW_p/yr to 500 MW_p/yr.

(a) 1 MW_p/yr

Investigator	Technology	Thickness (μm)	Efficiency	Cost (per W _p)
Hill [44]	Cz-Si ^a	N/A ^a	16%	\$4.50
	mc-Si ^a	N/A ^a	14%	\$4.50
Hynes and Hill [52]	Cz-Si	N/A	N/A	\$4.70
	mc-Si	N/A	N/A	\$4.70

^a Contact technology and device thickness are not specified, but presumed from other information provided to be screen printing and approximately 300 μm, respectively.

(b) 2 MW_p/yr/working shift

Investigator	Technology	Thickness (μm)	Efficiency	Cost (per W _p)
Margadonna and Ferrazza [50]	Screen-printed mc-Si	N/A ^a	13.5%	\$4.50

^a No thickness is explicitly specified in Margadonna and Ferrazza [50], but the article analyzes current production costs. Therefore, cell thickness is likely to be approximately 300 μm.

(c) 2.5 MW_p/yr

Investigator	Technology	Thickness (μm)	Efficiency	Cost (per W _p)
Alonso et al. [45]	Screen-printed Cz-Si	N/A	13%	€3.50

(d) 10 MW_p/yr

Investigator	Technology	Thickness (μm)	Efficiency	Cost (per W _p)
Wohlgemuth et al. [42]	Screen-printed mc-Si ^a	N/A	12.8%	\$3.29
Darkazalli et al. [43]	Cz-Si	N/A	14.5%	\$2.99
	mc-Si	N/A	13.5%	\$3.02
Hill [44]	Cz-Si ^b	N/A ^b	16%	\$2.30
	mc-Si ^b	N/A ^b	14%	\$1.80
Frantzis et al. [51]	Cz-Si ^b	N/A ^b	15%	\$2.45
	mc-Si ^b	N/A ^b	14%	\$2.10
Hynes and Hill [52]	Cz-Si	N/A	N/A	\$2.20
	mc-Si	N/A	N/A	\$1.90
Maycock [53]	Screen-printed mc-Si	350	13%	\$2.59

^a A number of variations on this process were also investigated, with module manufacturing costs ranging from \$3.08/W_p to \$3.93/W_p.

^b Contact technology and device thickness are not specified, but presumed from other information provided to be screen printing and approximately 300 μm, respectively.

Table 2.1: Continued

(e) 25 MW_p/yr

Investigator	Technology	Thickness (μm)	Efficiency	Cost (per W _p)
Carbajal [39]	Tandem junction mc-Si	N/A ^a	16%	\$2.00
Grenon and Coleman [40] ^b	Diffused Cz-Si	N/A	14%	\$1.84
	Ion-implanted Cz-Si	N/A	14%	\$1.61
Alonso et al. [45]	Screen-printed Cz-Si	N/A	13%	€2.57
Little and Nowlan [49]	Screen-printed mc-Si	300	15%	\$1.78
Rohatgi [55]	Screen-printed mc-Si	300	13.5%	\$1.98
	Screen-printed mc-Si	175	17%	\$1.06

^a Wafer thickness plus kerf was specified at 460 μm with multiblade ID sawing.^b This study investigated the sensitivity of manufacturing cost to annual production volume; however, only the values for the nominal 25 MW_p/yr case appear in this table.(f) 100 MW_p/yr

Investigator	Technology	Thickness (μm)	Efficiency	Cost (per W _p)
Grenon and Coleman [41]	Cz-Si flat plate	200	15%	\$1.45
	FZ-Si concentrator	200	15%	\$1.86
Hill [44]	Cz-Si ^a	N/A ^a	16%	\$2.30
	mc-Si ^a	N/A ^a	14%	\$1.80
Bruton et al. [47]	Various technologies	N/A	N/A	€1.50–2.00
Frantzis et al. [51]	Cz-Si ^a	N/A ^a	18%	\$1.45
	mc-Si ^a	N/A ^a	17%	\$1.15
Hynes and Hill [52]	Cz-Si	N/A	N/A	\$1.40
	mc-Si	N/A	N/A	\$1.20
Maycock [53]	Screen-printed Cz-Si	N/A	N/A	\$1.40
	Screen-printed mc-Si	N/A	N/A	\$1.20
	Screen-printed Si ribbon	N/A	N/A	\$1.20
Rohatgi [55]	Screen-printed mc-Si	175	17%	\$0.79–0.91

^a Contact technology and device thickness are not specified, but presumed from other information provided to be screen printing and approximately 300 μm, respectively.(g) 250 MW_p/yr

Investigator	Technology	Thickness (μm)	Efficiency	Cost (per W _p)
Alonso et al. [45]	Screen-printed Cz-Si	N/A	13%	€2.22

Table 2.1: Continued
(h) 500 MW_p/yr

Investigator	Technology	Thickness (μm)	Efficiency	Cost (per W _p)
Bruton et al. [46–48]	Screen-printed EFG Si	200	14.4%	€0.71
	Screen-printed mc-Si	200	15%	€0.91
	Buried-contact Cz-Si	200	18%	€1.15
	Screen-printed Cz-Si	200	16%	€1.25
Bruton [54]	Screen-printed mc-Si	150	17%	€0.77
	Buried-contact Cz-Si	150	20%	€0.97

to 100 MW_p between 2005 and 2010. It is not clear how much of this expected reduction he attributes to scale effects and how much he attributes to technological improvement.

Finally, while reducing solar cell thickness has long been regarded as an expedient means to reduce manufacturing cost, it has also been perceived as problematic because of high rates of breakage that accompany the thinning of the cells. However, research has been conducted into improving automation in the handling of thin cells, with an eye toward preserving product yields [58]. Furthermore, high yields for production on thin wafers have been demonstrated, including mechanical yields of 85% on 140 μm Cz-Si wafers and 90–95% on 200 μm multicrystalline wafers; the latter is only slightly lower than for 330 μm wafers [57]. Thus, the manufacturability of thin solar cells appears to be improving rapidly.

2.2 HISTORICAL DEVELOPMENT OF PHOTOVOLTAIC DEVICE MODELS

The first numerical device simulation was reported in 1964 by Gummel [59]. It was a one-dimensional simulation of a bipolar junction transistor based on a set of differential equations established 14 years earlier by Van Roosbroeck [60]. Numerical simulations in two dimensions first appeared in simplified form in 1968 [61, 62], then in complete form in the following year [63]. Two-dimensional simulators became a common part of device design in the 1970s; however, the first three-dimensional simulators did not appear until 1980 [64, 65]. The first successful general-purpose three-dimensional simulator did not appear until 1991 [66].

Numerical simulation of solar cells began in 1976 when Fossum [67] adapted a code

originally written for the analysis of silicon diodes. By 1982 Purdue University had developed SCAP1D and SCAP2D, one- and two-dimensional numerical models, respectively, intended specifically for silicon photovoltaic device work [68, 69]. These packages were limited to silicon device simulation only, though separate simulators for gallium arsenide were available through Purdue [70]; furthermore, Purdue's 1D models required a minicomputer and their 2D models required a supercomputer. This limited their accessibility and, therefore, their usefulness to the PV community. By this time the quasi-analytical models SPCOLAY (1D) and DCSSMODEL (2D) were also available [71, 72].

In 1985 the first numerical photovoltaic device model for personal computers, PC-1D, was released [73]. Initially it was a strictly one-dimensional model, but was upgraded to a quasi-one-dimensional model in 1988 [72]. Because it could run on a desktop computer and yielded comparable results to resource-hungry models like SCAP1D [74] it quickly became the leading device model in the PV community, a distinction that it holds to this day.¹

Many high-efficiency solar cell design features are inherently two- or three-dimensional, and for this reason multidimensional modeling is gradually assuming a larger role in photovoltaic device analysis. Software such as SCAP2D has largely disappeared because of its demanding computational requirements, but over the past 15 years new models have appeared that are able to run on small workstations and, more recently, personal computers. Purdue University's ADEPT was the first of these with an emphasis on solar cells [75], but recently the more general semiconductor device modeling package DESSIS_{ISE} [76] has gained favor in the PV community.

2.3 FOUNDATIONS OF PHOTOVOLTAIC DEVICE, SYSTEM, AND ECONOMIC MODELING

Analytical and numerical models of PV devices, systems, and economics have long been used in conjunction with experimental research and commercial experience to improve the performance and reduce the cost of PV modules. Furthermore, the models and methods

¹With the release of version 4 of the program in 1996 the hyphen was dropped from its name [27]. Therefore, it is referred to as PC1D throughout this document.

available to PV researchers have grown increasingly sophisticated as both PV and computer technology have evolved over the last several decades. While analytical models are still frequently used to promote intuitive understanding of fundamentals, particularly in device modeling, numerical models dominate for analysis of real devices and systems.

The following sections review the numerical models that are currently most commonly used in the PV industry to study three areas of primary interest: solar cells (devices), PV systems, and solar energy economics. The intent of these sections is to provide context and foster a better understanding of the current state of the art in PV modeling.

2.3.1 DEVICE MODELS

Numerous models have been developed to simulate the operation of a solar cell based on its physical parameters. By quantifying and specifying properties such as dopant densities and profiles, bulk and surface recombination rates, antireflection coating characteristics, and electrical contact quality, one may predict how efficiently a particular solar cell design will convert sunlight to electricity. While most general-purpose semiconductor device models are capable, on some level, of modeling solar cell performance, several models currently in use have been developed specifically with PV in mind.

Arguably the most popular device model is PC1D, first released in 1985, a quasi-1D model designed to run on personal computers [73]. PC1D has minimal processing requirements by modern computing standards and it has been experimentally well validated. Combined with its low price, these attributes have made it an extremely popular simulator whose output is widely accepted within the PV community. On the downside, PC1D models are stored in a proprietary binary data format and the program makes virtually no provision for user customization or inter-application communication. These limitations extend to program output, which can complicate analysis when simulations are performed in large numbers. Because of this, opportunities to apply new simulation methods using PC1D are limited.

More recently, DESSIS_{ISE}, a part of the ISE-TCAD suite of models, has gained popularity for solar cell modeling. It is a general multidimensional semiconductor device model developed with solar cell modeling in mind [77]; as such, it includes a number of capabilities of

particular interest to solar cell modelers. Furthermore, $\text{DESSIS}_{\text{ISE}}$ may be customized via a plug-in architecture, and input and output are accomplished through plain text files so that auto-generation of input and programmatic analysis of output are relatively simple. Most importantly, however, $\text{DESSIS}_{\text{ISE}}$ allows simulation of device structures that are inherently two- and three-dimensional, which PCID cannot do. While this capability is not critical for all device structures, many device structures exist that require this sort of functionality to provide meaningful insight to device operation through simulation. However, $\text{DESSIS}_{\text{ISE}}$ is much more computationally intensive than PCID, particularly when simulating multidimensional structures, so it is less practical to perform simulations in large numbers than with PCID.

2.3.2 SYSTEM MODELS

A very large number of PV system models are available, none of which have achieved the broad acceptance or dominant market share that PCID and $\text{DESSIS}_{\text{ISE}}$ have among device models. However, TRNSYS, developed by the Solar Energy Laboratory at the University of Wisconsin [78], is arguably the most important and influential such model. It is an extremely general model designed to perform detailed simulations of time-dependent energy systems. As such, it has been used not just for photovoltaic system simulations, but other renewable energy systems, low-energy buildings, HVAC systems, and fuel cells. TRNSYS is expensive and overly general for some applications, so while it has been used extensively for PV system simulations by Sandia National Laboratories and a number of other researchers, many investigators have found or developed alternatives.

One popular and well regarded alternative is PV-DesignPro [79], which differs from TRNSYS in that it emphasizes PV system design over detailed analysis. To this end, PV-DesignPro relies heavily on well validated empirical models of PV panels and other system components. This makes PV-DesignPro excellent for understanding and evaluating the impact of design decisions on PV system energy production, though because it is not based on empirical models rather than physical models it does not necessarily offer the physical insight that TRNSYS does. GeTPV, a model developed at Georgia Tech, is based upon

PV-DesignPro, but uses an improved thermal model to estimate PV module operating temperature [80]. It has not seen a public release and, therefore, cannot be considered a highly influential model, but its accuracy has been validated experimentally; furthermore, since its source code is readily available for modification it can be used to perform simulations that PV-DesignPro cannot.

More recently, the U.S. Department of Energy (DOE) has released the Solar Advisor Model (SAM) [81]. Intended primarily as a policy analysis tool for DOE to use in making research funding decisions, SAM uses a subset of TRNSYS as its PV system modeling tool. Its design and physical analysis capabilities are limited, but in combination with its economic modeling tools (which will be discussed further in section 2.3.3) it is well suited to examining the financial impacts of different PV technologies on the basis of LCOE.

Aside from these, an enormous number of other PV system models are in use. These range from models that are highly specialized to extremely general, and come in a variety of forms running the gamut from custom-generated spreadsheet models used by individual consultants to commercially available software suites targeted at whole-building energy simulations. Of particular note are PV F-CHART [82], a PV-specific implementation of TRNSYS developed by the original TRNSYS developers, and the National Renewable Energy Laboratory's (NREL) HOMER [83], a design-oriented (as opposed to policy-oriented) predecessor to SAM capable of simulating a variety of renewable energy technologies. DOE maintains an online directory of building energy software tools [84] that includes many popular PV system models.

2.3.3 ECONOMIC MODELS

Models of PV module manufacturing cost have been developed in the past, but were fairly cumbersome and required extremely detailed input to make their calculations. For a number of reasons, development of these models largely ceased in the 1980s (this will be discussed in greater detail in Chapter 2). While a number of numerical models do exist that could be used for the purpose of modeling PV module manufacturing costs, they tend to be computer-aided manufacturing (CAM) models designed for detailed factory layout and process optimization; as such, they too suffer from the need for extremely detailed inputs and are poorly suited for

rapid estimation of manufacturing costs. Consequently, economic models developed for PV use tend to focus on evaluating PV system costs and estimation of LCOE.

While analytical models of PV system economics have existed for some time, more detailed numerical models are a relatively recent development. In the United States, SAM has rapidly become the most significant of these models. Since 2006, applicants for federal PV research grant money under the Solar America Initiative (SAI) have been required to use SAM to perform economic self-assessments of their research proposals. SAM calculates LCOE using a well established financial analysis procedure described in [26], using installed PV system cost, ongoing operating and maintenance (O&M) costs, tax rates, financial incentives, and PV system performance estimates as its inputs. While SAM is arguably the most comprehensive economic analysis tool available for PV systems, its shortcomings in estimating energy production (resulting from its focus on policy analysis) limit its usefulness in analyzing the economics of real-world systems.

Elsewhere, Natural Resources Canada has developed RETScreen [85], a set of renewable energy analysis tools with extensive financial analysis capabilities. However, as spreadsheet-based tools, they are not capable of rigorous simulations to estimate energy production. Furthermore, like SAM, they are intended as policy analysis tools and lack many of the features desired for PV system design. A similar tool with more of a design orientation is the OnGrid Solar Financial Analysis Tool [86], though it is targeted at professional PV system installers who wish to calculate economic return-on-investment (ROI) for their customers in California, where retail electricity rate schedules and the state's PV incentive program can be very complex. ROI is frequently of greater interest to end-users than LCOE, which has been used primarily for setting policy and industry targets, though LCOE is now gaining wider acceptance as a more general indicator of cost-effectiveness for renewable energy projects.

CHAPTER 3

ANALYTICAL MODELING OF PV MODULE AND SYSTEM COST

The goal of this chapter is to assess crystalline silicon solar cell technologies analytically against thin-film technologies to determine under what conditions they remain economically competitive with one another. While accomplishing this numerically with established simulation tools would be relatively straightforward, an analytical approach is taken here in an effort to establish a fundamental understanding of the ways in which cost and efficiency affect one another. This approach necessarily requires a few simplifying assumptions, but yields a concise backdrop against which to better understand the more detailed numerical modeling to follow in later chapters.

While the model in this chapter was independently derived, similar investigations have been conducted previously [87–92] and found that module efficiency can have great economic leverage upon area-related PV system costs. However, these studies either fail to quantify the impact of this leverage or do so only for a limited set of circumstances. As a result of this, conclusions about the role of module efficiency in PV system economics are difficult to draw. Of these studies, Redfield’s approach, which compares two similar PV systems using low- and high-efficiency modules, showed the most promise for yielding a clear, concise, and quantitative economic assessment of module efficiency [88]. However, Redfield left many of the implications of his model unexplored, applying it only to a single hypothetical example comparing a flat-plate crystalline silicon PV system to a 300-sun gallium arsenide (GaAs) concentrator. As a result, his work, while still valid, provides little insight into modern PV systems.

In this chapter, an approach similar to that of Redfield is used to first to derive a model that directly compares PV modules of differing technologies in order to determine whether reducing manufacturing cost or increasing efficiency provides the more expedient path to

reducing cost per peak watt. Next, the approach is applied to PV systems in order to assess the leverage of efficiency on BOS costs, resulting in a model very similar to that derived by Redfield. This model is then extended to include systems with differing service lifetimes, facilitating comparisons of durable technologies with those that are less durable. Finally, the implications of these models are studied for current PV technology and short-term PV industry goals.

3.1 RELATIONSHIP BETWEEN PV MODULE MANUFACTURING COST AND EFFICIENCY

The initial model compares the manufacturing costs of low- and high-efficiency PV modules to determine whether module efficiency or manufacturing cost has the greatest influence on the module's cost per peak watt, which is the figure of greatest merit to consumers. It does this by relating module manufacturing cost and efficiency to the module cost per peak watt, then computing the sensitivity of cost per peak watt to changes in manufacturing cost and efficiency. The model is easily extended to comparisons of completely different PV modules and technologies.

3.1.1 NOMENCLATURE

For the sake of clarity, the following terminology and mathematical conventions are adopted in this section:

- *Design change* refers to any change in the design of a PV module, manufacturing process, or component thereof that affects the module's cost, efficiency, or both. This most obviously refers to changes in solar cell efficiency, but can include anything at all that affects the module's manufacturing cost or efficiency.
- *Manufacturing cost* refers to the area-related module manufacturing cost, expressed in terms of dollars per square meter. While the same cost, when converted to dollars per peak watt, is technically also a manufacturing cost, it is scaled by efficiency. Area-related cost is more indicative of the gross cost, in dollars, of an individual PV module.

- C refers to a power-related cost — that is, a cost expressed in terms of dollars per peak watt. This is the figure of merit most interesting to end-users of the module.
- A refers to area-related cost, expressed in dollars per square meter. This is the figure used to represent manufacturing cost.
- η refers to photovoltaic *module* (as opposed to *cell*) efficiency.

The variables C , A , and η may be subscripted with a number. A subscript of one indicates the variable refers to a module in its original state, while a subscript of two indicates that it refers to the module after a design change. For example, prior to improving the production yield of a manufacturing line, the area-related manufacturing of a module is A_1 ; after, it is A_2 . Note that while a specific design change is cited for purposes of this example, the model does not depend on the nature of the change, only the effects of the change on module manufacturing cost and efficiency.

3.1.2 DERIVATION OF THE MODEL

Given a module efficiency η and area-related manufacturing cost A , the module's power-related manufacturing cost C is

$$C = \frac{A}{I\eta}, \quad (3.1)$$

where I is the light intensity at which η is specified (1000 W/m^2 by industry convention). As previously stated, the power-related cost is the most useful figure of merit to consumers. This is because it combines both the area-related cost and the module efficiency into a single convenient value that is both meaningful and independent of module technology: A PV module that costs \$400 and has a power-related cost of $\$4.00/W_p$ will produce $100 W_p$ regardless of its efficiency or material composition. This relationship is illustrated in Figure 3.1.

Consider a PV module with efficiency η_1 and manufacturing cost A_1 . Suppose a design change is applied to the module, and the module's efficiency and manufacturing cost after the design change are η_2 and A_2 , respectively. The design change is cost-effective only if the module's cost per peak watt is less after the design change than it was before it, expressed

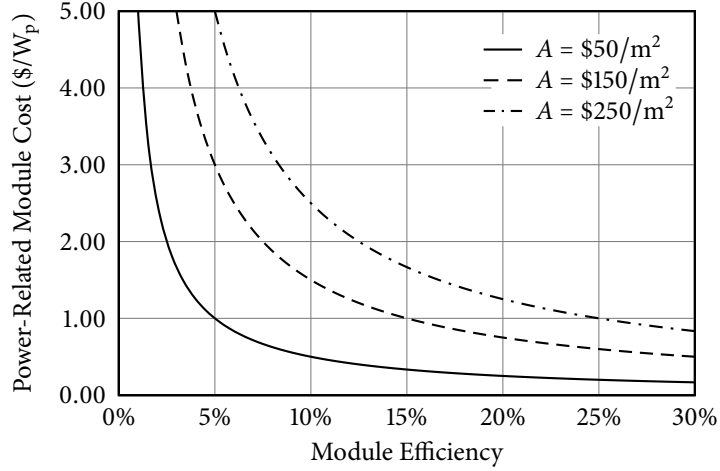


Figure 3.1: Power-related module cost as a function of efficiency. Each line represents a different area-related module cost and follows the relationship given by equation (3.1).

mathematically by the inequality $C_2 < C_1$. Applying equation (3.1) to this criterion and simplifying yields

$$\frac{A_2}{A_1} < \frac{\eta_2}{\eta_1}. \quad (3.2)$$

Thus, the cost criterion can be expressed as a simple inequality between ratios. Provided the ratio of manufacturing cost after the design change to that before it is less than the same ratio between module efficiencies, the design change is cost effective. This finding is neither new nor surprising.

Greater insight may be gained by working with the differences between the modules before and after the design change:

$$\Delta A = A_2 - A_1, \quad (3.3)$$

$$\Delta \eta = \eta_2 - \eta_1, \quad (3.4)$$

$$\Delta C = C_2 - C_1. \quad (3.5)$$

Using equation (3.1) one finds:

$$\begin{aligned} C_2 &= C_1 + \Delta C \\ &= \frac{A_1 + \Delta A}{I(\eta_1 + \Delta\eta)}. \end{aligned} \quad (3.6)$$

Noting from equation (3.1) that $A_1 = C_1 I \eta_1$ and solving for ΔC yields

$$\Delta C = \frac{\Delta A - C_1 I \Delta\eta}{I(\eta_1 + \Delta\eta)}. \quad (3.7)$$

Thus, equation (3.7) uses information about the current power-related cost and module efficiency to calculate the change in power-related cost resulting from expected changes in area-related cost and module efficiency.

Ultimately, C must be minimized in order to minimize the PV system cost. As a result, for a design change to be cost-effective requires $\Delta C < 0$ (note that this does *not* imply $\Delta A < 0$). Solving equation (3.7) for $\Delta C < 0$ yields

$$\Delta A < C_1 I \Delta\eta. \quad (3.8)$$

Equation (3.8) serves as a test in order to determine whether a change in design is cost-effective. More specifically:

1. If $\Delta A < C_1 I \Delta\eta$, the design change is cost-effective. That is, it will reduce the module manufacturing cost per peak watt.
2. Conversely, if $\Delta A > C_1 I \Delta\eta$, the design change is cost-ineffective — it will increase the module manufacturing cost per peak watt.
3. Finally, if $\Delta A = C_1 I \Delta\eta$, the design change is cost-neutral, and will neither increase nor decrease the manufacturing cost per peak watt.

Equation (3.8) may be used to determine whether a design change is cost-effective knowing only the current power-related manufacturing cost of the module, the change in efficiency,

and the change in area-related manufacturing cost. No knowledge of the module's starting efficiency is required.

Since C_1 and I in equation (3.8) must always be positive, the sign of $\Delta\eta$ determines whether ΔA may be positive. If $\Delta\eta$ is positive, then equation (3.8) indicates that ΔA may also be positive. This means that when efficiency increases, it is possible to reduce C while simultaneously increasing A .

As an example, consider a crystalline silicon PV module with $C_1 = \$3.00/W_p$. Suppose a design change increases efficiency by 1% absolute ($\Delta\eta = 0.01$). By equation (3.8), $\Delta A < \$30/m^2$ is required to achieve the desired outcome of $\Delta C < 0$. That is, with a 1% absolute increase in module efficiency, an *increase* in manufacturing cost is still cost-effective provided it amounts to less than $\$30/m^2$. On the other hand, a design change that *reduces* efficiency by 1% absolute ($\Delta\eta = -0.01$) is only cost-effective if $\Delta A < -\$30/m^2$, requiring a manufacturing cost reduction to avoid an undesirable increase in C .

An alternative expression for equation (3.8) results from substituting equation (3.1) and simplifying,

$$\frac{\Delta A}{A_1} < \frac{\Delta\eta}{\eta_1}. \quad (3.9)$$

This formulation expresses the cost-effectiveness criterion in terms of *relative* changes in area-related manufacturing cost and module efficiency. It states that a design change will achieve a reduction in C if the relative change in area-related manufacturing cost is less than the relative change in efficiency. Thus, an increase in η accompanied by a decrease in A is *always* cost-effective, while a reduction in η accompanied by an increase in A is *never* cost effective. If both η and A increase, or if they both decrease, the change *may* be cost-effective depending upon the result obtained from equation (3.9). This relationship is reaffirmed in the next section and plays an important role in determining whether efficiency or area-related cost has a greater impact on cost-effectiveness.

3.1.3 ASSESSING THE RELATIVE IMPORTANCE OF EFFICIENCY AND MANUFACTURING COST

Having determined the conditions under which a design change is cost-effective, the next step is to determine whether cost-effectiveness is more easily attained by increasing efficiency or reducing area-related manufacturing cost. To accomplish this, the following identities are useful:

$$\Delta A = \left(\frac{\Delta A}{A_1} \right) A_1, \quad (3.10)$$

$$\Delta \eta = \left(\frac{\Delta \eta}{\eta_1} \right) \eta_1. \quad (3.11)$$

Equations (3.10) and (3.11) express ΔA and $\Delta \eta$, respectively, in terms of their relative changes with respect to A_1 and η_1 . For example, a 10% reduction in manufacturing cost is expressed by $\Delta A/A_1 = -0.10$, and a 5% relative increase in efficiency by $\Delta \eta/\eta_1 = +0.05$.

Substituting equations (3.10) and (3.11) into equation (3.7) and simplifying yields

$$\frac{\Delta C}{C_1} = \frac{1 + \left(\frac{\Delta A}{A_1} \right)}{1 + \left(\frac{\Delta \eta}{\eta_1} \right)} - 1. \quad (3.12)$$

Equation (3.12) describes ΔC solely in terms of relative changes to A_1 and η_1 for a given value of C_1 . Furthermore, it expresses ΔC in a manner independent of A_1 and η_1 so that their relative effects on ΔC may be more clearly assessed. Note that if equation (3.12) is solved for $\Delta C < 0$, one recovers the cost-effectiveness criterion of equation (3.9).

Addressing changes in cost and efficiency in relative terms is appealing because it is more generally reflective of the amount of effort required to bring about a particular change. For example, one would expect that it is a great deal more difficult to produce a 1% absolute increase in efficiency on a low-efficiency material than it is on a high-efficiency material. Such an improvement represents about a 17% relative increase in efficiency for an amorphous silicon module with $\eta_1 = 6\%$, but only about an 8% relative increase for a multicrystalline silicon module with $\eta_1 = 12\%$. On the other hand, a 10% relative improvement in efficiency amounts to 0.6% absolute for the amorphous module and 1.2% absolute for the multicrystalline module, providing for a fairer and more realistic comparison of the two technologies.

To separately assess the impacts of $\Delta A/A_1$ and $\Delta\eta/\eta_1$ on cost-effectiveness, consider what happens to ΔC when each of the quantities is varied independently. Figure 3.2 displays ΔC as a function of $\Delta A/A_1$ with $\Delta\eta/\eta_1 = 0$ and as a function of $\Delta\eta/\eta_1$ with $\Delta A/A = 0$. Note that ΔC is linear in $\Delta A/A_1$ and nonlinear in $\Delta\eta/\eta_1$. From this, two clear trends emerge:

1. Given a choice between the *same* relative improvement in either A or η , the improvement in A will produce the greater reduction in C . The difference between the two is small for small improvements, but becomes more pronounced as the improvements grow. For example, a 10% reduction in A reduces C by 10% while a 10% increase in η reduces C by 9.1%; however, a 50% reduction in A reduces C by 50% while a 50% increase in η reduces C by only 33%. Taken to an extreme, a 100% reduction in manufacturing cost reduces C to zero while a 100% increase in efficiency reduces C by only 50%, and even a 300% increase in efficiency — a quadrupling — only reduces C by 75%.
2. Conversely, when the design change is not cost-effective and $\Delta C > 0$, a reduction in module efficiency will produce a greater increase in C than an increase in manufacturing cost. For example, an increase in A of 25% increases C by 25%, while a reduction in η of 25% increases C by 33%.

These trends suggest that a reduction in manufacturing cost is more helpful than an increase in module efficiency of the same relative magnitude, but a reduction in efficiency is more harmful than an increase in manufacturing cost of the same relative magnitude.

In reality, PV manufacturers will rarely, if ever, be forced to choose between a design that affects efficiency without affecting area-related manufacturing cost or vice versa. However, this finding suggests that design changes that emphasize cost savings will generally be more cost-effective than those that emphasize efficiency increases. For example, consider a design change that increases efficiency by 10% relative while reducing area-related manufacturing cost by 5%, and another design change that increases efficiency by 5% while reducing area-related manufacturing cost by 10%. By equation (3.12), the first design change will reduce power-related manufacturing cost by 13.6% while the second will reduce it by 14.3%. This

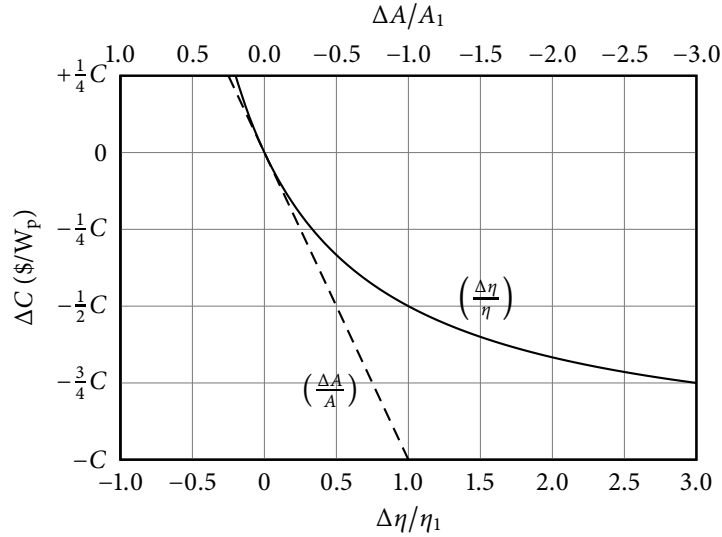


Figure 3.2: Relative impacts of efficiency and direct manufacturing cost on power-related module cost. Note top and bottom x -axes — moving left-to-right along either axis represents *improvement* in the associated characteristic.

difference may seem small, but for $C_1 = \$2.50/W_p$ in a 100-MW_p plant it amounts to an annual savings of \$1.75 million.

The relationship between $\Delta A/A_1$ and $\Delta \eta/\eta_1$ is illustrated graphically in Figure 3.3, which shows the value of ΔC resulting from various combinations of the two variables. It shows, for example, that a 40% reduction in C may be attained from a combination of 20% relative increase in efficiency and 28% reduction in area-related manufacturing cost. However, if the area-related manufacturing cost is instead reduced by 30%, a relative increase in efficiency of only 16.7% is required to achieve the same reduction in power-related manufacturing cost. The slopes of the lines in Figure 3.3 decrease with decreasing ΔC , reflecting the stronger influence of area-related manufacturing cost (compared to module efficiency) on improvements in cost-effectiveness. Conversely, the increasing slopes as ΔC increases reflects the stronger influence of module efficiency on reductions in cost-effectiveness.

3.1.4 PRELIMINARY CONCLUSIONS

In this section, a model was developed to describe the relationship between module efficiency and manufacturing cost. Manufacturing cost was subdivided into power- and area-related

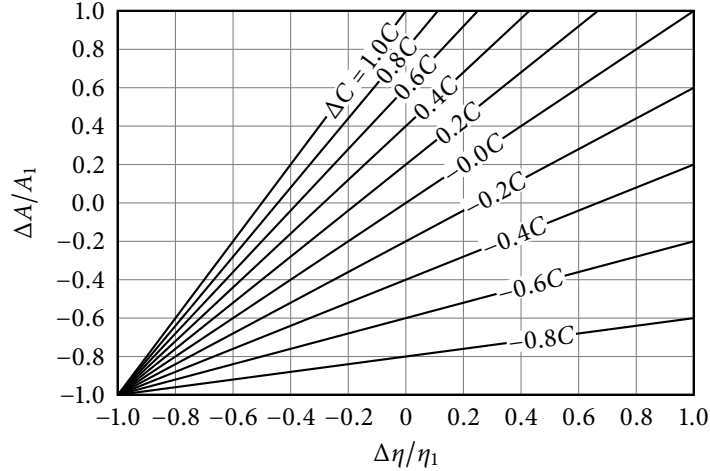


Figure 3.3: Contour plot displaying change in power-related module manufacturing cost, ΔC , as a function of relative changes in area-related manufacturing cost, $\Delta A/A$, and module efficiency, $\Delta\eta/\eta_1$.

categories linked, via equation (3.1), through efficiency. The cost-effectiveness of a design change resulting in a change in module efficiency or manufacturing cost was defined by its ultimate effect on power-related manufacturing cost, the most popular metric of PV module cost. Design changes resulting in reductions in power-related manufacturing cost were deemed cost-effective, those resulting in increases were deemed cost-ineffective, and those resulting in no change were deemed cost-neutral.

Next, the individual impacts of improvements in module efficiency and area-related cost were investigated. This investigation determined that a reduction in area-related cost will reduce power-related cost by a slightly, but significantly, larger margin than an increase in module efficiency of the same relative magnitude. Conversely, a reduction in module efficiency will increase power-related cost by a slightly, but significantly, larger margin than an increase in area-related cost of the same relative magnitude.

This analysis reveals no inherent cost advantage to high efficiency. As long as area-related module costs vary in proportion to efficiency, power-related cost is entirely independent of efficiency. More importantly, this analysis suggests that a 6%-efficient module that costs $\$3.50/W_p$ is completely interchangeable with a 20%-efficient module that also costs $\$3.50/W_p$.

If these conclusions are to be believed, efficiency does not matter if the power-related price is right. However, these conclusions fail to take into account the leverage of efficiency on downstream BOS costs. This is the subject of the next section.

3.2 IMPACT OF EFFICIENCY ON PV SYSTEM COST

The analysis presented in section 3.1 suggests that high module efficiency conveys no inherent advantage in power-related cost. It further suggests that increases in efficiency are only worth pursuing if they can be implemented at little to no additional cost. However, these conclusions neglect the fact that the ultimate goal of the end-user is to assemble a complete PV *system* at the lowest possible cost, and PV modules are just one of several components of a PV system.

In this section, a model is developed to assess the impact of module efficiency on the installed cost of PV systems. From this model, the concept of an *efficiency premium* is developed. This premium characterizes the impact of selecting high- versus low-efficiency modules for a system on the total installed system cost. A formal mathematical definition of the efficiency premium is proposed in section 3.2.5, but it may be qualitatively defined as the difference in high- and low-efficiency module costs for two otherwise identical PV systems such that the total installed costs of both systems are equal.

Note that while section 3.1 addressed PV module *manufacturing* costs, all of the costs discussed in this section are retail prices as paid by the end-user. Since prices are set by the market, it is not necessarily practical or desirable to assume a particular relationship between end-user prices and manufacturing costs. Therefore, *it is important to keep in mind that the values of A and C discussed in this section are not necessarily the same as those discussed in section 3.1.*

3.2.1 NOMENCLATURE

The model in this section is developed from the point of view of an end user who is building a PV system and trying to decide which modules to use. For this purpose, the system is segmented into the following cost components:

- PV Modules: Retail price of the PV modules.
- Inverter: Retail price of the inverter.
- Hardware: Retail price of the equipment and wiring required to mount and interconnect the modules, along with any additional permanent equipment required to complete installation.
- Installation: Fee for the physical labor, supervision, and equipment required to install the PV modules, inverter, and hardware.
- Indirect Costs: All costs not directly related to items in the other categories. These costs typically include engineering, permitting, grid interconnection fees, and similar costs.

The sum of hardware, installation, and indirect costs is the *balance-of-systems*, or BOS, cost. Traditionally BOS also includes the inverter, but the inverter is left out here for reasons that will become clear in section 3.2.2.

The sum of all five cost components is the *installed cost* of the PV system and encompasses all of the capital costs due at the time of system construction. Each component must include all relevant distribution and shipping costs, and all applicable taxes. Therefore, the module cost used in this section is not equal to that discussed in section 3.1, which concerned manufacturing costs. While it is important to bear this in mind, it does not diminish the conclusions that will be reached in this section since reducing retail prices while maintaining profit margins necessarily requires a proportional reduction in manufacturing cost. This issue will be briefly revisited in section 3.5.

As noted in section 1.1.1, it is often argued that PV module efficiency has an effect on the downstream components of the PV system. When efficiency is high, the argument goes, fewer modules are required to meet output power requirements. This, in turn, reduces the amount of hardware required for mounting and the amount of labor required for installation. It can also reduce other costs, such as site preparation costs that vary with the physical size

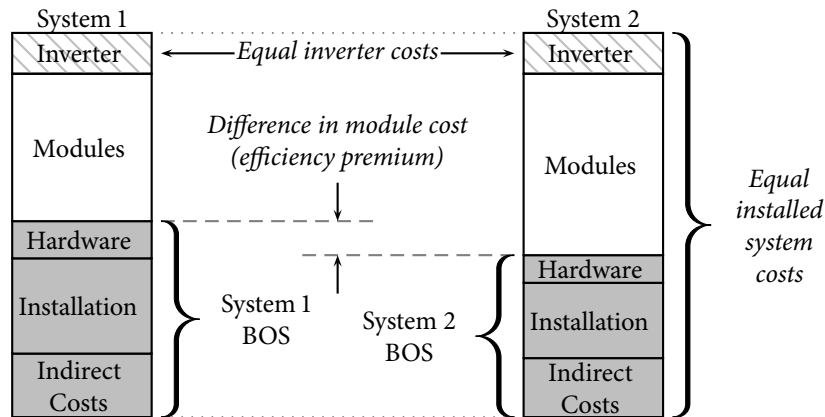


Figure 3.4: Comparison of cost components for two grid-connected PV systems of equal cost and capacity.

of the site. Therefore, when an end user chooses between low- and high-efficiency modules, he or she cannot assume the choice will not affect the other cost components of the system.

Assuming the choices available to the end user have equal service lives, the PV system with the greatest appeal to the end user will be the one that provides the required amount of energy at the lowest cost. The component costs for two hypothetical PV system that provide the same amount of energy at equal cost are shown schematically in Figure 3.4. Note that while the inverter costs shown in the diagram are equal, since both systems produce the same amount of energy, the other component costs are not necessarily equal: The BOS costs of system two are less than those of system one and the difference spent on PV modules.

Clearly, the module cost illustrated for system two in Figure 3.4 is the maximum that those modules may cost without rendering system one the more cost-effective choice. Conversely, if the cost of the system two modules were reduced — even if they remained more expensive than the system one modules — system two would be more cost-effective. In other words, one system may have more expensive PV modules than the other while simultaneously maintaining a lower installed system cost. The efficiency premium is the margin by which one system's modules may be more expensive than those in the other system without sacrificing cost-effectiveness; as shown in Figure 3.4, the efficiency premium is equal to the difference in BOS costs.

The model developed in section 3.2.2 uses ratios in a manner similar to the module manufacturing cost model of section 3.1 to compute the required module cost for system two to be more cost-effective than system one. It takes into account the differences in high-temperature performance that occur between the various PV module technologies, and a sample calculation is presented to show that the goal of selecting the more cost-effective system is satisfied. Finally, in section 3.2.5, an equation is derived to allow the more cost-effective module to be determined more directly.

3.2.2 DEVELOPMENT OF THE SYSTEM COST MODEL

The total installed cost of a PV system can be expressed,

$$S = S_m + S_{inv} + S_{bos}, \quad (3.13)$$

where S_m is the cost of the PV modules, S_{inv} is the cost of the inverter, and S_{bos} is the cost of BOS. Since systems one and two are both designed to produce the same annual energy output, system two is more cost-effective than system one when

$$S_2 < S_1, \quad (3.14)$$

where the numerical subscripts denote systems one and two. As noted in section 3.2.1, the two systems produce the same amount of energy by design and it is reasonable to assume that $S_{inv,2} \approx S_{inv,1}$. Thus, equation (3.14) may be written:

$$S_{m,2} + S_{bos,2} < S_{m,1} + S_{bos,1}. \quad (3.15)$$

Since both systems produce, by design, the same amount of energy,

$$\alpha_2 \eta_2 (1 - \ell_2) \equiv \alpha_1 \eta_1 (1 - \ell_1), \quad (3.16)$$

where α represents total module area and ℓ represents the fraction of energy production consumed by system losses. System cost and efficiency can then be related by dividing equation (3.15) through by equation (3.16):

$$\frac{S_{m,2} + S_{bos,2}}{\alpha_2 \eta_2 (1 - \ell_2)} < \frac{S_{m,1} + S_{bos,1}}{\alpha_1 \eta_1 (1 - \ell_1)}. \quad (3.17)$$

Noting that S/α is nothing more than an area-related cost and rearranging yields:

$$\frac{A_{m,2} + A_{bos,2}}{A_{m,1} + A_{bos,1}} < \frac{\eta_2(1 - \ell_2)}{\eta_1(1 - \ell_1)}, \quad (3.18)$$

where A_m is the area-related module cost and A_{bos} is the area-related BOS cost.

The right-hand side of equation (3.18) is the ratio of energy production *per unit area* of system two to that of system one. It includes two parameters for each system: module efficiency and system loss fraction. The loss fraction can be more precisely written as the product of each inefficiency that exists within the system:

$$(1 - \ell) = (1 - \ell_a)(1 - \ell_b)\dots \quad (3.19)$$

However, since the two systems are similar it is reasonable to assume that they will have similar loss mechanisms and that the losses will cancel one another. The exception is thermal losses, which are determined by the temperature coefficient associated with the semiconductor materials underlying the choice of PV module technology. The ratio on the right-hand side of equation (3.18) may then be written:

$$r = \frac{\eta_2(1 - \ell_{T,2})}{\eta_1(1 - \ell_{T,1})} \quad (3.20)$$

where $\ell_{T,1}$ and $\ell_{T,2}$ are the average losses due to temperature coefficient for the modules in systems one and two, respectively.

By equation (3.20), the entire comparison of energy production per square meter is reduced to a single dimensionless parameter, r . However, equation (3.18) still contains four different economic parameters. Keeping in mind that the purpose of this model is to determine the impact of PV module efficiency on the required cost of PV modules, define an additional pair of dimensionless system characteristics ν and ω such that:

$$A_{bos,1} = \nu A_{m,1} \quad (3.21)$$

$$A_{bos,2} = \omega A_{bos,1} \quad (3.22)$$

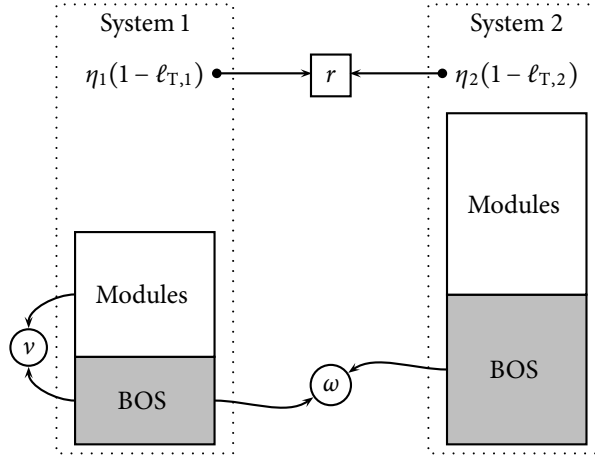


Figure 3.5: Schematic representation of the area-related energy outputs and cost parameters of systems one and two and the relationships resulting in the dimensionless quantities r , ν , and ω .

Now, given $A_{m,1}$, $A_{bos,1}$ is characterized by ν and $A_{bos,2}$ by ω (or, perhaps more precisely, the product of ν and ω). These relationships are shown schematically in Figure 3.5, where the cost components are illustrated in terms of area-related cost rather than total cost as they were in Figure 3.4. Substituting equations (3.20) to (3.22) into equation (3.18) and rearranging yields

$$\frac{A_{m,2}}{A_{m,1}} < r + (r - \omega)\nu. \quad (3.23)$$

This result is substantially the same as that obtained by Redfield [88].

Equation (3.23) describes the requirement on the area-related module cost of system two, $A_{m,2}$, relative to that of system one, $A_{m,1}$, in order for system two to be the more economical choice. The ratio is described in terms of dimensionless values representing the difference in area-related energy production (r) and BOS cost (ν and ω). Section 3.2.3 will describe how r , ν , and ω affect the ratio $A_{m,2}/A_{m,1}$. Section 3.2.4 characterizes existing PV systems to determine realistic values for ν and ω , and in section 3.2.5 a mathematical expression is derived for the efficiency premium. From these, cost and efficiency implications for various PV technologies are calculated and discussed.

3.2.3 ANALYSIS OF THE SYSTEM COST MODEL

While equation (3.23) is a fairly simple equation, understanding it can be difficult because of the number of parameters it entails. To focus the discussion, it is helpful to reiterate that the goal of this analysis is to investigate the effect of module efficiency on PV system economics. Therefore, for purposes of the present discussion, ν and η will be regarded as PV system characteristics (a topic that will be revisited in section 3.2.4); thus, r may be determined from PV module efficiency and temperature coefficient and, given $A_{m,1}$, the maximum cost-effective value of $A_{m,2}$ may be determined by simply plugging these parameters into equation (3.23).

That $A_{m,1}$ is assumed given for purposes of this discussion is significant. By equation (3.21), if $A_{m,1}$ is fixed then ν is directly proportional to the BOS cost of system one. Similarly, ω is directly proportional to the BOS cost of system two. Therefore, for purposes of analyzing equation (3.23) and its implications, ν and ω serve as proxies for the BOS costs of systems one and two, respectively. It is important to note that $A_{m,1}$ is assumed given purely for convenience and clarity in the following discussion — the choice has no effect on the conclusions, and the same conclusions may be reached by alternative analysis methods.

3.2.3.1 Relationship between Module Efficiency and Balance-of-Systems Cost

It is already established that the ratio on the left-hand side of equation (3.23) must satisfy the inequality expressed in that equation for system two to be more cost-effective than system one. However, if the left-hand side is *equal* to the right-hand side then the installed cost of system two is equal to that of system one and neither system is more cost-effective than the other. This is expressed mathematically by converting equation (3.23) to an equality,

$$\left(\frac{A_{m,2}}{A_{m,1}} \right)_{\text{eq}} = r + (r - \omega)\nu, \quad (3.24)$$

where $(A_{m,2}/A_{m,1})_{\text{eq}}$ is the value of $A_{m,2}/A_{m,1}$ for which systems one and two have equal cost.

By equation (3.20), r represents the ratio of the amount of energy generated per unit area in system two to that of system one. If the impact of the BOS costs, represented in equation (3.24) by ν and ω , are neglected for the moment, $(A_{m,2}/A_{m,1})_{\text{eq}} = r$. In this case,

the maximum economical module cost of system two is dictated purely by its energy density relative to system one. If $r = 1.5$, for example, then system two produces 1.5 times as much energy per square meter as system one and the maximum economical value of $A_{m,2}$ is 1.5 times $A_{m,1}$. If r changes, then for fixed $A_{m,1}$ the maximum economical value of $A_{m,2}$ changes proportionately. Not surprisingly, this is consistent with the findings of section 3.1, which considered module manufacturing cost and efficiency without regard to BOS cost. However, by equation (3.24), this situation will only arise when $\omega = r$ — that is, when the difference in BOS costs for the two systems is *also* proportional to the difference in performance.¹ Since this will happen only by coincidence, the maximum cost-effective value of $A_{m,2}$ is never determined solely by module efficiency.

Clearly, the above implies that if $(A_{m,2}/A_{m,1})_{\text{eq}} \neq r$, the true maximum cost-effective value of $A_{m,2}$ will differ from that expected based solely upon differences in module efficiency. When $(A_{m,2}/A_{m,1})_{\text{eq}} > r$, the maximum cost-effective value of $A_{m,2}$ will be disproportionately higher than expected based on the value of r alone, indicating that extra money may be spent on PV modules in system two without compromising its cost-effectiveness. On the other hand, when $(A_{m,2}/A_{m,1})_{\text{eq}} < r$, the maximum cost-effective value of $A_{m,2}$ will be disproportionately *lower* than expected based on r , indicating that *less* money may be spent on PV modules in system two if it is to remain economically competitive with system one. Since ν is a ratio of two economic costs, it must always be positive. By equation (3.24), this means that $(A_{m,2}/A_{m,1})_{\text{eq}} > r$ when $r > \omega$, and $(A_{m,2}/A_{m,1})_{\text{eq}} < r$ when $r < \omega$. Therefore, $r > \omega$ favors system two while $r < \omega$ favors system one.

Figure 3.6 displays equation (3.24) in the form of contours of $(A_{m,2}/A_{m,1})_{\text{eq}}$ as a function of ν and ω , with $(A_{m,2}/A_{m,1})_{\text{eq}}$ and ω expressed as multiples of r . The case where $\omega = r$ is evident as a horizontal line for which $(A_{m,2}/A_{m,1})_{\text{eq}} = r$. To understand the impact of BOS cost on the maximum cost-effective value of $A_{m,2}$, consider the partial derivatives of

¹Mathematically speaking it can also arise in the case that $\nu = 0$, which should never occur in practice since, by equations (3.21) and (3.22), it would require $A_{\text{bos},1} = 0$ and leave $A_{\text{bos},2}$ undefined.

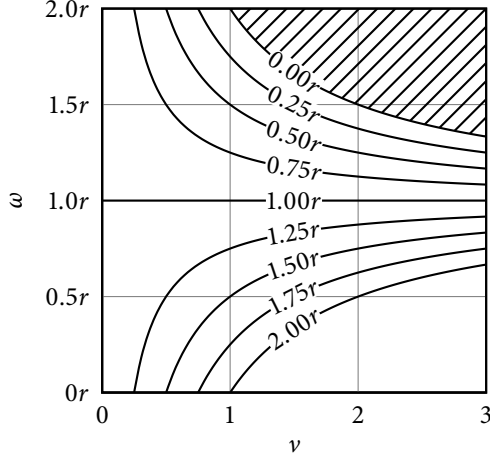


Figure 3.6: Contours of $(A_{m,2}/A_{m,1})_{eq}$ as a function of ν and ω . The values of $(A_{m,2}/A_{m,1})_{eq}$ and ω are expressed as multiples of r . In the hatched region, system one is always the more economical system.

equation (3.24) with respect to ν and ω :

$$\frac{\partial}{\partial \nu} \left(\frac{A_{m,2}}{A_{m,1}} \right)_{eq} = r - \omega \quad (3.25)$$

$$\frac{\partial}{\partial \omega} \left(\frac{A_{m,2}}{A_{m,1}} \right)_{eq} = -\nu. \quad (3.26)$$

Note that ω appears only in equation (3.25) and ν only appears in equation (3.26); as a result, the effect on $(A_{m,2}/A_{m,1})_{eq}$ of a change in the BOS cost component of one system is governed by the magnitude of the BOS cost component of the other system.

Consider equation (3.25). When $r > \omega$, the partial derivative is positive. Consequently, an increase in ν (or, equivalently, the BOS cost of system one) increases $(A_{m,2}/A_{m,1})_{eq}$ and favors system two. However, when $r < \omega$, the partial derivative is negative and an increase in ν reduces $(A_{m,2}/A_{m,1})_{eq}$, favoring system one. Furthermore, when $r > \omega$ then $(A_{m,2}/A_{m,1})_{eq}$ is already greater than r , and when $r < \omega$ then $(A_{m,2}/A_{m,1})_{eq}$ is already less than r . Therefore, the value of ν cannot affect *which* system is favored, only the *degree* to which it is favored. This trend is observed clearly in Figure 3.6 by following lines of constant ω for increasing values of ν .

Next, consider equation (3.26). As ω increases, $(A_{m,2}/A_{m,1})_{eq}$ decreases at a rate equal to the magnitude of ν regardless of the values of r and ω . Therefore, increases in ω favor system one while reductions favor system two. This trend is readily apparent in Figure 3.6, where following lines of constant ν for increasing values of ω reveals a rate of decline in $(A_{m,2}/A_{m,1})_{eq}$ that is proportional to the selected value of ν . In every case, $(A_{m,2}/A_{m,1})_{eq}$ is greater than r when $r < \omega$ and less than r when $r > \omega$, leaving the horizontal line represented by $\omega = r$ as the selection frontier that indicates whether system one or two is more cost-effective.

Simply put, system two is favored when $r > \omega$ and system one is favored when $r < \omega$, with the value of ν controlling the strength of the advantage enjoyed by the favored system. This is shown qualitatively in Figure 3.7. Since ν and ω are proxies for the BOS costs of systems one and two, respectively, these trends may be recast in a more tangible fashion. Which system is more economical is determined by a combination of system two BOS costs and PV module efficiency. Increasing or reducing system one BOS costs strengthens or weakens, respectively, the economic advantage enjoyed by the preferred system, whichever it may be. In practical terms, this is nothing more than a mathematical characterization, as either of the systems being compared can be designated system one or two without changing the results. However, as will be shown in section 3.2.6, this characterization can be very helpful in understanding the influence of BOS costs on PV system economics.

3.2.3.2 *Effect of Changes in Module Efficiency and Area-Related Cost on Installed System Cost*

In section 3.1.3 the model relating PV module manufacturing cost and efficiency was used to assess whether it is more cost-effective to increase module efficiency or to reduce module manufacturing cost. That assessment produced a slight preference for reducing manufacturing cost over increasing efficiency. However, the model developed in section 3.2.2 clearly shows that BOS costs can affect the relationship between module cost and efficiency. Therefore, it is instructive to apply the same approach used with the module manufacturing cost model to the system cost model to see whether it produces the same conclusions.

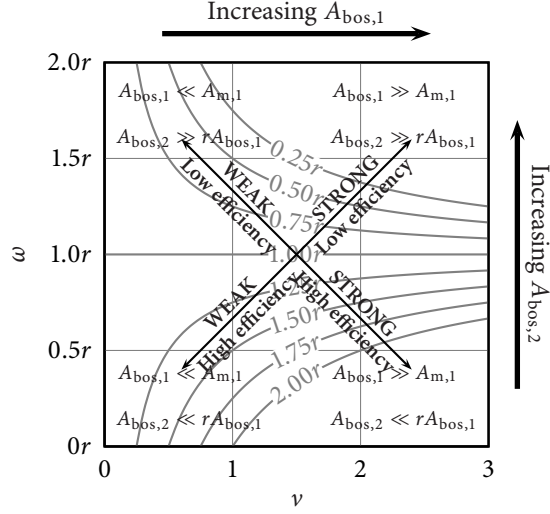


Figure 3.7: Qualitative assessment of Figure 3.6 showing the relationships between BOS costs that most strongly favor low- and high-efficiency PV modules.

Analogously to section 3.1.3, let the PV modules of system two be nothing more than improved versions of the modules used in system one — improved efficiency, reduced cost, or both. Therefore, the following relationships hold:

$$A_{m,2} = A_{m,1} + \Delta A_m \quad (3.27)$$

$$\eta_2 = \eta_1 + \Delta \eta \quad (3.28)$$

$$\ell_{T,2} = \ell_{T,1}. \quad (3.29)$$

Furthermore, since the modules of system two are nothing more than updated versions of those in system one,

$$A_{bos,2} \approx A_{bos,1}. \quad (3.30)$$

The installed system cost itself changes according to,

$$C_2 = C_1 + \Delta C. \quad (3.31)$$

Equations (3.27) and (3.28) parallel equations (3.3) and (3.4) from the module manufacturing cost model. Equation (3.30), combined with equation (3.22), implies $\omega \approx 1$ and, by

equation (3.21), $A_{\text{bos},2} = \nu A_{\text{m},1}$. Equation (3.29) arises from the modules in the two systems being not just the same technology, but nearly identical products and simply means that rated efficiencies may be used without consideration of potential losses.

The effect of these changes on installed system cost can be determined by revisiting equation (3.23). Substituting equation (3.29) into equation (3.20) yields,

$$r = \frac{\eta_2}{\eta_1}. \quad (3.32)$$

Using this with equations (3.27) and (3.28) to solve equation (3.23) for $(\Delta A/A_{\text{m},1})$, recalling that in this scenario $\omega \approx 1$, gives

$$\frac{\Delta A}{A_{\text{m},1}} < \frac{\Delta \eta}{\eta_1} (1 + \nu), \quad (3.33)$$

Compare to equation (3.9), the equivalent cost-effectiveness criterion for PV module manufacturing cost. Note that when $\nu = 0$ — that is, when BOS costs are zero — equations (3.9) and (3.33) are equivalent. Under this new criterion, the influence of efficiency on cost-effectiveness is enhanced by a factor of $(1 + \nu)$.

This enhanced influence is best illustrated by a numerical example. Suppose the modules in system two are 10% (relative) more efficient than those in system one, but that the increase in efficiency required a 15% increase in area-related module cost. Thus, $(\Delta \eta/\eta_1) = 0.10$ and $(\Delta A/A_{\text{m},1}) = 0.15$. Since $(\Delta A/A_{\text{m},1}) \not< (\Delta \eta/\eta_1)$, by equation (3.9) this increase in module efficiency is not cost-effective. However, if the systems' BOS costs are such that $\nu = 0.70$, the right-hand side of equation (3.33) evaluates to 0.17; since $(\Delta A/A_{\text{m},1})$ is less than this, the increase in module efficiency *is* cost-effective for this system once the BOS cost is taken into account. By leveraging the BOS cost, the higher efficiency becomes economical despite increasing the cost of the module.

The effect on installed system cost per peak watt may be seen by substituting equations (3.27) to (3.31) into equation (3.18) and simplifying to yield,

$$\frac{\Delta C}{C_1} = \frac{1 + \frac{\Delta A}{A_{\text{m},1}} \cdot \frac{1}{1+\nu}}{1 + \frac{\Delta \eta}{\eta_1}} - 1. \quad (3.34)$$

Note the similarity of equation (3.34) to equation (3.12) from the module manufacturing cost model. As with equations (3.9) and (3.33), the difference is a factor of $(1 + \nu)$. As written in equation (3.34) it reduces the influence of the change in module cost rather than increasing the influence of the change in module efficiency, but the effect is the same: High BOS costs reduce the importance of module cost and increase the importance of module efficiency.

Equation (3.34) is plotted in Figure 3.8(a) as a function of $(\Delta\eta/\eta_1)$ with $(\Delta A/A_{m,1}) = 0$, and as a function of $(\Delta A/A_{m,1})$ with $(\Delta\eta/\eta_1) = 0$ for increasing values of ν . This is analogous to the way equation (3.12) was plotted in Figure 3.3 for the PV module manufacturing cost model in section 3.1.3. When $\nu = 0$ the result is exactly the same as that shown in Figure 3.3 and both lines intersect at the origin. However, for $\nu > 0$ the slope with respect to $(\Delta A/A_{m,1})$ decreases. Since $(\Delta C/C_1)$ is unaffected by ν when $(\Delta A/A_{m,1}) = 0$, the slope with respect to $(\Delta\eta/\eta_1)$ does not change. The two lines continue to intersect at the origin, but the change in slope with respect to $(\Delta A/A_{m,1})$ gives rise to a second intersection point. The significance of this is that between the origin and the new intersection point, an increase in module efficiency has a greater effect on installed system cost than a reduction in module cost of the same relative magnitude.

The location of the new point of intersection may be determined by letting x equal the magnitude of the improvement in module efficiency or area-related cost. Then, equation (3.34) simplifies to

$$\frac{\Delta C}{C_1} = \frac{1}{1+x} - 1 \quad (3.35)$$

when $(\Delta A/A_{m,1}) = 0$ and

$$\frac{\Delta C}{C_1} = -\frac{x}{1+\nu} \quad (3.36)$$

when $(\Delta\eta/\eta_1) = 0$ (the negative sign in equation (3.36) reflects the fact that installed system cost is improved by *increasing* module efficiency, but *decreasing* module cost). Setting equations (3.35) and (3.36) equal to one another and solving for x yields

$$x = \nu. \quad (3.37)$$

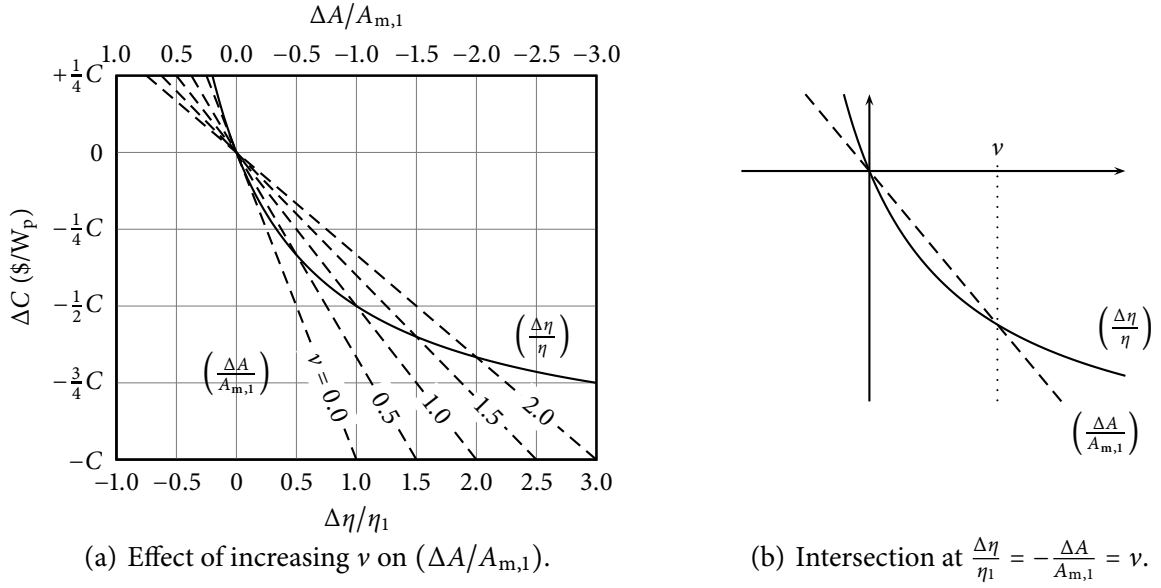


Figure 3.8: Relative impacts of changes in module efficiency and area-related cost on installed system cost when $\nu > 0$. For the same relative improvement, efficiency has a greater impact than area-related cost when the magnitude of the improvement is between zero and ν .

Thus, an increase in module efficiency or reduction in area-related cost will produce the same change $(\Delta C/C_1)$ in installed system cost when

$$\frac{\Delta\eta}{\eta_1} = -\frac{\Delta A}{A_{m,1}} = \nu. \quad (3.38)$$

This is shown schematically in Figure 3.8(b). As a result, the rule of thumb derived from the manufacturing cost model must be revised.

Now, given a choice between an increase in module efficiency or a reduction in area-related cost, both of equal relative magnitude, the increase in efficiency is the more cost-effective choice when the magnitude of the change is greater than zero and less than ν . When the magnitude of the change is greater than ν — that is, when $(\Delta\eta/\eta_1) > \nu$ or $-(\Delta A/A_{m,1}) > \nu$ — the reduction in module cost is the more cost-effective choice. Finally, when the magnitude of the change is negative (denoting a reduction in efficiency or an increase in area-related cost), the change in area-related cost is always the better choice. In fact, the moderating effects of $\nu > 0$ on $(\Delta A/A_{m,1})$ also minimize the detrimental effects of an increase in area-related cost, strengthening the notion that module efficiency should never be permitted to

drop. It should also be noted that since area-related module cost can never be reduced more than 100%, when $\nu > 1$ then increases in efficiency will *always* be more cost-effective than reductions of the same relative magnitude in area-related cost. This suggests that efficiency leverage is maximized when BOS costs exceed module costs.

3.2.4 INPUT PARAMETER DETERMINATION

Using the model described in this section requires realistic values for the model parameters. The value of r is strictly dependent upon system technology and can be determined using equation (3.20), provided the expected thermal losses are known. The remaining parameters, ν and ω , are economic and depend on the retail prices paid by end-users for system components. These prices are subject to a wide variety of market forces, many of which are unrelated to technology or manufacturing cost and beyond the control of component manufacturers. As a result, determination of appropriate values for ν and ω is not straightforward.

The following sections deal with each of these issues. First, section 3.2.4.1 discusses a method for estimating thermal losses in a PV system in a manner that is compatible with a simple analytical model like the one presented here. This takes into account differences in the PV technologies proposed for each system and, since one would expect thermal losses to be less significant in cooler climates, also accounts for the geographical location of the proposed system. Next, section 3.2.4.2 discusses various methods of estimating area-related BOS cost as a function of module efficiency. A method is selected on the basis of its potential to provide insight into US-based PV systems over the next decade, which enables the calculation of ν and ω for a variety of PV system types. The methods for determining r , ν , and ω developed here are applied in sections 3.2.6 and 3.2.5 to assess the cost-effectiveness of various PV module technologies.

3.2.4.1 *Thermal Losses and Determination of r*

In equation (3.20), r is defined as the ratio of the energy produced per square meter by system two to that of system one. Because the systems being compared are assumed identical, the only major loss mechanism considered in this model is related to the temperature coefficients

Table 3.1: Band gap energies (E_g) and typical temperature coefficients (α_T) for four commercially important terrestrial PV materials [23, 94, 95].

Material	E_g (eV)	α_T (%/°C)
Crystalline silicon (c-Si)	1.12	-0.50
Copper indium gallium diselenide (CIGS)	1.02-1.64	-0.34
Cadmium telluride (CdTe)	1.44	-0.25
Amorphous silicon (a-Si)	1.4-1.9	-0.20

of the PV modules. As the operating temperature of a solar cell increases the intrinsic carrier concentration in the underlying semiconductor material also increases, causing the band gap of the material to narrow [23]. This narrowing leads to a slight increase in current, but an appreciably larger drop in open-circuit voltage (V_{OC}), producing a net decrease in power conversion efficiency. It has long been established that this drop in efficiency is largely a function of the drop in V_{OC} , and that solar cells with high V_{OC} suffer smaller losses in efficiency when operating at high temperatures [93]. Since V_{OC} is itself a function of band gap energy (E_g), semiconductor materials with wide band gaps tend to be the least affected by high temperatures.

Band gap energies and typical temperature coefficients (α_T) for four important PV materials are shown in Table 3.1. Thermal loss is computed:

$$\ell_T = (T - 25^\circ\text{C})\alpha_T, \quad (3.39)$$

where T is the operating temperature of the solar cell. Once ℓ_T is computed for each PV system, the result is substituted into equation (3.20) along with η_1 and η_2 to compute r . However, at this point T is unknown.

The operating temperature of a solar cell can be difficult to quantify. It is influenced by the ambient air temperature, the amount of insolation it receives, wind velocity, mounting location and orientation, and a host of other local variables. Furthermore, even when the temperature of the cells can be carefully monitored, the operating temperature is difficult to measure with less uncertainty than $\pm 2^\circ\text{C}$ because of the encapsulation around it [96]. Finally, the desired value of T for use in equation (3.39) is not an instantaneous temperature, but a

Table 3.2: Coefficients used in determining solar cell operating temperatures for open-rack-mounted PV modules of various constructions [97].

Module construction	a	b	ΔT (°C)
Glass/cell/glass	-3.47	-0.0594	3
Glass/cell/polymer sheet	-3.56	-0.0750	3
Polymer/thin film/steel	-3.58	-0.113	3

representative average that will accurately account for thermal losses over the course of an entire year. Unfortunately, this task cannot be easily accomplished using an analytical approach. However, it can be accomplished numerically in a manner that does not compromise the instructive value of the analytical PV system model developed earlier.

To accomplish this, the instantaneous solar cell operating temperature is first estimated using an empirical model due to King [97]:

$$T_c = T_a + G \left(e^{a+bw} + \frac{\Delta T}{G_0} \right), \quad (3.40)$$

where T_a is the ambient temperature, G is the instantaneous irradiance on the module, G_0 is the irradiance at STC (1000 W/m²), w is the wind speed (m/s), a and b are empirically determined coefficients, and ΔT is the difference between the temperature of the back of the module and the temperature of the solar cell itself. Values of a , b , and ΔT for open-rack-mounted PV modules of various constructions are shown in Table 3.2.

The instantaneous value of T_c calculated in equation (3.40) is then used to compute an average weighted operating cell temperature (AWOCT) using a method described by Bücher [98]:

$$\bar{T} = \frac{\sum T_c G}{\sum G}, \quad (3.41)$$

where \bar{T} is the AWOCT. By performing the summations in equation (3.41) over the course of an entire year, a representative annual value of \bar{T} may be computed for a given module and location. Substituting equations (3.39) and (3.41) into equation (3.20) yields:

$$r = \frac{\eta_2 \left[1 + \alpha_{T,2} (\bar{T}_2 - 25^\circ\text{C}) \right]}{\eta_1 \left[1 + \alpha_{T,1} (\bar{T}_1 - 25^\circ\text{C}) \right]}, \quad (3.42)$$

Table 3.3: Computed AWOCT (°C) for selected U.S. cities and PV module constructions for south-facing open-rack-mounted PV arrays at latitude tilt and 22.6° tilt.

	Glass/cell/glass		Glass/cell/polymer		Polymer/thin film/steel	
	Latitude	22.6°	Latitude	22.6°	Latitude	22.6°
Atlanta, GA	38.1	38.2	35.8	35.9	33.6	33.7
Boston, MA	29.6	29.7	27.3	27.5	24.9	25.2
Boulder, CO	35.4	35.2	33.0	33.0	30.9	30.9
Detroit, MI	29.9	30.1	27.7	28.0	25.6	26.0
Houston, TX	41.0	41.0	38.8	38.8	36.7	36.7
Las Vegas, NV	45.5	45.5	42.9	42.9	40.5	40.5
Los Angeles, CA	38.2	37.9	35.7	35.5	33.2	33.0
Newark, NJ	31.8	31.9	29.6	29.8	27.4	27.7
Phoenix, AZ	49.9	49.9	47.3	47.3	45.1	45.1
San Francisco, CA	34.4	34.0	31.9	31.6	29.4	29.1

where the numerical subscripts indicate systems one and two. Values of \bar{T} computed from the TMY2 solar radiation database for south-facing modules at selected U.S. locations are shown in Table 3.3.

The table displays \bar{T} for each of the module constructions in Table 3.2 and for tilt angles equal to latitude. Since roof-mounted PV modules will often be tilted at an angle corresponding to roof pitch, particularly in residential installations, \bar{T} is also displayed for a tilt angle of 22.6°, a common roof pitch for buildings in the U.S. The table clearly shows that tilt angle has a negligible effect on annual AWOCT and may be safely ignored when computing r using equation (3.42). This should not be taken to suggest that tilt angle has negligible effect on annual energy production, as it does have a significant effect on plane-of-array insolation; rather, it indicates only that tilt angle does not affect r .

The differences in annual AWOCT between locations are quite large in some cases, suggesting that geography can have a significant affect on r . Consider an a-Si module with 6% efficiency and glass/thin film/steel construction, and a c-Si module with 13.5% efficiency and glass/cell/polymer construction, each with the temperature coefficients shown in Table 3.1. If the a-Si and c-Si modules are used in systems one and two, respectively, and mounted at a

tilt angle of 22.6° then:

$$r = \frac{0.135 \times [1 - 0.005 \text{ } ^\circ\text{C}^{-1} (47.3 \text{ } ^\circ\text{C} - 25 \text{ } ^\circ\text{C})]}{0.06 \times [1 - 0.002 \text{ } ^\circ\text{C}^{-1} (45.1 \text{ } ^\circ\text{C} - 25 \text{ } ^\circ\text{C})]}$$

$$= 2.08 \quad (3.43)$$

in Phoenix and

$$r = \frac{0.135 \times [1 - 0.005 \text{ } ^\circ\text{C}^{-1} (27.5 \text{ } ^\circ\text{C} - 25 \text{ } ^\circ\text{C})]}{0.06 \times [1 - 0.002 \text{ } ^\circ\text{C}^{-1} (25.2 \text{ } ^\circ\text{C} - 25 \text{ } ^\circ\text{C})]}$$

$$= 2.22 \quad (3.44)$$

in Boston. In other words, for every square meter of c-Si modules required, an equivalent system using a-Si will require 2.08 m² of modules in Phoenix and 2.22 m² of modules in Boston. The economic implications of this will be explored in section 3.2.6.

3.2.4.2 *Determination of Area-Related BOS Cost*

As previously noted, to calculate ν and ω requires that the relationship between module efficiency and retail BOS cost be quantified. However, the market forces that determine these prices are numerous and make quantification difficult. On a global scale, fluctuations in supply and demand, variations in currency exchange rates, and technological progress can cause the retail price to vary with time. Complicating matters further, local, regional, and national variations in supply and demand, marketing and construction regulations, and incentive programs can introduce geographical variability in pricing. Finally, the variety of products available on the market ensures further variability in pricing; a 100-W_p module from Evergreen Solar, for example, generally will not cost exactly the same as one from BP Solar. All of these factors act collectively to determine the retail price of each component of a PV system; consequently, the retail price does not necessarily bear any relationship to the manufacturing cost.

Because of the high degree of price variability these factors create, it is impossible to quantify the relationship between module efficiency and BOS cost in a deterministic manner.

Table 3.4: MYPP benchmarks for residential, commercial, and utility PV system costs in 2005, and reference systems for 2011 and 2015 [99].

System Element	Residential			Commercial			Utility		
	2005	2011	2015	2005	2011	2015	2005	2011	2015
Module efficiency (%)	13.5	16	20	13.5	16	20	13.5	16	20
PV module cost (\$/W _p)	4.00	2.20	1.00–1.50	4.00	2.20	1.00–1.50	3.30	2.20	1.00–1.50
Inverter cost (\$/W _p)	0.90	0.69	0.30	0.60	0.51	0.25	0.46	0.35	0.25
Hardware cost (\$/W _p)	0.61	0.40	0.33	0.55	0.17	0.08	0.97	0.73	0.61
Installation cost (\$/W _p)	1.66	0.57	0.42	0.54	0.36	0.13	0.27	0.16	0.10
Indirect cost (\$/W _p)	1.30	1.14	1.00	1.10	0.76	0.50	0.55	0.46	0.37

Furthermore, because these factors can change over time it is necessary to base speculation on the future economics of PV systems on projections about PV systems rather than field data. The projections used here come from U.S. Department of Energy (DOE) *Multi-Year Program Plan 2007–2011* (MYPP) [99]. This document cites benchmarks for U.S. PV system costs in 2005 and establishes reference systems for 2011 and 2015 that illustrate how the goals of the SAI might be met.² The reference systems were established for three sectors: residential, commercial, and utility. These are summarized in Table 3.4. The rows of the table are labeled in accordance with the nomenclature established in section 3.2.1.

The the method used here for relating module efficiency and BOS cost is a variation on a method first used by Cornelius [101]. He computed the required cost for PV modules of varying efficiency under the constraint that total system cost be equal for all efficiencies. (This differs from the present model in that the present model seeks the lower cost per unit of annual energy production.) In doing so, he assumed that the indirect costs expressed in Table 3.4 were fixed and that hardware and installation costs varied with efficiency. Mathematically, this is expressed:

$$C_{bos} = C_{ind} + \frac{\eta_{ref}(C_{hdw} + C_{ins})}{\eta}, \quad (3.45)$$

where C_{ind} , C_{hdw} , and C_{ins} are the indirect, hardware, and installation costs per peak watt, as shown in Table 3.4, and η_{ref} is the efficiency to which the costs in the table are referenced.

²The MYPP actually sets goals for 2011 and 2020, but the subsequent Solar America Initiative accelerates the timetable, moving the 2020 goals to 2015 [100].

Table 3.5: Derived values of A_{var} and A_{fix} ($\$/\text{m}^2$) MYPP reference systems.

	2005		2011		2015	
	A_{var}	A_{fix}	A_{var}	A_{fix}	A_{var}	A_{fix}
Residential	306	1300	155	1140	150	1000
Commercial	147	1100	84.8	760	42.0	500
Utility	167	550	142	460	142	370

For example, for the 2005 residential benchmark the BOS cost was expressed:

$$\begin{aligned}
 &= 1.30 + \frac{0.135 \times (0.61 + 1.66)}{\eta} \\
 &= 1.30 + \frac{0.306}{\eta}.
 \end{aligned} \tag{3.46}$$

While this yields BOS cost for an arbitrary module efficiency expressed in terms of dollars per peak watt, the present model requires BOS cost in terms of dollars per square meter. Transforming equation (3.45) by multiplying both sides by 1000η , the peak power output per square meter at standard test conditions (STC), yields:

$$\begin{aligned}
 A_{\text{bos}} &= 1000\eta_{\text{ref}}(C_{\text{hdw}} + C_{\text{ins}}) + 1000C_{\text{ind}}\eta \\
 &= A_{\text{var}} + A_{\text{fix}}\eta,
 \end{aligned} \tag{3.47}$$

where A_{var} is the variable BOS cost per square meter and A_{fix} is the fixed cost per square meter for a module efficiency of 100%. For the 2005 residential benchmark, this is:

$$A_{\text{bos}} = 306 + 1300\eta. \tag{3.48}$$

Repeating this procedure for each of the other cases in Table 3.4 yields a separate equation for each case, summarized in Table 3.5.

It seems counterintuitive at first that the factor of η should be attached to the fixed cost term, but it is a perfectly logical consequence of the transformation from equation (3.45). Adding an additional square meter of module area incurs additional BOS costs for hardware and installation labor. Using equation (3.48) as an example, each additional square meter of

module area added to the system increases BOS costs by \$306. Increasing module efficiency shrinks the physical size of the system and causes the fixed costs to be spread over a smaller area; thus, increasing efficiency also increases A_{bos} . However, as long as the increase in fixed cost per square meter does not exceed the variable cost per square meter, *total* BOS costs fall as efficiency rises. As an example, consider a 50 m² system with 10%-efficient modules rated at 5 kW_p. By equation (3.48), such a system would have $A_{\text{bos}} = \$436/\text{m}^2$ and a total BOS cost of \$21 800. If module area is reduced to 40 m² and module efficiency increased to 12.5% the system is still rated at 5 kW_p and A_{bos} increases to \$468.50/m², but total BOS cost drops to \$18 740.

By substituting the expressions for A_{bos} from Table 3.5 into equations (3.21) and (3.22), values for ν and ω may be calculated for arbitrary efficiencies in any year for any of the three system types. Thus:

$$\nu = \frac{A_{\text{var}} + A_{\text{fix}}\eta_1}{A_{\text{m},1}} \quad (3.49)$$

$$\omega = \frac{A_{\text{var}} + A_{\text{fix}}\eta_2}{A_{\text{var}} + A_{\text{fix}}\eta_1}. \quad (3.50)$$

It is worth taking a closer look at ω . Equation (3.23) suggests that efficiency leverage over BOS cost depends primarily on the difference between r and ω — the greater the difference, the greater the economic advantage to the system with the higher efficiency. As A_{var} approaches zero:

$$\lim_{A_{\text{var}} \rightarrow 0} \omega = \frac{\eta_2}{\eta_1} \approx r. \quad (3.51)$$

In this case, $r - \omega \approx 0$ and efficiency leverage on BOS cost disappears. This is because efficiency cannot leverage fixed BOS costs, which are the same for all PV systems regardless of module efficiency. Thus, low-efficiency modules are economically best suited to systems with low variable BOS costs. By inspection of Table 3.5, one would expect commercial PV systems to be the best candidates for low-efficiency modules.

3.2.5 COMPUTATION OF EFFICIENCY PREMIUM

The efficiency premium was defined in section 3.2 as the difference in module cost for which high- and low-efficiency modules will produce the same installed PV system cost. For example, if a high-efficiency module at $\$4.50/W_p$ leads to the same installed system cost as a low-efficiency module at $\$4.00/W_p$, the efficiency premium is $\$0.50/W_p$. This difference, where it exists, is a direct result of higher module efficiencies leveraging BOS costs in order to minimize the installed cost of PV systems. Thus, an efficiency premium allows one to achieve energy production targets at lower installed system cost, or to spend more per peak watt on high-efficiency modules without increasing the installed system cost.

Efficiency premium can be calculated from the model derived in section 3.2.2. First, substitute equation (3.1) into equation (3.23):

$$\frac{C_{m,2}}{C_{m,1}} < [r + (r - \omega)v] \frac{\eta_1}{\eta_2}. \quad (3.52)$$

Next, let $C_{m,2} = C_{m,1} + \Delta C_m$, where ΔC_m is the efficiency premium. Solving for ΔC_m yields:

$$\Delta C_m = \left\{ [r + (r - \omega)v] \frac{\eta_1}{\eta_2} - 1 \right\} C_{m,1}. \quad (3.53)$$

Note that the BOS leverage term $[r + (r - \omega)v]$ in equation (3.53) is scaled by the ratio of the rated module efficiencies. This reflects the discrepancy between conventional module pricing on the basis of rated power output at STC and the actual (loss-adjusted) energy production of modules deployed in the field. When the thermal losses in both systems are equal, $r = \eta_2/\eta_1$ and the effects of this pricing convention disappear, but when the thermal losses are not equal the efficiency premium is skewed in favor of the module with the smaller losses.

Using the values of v , ω , and r derived in sections 3.2.4.1 and 3.2.4.2, efficiency premium may be calculated for any combination of module technologies and efficiencies using equation (3.53). This is applied in section 3.2.6.

3.2.6 APPLICATION OF THE MODEL

With parameter values established, the model may now be applied for any combination of module efficiency, technology, and construction; geographical location; system type (residen-

Table 3.6: PV module assumptions for model calculations using 2005 MYPP benchmarks.

Technology	η (%)	Construction	α_T (%/°C)
c-Si	13.5	Glass/cell/polymer	-0.50
CIGS	9.0	Polymer/thin film/steel	-0.34
CdTe	8.0	Polymer/thin film/steel	-0.25
a-Si	6.0	Polymer/thin film/steel	-0.20

tial, commercial, or utility); and year of installation. The number of possible combinations of these factors is infinite and certainly not every plausible case can be addressed here. The following sections use the model to analyze a handful of highly informative cases using the 2005 benchmarks from Table 3.4, then assess the implications of the projected system costs in 2015 on PV module costs and technologies.

3.2.6.1 Efficiency Premium and Solar Cell Technology

The impact of module technology on PV system cost lies primarily in efficiency, though temperature coefficient and module construction also play a significant role. The benchmarks in Table 3.4 show a c-Si PV module efficiency of 13.5% at a cost of \$4.00/W_p in residential and commercial systems, and \$3.30/W_p in utility systems. Consider a-Si, CdTe, and CIGS modules having the efficiencies, constructions, and temperature coefficients shown in Table 3.6, all of which are typical for current PV modules of the selected technologies. Using this information in combination with the benchmarked cost of c-Si modules, the thin-film module price required for cost parity with c-Si may be computed using the model.

First, let system one be the system incorporating c-Si modules and system two be the one incorporating thin-film modules. Assuming the system is located in Phoenix and the modules are tilted at 22.6°, the appropriate AWOCT for a given module construction may be taken from Table 3.3. Then by equation (3.42):

$$r_{a-Si} = 0.48 \quad r_{CdTe} = 0.63 \quad r_{CIGS} = 0.70, \quad (3.54)$$

where the subscripts are used in place of the usual numeral 2 to indicate the module technology for which r is computed. Thus, the a-Si system will generate about half the energy

per square meter that the c-Si system will, while the CIGS system will generate just over two-thirds of the energy per square meter.

Next, determine ν and ω for a residential system. It is already established that c-Si modules cost $\$4.00/W_p$, so by equation (3.1), $A_{m,1} = \$540/m^2$. Module efficiency for this system is 13.5%, so by Table 3.5:

$$\begin{aligned} A_{bos,1} &= 306 + 1300 \times 0.135 \\ &= \$481.50/m^2. \end{aligned} \quad (3.55)$$

Substituting $A_{m,1}$ and $A_{bos,1}$ into equation (3.21) yields:

$$\nu = 0.89. \quad (3.56)$$

Determining the BOS costs for the thin-film systems and substituting into equation (3.22) yields:

$$A_{bos,a-Si} = \$384/m^2 \quad A_{bos,CdTe} = \$410/m^2 \quad A_{bos,CIGS} = \$423/m^2 \quad (3.57)$$

$$\omega_{a-Si} = 0.80 \quad \omega_{CdTe} = 0.85 \quad \omega_{CIGS} = 0.88. \quad (3.58)$$

Finally, equations (3.54), (3.56) and (3.57) may be substituted into equation (3.23) to compute the maximum area-related module prices for each of the thin-film module technologies to achieve cost parity with c-Si at $\$4.00/W_p$:

$$A_{m,a-Si} < \$106.43/m^2 \quad A_{m,CdTe} < \$237.06/m^2 \quad A_{m,CIGS} < \$291.08/m^2, \quad (3.59)$$

which, by equation (3.1), translates to the following power-related costs:

$$C_{m,a-Si} < \$1.77/W_p \quad C_{m,CdTe} < \$2.96/W_p \quad C_{m,CIGS} < \$3.23/W_p. \quad (3.60)$$

Thus, to compete economically with c-Si modules of 13.5% efficiency at $\$4.00/W_p$, a-Si modules should cost no more than $\$1.77/W_p$, CdTe no more than $\$2.96/W_p$, and CIGS

no more than $\$3.23/W_p$. Clearly, efficiency plays a much stronger role than temperature coefficient in determining leverage over BOS costs.

To check that the calculations are sensible, assume the system is required to produce 6000 kW·h/yr, its site in Phoenix receives 2350 kW·h/m²/yr in insolation, each system uses the same 3-kW inverter, and non-thermal losses in the system (inverter, wiring, dust, etc.) amount to 15%. The required module area is computed from these values using the appropriate module efficiency for each technology, adjusted for thermal losses. The system size in kW_p may then be computed from the STC efficiency. Using these values in conjunction with the BOS and module costs computed above, the total cost of the system using each technology can be computed. The results of this series of calculations are summarized in Table 3.7, using the maximum cost-effective module cost for each thin-film technology as computed in equation (3.60). Note that only the system size and total installed system cost depend upon the amount of energy the system generates — the model parameters themselves, as demonstrated above, do not require this information.

Since each system in Table 3.7 is designed to produce 6000 kW·h/yr and, as shown by the total installed system cost, each of the systems has equal installed cost, the table shows the conditions under which other PV technologies are economically equal to c-Si at $\$4.00/W_p$. BOS costs for c-Si are lower than for any other technology, which works in its favor. This price differential allows higher per-peak-watt module costs for c-Si than for any other technology, producing efficiency premiums relative to c-Si of $\$0.77/W_p$, $\$1.04/W_p$, and $\$2.23/W_p$ for CIGS, CdTe, and a-Si modules, respectively. The maximum economical cost of any of these technologies is then $\$4.00/W_p$ (the price of c-Si) minus the efficiency premium for the selected technology. Therefore, the maximum economical costs for the thin-film modules considered in Table 3.7 are $\$3.23/W_p$, $\$2.96/W_p$, and $\$1.77/W_p$ for CIGS, CdTe, and a-Si, respectively. Comparing to the average price of a thin-film PV module in 2006, which was $\$3.32/W_p$ [36], suggests that CIGS and CdTe are becoming competitive with typical c-Si for residential use, but that a-Si is not very competitive.

Note also that the system size, as measured in kW_p, is not the same for all four systems. This is a result of the unequal temperature coefficients of the four different PV technologies:

Table 3.7: Size, installed cost, and efficiency premium for residential PV systems using c-Si and thin-film module technologies to produce 6000 kW·h/yr at equal installed cost in Phoenix using 2005 BOS costs.

	c-Si	CIGS	CdTe	a-Si
System size (m ²)	25.0	35.8	39.5	52.2
System size (kW _p) ^a	3.38	3.22	3.16	3.13
<i>Module^b</i>				
A _m (\$/m ²)	540.00	291.08	237.06	106.43
C _m (\$/W _p)	4.00	3.23	2.96	1.77
Total cost (\$)	13 523	10 427	9372	5551
<i>BOS</i>				
A _{bos} (\$/m ²)	481.50	423.00	410.00	384.00
C _{bos} (\$/W _p)	3.57	4.70	5.13	6.40
Total cost (\$)	12 058	15 153	16 209	20 029
<i>Inverter</i>				
Size (kW)	3	3	3	3
C _{inv} (\$/W _p)	0.90	0.90	0.90	0.90
Total cost (\$)	2700	2700	2700	2700
<i>Installed cost of the system</i>				
C _{sys} (\$/W _p) ^a	8.37	8.77	8.94	9.04
Total cost (\$)	28 281	28 281	28 281	28 281
<i>Efficiency premium with respect to c-Si</i>				
ΔC _m (\$/W _p)	—	0.77	1.04	2.23

^a While each system is sized to produce 6000 kW·h/yr, system ratings and installed cost per W_p differ because of differences in temperature coefficient for each technology.

^b The module cost shown for the thin film technologies is the maximum that is economically competitive with c-Si.

Table 3.8: Model calculations for c-Si and thin-film PV modules using 2005 MYPP benchmarks for commercial and utility systems.

	Commercial				Utility			
	c-Si	CIGS	CdTe	a-Si	c-Si	CIGS	CdTe	a-Si
<i>Module</i>								
A_m (\$/m ²)	540.00	338.06	294.24	188.13	445.50	263.57	224.02	129.72
C_m (\$/W _p)	4.00	3.76	3.68	3.14	3.30	2.93	2.80	2.16
<i>BOS</i>								
A_{bos} (\$/m ²)	295.50	246.00	235.00	213.00	241.25	216.50	211.00	200.00
C_{bos} (\$/W _p)	2.19	2.73	2.94	3.55	1.79	2.41	2.64	3.33
<i>Efficiency premium with respect to c-Si</i>								
ΔC_m (\$/W _p)	—	0.24	0.32	0.86	—	0.37	0.50	1.14

Notice that the system size decreases with decreasing magnitude of the temperature coefficient. This same effect produces an increase in installed system cost per W_p with decreasing thermal losses, which may give the illusion that the c-Si system is the least expensive of the four. In reality, however, each system produces the same amount of energy for the same amount of money.

3.2.6.2 Efficiency Premium and Market Segment

The calculations above are repeated for commercial and utility systems using the 2005 benchmarks in Table 3.4 and the values of A_{var} and A_{fix} in Table 3.5 to compute BOS costs. The results for commercial and utility systems are shown in Table 3.8. For brevity, system size and total cost calculations are omitted, as they were performed for the residential case only to show that the model does indeed calculate system requirements for producing equal amounts of energy at equal cost. Efficiency premium calculations with respect to the c-Si modules are also integrated into Table 3.8.

The most notable trend in comparing Table 3.8 with Table 3.7 is the drastic difference in the economical cost of thin-film PV modules between commercial and residential systems. For a-Si modules, the efficiency premium with respect to c-Si drops from \$2.23/ W_p in residential systems to just \$0.86/ W_p in commercial systems. The difference between residential and utility system is also significant. In both cases, the difference is a function of variable BOS

costs. Note from Table 3.5 that variable BOS costs drop for \$306/m² for residential systems to \$167/m² for utility systems and just \$147/m² for commercial systems. As anticipated in section 3.2.4.2, high efficiency has less leverage over BOS costs as the variable BOS costs drop. Thus, thin films are much more competitive with c-Si in large-scale commercial and utility applications.

3.2.6.3 *Influence of Geographical Location on Efficiency Premium*

Variations in AWOCT with geographical location might reasonably be expected to produce regional variations in efficiency premium. Figure 3.9 displays efficiency premium as a function of AWOCT for 13.5%-efficient c-Si modules relative to the thin-film modules used in the previous analyses. Residential, commercial, and utility systems are analyzed according to the 2005 benchmarks. The graphs make the simplifying assumption that AWOCT is the same for both the c-Si and thin-film modules. Not surprisingly, efficiency premium varies most when c-Si modules are compared to a-Si modules, which are least affected by temperature and therefore gain the most when AWOCT is high. Efficiency premium for c-Si compared to CIGS is relatively invariant with increasing AWOCT, since the temperature coefficient of CIGS most closely matches that of c-Si.

By comparing Figure 3.9 with Table 3.3 one sees that thin-film PV modules are most competitive for commercial and utility PV systems in the southwestern United States where AWOCT is very high. Outside of that region, AWOCT drops rapidly and erodes the advantage the thin-film modules have in temperature coefficient, even in certain very sunny locations such as Los Angeles. In cooler northern climates, such as those of Boston, Detroit, and even San Francisco, AWOCT is nearly equal to the STC temperature of 25 °C. In such locales, differences in temperature coefficient are relatively unimportant.

These results suggest that throughout much of the United States, the smaller temperature coefficients that thin-film modules have may not translate into a significant economic benefit. They remain, however, an important consideration in the nation's hottest locations, which also tend to be the sunniest. In places like Phoenix and Las Vegas, temperature coefficients must certainly be taken into account and can significantly reduce efficiency premium relative

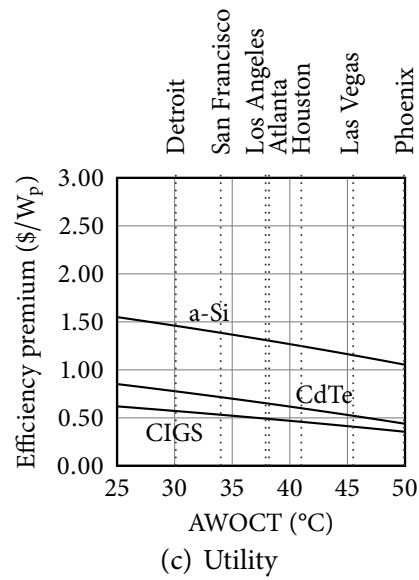
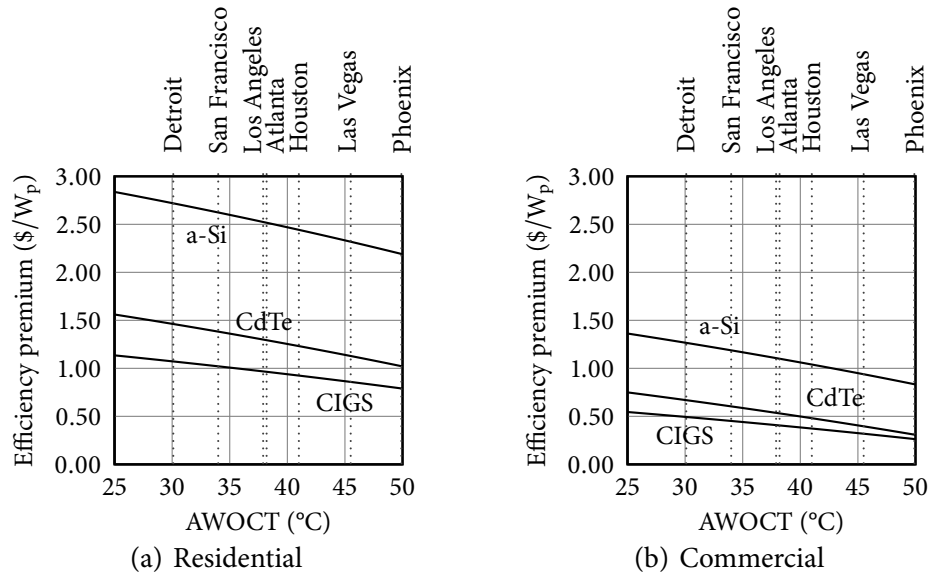


Figure 3.9: Efficiency premium as a function of AWOCT using 2005 MYPP benchmarks for c-Si PV modules with 13.5% efficiency relative to CIGS, CdTe, and CIGS PV modules with efficiencies of 9.0%, 8.0%, and 6.0%, respectively.

to STC. In locations like Detroit and Boston, however, the module temperature coefficient has virtually no impact on efficiency premium.

3.2.6.4 PV Module Cost and Efficiency Targets for Achieving Grid Parity in 2015

In section 3.2.4.2, fixed and variable BOS costs for PV systems in 2011 and 2015 were derived from the MYPP reference systems in Table 3.4. These BOS costs were summarized in Table 3.5. Using the c-Si module-based reference systems, the methods of the previous sections may be used to project retail price requirements for all major PV technologies in the near future.

Before doing so, however, it is important to recognize that the MYPP reference systems are based on projections of future c-Si module cost and efficiency. If these projections are not realized it does not mean the SAI goals have not been met; rather, they comprise one vision of how the goals are *likely* to be met. Since they do not preclude meeting the goals by other means they do not constitute true cost targets. This would seem to complicate analysis considerably, since *actual* costs in 2015 may differ significantly from those in the reference systems for that year without missing the SAI targets for LCOE. However, because of the insights provided by the model derived here, this analysis is not nearly as complicated as it might first seem.

For now, assume the previously derived relationships between BOS cost and module efficiency hold (departures from this assumption will be considered shortly). The 2011 reference systems assume 16% c-Si module efficiency at a retail cost of \$2.20/W_p. As mentioned above, however, this does not constitute an efficiency or cost goal and the event that c-Si module efficiency falls short of or exceeds 16% must be considered. Required PV module costs for 2011 as a function of module efficiency are shown for all four major module technologies are plotted in Figure 3.10. Note from Table 3.5 that the variable BOS costs for residential and utility PV systems are very similar; as a result, the parity prices for PV modules in these systems are nearly identical. Note that this occurs despite the very large difference in fixed BOS costs, which strongly suggests that module efficiency can leverage only the variable BOS costs. As for the 2005 benchmarks, commercial systems are projected to have the lowest variable BOS costs in 2011 and will therefore continue to be the most attractive market for

low-efficiency modules.

Another significant trend in Figure 3.10 is that the economic impact of efficiency is greatest for module efficiencies below about 10%, after which increasing efficiency has a reduced, but still significant, impact. The effect of temperature coefficient is subtle, but may be seen by comparing Figures 3.10(a), (b), (c), and (d). As the magnitude of the temperature coefficient decreases, the parity cost of the PV module increases. This effect erodes the efficiency premium enjoyed by high-efficiency c-Si PV modules and suggests that thin film modules may attain cost parity at slightly lower efficiencies.

Figure 3.11 shows projected parity costs for PV modules in 2015. The MYPP reference systems for that year specify 20%-efficient c-Si PV modules at a cost between $\$1.00/W_p$ and $\$1.50/W_p$; this range corresponds to the LCOE ranges targeted by the SAI. Since the module cost is specified as a range, the target costs for each PV module technology in the figure are also specified as a range and displayed as bands for each technology and market sector. These bands represent only the range of target costs; cost/efficiency combinations that fall below the bands exceed the SAI goals and provide electricity at an even lower cost than targeted. Once again, the variable BOS costs for residential and utility systems are nearly identical, and the bands corresponding to those systems lie atop one another. The commercial sector again has the lowest variable BOS cost and is the most favorable to low-efficiency modules.

Comparing the slopes of the curves in Figures 3.10 and 3.11 suggests that the economic impact of efficiency will be much greater in 2015 at low efficiencies, but lower at high efficiencies. However, where the transition from rapid improvement to slow improvement occurred at about 10% efficiency in 2011, it occurs at about 15% efficiency in 2015. Therefore, PV modules with efficiencies less than about 15% will be at a significant economic disadvantage compared to the reference system. Because the curves in Figure 3.11 flatten out above about 15% efficiency, even if c-Si module efficiencies improve by only a few percent (absolute) over the next eight years their price need not differ considerably from the $\$1.00/W_p$ to $\$1.50/W_p$ of the 2015 MYPP reference systems to reach the SAI targets. However, this result suggests that thin-film manufacturers will be pressured to either make substantial gains in efficiency or reduce module costs per peak watt far below those of c-Si manufacturers.

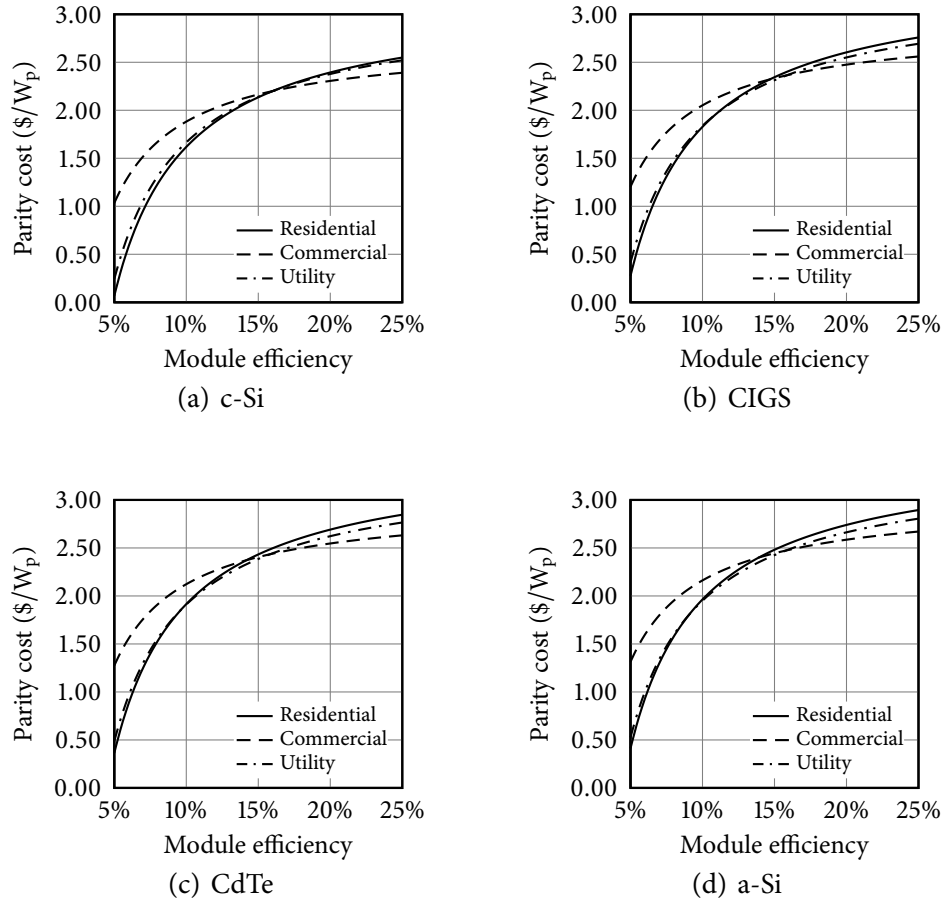


Figure 3.10: PV module cost to achieve parity with 2011 MYPP c-Si reference system as a function of module technology, efficiency, and market sector for PV systems located in Phoenix.

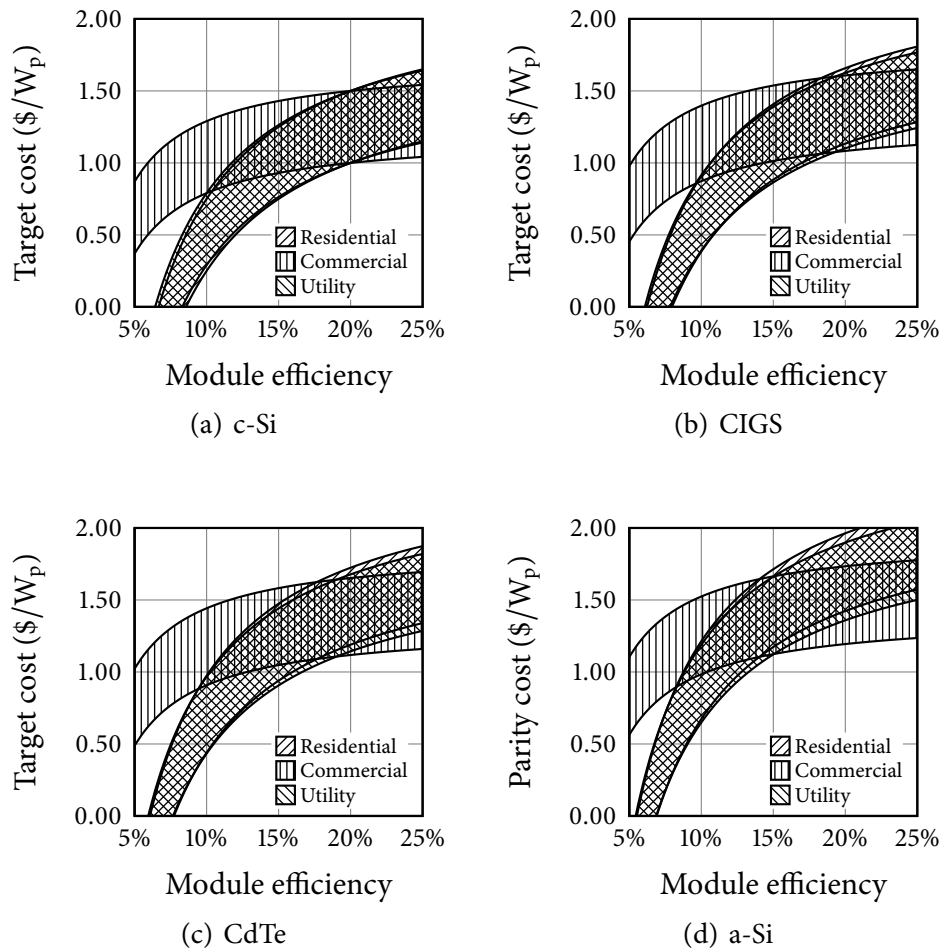


Figure 3.11: PV module cost to achieve grid parity according to the 2015 MYPP reference scenario as a function of module technology, efficiency, and market sector for PV systems located in Phoenix.

To make these trends more concrete, Table 3.9 summarizes the PV module prices required to achieve grid parity by 2015 for current commercial and record solar cell and module efficiencies. These values suggest that typical c-Si module efficiencies should increase significantly from their current level around 13.5% to achieve grid parity at the target module cost range of \$1.00/W_p to \$1.50/W_p. However, the current best commercial module efficiency is high enough that continuing development efforts should focus more on reducing cost than on increasing efficiency. In the race for grid parity, the difference between the commercial-best 17.0% efficiency and laboratory-record 22.7% efficiency is only \$0.06/W_p to \$0.22/W_p using BOS cost assumptions for 2015.

At current typical commercial module efficiencies, both CIGS and CdTe will have to surpass the \$1.00/W_p to \$1.50/W_p target by a large margin to achieve grid parity. This requirement is relaxed considerably in the commercial market, where BOS costs are low. Even the current best CdTe efficiency of 11.1% will have to surpass the target in residential and utility systems. Only if CIGS and CdTe can be produced commercially at their current laboratory record module efficiencies will they be able to compete with high-efficiency c-Si on equal economic footing.

Amorphous silicon simply cannot achieve grid parity at current efficiencies except when BOS costs are very low, as expected in the commercial market segment in 2015. Even at the current record cell and module efficiencies, a-Si will still have to surpass the \$1.00/W_p to \$1.50/W_p target by a large margin to be competitive in residential and utility markets.

Figure 3.11 and Table 3.9 seem to suggest that 20% efficiency is the “sweet spot” where further increases in efficiency result in rapidly diminishing returns. Indeed, using this model one can calculate a target cost of \$1.45/W_p to \$1.95/W_p for a hypothetical PV module of 50% efficiency in a residential system in 2015. In other words, *tripling* the current best commercial c-Si efficiency must cost less than \$0.45/W_p to be cost-effective. The location of this “sweet spot” is a function of BOS cost, and the lower the BOS cost the less sensitive the installed system cost is to module efficiency.

It is highly unlikely that PV can achieve grid parity without reducing BOS costs to the levels in the MYPP reference case for 2015. Thus, it is safe to say that module efficiencies

Table 3.9: Retail module prices required for grid parity in 2015 for current and record PV cell and module efficiencies.

Technology	Efficiency (%)	Target cost (\$/W _p)			Comment
		Residential	Commercial	Utility	
c-Si	13.5	0.64–1.14	0.90–1.40	0.66–1.16	Current typical commercial module efficiency
	17.0	0.87–1.37	0.96–1.46	0.87–1.37	Current best commercial module efficiency
	20.0	1.00–1.50	1.00–1.50	1.00–1.50	Target module cost and efficiency
	22.7	1.09–1.59	1.02–1.52	1.08–1.58	Current record module efficiency [102]
CIGS	9.0	0.22–0.74	0.83–1.35	0.23–0.76	Current typical commercial module efficiency
	16.6	0.98–1.50	1.04–1.56	0.96–1.48	Current record module efficiency [102]
CdTe	8.0	0.06–0.60	0.80–1.34	0.08–0.61	Current typical commercial module efficiency
	11.1	0.58–1.11	0.95–1.48	0.56–1.10	Current best commercial module efficiency
	16.5	1.03–1.56	1.07–1.61	0.99–1.53	Current record module efficiency [102]
a-Si	6.0	0.00–0.01	0.65–1.19	0.00–0.05	Current typical commercial module efficiency
	10.4	0.53–1.07	0.94–1.48	0.51–1.05	Current record module efficiency (stabilized) [102]
	13.3	0.84–1.38	1.03–1.57	0.81–1.35	Current record cell efficiency (stabilized) [103]

approaching 20% are a desirable goal. However, if BOS costs continue to decline beyond that time then the efficiency required for cost-effective PV will also continue to decline. As a result, it is plausible that if low-efficiency technologies like current a-Si can survive long enough in low-BOS niche applications they may find new life many years down the road.

3.2.7 CAVEATS AND LIMITATIONS

It bears repeating that the model presented in this section was developed with the aid of a number of simplifying assumptions. Most notably, it assumes that the two systems being compared are identical in all respects except the choice of PV module, and that the PV modules in each system are mounted in a similar fashion. In reality, different modules may have different mounting requirements and one or both of these assumptions may not be met.

Consider, for example, a commercial system being installed on a flat roof with no protrusions, with the buyer comparing roll-out a-Si modules to conventional rack-mounted c-Si modules. The roll-out modules would be expected to have a greatly reduced variable BOS cost compared to the rack-mounted modules because of their simpler installation. They might also have lower fixed BOS cost because of the greater simplicity of the system design. If the roll-out a-Si modules are designated system one and the rack-mounted c-Si modules system two, this would correspond to smaller values of ν and larger values of ω than would be expected from using the BOS costs described in section 3.2.4.2. However, without the additional mounting hardware of the rack-mounted modules in system two, these modules would be mounted with zero tilt angle. The modules in system two, on the other hand, could be mounted at an ideal tilt angle. This would increase, perhaps drastically, the value of r that would be computed under the assumption of equal tilt angles. In this situation, the only way to know which system is more economical is to explicitly compute the levelized cost of energy from each system.

The best available data on BOS costs were used to produce the BOS-cost-generating functions, which were conceived as linear functions of efficiency based on fixed and variable BOS costs. The idea that these costs can be viewed as having fixed and variable components is both plausible and appealing, and in section 3.2.4.2 produced the conclusion that efficiency

premium is governed almost entirely by variable BOS cost. While this conclusion appears to be novel, it is eminently sensible since efficiency cannot leverage fixed BOS costs, which are the same for all systems regardless of module efficiency.

Another characteristic not fully accounted for in this model is the enhanced energy production from thin-film modules (notably a-Si) relative to c-Si modules [104]. The number of kW·h produced per rated kW_p has been observed to be greater for a-Si modules than for c-Si modules, primarily because of their lower temperature coefficients. While this difference is accounted for in the model, other factors contributing to this enhancement are differences in spectral response and enhanced self-annealing of optically induced defects at high operating temperatures in a-Si modules. However, it has been speculated that the enhancement is also a result, at least in part, of measurement errors. Furthermore, there are indications that the enhancement due to differences in spectral response are dependent upon module tilt angle, and that for many tilt angles spectral effects favor c-Si modules rather than thin films [105].

Perhaps the most significant PV system characteristic not accounted for in this model is that of system life. By not explicitly taking system life into consideration and performing its computations on the basis of cost per peak watt (or per square meter), the model implicitly assumes that both systems have equal life. While c-Si and a-Si modules have similar service life expectations, it is not yet clear how long CdTe and CIGS modules, which have shorter commercial histories from which to draw, will last in the field. However, accounting for differences in service life requires comparison on the basis of levelized cost of energy, rather than installed system cost. This, in turn, requires consideration of economic parameters beyond the control of the design engineer and introduces an additional level of complexity. Nonetheless, an attempt to treat this case is made in section 3.3.

All things considered, the analytical model presented here should be relatively accurate for the general case of two directly comparable systems. In that spirit, the predictions of section 3.2.6.4 are offered with the caveat that the assumptions about BOS costs are based upon one view of how such costs may evolve in the future. Alternative viewpoints may be easily accommodated by the model by simply changing the BOS and module efficiency assumptions, recomputing r , ν , and ω , and using the recomputed values to update $(A_{m,2}/A_{m,1})_{eq}$ and the

efficiency premium ΔC_m . These issues will be revisited in section 3.5.

3.3 INFLUENCE OF SYSTEM SERVICE LIFE ON EFFICIENCY PREMIUM

The installed system cost model derived in section 3.2 correctly compares the installed costs of two PV systems. However, this is only a useful metric for comparing systems when both systems have equal service lives. If one system will remain in service for a substantially longer time than the other, its costs will be distributed over a proportionally greater amount of energy production. Accounting for this complicates the analysis by introducing issues of system financing, inflation, and the time value of money; however, it may be accomplished through levelized cost analysis.

This scenario is important because it is yet unclear how long newer thin film technologies might last in the field. Cadmium telluride PV modules, for example, have accumulated little failure history upon which to assess their reliability, and uncertainty exists about how long they might last in the field. Evidence of this is found in the warranty offered by First Solar, the world's largest producer of CdTe PV modules. While the company backs its products with a 25-year warranty on power output, it provides only a 5-year warranty on defects. Furthermore, under the power warranty it reserves the right to make up power shortfalls by providing additional modules instead of replacing degraded modules [106]. Therefore, it is prudent to see how sensitive the efficiency premium is to module service life.

This is accomplished by adjusting the efficiency premium calculation to account for the levelized cost of electricity (LCOE). Simply stated, LCOE is the unit cost of electricity at which cumulative electricity production over the lifetime of a generator equals its total life-cycle cost. The total life-cycle cost is computed from all of the expenditures on the system over its service life, summed after adjusting for inflation and the time value of money. LCOE computations are treated in detail in Appendix A, but a few key results will be used here to model the influence of service life on LCOE and the impact it has on efficiency premium.

Figure 3.12 illustrates the importance of long service life in reducing LCOE. It displays LCOE as a function of system service life for a residential PV system modeled using the 2005 MYPP benchmarks. As service life increases, LCOE decreases asymptotically. The shaded

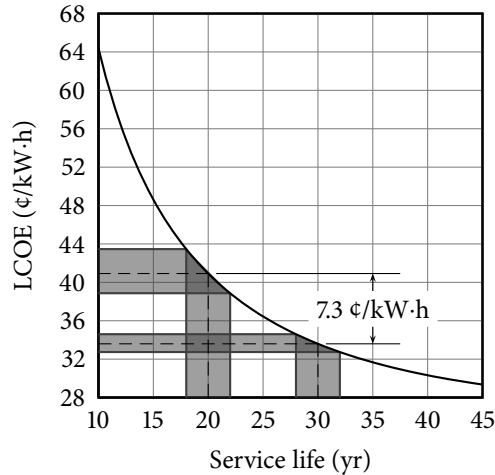


Figure 3.12: Effect of PV system service life on LCOE for 2005 MYPP residential benchmark system.

regions show that for slight variations in service life, the impact on LCOE is smaller for a system with a 30-yr life than for one with a 20-yr life; therefore, longer service life reduces uncertainty in LCOE due to uncertainty in actual (versus planned) service life.

In addition, the LCOE for a system lasting 20-yr is 7.3 ¢/kW·h greater than for one lasting 30-yr. This is a margin of 22% and is equivalent to spending an additional \$730 on electricity each year for the average U.S. household at the 30-yr LCOE. Even at U.S. average grid rates, it amounts to an additional \$220 every year. Thus, PV modules that are shorter-lived than their c-Si counterparts must cost commensurately less to achieve grid parity.

3.3.1 COMPUTING THE LEVELIZED COST OF ELECTRICITY

The LCOE L of a PV system is:

$$L = \frac{A_T}{\sum_{i=0}^N \frac{Q_i}{(1+d_r)^i}}, \quad (3.61)$$

where A_T is the total life-cycle cost of the system, Q_i is the amount of energy generated by the system in year i , N is the expected service life of the system, and d_r is the real (inflation-adjusted) discount rate applied to cash flows over the N years of the system's life. If A_T is

expressed in \$/m² then Q_i is expressed in kW·h/m² and:

$$A_T = (A_m + A_{\text{bos}}) \frac{F}{D_n}. \quad (3.62)$$

Note that, as in previous sections, inverter costs are neglected. In equation (3.62), F is the *uniform capital recovery factor* (UCRF):

$$F = \frac{f(1+f)^N}{(1+f)^N - 1}, \quad (3.63)$$

where f is the finance rate for the PV system and N is the number of years the system is financed. The remaining parameter, D_n , is:

$$D_n = \frac{d_n(1+d_n)^N}{(1+d_n)^N - 1}, \quad (3.64)$$

where d_n is the nominal (current, or non-inflation-adjusted) discount rate applied to cash flows over the system's service life N . The two discount rates, d_r and d_n , are related by:

$$d_r = \frac{1+d_n}{1+e} - 1, \quad (3.65)$$

where e is the rate of inflation.

If the system produces the same amount of energy every year, Q_i will be constant. Assuming, for simplicity, that this will be the case and letting $Q_i = Q$, equation (3.61) may be reduced to

$$L = \frac{A_T}{Q} D_r, \quad (3.66)$$

where:

$$\begin{aligned} D_r &= \frac{1}{\sum_{i=0}^N \frac{1}{(1+d_r)^i}} \\ &= \frac{d_r(1+d_r)^N}{(1+d_r)^N - 1}. \end{aligned} \quad (3.67)$$

Substituting equation (3.62) into equation (3.66) yields:

$$L = \frac{(A_m + A_{bos})FD_r}{QD_n}, \quad (3.68)$$

which expresses LCOE in terms of the installed cost of the PV system, the energy generated per unit area, the finance rate, and the real and nominal discount rates (which, by equation (3.65), implicitly account for inflation).

3.3.2 EFFICIENCY PREMIUM FOR SYSTEMS WITH UNEQUAL SERVICE LIVES

To compare the energy costs of two PV systems, use equation (3.68) to compute the ratio of the LCOE of system two to that of system one:

$$\frac{L_2}{L_1} = \frac{(A_{m,2} + A_{bos,2})Q_1F_2D_{r,2}D_{n,1}}{(A_{m,1} + A_{bos,1})Q_2F_1D_{r,1}D_{n,2}}, \quad (3.69)$$

where the numerical subscripts denote systems one and two. Since Q_1 and Q_2 are the energy output per unit area of systems one and two, respectively, $Q_2/Q_1 = r$. Substituting this, along with equations (3.63), (3.64) and (3.67), into equation (3.69) and simplifying yields:

$$\frac{L_2}{L_1} < \frac{A_{m,2} + A_{bos,2}}{A_{m,1} + A_{bos,1}} \times \frac{\lambda_F \lambda_D}{r}, \quad (3.70)$$

where

$$\lambda_F = \frac{F_2}{F_1} = \frac{(1+f)^{N_2} - (1+f)^{N_2-N_1}}{(1+f)^{N_2} - 1} \quad (3.71)$$

and

$$\lambda_D = \frac{D_{r,2}D_{n,1}}{D_{r,1}D_{n,2}} = \frac{(1+e)^{N_1} [(1+d_r)^{N_1} - 1] \{[(1+d_r)(1+e)]^{N_2} - 1\}}{(1+e)^{N_2} [(1+d_r)^{N_2} - 1] \{[(1+d_r)(1+e)]^{N_1} - 1\}} \quad (3.72)$$

That is, L_2/L_1 is simply the ratio of the installed system cost of system two to that of system one, modified by the inflation and discount rates through λ_D and the finance rate through

λ_F . When $L_2/L_1 < 1$, the LCOE of system two is less than that of system one, and system two is more economical. When $L_2/L_1 > 1$, the LCOE of system two is greater than that of system one, and system one is more economical. Finally, when $L_2/L_1 = 1$, both systems have the same LCOE and neither has an economic advantage over the other.

Imposing the condition that $L_2/L_1 < 1$ — that is, that system two is more economical than system one — on equation (3.70) and simplifying yields:

$$\left(\frac{A_{m,2} + A_{bos,2}}{A_{m,1} + A_{bos,1}} \right) \lambda_F \lambda_D < r. \quad (3.73)$$

Substituting equations (3.22) and (3.21) into equation (3.73) and solving for $A_{m,2}/A_{m,1}$ yields:

$$\frac{A_{m,2}}{A_{m,1}} < \frac{r}{\lambda_F \lambda_D} + \left(\frac{r}{\lambda_F \lambda_D} - \omega \right) v. \quad (3.74)$$

Equation (3.74) expresses the condition for system two to be more economical than system one in terms of r , v , and ω . Comparing to equation (3.23), the only difference between it and equation (3.74) is that the r term is modified by the product of λ_F and λ_D . Therefore, the effect of differing service lifetimes on PV system economics is either to amplify ($\lambda_F \lambda_D < 1$) or attenuate ($\lambda_F \lambda_D > 1$) the economic impact of the difference in energy densities of the two systems. Not surprisingly, when $N_1 = N_2$, both λ_F and λ_D are unity and equations (3.23) and (3.74) are identical. That λ_F and λ_D operate only on module parameters and not on BOS parameters is fitting, since BOS costs are independent of system life and total energy production is not.

The efficiency premium for modules in PV systems of unequal service life is derived from equation (3.74) in precisely the same manner that equation (3.53), the equation defining efficiency premium for systems with equal service lives, was in section 3.2.5. This yields:

$$\Delta C_m = \left\{ \left[\frac{r}{\lambda_F \lambda_D} + \left(\frac{r}{\lambda_F \lambda_D} - \omega \right) v \right] \frac{\eta_1}{\eta_2} - 1 \right\} C_{m,1}. \quad (3.75)$$

As above, the $\lambda_F \lambda_D$ product amplifies the economic impact of energy density when it is less than unity and attenuates it when it is greater than unity. Furthermore, when it is equal to unity, equations (3.53) and (3.75) are identical. Since $\lambda_F \lambda_D = 1$ when $N_1 = N_2$, equations (3.23) and (3.53) may be seen as special cases of equations (3.74) and (3.75).

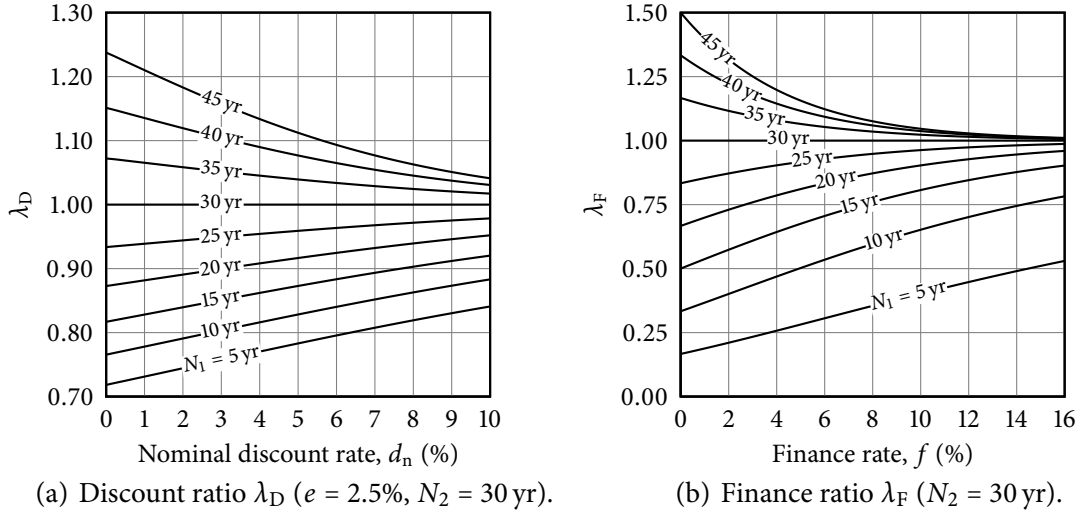


Figure 3.13: Financial parameters affecting the LCOE ratio L_2/L_1 as a function of inflation, discount rate, and inflation.

3.3.3 ANALYSIS OF THE LEVELIZED COST MODEL

Because equation (3.74) is so similar to equation (3.23), analysis of the levelized cost model closely parallels that of the system cost model as described in section 3.2.3. The key element in evaluating the effect of module service life on cost is the UCRF ratio λ_F , plotted in Figure 3.13 for various values of f and N_1 , assuming $N_2 = 30$ yr. This ratio acts to inflate (when $\lambda_F < 1$) or deflate (when $\lambda_F > 1$) the impact of the performance ratio r .

Because it has four independent parameters, equation (3.74) is very difficult to visualize in a compact manner. However, Figure 3.14 illustrates the effect of the UCRF ratio λ_F by re-plotting Figure 3.6 for λ_F values of 0.9 and 1.1. Note, by comparison of Figure 3.14(a) with Figure 3.6, that when $\lambda_F < 1$ the level curves of $(A_{m,2}/A_{m,1})_{eq}$ shift upward. As a result, $(A_{m,2}/A_{m,1})_{eq}$ increases for a given combination of ν and ω . Conversely, when $\lambda_F > 1$ as shown in Figure 3.14(b), the level curves shift downward and $(A_{m,2}/A_{m,1})_{eq}$ decreases for a given combination of ν and ω . Since, as shown in Figure 3.13, $\lambda_F < 1$ when $N_1 < N_2$ and $\lambda_F > 1$ when $N_1 > N_2$, these trends indicate that short-lived modules must be cheaper than long-lived modules in order to produce electricity at equal cost. Furthermore, since the gradient of $(A_{m,2}/A_{m,1})_{eq}$ is steepest for high values of ν it suggests that the impact of module

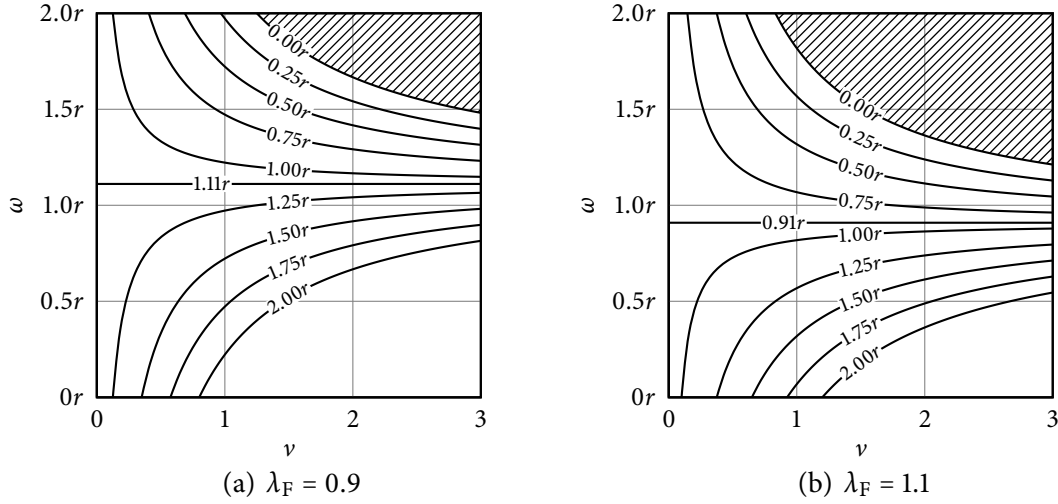


Figure 3.14: Contours of $(A_{m,2}/A_{m,1})_{eq}$ as a function of ν and ω for UCRF ratios of (a) 0.9 and (b) 1.1. The values of $(A_{m,2}/A_{m,1})_{eq}$ and ω are expressed as multiples of r . Compare with Figure 3.6, for which the UCRF ratio is implicitly unity.

life is greatest when BOS costs are high. Combined with the conclusions from section 3.2.3, this indicates that both module efficiency and service life can have tremendous leverage on PV system economics, particularly when BOS costs are high.

The change in $A_{m,2}/A_{m,1}$ introduced by accounting for differences in service life may be seen more clearly by subtracting equation (3.23) from equation (3.74),

$$\Delta \left(\frac{A_{m,2}}{A_{m,1}} \right) = \left(\frac{1}{\lambda_F \lambda_D} - 1 \right) (1 + \nu) r. \quad (3.76)$$

Note that this change is unaffected by ω , the ratio of the area-related BOS cost of system two to that of system one. Thus, the impact of the service life difference depends only upon system one BOS cost, the difference in system performance, and the finance, discount, and inflation rates. By Figure 3.13, λ_F and λ_D decrease with decreasing N_1 , and by equation (3.20), r increases with increasing system two module efficiency. Therefore, equation (3.76) indicates that long-lived, high-efficiency PV modules have significantly greater economic value than short-lived, low-efficiency PV modules, particularly when BOS cost is high relative to the cost of the low-efficiency modules. The implications of this finding for existing PV technologies are explored further in section 3.4.

3.3.4 LIMITATIONS OF THE FINANCIAL MODEL

Several simplifying financial assumptions were made in assessing the influence of module service life on PV system economics. These assumptions are consistent with the stated goal of producing an analytical model that promotes fundamental understanding of the balance between BOS cost and module efficiency, but it is important to understand their limitations and implications.

The financing calculation makes several simplifying assumptions. First, it implicitly assumes that no downpayment is made on either of the PV systems. This is mitigated in part by the initial assumption that each of the PV systems under consideration is designed to produce the same amount of energy at a similar total cost — a 30% downpayment on one system, for example, will also amount to a downpayment of about 30% on the other system. Whether a downpayment favors longer- or shorter-lived modules depends on size of the downpayment and the finance, discount, and inflation rates, but in most cases the effect on efficiency premium will be negligible.

Second, the model implicitly assumes the term over which the system is financed is equal to the life of the system. While this is not an unreasonable assumption, in reality purchasers are free to finance the system over a shorter term if they wish. In addition, loans of differing terms typically carry different interest rates. The difference in interest rates is usually slight, so this is not a major concern. Equation (3.71) can easily accommodate differences in term by using appropriate values of N_1 and N_2 , but the accuracy gained by doing so is negligible.

Assumptions about discount rate are less of a concern than for finance rate. It is often appropriate to assign different discount rates to projects of differing length; for example, a commercial investor may require a higher rate of return on lengthier projects. The model can, in principle, account for this by computing D_n and D_r using different discount rates for different systems, but as for the financing calculation, the accuracy gained is negligible.

Finally, average inflation rates may not be equal over two unequal time periods. However, the long-term inflation rate in the United States has varied little since the mid-1970s [107]. Therefore, this is not a likely source of error for calculations on systems located in the US.

Table 3.10: Retail module prices required for grid parity in 2015 for CIGS and CdTe PV modules with current and record PV module efficiencies, assuming 20-yr service life.

Technology	Efficiency (%)	Target cost (\$/W _p)			Comment
		Residential	Commercial	Utility	
CIGS	9.0	0.00–0.19	0.54–0.98	0.00–0.32	Current typical commercial module efficiency
	16.6	0.52–0.96	0.75–1.19	0.61–1.05	Current record module efficiency [102]
CdTe	8.0	0.00	0.51–0.96	0.00–0.17	Current typical commercial module efficiency
	11.1	0.12–0.57	0.66–1.10	0.22–0.67	Current best commercial module efficiency
	16.5	0.56–1.01	0.78–1.23	0.64–1.08	Current record module efficiency [102]

3.3.5 GRID PARITY COST FOR PV MODULES WITH 20-YEAR SERVICE LIFE

Now the financial model is applied to the results of section 3.2.6.4 for the two module technologies with uncertain service lives, CIGS and CdTe. Assuming a finance rate f of 8.0%, an inflation rate e of 2.5%, and a nominal discount rate d_n of 12.0%, the range of module costs required to achieve grid parity are shown in Table 3.10.

The results indicate that CIGS and CdTe will require either substantial improvements in efficiency or drastic reductions in cost to achieve grid parity on 20-yr service lives. Much like a-Si, current commercial efficiencies will have a very difficult time competing except in cases where BOS costs are very low. Furthermore, even if today’s record efficiencies are successfully transferred to commercial products they will still have to surpass the \$1.00/W_p to \$1.50/W_p target to achieve grid parity.

3.4 USING THE ANALYTICAL COST MODEL

In the previous sections a highly general analytical model was derived for quantifying the impact of power conversion efficiency on the economic equivalence of competing PV system designs. Keeping the model analytical and computationally simple, however, required a high degree of abstraction, resulting in an expression for efficiency premium with dimensionless

parameters having only a loose relationship to physical and economic quantities. While such equations are not uncommon in engineering and science, it can be difficult to understand how to apply them correctly.

This section lays out a step-by-step procedure for using this analytical model that should alleviate any confusion that might result from trying to understand the 76 equations presented in the course of deriving the model. Its basis is the generalized model represented by the equations derived in section 3.3 for PV systems having unequal service lives, but in the case that the service lives are equal the result will be the same as if the less general equations derived in section 3.2 were used.

1. Gather the following information for each of the two PV systems involved in the comparison, converting power-related module and BOS costs C_m and C_{bos} , respectively, to the required area-related costs using equation (3.1) if necessary:
 - Module efficiency, η .
 - Module cost, A_m ($\$/m^2$).
 - Module temperature coefficient, α_T ($\%/^{\circ}C$).
 - Expected AWOCT, \bar{T} ($^{\circ}C$). See, for example, Table 3.3.
 - BOS cost, A_{bos} ($\$/m^2$), excluding the inverter.
 - Expected system life, N (yr).

The BOS cost may be determined in whatever manner deemed appropriate; however, unless noted otherwise, all of the examples presented in subsequent sections will be based on US DOE projections as described in section 3.2.4.2.

If $N_1 \neq N_2$, additional information is required:

- System finance rate f .
- Nominal discount rate, d_n .
- Real discount rate, d_r .

Typically d_r will be unknown, but d_n and the inflation rate, e will be known. In that case, compute d_r using equation (3.65).

2. Compute r :

$$r = \frac{\eta_2 \left[1 + \alpha_{T,2} (\bar{T}_2 - 25^\circ\text{C}) \right]}{\eta_1 \left[1 + \alpha_{T,1} (\bar{T}_1 - 25^\circ\text{C}) \right]}. \quad (3.42)$$

3. Compute the BOS cost parameters ν and ω :

$$\nu = \frac{A_{\text{bos},1}}{A_{\text{m},1}} \quad (3.21)$$

$$\omega = \frac{A_{\text{bos},2}}{A_{\text{bos},1}}. \quad (3.22)$$

4. If $N_1 = N_2$ then let $\lambda_F = \lambda_D = 1$ and skip to step 9. Otherwise, compute the UCRFs F_1 and F_2 for each system:

$$F = \frac{f(1+f)^N}{(1+f)^N - 1}, \quad (3.63)$$

using $N = N_1$ for F_1 and $N = N_2$ for F_2 .

5. Compute λ_F :

$$\lambda_F = \frac{F_2}{F_1}. \quad (3.71)$$

6. Compute the uniform nominal discount factors $D_{n,1}$ and $D_{n,2}$ for each system:

$$D_n = \frac{d_n(1+d_n)^N}{(1+d_n)^N - 1}, \quad (3.64)$$

using $N = N_1$ for $D_{n,1}$ and $N = N_2$ for $D_{n,2}$.

7. Compute the uniform real discount factors $D_{r,1}$ and $D_{r,2}$ for each system:

$$D_r = \frac{d_r(1+d_r)^N}{(1+d_r)^N - 1}, \quad (3.67)$$

using $N = N_1$ for $D_{r,1}$ and $N = N_2$ for $D_{r,2}$.

8. Compute λ_D :

$$\lambda_D = \frac{D_{r,2}D_{n,1}}{D_{r,1}D_{n,2}}. \quad (3.72)$$

9. Working from equation (3.74), compute the ratio of $A_{m,2}$ to $A_{m,1}$ for the systems to be equally cost-effective:

$$\left(\frac{A_{m,2}}{A_{m,1}}\right)_{\text{eq}} = \frac{r}{\lambda_F \lambda_D} + \left(\frac{r}{\lambda_F \lambda_D} - \omega\right)v. \quad (3.77)$$

10. Compute the efficiency premium:

$$\Delta C_m = \left[\left(\frac{A_{m,2}}{A_{m,1}}\right)_{\text{eq}} \times \frac{\eta_1}{\eta_2} - 1 \right] C_{m,1}. \quad (3.75)$$

The next section exemplifies the use of this procedure for a comparison between typical c-Si modules available today and typical thin-film modules using a-Si in a residential PV system. Additional examples may be found in Appendix B.

3.4.1 CALCULATION OF EFFICIENCY PREMIUM FOR CRYSTALLINE SILICON VS. AMORPHOUS SILICON PV MODULES

An insightful comparison to make using the efficiency premium model is to compare today's typical c-Si module technology to today's typical thin-film technology. For c-Si, this means using a module of average efficiency having the thermal characteristics observed in most c-Si PV modules. For this task, a BP Solar module with 13.0% efficiency and a temperature coefficient of $-0.50\%/^{\circ}\text{C}$ was selected. For the thin-film module, a-Si was selected since it was the commercially dominant thin film until very recently. The comparison assumes an a-Si module from Unisolar with a 6.3% efficiency and a temperature coefficient of $-0.20\%/^{\circ}\text{C}$. Both modules are assumed to cost $\$3.75/W_p$, which is currently a typical retail price for both types of modules.

Assigning the c-Si module to system one and the a-Si module to system two, the comparison proceeds as follows:

Table 3.11: Input data for efficiency premium calculations on c-Si PV modules with efficiencies of 13.0% (System 1) against 6.3%-efficient a-Si PV modules (System 2).

Parameter	System 1	System 2
Module efficiency, η	0.130	0.063
Module cost, A_m (\$/m ²)	487.50	236.25
Module temperature coefficient, α_T (%/°C)	-0.50	-0.20
Expected AWOCT, \bar{T} (°C)	47.3	45.1
BOS cost, A_{bos} (\$/m ²)	475	388
Expected system life, N (yr)	30	30

1. Using equation (3.1), the area-related cost of each module is computed. BOS costs are determined using module efficiency and the function derived for residential systems in 2005 as shown in Table 3.5. Finally, the values for AWOCT are taken from Table 3.3 for glass/cell/polymer module architecture tilted at 22.6°. The data gathered are displayed in Table 3.11.

2. Compute r from equation (3.42) using these values:

$$\begin{aligned}
 r &= \frac{0.130 \times [1 - 0.0050 \times (47.3^\circ\text{C} - 25^\circ\text{C})]}{0.063 \times [1 - 0.0020 \times (45.1^\circ\text{C} - 25^\circ\text{C})]} \\
 &= 0.52.
 \end{aligned} \tag{3.78}$$

3. From the values in Table 3.11, the BOS parameters ν and ω are:

$$\begin{aligned}
 \nu &= \frac{\$475/\text{m}^2}{\$488/\text{m}^2} \\
 &= 0.97
 \end{aligned} \tag{3.79}$$

$$\begin{aligned}
 \omega &= \frac{\$388/\text{m}^2}{\$475/\text{m}^2} \\
 &= 0.82.
 \end{aligned} \tag{3.80}$$

4. Since $N_1 = N_2$, let $\lambda_F = \lambda_D = 1$ and skip to step 9.

9. Compute $(A_{m,2}/A_{m,1})_{eq}$:

$$\begin{aligned}
 \left(\frac{A_{m,2}}{A_{m,1}} \right)_{eq} &= 0.52 + (0.52 - 0.82) \times 0.97 \\
 &= 0.24.
 \end{aligned} \tag{3.81}$$

Table 3.12: Results of efficiency premium computation comparing a PV system using typical c-Si PV module technology to that using typical a-Si technology.

	System 1 BP Solar	System 2 Unisolar	ΔC_m (\$/W _p)	Maximum $C_{m,2}$ (\$/W _p)
Efficiency (%)	13.0	6.3		
Module price C_m (\$/W _p)	3.75	3.75		
α (%/°C)	-0.50	-0.20		
AWOCT (°C)	47.3	45.1		
BOS (\$/m ²)				
<i>Residential</i>	475	388	-1.91	1.84
<i>Commercial</i>	290	216	-0.70	3.05
<i>Utility</i>	239	202	-0.90	2.85

10. Compute the efficiency premium:

$$\begin{aligned}\Delta C_m &= \left(0.24 \times \frac{0.130}{0.063} - 1\right) \times \$3.75/W_p \\ &= -\$1.91/W_p,\end{aligned}\tag{3.82}$$

yields a \$1.91/W_p premium that the negative sign indicates favors system one.

This efficiency premium means that the maximum economical price $C_{m,2}$ for the a-Si PV modules in system two is \$1.84/W_p. Since a-Si modules cost about the same as c-Si modules, at \$3.75/W_p they are not economical. Table 3.12 summarizes these results, along with those computed as above using commercial and utility BOS cost assumptions. In every case, the maximum economical value of $C_{m,2}$ is significantly less than the current price of a-Si modules. This may explain, in part, why c-Si modules dominate the PV market.

3.4.2 CALCULATION OF EFFICIENCY PREMIUM FOR CRYSTALLINE SILICON VS. CADMIUM TELLURIDE PV MODULES

A similar calculation to the one in section 3.4.2 is summarized in Table 3.13. This compares the *best* c-Si modules currently available to the *best* thin-film modules currently available. The c-Si modules are represented by Sunpower’s 17%-efficient modules with a temperature coefficient of -0.36 %/°C, while thin films are represented by First Solar’s CdTe modules with 11.1% efficiency and a temperature coefficient of -0.25 %/°C. The calculation is shown step-by-step for residential PV systems in Appendix B.

Table 3.13: Results of efficiency premium computation comparing a PV system using typical c-Si PV module technology to that using typical a-Si technology.

	System 1 Sunpower	System 2 First Solar	ΔC_m (\$/W _p)	Maximum $C_{m,2}$ (\$/W _p)
Efficiency (%)	17.0	11.1		
Module price C_m (\$/W _p)	3.75	1.75		
α (%/°C)	-0.36	-0.25		
AWOCT (°C)	47.3	45.1		
BOS (\$/m ²)				
<i>Residential</i>	527	450	-0.73	3.02
<i>Commercial</i>	334	269	-0.27	3.48
<i>Utility</i>	261	228	-0.35	3.40

While Table 3.12 suggested a reason why c-Si has come to dominate the PV market, Table 3.13 hints at why thin films have begun to take market share from c-Si in recent years. The higher-efficiency c-Si module enjoys a substantial efficiency premium advantage over the lower-efficiency CdTe module, particularly in the high-BOS residential market segment, but First Solar’s CdTe modules undercut Sunpower’s c-Si modules in price by such a large margin that the efficiency premium cannot overcome it. These extremely competitive prices are a major contributor to the rising market share of CdTe.

In Table 3.14 this calculation is extended to estimated required future CdTe module costs for module service lives between 15 yr and 30 yr. The calculation for the 20-yr case is laid out step-by-step in Appendix B. Table 3.14 compares c-Si modules with the 2015 target efficiency and cost of 20% and \$1.50/W_p, respectively, to CdTe modules having the current record module efficiency of 16.5%. Thus, the table shows the required CdTe module cost to achieve grid parity in 2015 as a function of service life.

As expected, the magnitude of the efficiency premium grows rapidly with decreasing CdTe service life. If the current record efficiency for CdTe modules can be transferred from the laboratory to the production line *and* achieve a 30-yr service life, they can achieve grid parity at the same module cost as c-Si. However, if either of these requirements is not met, CdTe will have to undercut c-Si by a significant margin if it is to compete on equal economic footing.

Table 3.14: Efficiency premium calculations on a residential PV system using 2015 BOS costs comparing c-Si modules with 20% efficiency at $\$1.50/W_p$ (System 1) to CdTe modules with 16.5% (System 2).

Parameter	N_2 (yr)			
	15	20	25	30
Energy density ratio, r			0.88	
System 1 BOS parameter, ν			0.92	
System 2 BOS parameter, ω			0.93	
Finance ratio, λ_F	1.32	1.15	1.05	1.00
Discount ratio, λ_D	1.07	1.04	1.02	1.00
Cost equality ratio, $(A_{m,2}/A_{m,1})_{eq}$	0.35	0.56	0.72	0.84
Efficiency premium, ΔC_m ($\$/W_p$)	-0.87	-0.47	-0.18	-0.02
Maximum $C_{m,2}$ ($\$/W_p$)	0.63	1.03	1.32	1.48

3.5 CONCLUSIONS

When comparing PV systems of comparable architecture, differences in BOS costs between systems using high- and low-efficiency modules can give rise to a premium that must be paid for using low-efficiency modules. The magnitude of this premium is strongly dependent upon the variable BOS cost associated with the common architecture, with lower variable BOS cost resulting in a smaller efficiency premium.

In this chapter, a model was developed to quantify this premium for current and future residential, commercial, and industrial PV systems on the basis of cost projections established by the U.S. Department of Energy. According to calculations performed with the model using DOE benchmarks and SAI goals as inputs, c-Si PV modules enjoy a substantial efficiency premium over current thin-film technology. Efficiency premium decreases with decreasing BOS cost, suggesting that low-efficiency modules can be economically competitive with high-efficiency modules in some applications. It appears that some thin-film technologies, particularly the CdTe modules produced by First Solar at $\$1.25/W_p$ and sold for $\$1.75/W_p$, are currently more economical than c-Si at 13.5% efficiency and $\$4.00/W_p$ even after accounting for the efficiency premium. However, if c-Si can reach the cost and efficiency target of 20% at $\$1.00/W_p$ to $\$1.50/W_p$ for 2015 laid out by the SAI then thin-film modules will have to either substantially increase efficiency and longevity or reduce costs to a fraction of those required

for c-Si just to remain competitive.

The challenge, therefore, for c-Si is to reduce retail module costs to approximately $\$1.00/W_p$ to $\$1.50/W_p$ while increasing module efficiencies to 18% to 20%. The latter task has already nearly been achieved by the highest-efficiency modules on the market. However, the former task requires an approximately four-fold reduction from current module costs. This sets the stage for the remainder of this thesis, which explores the obstacles to attaining these goals and attempts to identify in a systematic way the most expedient paths to achieving them.

Sections 3.2.7 and 3.3.4 discussed the major assumptions of the model. These included the method by which BOS costs were estimated, the assumption that PV modules in competing system designs would always be mounted with the same orientation and respond to the solar spectrum in the same manner, and the assumptions of equal financing and discounting for each of the systems being compared. While there are clearly cases of particular system designs that cannot be compared by this model, it is accurate enough to draw conclusions about the magnitude of the economic differences between competing PV module technologies. Assessing the cost of a particular PV system to a high degree of precision is not what this model is intended to do; rather, it is intended for drawing *general* conclusions about the differences between competing design options.

CHAPTER 4

DEVICE MODELING AND DESIGN OPTIMIZATION TO MITIGATE THE EFFECTS OF MATERIAL- AND PROCESS-INDUCED VARIABILITY IN SOLAR CELL PERFORMANCE

Differences in the physical properties of the silicon wafers from which solar cells are fabricated are well known to impact the efficiencies of finished devices. For example, solar cells produced from high-quality float-zone (FZ) refined wafers have traditionally produced solar cells with much higher efficiencies than those produced from comparatively low-quality cast multicrystalline silicon. However, cast multicrystalline silicon and single-crystal wafers produced by the Czochralski (Cz) method dominate the commercial solar cell market because of their much lower cost. As a result, there is considerable interest in determining how close these low-cost materials can come to matching the performance of FZ, and under what conditions the differences between them can be minimized or eliminated.

The purpose of this chapter is twofold: first, to model the impact on solar cell efficiency of this variability; and second, to use the modeling results to develop solar cell design guidelines that maximize efficiency while simultaneously mitigating the effects of this variability. The modeling is informed by estimates of PV module manufacturing cost made using the cost model that is developed in Chapter 5. In this manner, a process is developed to produce solar cell designs that balance cost and efficiency in a near-optimal manner.

This chapter presents the results of extensive device modeling aimed at establishing material and device design parameters that minimize the gap in performance between screen-printed commercial solar cells made from high-quality and low-quality silicon. This will allow the use of cheaper feedstock silicon and crystal growth techniques and promote production of solar cells on thinner wafers, all without sacrificing cell efficiency. This effort addresses the biggest challenge in PV: development of low-cost, high-efficiency solar cells.

4.1 DEVICE MODELING

All device modeling in this chapter was performed using PC1D [27]. The simulated device structure was a planar n^+pp^+ device like that shown in Figure 1.3 on page 6, with a rear optical interface consistent with that of a widely used aluminum back surface field (Al-BSF). To simulate this interface in PC1D, the front internal reflectance was set to 77% for the first reflection and 92% for subsequent reflections, while the rear internal reflectance parameters were set to 82% for all reflections [108]. The front external reflectance profile corresponded to that of a single layer antireflection coating composed of silicon nitride with a refractive index of 2.03 at 632.8 nm, and a thickness of 78 nm. Base doping was $1.14 \times 10^{16} \text{ cm}^{-3}$ unless noted otherwise, and the emitter sheet resistivity of all simulated devices was $40 \Omega/\square$. Simulations were performed over a wide range of bulk lifetimes, device thicknesses, and back surface recombination velocities (BSRVs). The results of these initial calculations are shown in Figure 4.1 on the next page.

Optimum thickness, defined as the wafer thickness at which efficiency is maximized, clearly varies with both bulk lifetime and BSRV. However, the relationships between these three parameters are not clear from Figure 4.1. Furthermore, it is difficult to visualize a simple relationship between efficiency and material quality from these results. Therefore, an attempt was made to express efficiency in a manner that is largely independent of material quality. Material quality relates directly to the diffusion length, L , which represents the average distance that free carriers travel through the bulk:

$$L = \sqrt{D\tau_b}, \quad (4.1)$$

where D is the diffusion coefficient and τ_b the bulk lifetime. This distance was used to scale the wafer thickness, creating a single dimensionless design parameter that represents both wafer thickness and material quality. This scaled parameter is simply the ratio of L to wafer thickness, W . The value of L/W at which efficiency peaks is referred to as the optimum L/W ratio, $(L/W)_{\text{opt}}$.

Figure 4.2 on page 95 shows that when $(L/W)_{\text{opt}}$ is plotted as a function of BSRV and solar cell efficiency, it more directly shows the relationships between L , W , and BSRV required to

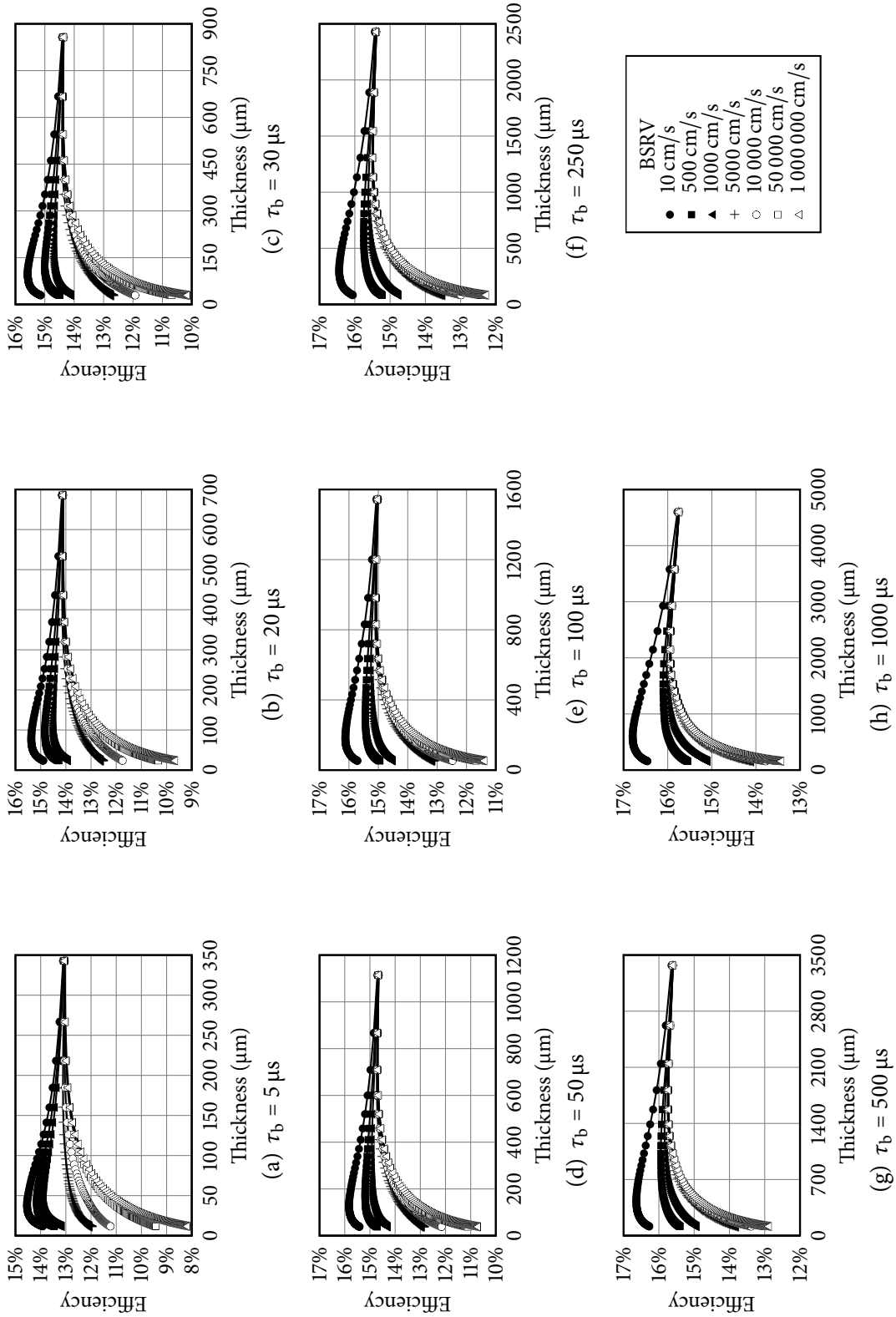
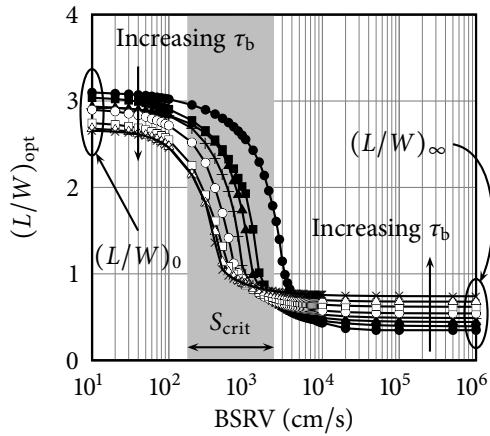
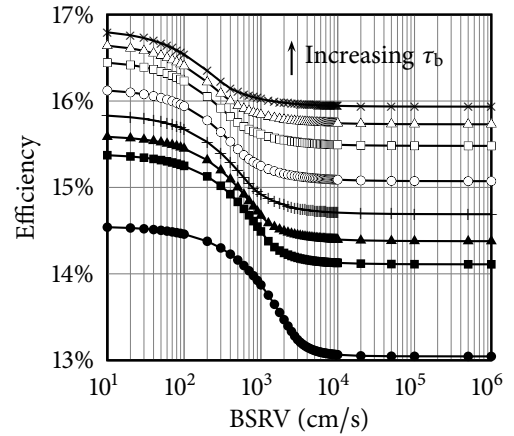


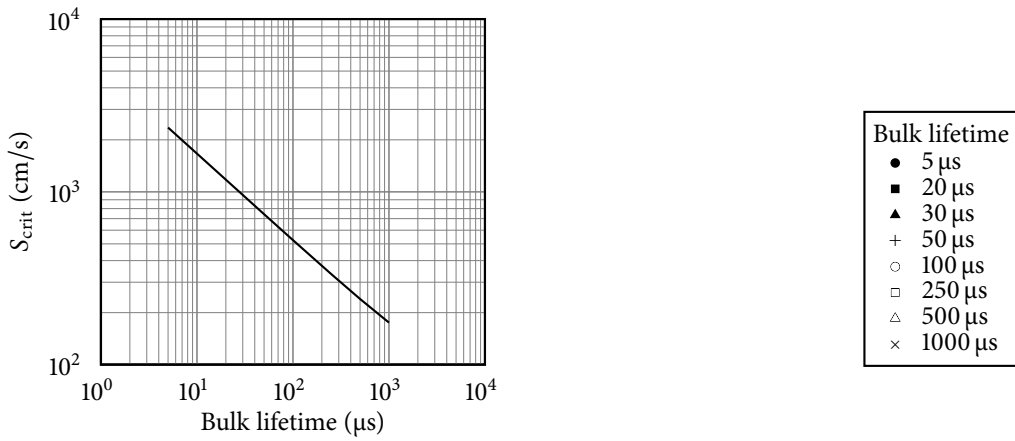
Figure 4.1: Simulated solar cell efficiency as a function of thickness, bulk lifetime, and back-surface recombination velocity.



(a) Optimum L/W ratio.



(b) Efficiency at $(L/W)_{opt}$.



(c) S_{crit} and τ_b .

Figure 4.2: Effect of back surface recombination velocity on optimum L/W ratio and efficiency for $1.3 \Omega\cdot\text{cm}$ base resistivity.

maximize efficiency. For a given bulk lifetime and BSRV, Figure 4.2(a) shows the value of $(L/W)_{\text{opt}}$, which indicates the device thickness W that will maximize solar cell efficiency. Figure 4.2(b) then gives the corresponding efficiency for that $(L/W)_{\text{opt}}$ and BSRV. Note that the value of $(L/W)_{\text{opt}}$ varies only slightly with respect to τ_b for high and low values of BSRV. Only for intermediate values of BSRV is $(L/W)_{\text{opt}}$ significantly dependent upon τ_b , shown by the shaded region in Figure 4.2(a). The reason for this can be explained on the basis of the F parameter of the dark saturation current equation for the base:

$$J_{\text{ob}} = \frac{qDn_i^2}{LN_A} \times F, \quad (4.2)$$

where

$$F = \frac{\frac{S_b L}{D} + \tanh\left(\frac{W}{L}\right)}{1 + \frac{S_b L}{D} \tanh\left(\frac{W}{L}\right)}, \quad (4.3)$$

n_i is the intrinsic carrier density of silicon, N_A is the base doping density, and S_b is the BSRV. When F is unity the effect of the rear surface on J_{ob} disappears. For F greater than unity J_{ob} will increase, and for F less than unity J_{ob} will decrease. Thus, “good” passivation may be defined by values of S_b such that $F < 1$, and “bad” passivation may be defined by values of S_b such that $F > 1$.

Solving equation (4.3) for the critical value S_{crit} at which F is unity yields:

$$S_{\text{crit}} = \frac{D}{L}. \quad (4.4)$$

Thus, S_{crit} is a function of material quality and ranges from 175 cm/s for $\tau_b = 1000 \mu\text{s}$ to 2356 cm/s for $\tau_b = 5 \mu\text{s}$. When $S_b \rightarrow 0$, $F \rightarrow \tanh(W/L) \leq 1$, and when $S_b \rightarrow \infty$, $F \rightarrow \coth(W/L) \geq 1$. Thus, $(L/W)_{\text{opt}}$ may be defined as a binary-valued design parameter dependent upon the value of S_b :

$$\left(\frac{L}{W}\right)_{\text{opt}} = \begin{cases} (L/W)_0 & S_b < S_{\text{crit}} \\ (L/W)_\infty & S_b > S_{\text{crit}} \end{cases} \quad (4.5)$$

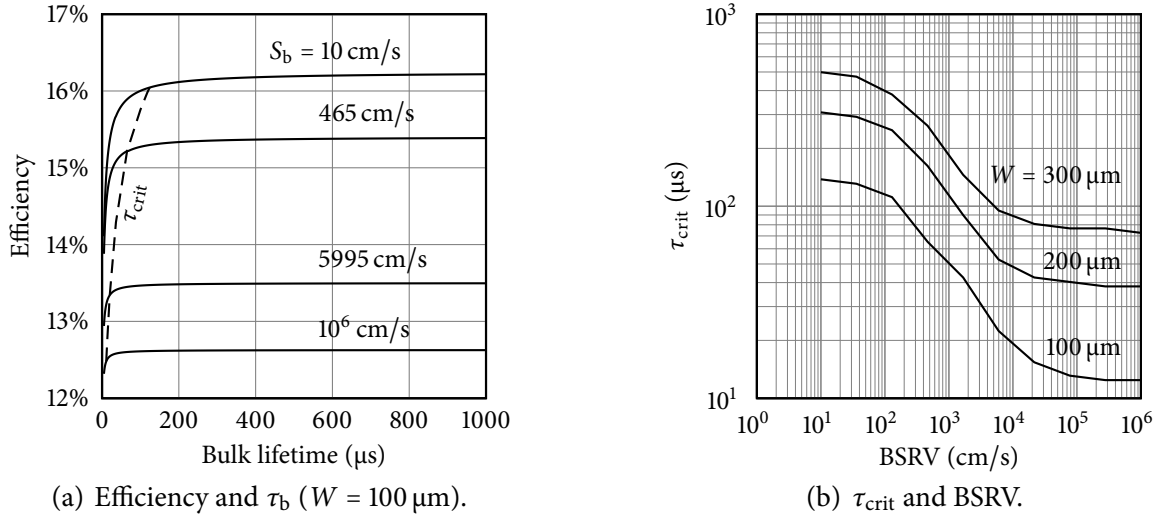


Figure 4.3: Determination of τ_{crit} , the value of bulk lifetime at which further improvement has no appreciable effect on efficiency.

Since $(L/W)_0 > (L/W)_\infty$, optimum efficiencies are attained with thin substrates when $S_b < S_{\text{crit}}$ and with thick substrates when $S_b > S_{\text{crit}}$. Furthermore, because S_{crit} increases nonlinearly with decreasing τ_b , as shown in Figure 4.2(c), high-quality material requires better passivation at the rear surface than low-quality material does to enable thin designs with $(L/W)_{\text{opt}} = (L/W)_0$. As a result, the ability to make high-efficiency, low-cost solar cells on high-quality material depends on having low-cost technology for producing excellent surface passivation.

While the dependence of $(L/W)_0$ itself on τ_b is not great, as shown in Figure 4.2(a), it may be explained by observing that when $S_b < S_{\text{crit}}$, the rate of recombination is less at the surface than it is in the bulk. Thus, a thinner bulk layer is desirable in order to couple more carriers to the surface. Bulk recombination increases further as τ_b decreases, favoring even thinner substrates and therefore higher values of $(L/W)_0$ for lower values of τ_b . When $S_b > S_{\text{crit}}$, the rate of recombination is higher at the surface than in the bulk and a thicker substrate is desirable to decouple carriers in the bulk from the surface. As a result, lower values of $(L/W)_\infty$ are favored for lower values of τ_b .

It is important to note from Figure 4.2(b) that even though efficiency is less dependent

upon τ_b at low BSRV than at high BSRV, it is still quite strongly dependent on τ_b at any given BSRV. Hence, independence of material quality is not achieved by simple optimization with respect to L/W because high- τ_b substrates always produce a lower value of $(L/W)_{opt}$ and higher optimum efficiency regardless of the BSRV value. However, the slope of the efficiency vs. bulk lifetime curve may be used to determine a critical value of τ_b above which further improvements in τ_b will not produce a meaningful increase in efficiency. The value of τ_b at which the slope drops below a predetermined threshold is defined as the critical value, τ_{crit} . The threshold value itself is rather subjective, but defined in this research as the slope corresponding to a 10% relative increase in efficiency resulting from an order of magnitude increase in τ_b . Thus, the threshold may be computed from:

$$\begin{aligned}\frac{\Delta\eta}{\Delta\tau_b} &= \frac{1.1\eta - \eta}{11\tau_b - \tau_b} \\ &= \frac{0.1\eta}{10\tau_b}.\end{aligned}\tag{4.6}$$

The value of τ_{crit} is equal to the value of τ_b for which the slope of the efficiency vs. bulk lifetime curve drops below the value of $\Delta\eta/\Delta\tau_b$ computed by equation (4.6). The results of this analysis for the 100- μm -thick device design modeled in this section are shown by the dashed line in Figure 4.3(a), which shows efficiency as a function of bulk lifetime and BSRV. The line indicates τ_{crit} , the value of τ_b above which further increases in τ_b do not produce significant increases in efficiency. The value of τ_{crit} is plotted explicitly as a function of BSRV and device thickness in Figure 4.3(b).

The most striking result from Figure 4.3(b) is that for 100- μm -thick devices, no significant increase in efficiency may be attained by increasing bulk lifetime beyond modest values of about 12 μs for high BSRVs and 140 μs for low BSRVs. For 200- and 300- μm -thick devices, modest lifetimes are sufficient for high BSRV values; however, at low BSRVs, τ_b must reach 300 μs on 200 μm devices and nearly 500 μs on 300 μm devices before further increases in bulk lifetime become futile. Clearly, device thickness should be as small as possible in order to maximize efficiency using low-cost materials. The efficiency of a 100- μm -thick device is independent of all but the lowest bulk lifetimes when BSRV is high, and can still be maximized

Table 4.1: Optimum solar cell thickness and efficiency associated with different bulk lifetime values for the device modeled in section 4.1 with BSRV of 10 cm/s.

τ_b (μs)	L_b (μm)	$(L/W)_{\text{opt}}$	W_{opt} (μm)	η_{opt} (%)	$\eta(W = 100 \mu\text{m})$ (%)
5	119.9	3.10	38.7	14.5	14.1
20	240.6	3.04	79.2	15.4	15.4
30	294.9	2.94	100	15.6	15.6
50	380.9	2.92	131	15.8	15.8
100	538.0	2.90	186	16.1	16.0
250	843.7	2.74	307	16.4	16.1
500	1174	2.68	438	16.6	16.2
1000	1608	2.67	605	16.8	16.2

with modest bulk lifetimes attainable through low-cost commercial processes when BSRV is low. By contrast, thicker devices need costly zone-refined silicon and careful processing to maintain the 300 μs to 500 μs lifetimes required to reach their full potential.

4.2 SOLAR CELL DESIGNS FOR MAXIMUM EFFICIENCY

According to the modeling performed in section 4.1, $(L/W)_{\text{opt}}$ is the L/W ratio at which power conversion efficiency is maximized. In practical terms, these results provide a roadmap to the optimum wafer thickness as a function of material quality and BSRV. Table 4.1 shows an example of that for a solar cell technology that can produce a BSRV of 10 cm/s. From Figure 4.2(a) one can find $(L/W)_{\text{opt}}$, and therefore the optimum thickness W_{opt} , for a given bulk lifetime. The optimum efficiency η_{opt} may then be read from Figure 4.2(b). Table 4.1 displays the results of this computation for a range of τ_b values from 5 μs to 1000 μs . The thicknesses prescribed for τ_b values greater than 250 μs are much higher than those used in modern commercial devices. Because manufacturers are pushing toward thin devices of 200 μm or less in order to save money on silicon feedstock, these thicknesses — as well as the 307 μm thickness prescribed for τ_b of 250 μs — are simply not practical in commercial production. As a result, L/W -optimized designs are not practical for high values of τ_b because wafer thickness must be increased by a factor of three to five in order to improve efficiency by just a few tenths of a percent. Given that silicon wafers account for more than 50% of the cost of a PV module today, this cannot be cost-effective in spite of the higher efficiency. However,

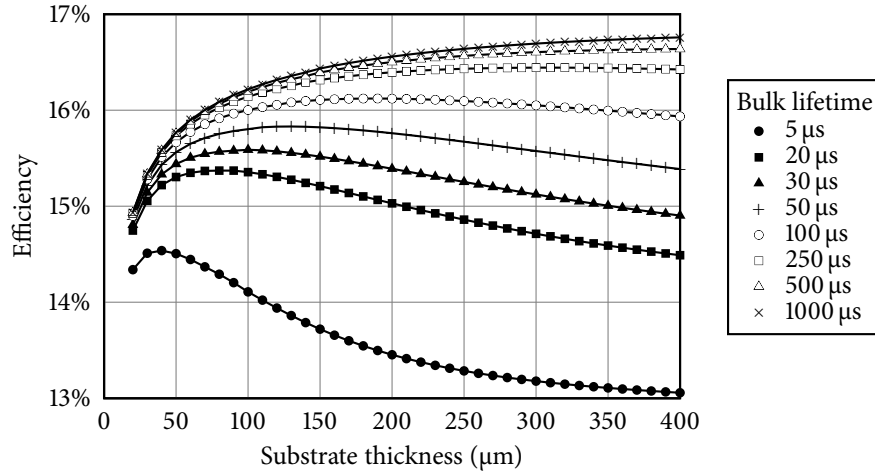


Figure 4.4: Solar cell efficiency as a function of τ_b for substrate thickness less than 400 μm and S_b equal to 10 cm/s .

$(L/W)_{\text{opt}}$ is a very useful design guide for values of τ_b below about 100 μs . Table 4.1 shows that if BSRV values can be reduced to 10 cm/s then for all materials with τ_b below 100 μs , one may reduce the device thickness to 100 μm without any appreciable loss in efficiency relative to the $(L/W)_{\text{opt}}$ design.

Figure 4.4 shows how efficiency varies for solar cells less than 400 μm thick with a low BSRV of 10 cm/s . Such low BSRV values are achieved by high-quality oxidation or deposition of amorphous silicon layers on the surface [109, 110]. Efficiency peaks are observed for all τ_b values of 250 μs and less. For these values of τ_b , efficiency peaks at some optimum thickness, shown as W_{opt} in Table 4.1. Solar cells with high values of τ_b also have higher values of W_{opt} than cells with low values of τ_b . As a result, as thickness decreases, efficiency decreases for cells with high τ_b and increases for cells with low τ_b , as shown in Figure 4.4. Consequently, the *difference* in efficiency between cells made on high quality material and those made on low quality material becomes smaller as substrate thickness shrinks. However, the difference

never shrinks to zero. This is because efficiency is related to τ_b through the equations [111]:

$$V_{OC} = \frac{kT}{q} \ln \left(\frac{J_{SC}}{J_{0b} + J_{0e}} \right) \quad (4.7)$$

$$\eta = \frac{V_{OC} J_{SC} FF}{I}, \quad (4.8)$$

where k is Boltzmann's constant, T is temperature, q is the electronic charge, V_{OC} is the open-circuit voltage, J_{SC} is the short-circuit current, η is efficiency, J_{0e} is the emitter saturation current, FF is the fill factor, and I is insolation. Since J_{SC} is a function of net carrier collection it decreases with decreasing τ_b . Furthermore, according to equations (4.1) and (4.2), J_{0b} is inversely proportional to the square root of τ_b . As a result, V_{OC} also decreases with decreasing τ_b . Fill factor, in turn, decreases with decreasing V_{OC} and is thus indirectly affected by τ_b . Therefore, for a given substrate thickness, V_{OC} , J_{SC} , and fill factor decrease with decreasing τ_b , and a device with high τ_b will always have higher efficiency than an otherwise-identical device with lower τ_b . However, Figure 4.4 shows that as substrate thickness decreases, this gap diminishes significantly. Table 4.1 shows that for 100- μm -thick substrates a factor of 10 reduction in τ_b (from 1000 μs to 100 μs) produces only a 0.2% absolute gain in efficiency.

This is a very important finding since commercial solar cells must be designed with both physics and economics in mind. In the current PV market, a shortage of silicon feedstock resulting in high feedstock prices is driving the economics in favor of thinner solar cells in the range of 100 μm to 200 μm . Table 4.1 shows that for a 100- μm substrate, solar cells with modest values of τ_b operate at or very near peak efficiency. By contrast, while 100- μm -thick cells with high values of τ_b still operate at slightly higher efficiency, their efficiencies can be appreciably less than those at their optimum values of L/W . The difference in optimum efficiency between devices with τ_b values of 1000 μs and 50 μs is a full one percent, but the one with the higher τ_b value consumes nearly five times as much silicon. Clearly, the higher efficiency is not worthwhile if the cost of the additional silicon required produces an increase in module cost per peak watt.

Since the figure of merit for affordable PV modules is ultimately their cost (e.g., dollars per peak watt), a model developed in Chapter 5 was used to estimate manufacturing costs

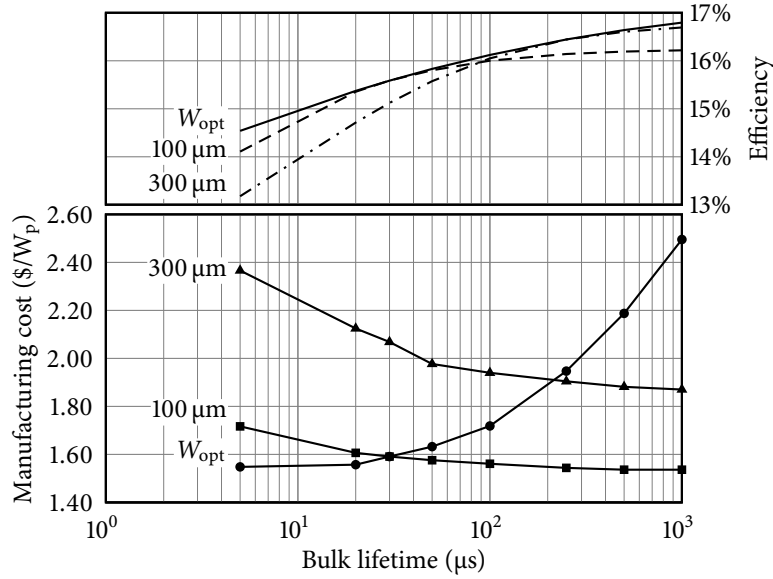


Figure 4.5: Solar cell efficiencies and PV module manufacturing costs for solar cells having optimized, 100- μm , and 300- μm thicknesses ($S_b = 10 \text{ cm/s}$).

for modules using each of the solar cell designs of Table 4.1, as well as an additional 300- μm design. These estimates are shown in Figure 4.5. One curve depicts the manufacturing cost associated with using cells of optimum thickness and efficiency, while the other shows that associated with using 100- μm -thick cells. Solar cells of optimum thickness are significantly less expensive for low values of τ_b because they consume much less silicon; however, the manufacturing cost levels off below about 30 μs . On the other hand, when the thickness is fixed at 100 μm , silicon consumption no longer affects the analysis. Solar cells with high values of τ_b have higher efficiencies, and manufacturing cost decreases with increasing bulk lifetime. However, the cost reduction is not significant for τ_b values greater than about 100 μs . Furthermore, the highest τ_b values are only attainable using expensive zone-refined silicon, which is not accounted for in this computation. Therefore, it is expected that a more accurate accounting would reveal a significant increase in manufacturing cost for τ_b values higher than several hundred microseconds even when the wafer thickness is fixed at 100 μm . Thus, τ_b values between 20 μs and 100 μs provide the best opportunity for low-cost crystalline silicon PV at 100- μm wafer thicknesses. As shown in Figure 4.5, values of τ_b below 20 μs will

degrade efficiency and increase cost, while values above 100 μs will not appreciably improve either efficiency or cost.

By contrast, the 300- μm design is substantially more expensive than the 100- μm design for all values of τ_b because of its increased silicon consumption. The manufacturing cost of this design drops rapidly with increasing τ_b up to about 50 μs and continues to drop at a significant rate up to about 500 μs . Furthermore, τ_b must reach 100 μs before the efficiency of the 300- μm design exceeds that of the 100- μm design. Thus, minimizing the cost of crystalline silicon PV at 300 μm requires τ_b values of several hundred microseconds. Bulk lifetimes as high as 150 μs have been reached with low-cost multicrystalline silicon in a pilot production setting [112], but it is not clear that such high lifetimes can be consistently realized on commercial production lines. As a result, the cost of PV modules produced with 300- μm -thick solar cells is limited by bulk lifetime, and increases in τ_b will always yield reductions in manufacturing cost.

This analysis shows that thin devices around 100 μm can reach near-optimum efficiencies with modest values of τ_b that are easily attained with existing multicrystalline silicon wafer technology. It also shows that devices with low to modest values of τ_b require less aggressive passivation to achieve these efficiencies, potentially reducing the amount of technology development required to realize them in practice. Finally, it shows that modules based on thicker devices, such as those in the 300 μm example, are more expensive despite their higher efficiencies because of their increased silicon consumption. It also shows that they require higher values of τ_b and much lower values of BSRV to realize near-optimum efficiency, indicating that substantial technology development must be done in order for these devices to match their potential. Consequently, working toward commercial production of thinner solar cells is the most expedient way to meet the roadmap's cost targets.

4.3 EFFECT OF DEVICE PARAMETER VARIABILITY ON OPTIMUM DESIGN

Sections 4.1 and 4.2 described how to optimize a solar cell design with a given set of design parameters (e.g., base doping concentration, BSRV, etc.). However, silicon utilization rates

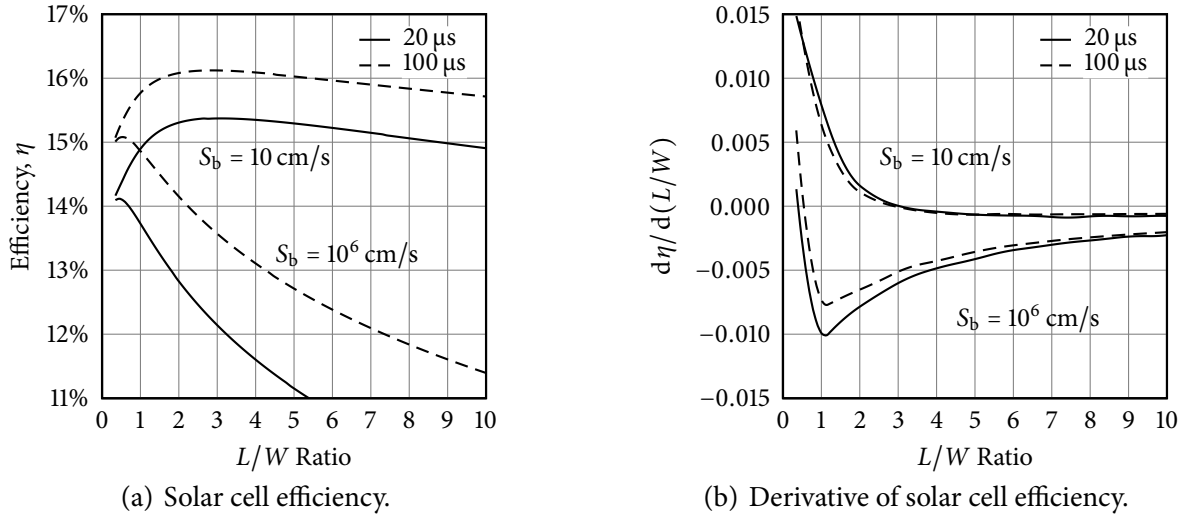


Figure 4.6: Derivative of device efficiency with respect to L/W .

have great bearing on solar cell manufacturing costs and, as a result, manufacturers are forced to use silicon wafers with a wide range of physical parameters. Consequently, a device optimized for a single set of design parameters is not necessarily optimized for commercial production. Thus, it is important to understand how a solar cell design will respond to variations in wafer parameters such as bulk lifetime, base doping density, and even wafer thickness.

Figure 4.6 shows efficiency, η , and its derivative with respect to L/W on low- and medium-quality substrates (τ_b values of $20 \mu\text{s}$ and $100 \mu\text{s}$, respectively) for excellent- and poor-quality back surface passivation (S_b values of 10 and 10^6 cm/s , respectively). In each case, peak efficiency — and therefore $(L/W)_{\text{opt}}$ — occurs where the derivative crosses the zero on the y-axis in Figure 4.6(b). For solar cells with low BSRV the derivative increases rapidly to the left of this point, while to the right of this point it becomes roughly constant. This indicates that low-BSRV devices whose L/W ratios are lower than optimum will suffer greater losses in efficiency than those whose L/W ratios are higher than optimum. Therefore, when BSRV is low, cells designed with higher-than-optimum L/W ratio will be more tolerant of variations in material quality (L) and wafer thickness (W).

This is seen in Figure 4.6(a) on the curves with S_b equal to 10 cm/s , for which $(L/W)_{\text{opt}}$ is

three. For the device with τ_b equal to 100 μs , efficiency at $(L/W)_{\text{opt}}$ is 16.1%. If variations in L and W reduce the L/W ratio to one, however, efficiency will drop to 15.8%, while variability resulting in an increase of L/W to five will only reduce the efficiency to 16.0%. In commercial production, values of L can vary by a factor of two or more, and as wafers become thinner the L/W quotient will become more sensitive to variations in W since the derivative of L/W with respect to W :

$$\frac{d}{dW} \left(\frac{L}{W} \right) = -\frac{L}{W^2}, \quad (4.9)$$

is inversely proportional to W^2 . As a result, it will be increasingly important to ensure that $L/W \geq (L/W)_{\text{opt}}$ by reducing device thickness and maximizing bulk lifetime.

When BSRV is high the value of the derivative changes rapidly on both sides of the zero crossing. This indicates a sharper peak in efficiency with respect to L/W , which can be seen clearly in Figure 4.6(a). As a result, significant deviations in L/W from $(L/W)_{\text{opt}}$ will result in far greater variations in efficiency than in the low-BSRV case, indicating that devices with high BSRV cannot be made more tolerant to variations in L and W . However, since $(L/W)_{\text{opt}}$ is approximately 0.6 for these devices, they tend to have thick substrates, which by equation (4.9) serves to reduce the sensitivity of the L/W ratio to variations in L and W . Therefore, the sensitivity of efficiency to L/W cannot be mitigated by engineering the L/W ratio as in the low-BSRV case, though it can be damped by high wafer thickness when BSRV is high. Since L/W must be close to $(L/W)_{\text{opt}}$ to maintain high efficiencies, efficiency variation is reduced in the high-BSRV case by maximizing τ_b and increasing wafer thickness as necessary to maintain $(L/W)_{\text{opt}}$. From a commercial standpoint, this optimization is not practical because the use of extremely thick wafers is undesirable.

Figure 4.6(b) shows the derivative of efficiency with respect to L/W for bulk lifetime values of 20 μs and 100 μs , and for BSRV values of 10 cm/s and 10^6 cm/s. When BSRV is low and $L/W > (L/W)_{\text{opt}}$ the two curves lie atop one another, showing little to no dependence of the derivative on τ_b . However, the curves lie distinctly apart when BSRV is high, indicating a significant dependent of the derivative upon τ_b when passivation is poor. Furthermore, when BSRV is high and $L/W > (L/W)_{\text{opt}}$, the absolute value of the derivative is significantly

greater for low- τ_b substrates at high BSRV than for high- τ_b substrates. This indicates that solar cells with low τ_b and high BSRV are more sensitive to variations in L/W than those with high τ_b and high BSRV. It also suggests that designs based on low BSRV values will better tolerate L/W variations when BSRV is low than when it is high, particularly when $L/W > (L/W)_{\text{opt}}$.

Finally, Figure 4.7 shows how variations in base resistivity, ρ_b , can affect $(L/W)_{\text{opt}}$ and efficiency, in this case for a substrate with a τ_b value of 30 μs . As ρ_b increases, $(L/W)_0$ — that is, $(L/W)_{\text{opt}}$ at low BSRV — increases as well, implying that high resistivities favor thinner wafers. Furthermore, Figure 4.7(b) shows that as ρ_b increases, the maximum efficiency available from the wafer decreases at all BSRV values. In such a scenario, the only way to maintain the optimum L/W ratio is to tailor the thickness of each device to its particular value of ρ_b . This is highly impractical, if not impossible; as a result, production-line variability in ρ_b leads to variability in efficiency. This may affect the conclusions rendered by the preceding analysis of efficiency with respect to L/W ratio. Furthermore, on an actual production line it is not just bulk resistivity that varies; wafer thickness, bulk lifetime, and virtually every other device design parameter will also vary. Therefore, in order to minimize solar cell efficiency variation it is important to understand how variations in all of the input parameters affect efficiency. This is the subject of the next section.

4.4 MODELING THE IMPACT OF DEVICE PARAMETER VARIABILITY USING MONTE CARLO SIMULATION

It was shown earlier, in Figure 4.2(b) on page 95, that different values of τ_b produce different efficiencies for the same solar cell design. Similarly, it was also shown in Figure 4.4 on page 100 that different values of device thickness produce different efficiencies. Along with the data presented in the previous section, it is clear that variations in these parameters will combine in complex ways to produce pronounced variations in efficiency. This is important for predicting variability in the output of a commercial production line with a large number of input variables. If a highly variable parameter introduces little variability into efficiency, for example, changes in that parameter are unlikely to have much influence over efficiency

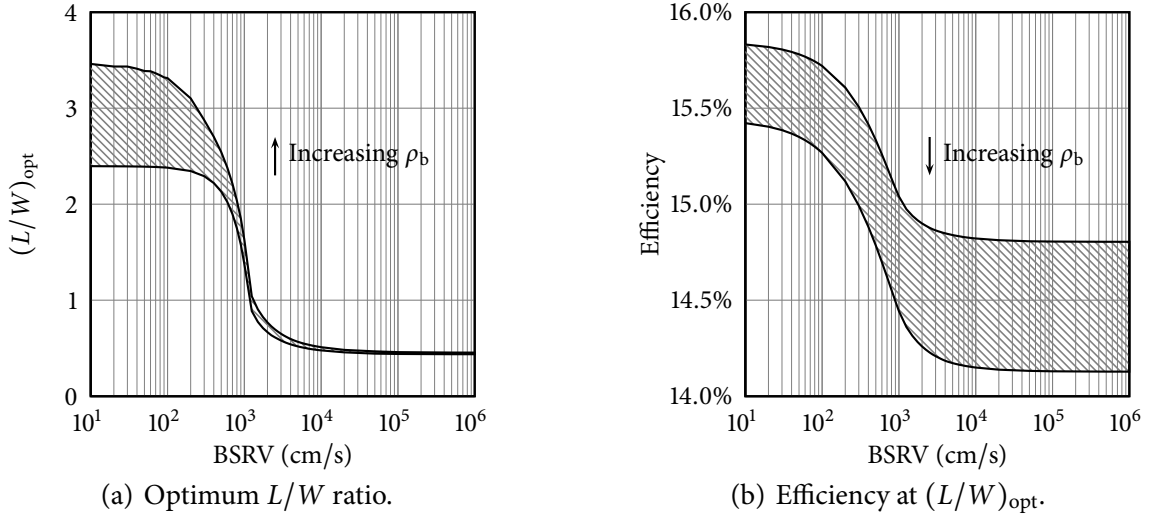


Figure 4.7: Effect of varying base resistivity from 0.5 to 2.0 $\Omega\cdot\text{cm}$ and BSRV from 10 to 10^6 cm/s on $(L/W)_{opt}$ and optimum efficiency for τ_b of 30 μs .

or variability in production output. On the other hand, if a small change in a parameter produces a large change in efficiency, it is highly influential and must be controlled carefully. Further complicating the issue, some design parameters may be highly influential under some circumstances, but not under others. A technology that works well in the laboratory can be undermined on the production line by uncontrolled variability in influential parameters. Understanding the variability in these parameters and its influence on efficiency can be key to transferring laboratory technologies to the production line.

In this task, the collective impact of multiple variables on solar cell efficiency has been modeled using Monte Carlo simulation. Each design parameter (e.g., thickness, bulk resistivity, or bulk lifetime) is represented by a random variable with a representative probability density function (pdf). Modeling proceeds by repeatedly sampling each of these variables and using the sample as an input to the device model, in this case PCID, to calculate cell efficiency. After a suitably large number of iterations one obtains a pdf of the output, in this case efficiency. To obtain accurate results, accurate probability distributions are required for the random variables. A very powerful advantage of Monte Carlo simulation is that correlations between variables may be taken into account, and very often these correlations

have profound effects on the output distribution. However, as with the input pdfs themselves, the correlations must be accurately characterized in order to produce accurate results.

As an example, consider Table 4.1 on page 99, which says that for a modest τ_b of 30 μs and an excellent BSRV of 10 cm/s, the optimum device thickness is 100 μm . Recall from section 4.1 that this device assumes N_A is $1.14 \times 10^{16} \text{ cm}^{-3}$, corresponding to a bulk resistivity of 1.3 $\Omega\text{-cm}$. Suppose that this device were to be produced on a manufacturing line where τ_b varies uniformly from 20 to 100 μs and ρ_b varies uniformly from 0.5 to 4.0 $\Omega\text{-cm}$. Variations in τ_b would produce values of L/W that are lower than $(L/W)_{\text{opt}}$ when τ_b is less than 30 μs , and higher than $(L/W)_{\text{opt}}$ when τ_b is greater than 30 μs . According to the preceding analysis of Figure 4.6(b), these variations in L/W should produce less-than-optimum efficiencies when τ_b is less than 30 μs and near-optimum efficiencies when τ_b is greater than 30 μs .

Variations in ρ_b will similarly affect efficiency according to Figure 4.7. When ρ_b is less than 1.3 $\Omega\text{-cm}$, the value of $(L/W)_{\text{opt}}$ will decrease, leaving L/W greater than $(L/W)_{\text{opt}}$ and suggesting, by Figure 4.6(b), that efficiency should be near-optimum. However, the reduction in ρ_b will decrease J_{0b} according to equation (4.2), in turn increasing V_{OC} and efficiency according to equations (4.7) and (1.3). When ρ_b is greater than 1.3 $\Omega\text{-cm}$ the opposite holds: L/W will be less than $(L/W)_{\text{opt}}$, and the increase in ρ_b will cause efficiency to decrease. Thus, one expects low values of ρ_b to lead to higher-than-expected efficiencies and high values of ρ_b to do the opposite.

The results of Monte Carlo simulation of this scenario after 20 000 samples are shown in the box plot of Figure 4.8(a), which indicates that the results anticipated by the above analysis are substantially correct. The simulation assumed uniform distributions of ρ_b between 0.5 $\Omega\text{-cm}$ and 4.0 $\Omega\text{-cm}$, and τ_b between 20 μs and 100 μs . It produced a median efficiency of 15.7% with the lower and upper quartiles at 15.5% and 15.9%, respectively, and a range of 15.0% to 16.1%. Note that while the design value of τ_b was 30 μs , the average τ_b resulting from the sampling process was 60 μs because of the uniform distribution between 20 μs and 100 μs . According to Table 4.1, a wafer thickness of 100 μm is not optimum for this value of τ_b and L/W is greater than $(L/W)_{\text{opt}}$ for 30 μs bulk lifetime. As a result, the mean efficiency of 15.7% is higher than the 15.6% expected from the 30- μs design selected from Table 4.1, but

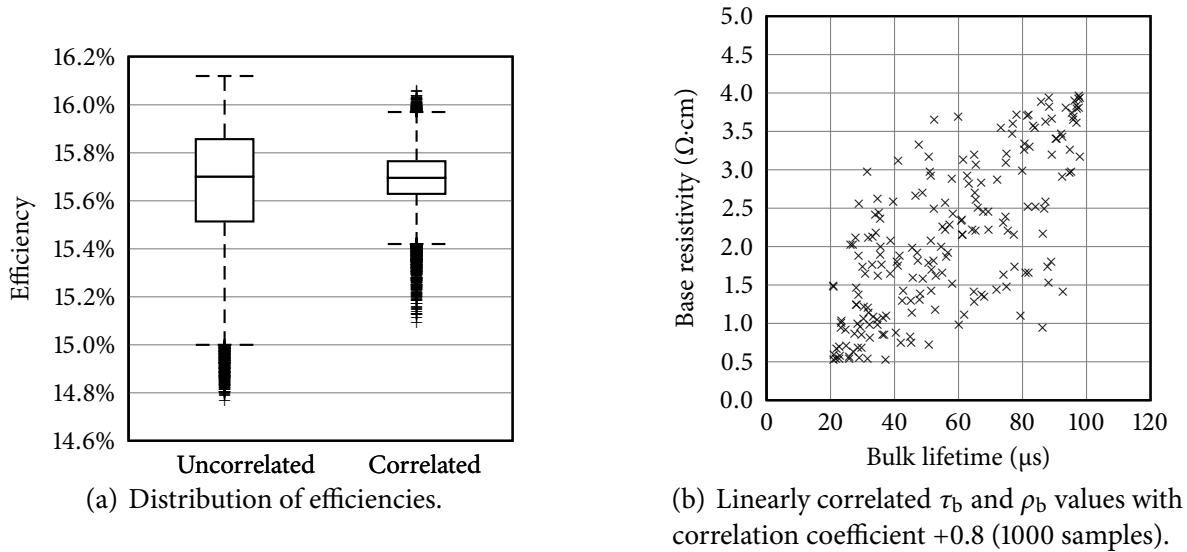


Figure 4.8: Results of Monte Carlo simulation of variability in bulk lifetime and base resistivity with and without correlation between the variables.

is less than the optimum efficiency of 15.8% to 16.0% for τ_b between 50 μs and 100 μs .

Now suppose that τ_b and ρ_b are linearly correlated with a correlation coefficient of +0.8. This relationship is shown in Figure 4.8(b), the positive sign on the correlation coefficient indicating that τ_b increases with increasing ρ_b . Because of this relationship between τ_b and ρ_b , the L/W ratio tends to increase as ρ_b increases. By Figure 4.7(a) on page 107, $(L/W)_{\text{opt}}$ increases with increasing ρ_b , so the correlation between τ_b and ρ_b tends to keep the value of L/W closer to $(L/W)_{\text{opt}}$ than when the two are not correlated. As a result, one expects to see less variability in efficiency from this arrangement.

As shown in Figure 4.8(a), repeating the simulation with correlated random variables still yields a median efficiency of 15.7%, but with narrower and more symmetric lower and upper quartiles of 15.6% and 15.8%, respectively, and a narrower range of 15.4% to 15.9%. Thus, in this case strong positive correlation between τ_b and ρ_b does, in fact, serve to reduce variability in efficiency with no adverse effect on its median value.

While in this simple example the results of the Monte Carlo simulation were correctly anticipated by careful analysis, the true power of Monte Carlo lies in more complex scenarios. Often, the probability distributions of the random variables will not be uniform,

and correlations between them may be nonlinear. In these situations, analysis is often not straightforward and requires statistical methods to determine which random variables have the greatest effect on efficiency.

4.5 ROADMAP FOR HIGH-EFFICIENCY CRYSTALLINE SILICON SOLAR CELLS

The principles derived in the preceding sections can be used to derive a series of incremental improvements with the potential to increase multicrystalline silicon solar cell efficiency from its current level of 14% to 15% up to 20%. These principles can be summarized as follows:

- Reduce S_b below S_{crit} to enable high $(L/W)_{opt}$.
- Increase τ_b to τ_{crit} for desired wafer thickness.
- Reduce wafer thickness to desired value.

For the basic design illustrated in the previous section, the ideal wafer thickness appears to be around 100 μm . The process of generating the roadmap to 20% efficiency is illustrated with the aid of PC1D simulations starting with a baseline solar cell design representative of today's commercial solar cells.

The baseline solar cell is fabricated on an untextured 250- μm -thick p-type multicrystalline silicon wafer with a bulk lifetime of 20 μs and a base resistivity of 1.3 $\Omega\cdot\text{cm}$. It has a co-fired back surface field producing a BSRV of 5000 cm/s . The front of the cell is diffused with a 50 Ω/\square phosphorus emitter and has an FSRV of 150 000 cm/s . The front contact is screen-printed silver with 7% front-surface coverage that is co-fired with the BSF to yield a fill factor of 0.75. It has a rear internal reflectance of 82% and a front internal reflectance of 77%, consistent with the imperfectly Lambertian reflector produced by aluminum BSFs [108]. The baseline solar cell design yields a power conversion efficiency of 14.4%.

Since the cell will ultimately be thin, light trapping will be important to maintaining high efficiency. To set the stage for this, the first improvement involves fine-line screen-printing techniques that not only maximize the amount of light entering the solar cell, but simultane-

ously reduce series resistance. This increases fill factor from 0.75 to 0.78 and boosts efficiency from 14.4% to 15.3%.

An increase in τ_b is next. Figure 4.3 suggests that τ_{crit} for this cell design at 100 μm is around 100 μs . Increasing τ_b to 100 μs raises efficiency further, to 15.7%.

With a high L/W ratio, a reduction in BSRV can be expected to yield significant benefits. In the next step, the aluminum BSF is replaced with silicon nitride dielectric passivation and a screen-printed back-surface reflector. This improves BSRV to 100 cm/s . It has the additional effect of improving light trapping by increasing rear internal reflectance to 95% and front internal reflectance to 92%. These measures yield an efficiency of 17.7%.

Now, with the L/W ratio high, the BSRV low, and light trapping greatly improved, solar cell thickness can be reduced without negatively impacting efficiency. Reducing the cell thickness to 100 μm increases the L/W even more and minimizes the amount of silicon feedstock consumed to produce a peak watt of power. Efficiency remains stable at 17.7%, but this step is expected to reduce manufacturing cost significantly.

The efficiency of a thick solar cell with poor bulk lifetime is limited by the dark saturation current in the base, J_{0b} , which is much greater than the dark saturation current in the emitter, J_{0e} . However, at this point the solar cell is very thin and has a high bulk lifetime, minimizing J_{0b} , and J_{0e} has grown in importance. Thus, a selective emitter with a sheet resistivity of 100 Ω/\square is employed to reduce J_{0e} and increase efficiency to 18.4%.

A further increase in efficiency may be obtained by improving light trapping. The light-trapping properties of the rear surface have already been improved significantly, so the best opportunity for improvement is through isotropic texturing of the front surface. This traps additional light inside the cell and improves efficiency to 19.8%.

Finally, V_{OC} can be increased by using a more heavily doped substrate. This is unwise when bulk lifetime is low, since heavy doping tends to reduce lifetime further. However, with a very high L/W ratio, heavier doping of the bulk can be done without compromising efficiency. This final step improves cell efficiency to 20.0%.

The input parameters to PCID that were changed at each step to produce these efficiency calculations are listed in Table 4.2; the associated efficiency values are shown in Figure 4.9.

Table 4.2: PCID inputs for modeling incremental improvements to base multicrystalline silicon solar cell technology.

Cell description	Cell parameters set or changed
A. Industrial solar cell (current)	$W = 250 \mu\text{m}$, $\tau_b = 20 \mu\text{s}$, $R_S = 1.1 \Omega\cdot\text{cm}^2$, $R_{SH} = 1000 \Omega\cdot\text{cm}^2$, $J_{02} = 5 \text{ nA}$, $N_2 = 2$, $S_f = 150\,000 \text{ cm/s}$, $S_b = 5000 \text{ cm/s}$. Also, SiN_x (2.03, 780 Å) SLAR, metallization coverage of 7%, $R_b = 82\%$, and 80% Lambertian character.
B. Improved screen printing	$R_S = 0.7 \Omega\cdot\text{cm}^2$, $R_{SH} = 5000 \Omega\cdot\text{cm}^2$, $J_{02} = 2.5 \text{ nA}$, $N_2 = 2$, metallization coverage 5%.
C. Lifetime enhancement	$\tau_b = 100 \mu\text{s}$.
D. Back surface reflector	$R_b = 95\%$ and perfectly diffuse, $S_b = 100 \text{ cm/s}$.
E. Reduce cell thickness to 100 μm	$W = 100 \mu\text{m}$.
F. Selective emitter	$\rho_S = 100 \Omega/\square$, $S_f = 30\,000 \text{ cm/s}$.
G. Random pyramids on front	3.535 μm pyramid height.
H. Reduce resistivity to 0.6 $\Omega\cdot\text{cm}$	$\rho_b = 0.6 \Omega\cdot\text{cm}$.

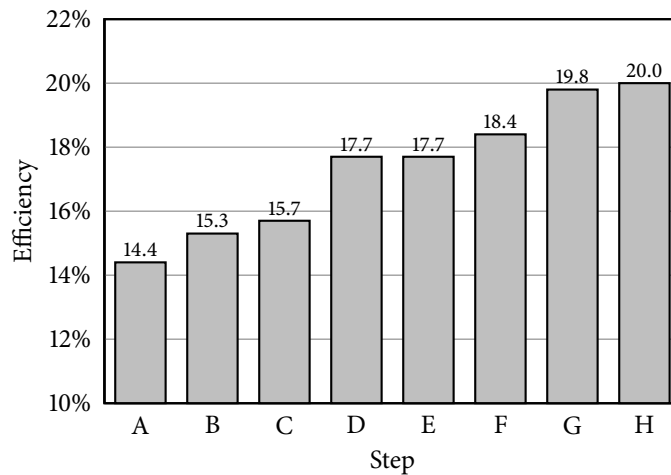


Figure 4.9: Improvements in base commercial multicrystalline silicon solar cell efficiency obtained by incremental progress in device design as described in Table 4.2.

The development of this roadmap shows how the principles derived in this chapter may be used to improve solar cell efficiency. More importantly, this chapter provides an example for deriving similar guidelines to improve other solar cell designs. In Chapter 5, the roadmap developed here will be combined with a manufacturing cost model to see how the design might be further improved to achieve solar energy at low cost.

4.6 CONCLUSIONS

This study established three simple guidelines to steer crystalline silicon solar cell development toward low cost with little sacrifice in efficiency. These guidelines are: (1) reduce back surface recombination velocity below the threshold value S_{crit} determined from equation (4.4); (2) increase bulk lifetime to the threshold value τ_{crit} appropriate for the wafer thickness; and (3) minimize wafer thickness. The last of these guidelines, minimizing wafer thickness, is the key to keeping manufacturing cost low. The other two guidelines simply enable thin solar cells to be produced with little loss in efficiency.

The study also investigated the effects of variability in the physical properties of solar cells on their efficiency. It was established that when BSRV is low, efficiency variability resulting from variability in bulk lifetime can be minimized by using a slightly larger L/W ratio than optimum. In addition, a Monte Carlo methodology was developed in conjunction with PC1D to explicitly assess the effects of parameter variability on efficiency even when the parameters are statistically correlated.

The guidelines established in this chapter were employed to establish a series of technological improvements that increase efficiency with an eye toward minimizing manufacturing cost. A roadmap was developed to improve solar cell efficiency from 14.4% to 20.0% while simultaneously minimizing cell thickness. Whether this roadmap succeeds in meeting the $\$1.50/W_p$ cost target established by DOE will be evaluated in Chapter 5.

CHAPTER 5

MODELING PHOTOVOLTAIC MODULE MANUFACTURING COST

Ultimately, the success of the PV industry is predicated not on technological achievements like maximizing solar cell efficiency, but on making electricity derived from PV economically competitive with conventional electricity sources. As demonstrated in Chapter 3, increased efficiency can make this goal easier to attain by reducing BOS contributions to installed system cost, but it cannot attain the goal without significant reductions in manufacturing cost.

As described in Chapters 2 and 4, a number of tools exist for estimating the efficiency of solar cells produced using a particular manufacturing sequence. However, no widely available tools exist for assessing the associated manufacturing cost. As a result, the cost implications of a great deal of PV research and development are described speculatively and in qualitative terms such as “low-cost” and “manufacturable,” rather than in easily comparable quantitative terms.

The aim of this chapter is to describe the development of a numerical model that estimates the manufacturing cost of PV cells and modules, given sufficient technical detail about their manufacturing processes. It estimates the one-time costs associated with building a PV plant and the operating costs incurred in the scope of the plant’s day-to-day operations, then combines this information in a manner that yields an estimate of manufacturing cost. The structure and base assumptions of the model are described in section 5.2.

The model developed in this chapter is highly generalized and, in theory, can be applied to any PV manufacturing process (including thin-film PV) given sufficient technical and economic information about the manufacturing process. However, it will be applied exclusively to crystalline silicon PV processes in this thesis.

5.1 OVERVIEW OF MANUFACTURING COST ESTIMATION

Prior to discussing the manufacturing cost model in detail, it is helpful to have an overview of the process to use as a guide. Roughly speaking, estimating a manufacturing cost requires an estimate of the capital required to build the plant and an estimate of the plant's operating expenses. Direct operating expenses figure into the direct manufacturing cost, also referred to as cost of revenue, cost of sales, cost of manufacturing (COM), or cost of goods sold (COGS). Indirect operating expenses, while not included in the direct manufacturing cost, affect the plant's net profit and, therefore, the price for which the plant can sell the finished solar panel.

In this section, the methods used by the model to estimate the plant's capital and operating costs are outlined. This is followed by a discussion of the accounting classification of these expenses and the computation of income tax liability, cash flows, and gross and net profit margins. These values are used to compute return on investment (ROI) and payout period, which are useful in estimating the minimum wholesale cost that will be profitable for a given manufacturing cost.

5.1.1 CAPITAL COST ESTIMATION

The manufacturing cost of any product can only be known precisely by selecting a site for the plant, building it, hiring workers, purchasing raw materials, and producing the product. Prior to reaching that stage, the manufacturing cost estimate necessarily requires assumptions about how much these elements will cost. Naturally, the better the assumptions reflect reality, the more accurate the estimate is likely to be.

The chemical process industry generally classifies capital cost estimates into one of five categories [113]:

1. Order of magnitude estimate
2. Study estimate
3. Preliminary estimate

4. Definitive estimate

5. Detailed estimate

Each type of estimate requires a progressively greater amount of information and, in turn, produces a progressively more accurate estimate of the capital required to build the plant. The information required and level of accuracy for each type of estimate is summarized in Table 5.1 on the next page. The cost of performing the capital cost estimate can range from a few thousand dollars for an order of magnitude estimate on a small plant to more than a million dollars for a detailed estimate on a large plant.

The model developed in this chapter demands a process flow diagram and list of major equipment requirements. The equipment is sized and its cost estimated on the basis of published equipment prices. The remainder of the plant's capital costs are then extrapolated from the cost of the major equipment, a procedure known as *factoring*. By Table 5.1, the manufacturing cost calculated by the model closely resembles a study estimate. In keeping with this, it is believed to have an accuracy of +30% to -20%, provided its underlying assumptions are met and the input data are accurate.

While this range of accuracy may seem broad, improving it requires a great deal more effort. The cost estimates produced by the MUSIC FM study discussed in Chapter 2, for example, were developed over a long period of time and involved more than a dozen participants. Even so, the final report on the study [47] suggests that it is consistent with a preliminary estimate, which improves accuracy only to +25% to -15%. While this additional effort served the purposes of MUSIC FM and would be an important step in estimating the cost of a commercial product, the motivation for developing the present model was to evaluate the relative economic merits of competing processes at the R&D stage; therefore, a high degree of accuracy is not necessary. Furthermore, the information required to produce better than a study estimate may not even be available for some newly developed processes.

The model also assumes that the plant is a “greenfield” project — that is, it is constructed on previously undeveloped land. Therefore, the estimate must include site preparation and building construction. The alternative, a “brownfield” development (which is performed

Table 5.1: Classifications of capital cost estimates (after [113]).

Estimate type	Required data	Accuracy
Order of magnitude	Cost information from a similar, previously built plant, adjusted for capacity and inflation. Requires only a block diagram of the production process.	+40% to -20%
Study	Process flow diagram and list of major equipment requirements, along with its approximate size and cost. The total cost of the equipment can be factored to yield an estimate of the total capital cost.	+30% to -20%
Preliminary	Process flow diagram, sketches of major equipment, and preliminary plot plan. More accurate sizing of equipment than in study estimate, plus approximate layout of equipment and services (plumbing, instrumentation, electricity, etc.). Utilities are estimated.	+25% to -15%
Definitive	Final process flow diagram, equipment sketches, plot plan, utility balances, and preliminary piping and instrumentation diagram. Preliminary specifications for all equipment, services, utilities, and off-site requirements.	+15% to -7%
Detailed	All diagrams that are required to complete construction of the plant, including final process flow and piping and instrumentation diagrams. Complete engineering of the process and all related off-site and utility requirements. Vendor quotes for all items of significant cost.	+6% to -4%

on previously developed land) is a more complicated case, since brownfields might require demolition of existing structures, abatement of pre-existing environmental problems, and other expenses that are difficult to anticipate without actually selecting a building site. This also means that the model will not predict manufacturing costs associated with plant expansions, which can be less costly than greenfield development. However, since the PV industry requires enormous growth before PV will contribute significantly to global electricity supply, greenfield developments are likely to be the norm for the foreseeable future.

Finally, the model is designed as a static model, meaning its assumptions are long-term averages and its outputs are long-term performance parameters. Thus, it cannot be used to study the flow of material through the plant or the effects of operational policies on manufacturing cost. Such studies require dynamic models and more detailed input data; therefore, they are most readily applied to existing plants or plant designs at the definitive or detailed estimate level [114]. Since the goal of this chapter is to estimate the manufacturing cost of solar cell design processes while they are in the research and development stage, a dynamic model is not appropriate to the task at hand.

5.1.2 OPERATING COSTS AND COMPUTATION OF MANUFACTURING COST

As with capital cost estimation, estimation and classification of operating costs can be complicated. However, cost engineers have developed a basic framework around which to estimate and classify these costs in the early stages of an engineering project [115]. Many variations on the basic method exist, so it is necessary to be explicit about the details of the calculation. As with the capital cost estimate, a number of assumptions and simplifications are required to evaluate a production process while it is still in the research and development phase.

The elements required to compute the COGS, total product cost, and selling price of a manufacturing product are shown in Figure 5.1. To build the model, each of the elements in the diagram must be re-cast in a fashion such that the cost of each can be estimated from available information. In other words, it may not be possible to estimate indirect labor costs as a classification unto itself, but they may be distributed between multiple categories.

The complete classification of operating costs assumed by the model is shown in Table 5.2.

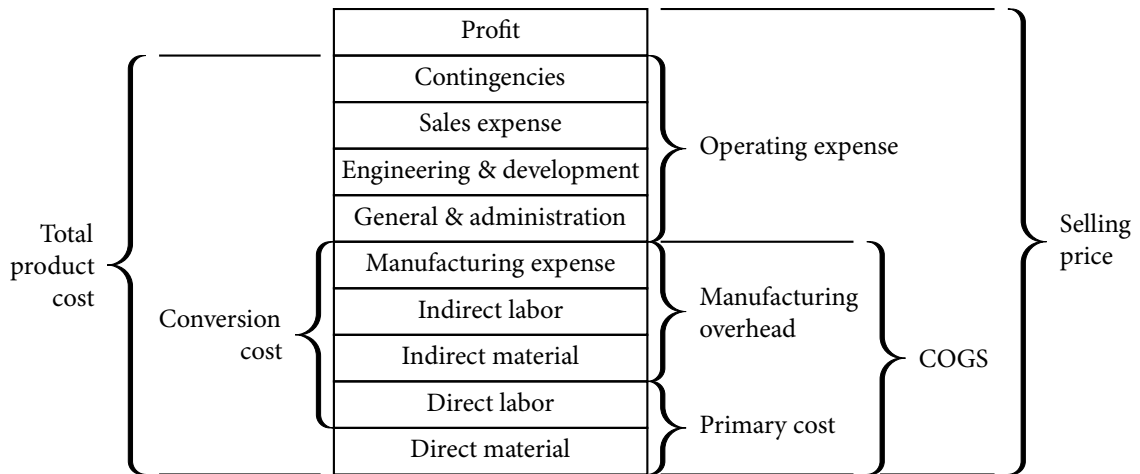


Figure 5.1: Elements of manufacturing and selling price of a manufactured product (after Tanner [116]).

Note that it does not have a one-to-one correspondence with the elements in Figure 5.1; however, all elements are counted. For example, indirect labor is distributed between maintenance & repair and laboratory charges, and indirect material is distributed amongst these plus operating supplies. These categories are more easily estimated than the ones shown in Figure 5.1.

The estimated expenses associated with each of these classifications are derived from the process specification. Plant sizing, which will be detailed in section 5.2.2, yields capital equipment, raw material, and direct labor requirements, and the remaining operating expenses follow from these. They are estimated primarily using economic analysis methods borrowed from the chemical processing industry, but model validation indicates that these methods are suitable for the present task.

The results of this analysis can be entered into an income statement to estimate gross and net profits, income tax liability, cash flows, and return on investment. A sample income statement is shown in Table 5.3. If the statement pertains to a 25 MW_p PV plant, the revenue in the table corresponds to a wholesale selling price of \$3.00/W_p and the cost of goods sold (COGS) corresponds to a direct manufacturing cost of \$2.50/W_p. Operating expenses amount to \$0.10/W_p. The income statement in Table 5.3 follows closely the format of corporate

Table 5.2: Classification of PV module manufacturing plant operating costs used by the model.

<i>Direct manufacturing expenses (DME)</i>
Raw materials
Operating labor
Direct salaries & overhead
Maintenance & repair
Operating supplies
Laboratory charges
<i>Fixed manufacturing expenses (FME)</i>
Depreciation
Local taxes & insurance
Overhead
<i>General manufacturing expenses (GME)</i>
Administration
Selling costs
Research & development
Royalties

income statements issued by publicly held corporations and is calculated as follows:

1. Revenue is shown on the first line and determined from the wholesale price of the PV modules produced in the plant.
2. The cost of goods sold, which is equal to the sum of the direct and fixed manufacturing expenses in Table 5.2, is subtracted from revenues to determine gross profit.
3. Operating expenses, which are equal to the general manufacturing expenses in Table 5.2, are subtracted from gross profit to determine operating income.
4. Taxable income is determined by subtracting depreciation from operating income.
5. If taxable income is less than zero, income tax liability is zero. Otherwise, taxable income is multiplied by the applicable tax rate to compute income tax liability.
6. Net profit is equal to operating income minus income tax liability.
7. Cash flow is equal to net profit plus depreciation.

Table 5.3: Illustrative income statement example for a PV module manufacturer (all figures in thousands of dollars).

Revenue	75000.0
Cost of goods sold (COGS)	62500.0
Gross profit	12500.0
Operating expenses	2500.0
Operating income	10000.0
Depreciation	4250.0
Taxable income	5750.0
Income tax	2012.5
Net profit	7987.5
Cash flow	12237.5

Gross and net profit are sometimes expressed in terms of percentage of revenue to aid comparison between companies, since revenue differs from company to company.

Return on investment (ROI) is:

$$\text{ROI} = \frac{\text{net profit}}{\text{capital investment}}, \quad (5.1)$$

and the payout period (PP) — that is, the time required to recover the initial capital investment — is:

$$\text{PP} = \frac{\text{capital investment}}{\text{cash flow}}. \quad (5.2)$$

If the capital investment that produced the sample income statement shown in Table 5.3 is \$45 million, then ROI is 17.75% and the payout period is 3.68 yr.

5.2 MODEL STRUCTURE

The model is segmented into three phases: specification, sizing, and evaluation. In the specification phase, which is described in greater detail in section 5.2.1, the process flow diagram is translated into a series of input files that the model can understand. These files specify the function of each step of the process and establish its equipment, raw material, and labor requirements. They also specify the order in which the steps are carried out and the intended production volume of the plant.

In the sizing phase, the desired production volume is translated into throughput requirements for each step. Once the model determines the number of (for example) modules, strings, or wafers that a particular step must handle, it calculates the number of pieces of equipment the step will require. From that, labor and raw material requirements may be quantified. This phase is detailed in section 5.2.2.

During evaluation, which is described in section 5.2.3, the model estimates the costs associated with each of these items. The sum total of the equipment costs is factored to yield an estimate of capital required to build the plant, while material and labor costs are used to estimate operating expenses. Finally, the capital and operating expenses are combined to produce an estimate of the product's manufacturing cost.

5.2.1 PROCESS SPECIFICATION

In most cases, the process specification may be taken from the process flow diagram. The process flow diagram should begin with a starting material, such as silicon feedstock or wafers, finish with a final product, such solar cells or PV modules, and list each significant activity in the fabrication process. For purposes of the model, a "significant activity" is defined as any process step requiring a piece of major equipment.

Process specification is a two-step process. First, the user specifies plant characteristics. These include:

1. Annual plant capacity, in peak watts.
2. Product capacity, in peak watts (e.g., $100 W_p$ if the plant produces $100-W_p$ modules).
3. Nominal solar cell power output, in peak watts.
4. Nominal solar cell thickness, in micrometers.
5. The number of solar cells per PV module.
6. The number of silicon bricks obtained from a single ingot.
7. The required production sequence in the form of a list of process steps.

The number of cells per module is not required if the modeled plant does not produce modules, and the number of bricks per ingot is not required if the plant purchases wafers instead of fabricating them in-house.

Process steps are described in a modular, stand-alone manner that completely encapsulates the step. These encapsulated descriptions are referred to as *workstations*, and each workstation defines a single process step in the production sequence. An emitter diffusion process step, for example, requires wafers to diffuse plus raw materials and labor to support the diffusion. It produces diffused wafers. All of these things must be present in the workstation specification. The items received from the previous workstation in the process are referred to as *input product*, and the items sent to the next workstation in the process are referred to as *output product*; in the emitter diffusion example, these correspond to the undiffused and the diffused wafers, respectively.

Complete specification of a workstation consists of the following elements:

1. Equipment requirement, including the cost and throughput capacity of a single piece of the required equipment and an estimate of uptime (taking into account both scheduled and unscheduled maintenance).
2. Raw material requirements, expressed as the quantity required per piece worked (e.g., per wafer or per module).
3. Labor requirements, expressed as the number of operators required per machine per shift.
4. The amount of material etched or lost to kerf at the process step, in micrometers.
5. The process yield of the step.
6. Input type, which refers to the type of piece being worked (e.g., wafer, cell, or module).
7. Output type, which refers to the type of piece produced for the next process step (e.g., wafer, cell or module).

The first step of the process takes a null input type and computes all material needs from the raw material requirements.

Each plant specification and process step must be defined clearly in a manner that the program can read and use. This is revisited in section 5.4, which describes the program's implementation.

5.2.2 THROUGHPUT AND EQUIPMENT SIZING

The throughput rates and equipment sizes required to achieve the plant's annual production capacity target are estimated using an algorithm originally developed for the SAMICS project. The original SAMICS algorithm is described in detail in [117]; this section describes it as adapted for the present model, though the differences are few and related primarily to program structure rather than theory.

Sizing a production step requires information about the quantity of product that must be accommodated by the step. As noted above, plant capacity is designated in peak watts. This agrees with conventional terminology used within the PV industry to describe plant size, but it is not a useful measure for discussing plant throughput. Therefore, the desired production volume for the plant must be converted from peak watts to a number of product units. For example, if the plant specification designates a 25 MW_p plant that produces PV modules rated at 100 W_p , the production volume is converted from 25 MW_p to 250 000 modules.

Once the required annual number of production units is known, the model works backward through the process sequence to determine the throughput required at each step. If the aforementioned plant operates 330 days/yr (7920 hr/yr) then it must produce modules at the rate of 31.6 per hour. Each workstation in the plant that processes modules must be sized to handle that rate of throughput. If each module contains 36 solar cells, the cell-processing workstations must be sized to handle a throughput of 31.6×36 or 1364 cells/hr. The sizing algorithm continues in this manner through the process specification until it has determined the quantity and size of the workstations required at each production step. This process is detailed below.

5.2.2.1 Machine Requirements

The model determines the number of machines required at each process step from the annual number of machine operating hours required to achieve the throughput required of the step. From this, the number of machines required is calculated from the number of annual operating minutes available from a single machine.

The required number of operating hours is:

$$R = \frac{Q}{T}, \quad (5.3)$$

where Q is the number of units the workstation must produce each year and T is the throughput rate of a single machine in units/hr. The plant production target determines Q as described above, while T is a design characteristic of the machine that is generally obtained from the equipment manufacturer's specifications. Thus, if a process step must complete a million units annually and the throughput rate of a single machine is 500 units/hr, $R = 2000$ hr/yr.

The number of machines required at each process step is determined from the number of hours the machine will actually operate each year. This, in turn, is determined from the plant's production schedule, the time required for scheduled and unscheduled maintenance on the machine, and the fraction of plant capacity at which the plant operates. The actual number of hours that a single machine operates in year is determined from:

$$A = FPN_sH(DW - E), \quad (5.4)$$

where F is the machine's duty cycle (taking into account maintenance, reliability, setup and cleaning time, etc.); P is the fraction of maximum capacity at which the plant operates; N_s is the number of shifts the plant operates per fiscal day; H is the number of fiscal hours per shift; D is the number of fiscal days per fiscal week; W is the number of fiscal weeks per fiscal year (accounting for scheduled shutdown periods, if any); and E is the number of plant holidays per fiscal year. Typical values for each of these parameters are shown in Table 5.4.

From the required number of operating hours, R , and the actual number of hours that a single machine operates in a year, A , the number of machines required to produce Q units of

Table 5.4: Typical values used for calculating the number of hours a machine operates each year.

Variable	Description	Typical value
F	Duty cycle	0.5–0.9
P	Operating capacity fraction	1.0
N_S	Number of shift per fiscal day	1, 2, or 3
H	Fiscal hours per shift	8
D	Fiscal days per fiscal week	5 or 7
W	Fiscal weeks per fiscal year	50–52
E	Plant holidays per fiscal year	0–10

product is simply:

$$n = \frac{R}{A}. \quad (5.5)$$

Note that this equation typically produces a non-integer value of n . Since it is not possible to purchase a fraction of a machine, the number of machines required for purposes of estimating the plant's capital cost is:

$$N = \lceil n \rceil, \quad (5.6)$$

where the brackets denote the ceiling function. Note that the difference between n and N translates into idle time for the machine in question. Since an idle machine requires no operator, n remains useful for determining a machine's labor requirements.

The average number of machines idle at any given time can be estimated by calculating the number of machines that would be required if there were no downtime and no extra plant capacity ($F = P = 1$):

$$M = \frac{R}{N_S H (DW - E)}. \quad (5.7)$$

The number of idle machines is then:

$$I = N - M. \quad (5.8)$$

Since I accounts not just for downtime due to excess capacity, but for all reasons, it is possible — even likely — to have $I > 0$. This might occur for machines that have long setup

times or those that require frequent cleaning. Furthermore, it is an average. Depending on how a plant schedules maintenance, the bulk of the downtime may occur simultaneously for all machines during a planned shutdown. Therefore, I is not a measure of how smoothly a process might run, but it can help in detecting machines that are over-sized for the process or desired production volume.

5.2.2.2 *Input Product Requirement*

The amount of input product required by a process step depends on the quantity of input product required to produce a single item of output product. It also depends on the process yield of the step. It is expressed:

$$Q_{\text{in}} = \frac{yQ_{\text{out}}}{c}, \quad (5.9)$$

where y is the process yield and c is the quantity of input product required to produce a single item of output product.

The value of c is dependent upon the types of products represented by Q_{in} and Q_{out} . If, for example, Q_{out} is a quantity of PV modules and Q_{in} is a quantity of solar cells, c is equal to the number of cells per module. The value of c defaults to unity and changes only in steps where silicon ingots are converted to bricks, bricks are sawn into wafers, or cells are interconnected to form modules.

5.2.2.3 *Raw Material Requirements*

After computing the number of machines required to complete a process step, the model computes raw material requirements. These are specified in terms of the amount of material required per unit input product processed. Thus, a raw material specification for a screen printing step might require, for example, 0.12 g of silver contact paste per wafer processed.

The annual quantity required of any raw material is simply:

$$q_{\text{mat}} = \dot{q}Q_{\text{in}}, \quad (5.10)$$

where \dot{q} is the quantity required per unit input product processed (e.g., the aforementioned 0.12 g/wafer). Values for \dot{q} , which should be specified in units of quantity per ingot, brick,

wafer, cell, or module, are determined from process requirements and manufacturer data for the machine.

5.2.2.4 Labor Requirements

The amount of labor required to complete a process step depends on the number of personnel required to operate and support a single machine, the number of machines that require operators, and the number of shifts the plant operates. The number of personnel required is:

$$q_{\text{lab}} = rnS, \quad (5.11)$$

where r is the number of personnel required per machine, n is the number of machines required as computed from equation (5.5), and S is the shift multiplier. Note that more than one type of laborer can be specified for a piece of equipment, each with its own values of r and, consequently, q_{lab} .

The shift multiplier represents the effective number of shifts the plant operates. It is based upon the actual number of shifts the plant operates, but includes an adjustment to account for the additional personnel who must be hired to work weekend and swing shifts and cover for those who are sick or on vacation. It is computed from:

$$S = \frac{N_s H(DW - E)}{h(dw - e - v - a)}, \quad (5.12)$$

where h is the number of working hours per person per shift, d is the number of working days per person per working week, w is the number of working weeks per person per fiscal year, e is the number of paid holidays per fiscal year, v is the average number of paid vacation days per person per fiscal year, and a is the average number of paid personal days per person per fiscal year. These variables, along with typical values, are summarized in Table 5.5 (recall that the variables in the numerator were already summarized in Table 5.4 on page 126). The numerator of equation (5.12) represents the number of hours the plant operates each year, while the denominator represents the number of hours the average worker comes to work during the fiscal year.

Table 5.5: Typical values used for calculating the shift multiplier.

Variable	Description	Typical value
h	Working hours/person/shift	8
d	Working days/person/week	5
w	Working weeks/person/year	50–52
e	Paid holidays/year	0–10
v	Paid vacation days/person/year	10–15
a	Paid personal days/person/year	50–52

5.2.3 MANUFACTURING COST EVALUATION

With plant sizing complete, the capital equipment requirements and annual material and labor requirements are known. This is most of the information required to compute the PV module manufacturing cost. However, a few additional pieces of information are required:

- Indirect capital costs, including the costs of buildings and service utilities required to support the manufacturing operation.
- Maintenance costs associated with manufacturing equipment.
- Direct overhead costs.

It is also prudent to include a contingency to cover unanticipated expenses.

These costs may all be estimated using procedures developed by the chemical processing industry [113]. However, applying these guidelines to PV manufacturing plants tends to significantly overestimate capital requirements. This is in large part because they were devised with custom-built chemical processing equipment in mind, rather than the “off-the-shelf” equipment typically used for processing semiconductors, including solar cells [118]. As a result, the guidelines make allowances for engineering and installation costs that are not incurred in PV plant construction.

The best way to address this would be to evaluate actual PV plant construction costs and determine appropriate factors for the PV industry. This is not only an enormous undertaking, it is also impractical since such information is not readily available. An alternative approach to estimating indirect capital costs is inspired by the concept of *Lang factors*, which are

sometimes used for rapid estimates of chemical plant capital costs. The concept was developed in the 1940s by H. J. Lang, who noted that the total capital cost of a major expansion to an existing chemical plant tended to be a constant multiple of major equipment cost for certain classes of chemical plants [113].

A Lang-like capital cost factor for the PV industry can be derived using data published by turnkey PV production line manufacturer Spire. These data are comprised of estimates of PV plant capital cost as a function of production volume for a standard crystalline silicon PV module manufacturing line [119]. This is the method used in the model to estimate indirect capital expenditures. It is derived and discussed in detail in section 5.3.1; it is used here without further comment.

The following sections address the manner in which each of the PV module manufacturing cost components is calculated. Recall that these components were summarized in Table 5.2 on page 120.

5.2.3.1 Capital Cost and Depreciation

Capital costs affect PV module manufacturing economics in two ways. The first way is through depreciation. In principle, capital investments are made once, when the plant is constructed. However, because the capital investment has value and is being kept by the company, rather than sold to customers, only its year-to-year decline in value may be considered an operating expense. For example, if the value of a piece of equipment costing \$100 000 declines to \$80 000 after one year, only \$20 000 may be charged to operating expenses. Depreciation is this decline in value.

The second way in which capital costs affect manufacturing economics is in determining the minimum price that must be charged to achieve a desired return on investment. When capital investment is high, larger profit margins are required to achieve the same return on investment as when capital investment is low. In other words, the lower the capital cost, the lower the profit margin need be to produce the same return on investment. While this does not factor in to the manufacturing cost estimate, it *does* factor in to profitability.

The total capital cost of the plant is computed by summing the costs of each piece of

major equipment required, as determined in section 5.2.2.1, and multiplying by the capital cost factor:

$$\begin{aligned} C_{\text{tot}} &= \kappa \sum_{i=1}^N C_{\text{me},i} \\ &= \kappa C_{\text{me}}, \end{aligned} \quad (5.13)$$

where $C_{\text{me},i}$ is the capital cost of the major equipment in step i and κ is the capital factor:

$$\kappa = 3.4P^{-0.095}. \quad (5.14)$$

In equation (5.14), P is the plant capacity in MW_p . (As mentioned previously, the expression for the capital cost factor κ is derived in section 5.3.1.)

To encourage capital investment, depreciation is tax-deductible in most countries. Because of this, the manner in which it is calculated is strictly regulated. The time value of money dictates that the faster an item depreciates, the greater the return on investment. For this reason, governments impose depreciation schedules on companies to ensure reasonable rates of depreciation. Currently, the United States Internal Revenue Service requires that semiconductor manufacturing equipment be depreciated over a period of five years [120].

Accelerated depreciation schedules are available, and they are generally advantageous in that they provide for greater tax deductions in the early years of the equipment's life (i.e., they generate greater return sooner). However, cost engineers warn against using accelerated depreciation schedules for engineering calculations, particularly at the level of a factor estimate. There are several arguments in support of this position. One is that the cost estimate contains enough uncertainty that accelerated depreciation is inappropriately precise. Another is that the choice of depreciation schedule is a management decision that should be handled by accountants rather than engineers, and to presume an accelerated schedule that management does not wish to use will skew the cost analysis. Finally, cost engineers have noted that most cost estimates do not account for the inevitable rise in maintenance and repair expenses as equipment ages, and some have suggested that the sum of accelerated depreciation and rising maintenance costs in a real plant is roughly constant from year to

year [115]. Therefore, the model follows their recommendations and uses unaccelerated straight-line depreciation.

The model leaves the rate of depreciation up to the user. Throughout this thesis, depreciation is calculated at a rate of 23.5% of major equipment cost. The basis for this figure is the 20% rate of depreciation corresponding to a five-year straight-line depreciation of major equipment. However, plant buildings, office furniture, and computer equipment are also depreciable. The bulk of these additional capital expenditures is in buildings, which are assumed to depreciate over 20 years. Since indirect capital cost C_{ind} is simply the total capital cost C_{tot} minus the direct capital cost C_{me} , by equation (5.13) it is equal to:

$$\begin{aligned} C_{\text{ind}} &= C_{\text{tot}} - C_{\text{me}} \\ &= (\kappa - 1)C_{\text{me}}. \end{aligned} \quad (5.15)$$

Some of these indirect costs are for land, engineering, construction, and other non-depreciable capital expenses. Conservatively (on the basis of chemical industry rules of thumb) estimating additional depreciable costs at 50% of C_{ind} and depreciating in a straight line over 20 years gives an additional 3.5% depreciation for $\kappa = 2.4$, which corresponds to a plant capacity P of 38 MW_p. Since the rate of depreciation calculated in this manner varies only from 23.0% at 100 MW_p to 23.8% at 25 MW_p and depreciation is ultimately responsible for only a small part of the manufacturing cost, a fixed value of 23.5% is used throughout this thesis.

5.2.3.2 Raw Material Cost

Raw material cost is estimated by first compiling the raw material requirements from each workstation into a master list. Once the plant-wide total required quantity of all materials is known, the price of each material is determined with the aid of a user-specified material cost catalog. The data in the catalog are used to compute a unit price for each material, and the unit price is then multiplied by the required quantity to compute the total cost of the material. The total raw material cost is simply the sum of the costs for each raw material.

The unit price for a given material can be affected by economies of scale and is computed using the relation:

$$u_{\text{mat}} = a q_{\text{mat}}^b, \quad (5.16)$$

where a and b are empirically determined coefficients and m is the required quantity of the material. The total cost for the required material is then:

$$C_{\text{mat}} = q_{\text{mat}} u_{\text{mat}}. \quad (5.17)$$

The determination of the coefficients a and b and their values for specific materials are detailed in section 5.3.

5.2.3.3 *Operating Labor Cost*

The number of laborers required for each production step is computed using equation (5.11). These are summed to determine the total number of laborers required to staff the plant. Then the annual salary owed to each laborer is looked up in a user-specified labor cost catalog. The wages listed in the catalog are used to compute the total cost of direct operating labor. The annual cost of operating labor is:

$$C_{\text{lab}} = q_{\text{lab}} u_{\text{lab}}, \quad (5.18)$$

where u_{lab} is the annual wage paid to a single laborer.

As described in section 5.2.2.4, the model is capable of handling laborers of various descriptions, each receiving a different wage. However, for purposes of this thesis, only equipment operators are considered in determining operating labor costs. Salaries for personnel working on the production line, such as supervisors and engineers, and wages for maintenance personnel are computed separately. According to the U.S. Bureau of Labor Statistics, the average equipment operator in the semiconductor industry in 2006 was paid a wage of about \$35 000 [121]; unless otherwise stated, this is the figure used for computing operating labor costs throughout this thesis.

5.2.3.4 *Direct Salaries*

The number of supervisors, engineers, and other salaried employees working on the production is dictated by the amount of direct labor hired to operate the production line. Therefore,

direct salaries are computed as a fixed percentage of operating labor. The percentage is typically in the range of 10% to 20%. The calculations in this thesis use a relatively conservative value of 18%.

5.2.3.5 Maintenance and Repair

Maintenance and repair costs are dictated by the amount of equipment and other real property present in the plant. These costs tend to be about 4% to 8% of depreciable capital. Unless otherwise stated, the calculations in this thesis assume that maintenance and repair costs are 6% of depreciable capital.

5.2.3.6 Operating Supplies

The cost of operating supplies is proportional to the cost of maintenance and repair. This typically ranges from 10% to 20% of maintenance and repair costs; unless stated otherwise, this thesis assumes a value of 15%.

5.2.3.7 Laboratory Charges

Laboratory charges pertain to testing required to maintain product quality and monitor process characteristics. They are expressed as a percentage of operating labor, typically between 10% and 20%. Unless otherwise stated, this thesis assumes laboratory charges amount to 15% of operating labor.

5.2.3.8 Local Taxes and Insurance

This category refers to property and other local taxes, as well as the cost of obtaining insurance for the plant. Since property taxes are levied upon real estate value and insurance covers the value of real property, local taxes and insurance are proportional to depreciable capital costs, usually to the tune of a few percent. This thesis assumes 3% of depreciable capital for local taxes and insurance.

5.2.3.9 *Overhead*

Overhead covers the cost of health insurance and other worker benefits, as well as various costs related to the hiring and maintenance of employees. It is proportional to the total cost of all of the direct labor required by the plant, including salaried employees and maintenance personnel. A commonly suggested value for overhead is 70% of the sum of operating labor, maintenance and repair, and direct salaries. This is the value used throughout this thesis unless otherwise noted.

5.2.3.10 *Administration*

Administrative costs are proportional to revenue. From a cost engineering perspective, however, revenue cannot be reliably projected. Therefore, administrative costs are calculated as a percentage of the total cost of manufacturing, which is a reliable proxy for revenue in a competitive market. This thesis assumes administrative costs of 2% of the total cost of manufacturing (the sum total of direct, fixed, and general manufacturing expenses).

5.2.3.11 *Selling Costs*

Selling costs are also proportional to revenue and, like administrative costs, are computed in the model as a percentage of the total cost of manufacturing. In the current PV market, most PV companies have already sold out their entire production runs well into the future — more than a year, in some cases — and sales staffs are thin. Thus, selling costs are assumed to be quite low at 1% of the total cost of manufacturing.

5.2.3.12 *Research and Development*

Research and development is typically budgeted on the basis of revenue. Since different companies place different emphasis on R&D there is no “correct” value to use here, but in the chemical industry it typically ranges from 0% to 10% of revenues. This thesis uses 5% of total manufacturing cost unless otherwise indicated.

5.2.3.13 Royalties

If the process being modeled uses a patented technology, royalties may need to be paid. These are typically expressed as a percentage of revenue. Unless otherwise specified, this thesis assumes that the modeled process does not contain any patented elements and sets royalties to zero.

5.2.3.14 Total Manufacturing Cost

The sum of all of these categories equals the total manufacturing cost. Table 5.6 summarizes the typical range of values for each cost category along with the baseline values assumed for the modeling performed in this thesis. Note that the baseline values may be used to express total manufacturing cost C_{mfg} analytically in terms of total plant material cost C_{mat} , total plant operating labor cost C_{lab} , and the sum of the capital costs of all major equipment C_{me} :

$$\begin{aligned} C_{\text{mfg}} &= C_{\text{mat}} + C_{\text{lab}} + 0.18C_{\text{lab}} + 0.06C_{\text{me}} + 0.15(0.06C_{\text{me}}) + 0.15C_{\text{lab}} \\ &\quad + 0.235C_{\text{me}} + 0.03C_{\text{me}} + 0.70(C_{\text{lab}} + 0.18C_{\text{lab}} + 0.06C_{\text{me}}) + 0.02C_{\text{mfg}} \\ &\quad + 0.01C_{\text{mfg}} + 0.05C_{\text{mfg}} \\ &= 1.087C_{\text{mat}} + 2.344C_{\text{lab}} + 0.409C_{\text{me}}. \end{aligned} \tag{5.19}$$

The coefficients of the resulting equation are, of course, dependent upon the assumptions used for the various manufacturing cost categories and will change — potentially significantly — if different assumptions are used. Nonetheless, some interesting observations can be made from this expression.

Note that while equation (5.19) implies that manufacturing cost is most sensitive to the cost of direct operating labor, this does *not* mean direct operating labor is the most significant cost component in PV module manufacturing. In fact, it will be shown later in the chapter that raw material costs are the most significant by virtue of the fact that $C_{\text{mat}} \gg C_{\text{lab}}$. However, the large coefficient of C_{lab} indicates that increases in labor costs should be avoided whenever possible, even if it means increasing material or capital costs. Of particular interest is the large difference between the coefficients of C_{lab} and C_{me} , since it implies that small reductions

Table 5.6: Operating cost factors for computation of PV module manufacturing cost.

Factor	Typical range	Values used in baseline model
<i>Direct manufacturing expenses (DME)</i>		
Raw materials	Direct calculation	Direct calculation
Operating labor	Direct calculation	Direct calculation
Direct salaries	10–25% of operating labor	18% of operating labor
Maintenance & repair	2–10% of depreciable capital	6% of major equipment cost
Operating supplies	10–20% of maintenance & repair	15% of maintenance & repair
Laboratory charges	10–20% of operating labor	15% of operating labor
<i>Fixed manufacturing expenses (FME)</i>		
Depreciation	Varies	23.5% of major equipment cost
Local taxes & insurance	1.4–5.0% of depreciable capital	3% of major equipment cost
Overhead	50–70% of operating labor, direct salaries, and maintenance & repair	70% of operating labor, direct salaries, and maintenance & repair
<i>General manufacturing expenses (GME)</i>		
Administration	1–3% of revenues	2% of total manufacturing cost
Selling costs	1–3% of revenues	1% of total manufacturing cost
Research & development	0–5% of revenues	5% of total manufacturing cost
Royalties	0–6% of revenues	0% of total manufacturing cost

in labor costs can be traded off for relatively large increases in capital cost; in other words, automation is likely to be highly cost-effective (depending, of course, on the cost of the automated equipment).

5.3 ECONOMIES OF SCALE

An important factor in assessing the economics of any manufactured good is the economy of scale. Roughly stated, this is the principle that the unit cost of a manufactured good decreases as the scale of production of that good increases. It applies to both raw materials and equipment, albeit in different ways, and to some degree it can even apply to overhead costs on labor (e.g., the per-employee cost of health insurance decreases as the size of the group insured increases). The end result is that the larger a manufacturing plant becomes, the lower the per-unit manufacturing cost of its products.

Since the scale of PV manufacturing is rapidly increasing it is important to understand its affect on PV module economics. It has been estimated that increasing the scale of manufacturing from 25 MW_p/yr to 100 MW_p/yr can itself, with no change to device design, reduce

PV module manufacturing cost by 10% [51]. Another study suggests that increasing scale to 500 MW_p/yr offers as much as a 25% reduction in manufacturing cost, though that study assumed vertical integration of silicon feedstock and glass production in addition to simple economies of scale [47, 54].

The model developed in this chapter is designed to capture as much of these economies of scale as possible. Available information on major equipment costs and raw materials was fit to a power law relationship of the form:

$$u = av^b, \quad (5.20)$$

where u is the unit price for a material or piece of equipment, v is a material quantity or equipment throughput rate, and a and b are regression coefficients. The details and origins of this relationship is described separately for materials and equipment in the following sections.

5.3.1 ESTIMATING CAPITAL COSTS

Capital costs are incurred for the equipment required to manufacture the PV wafers, cells, and modules, as well as the buildings that house the equipment and all support facilities. A number of methods have been developed to aid in estimating these costs, most notably by the chemical engineering industry; an overview of these is given in [113]. For the PV industry, costs of capital equipment may be estimated with the aid of regular market surveys of production equipment published in *Photon International*, an industry trade publication.

In general, manufacturing plant designers can choose from multiple pieces of equipment to perform a given manufacturing task. For example, consider a plant that must deposit silicon nitride antireflection coatings onto 2000 wafers per hour. More than one plasma-enhanced chemical vapor deposition (PECVD) system is available on the market that is capable of this task. Furthermore, PECVD systems capable of diffusing 1000 wafers/hr are also available and the plant can simply use two of them. It can even opt for four systems, each with a throughput rate of 500 wafers/hr. This raises the question of how to determine the capital cost of the required equipment.

In reality this choice is governed by a number of factors. A plant may spend extra to purchase a PECVD system with enhanced controls, loading and unloading mechanisms, or gas-handling capabilities. It might opt for a more basic system to reduce the cost of the machine. However, for purposes of cost estimation the only thing that is required is a reasonably accurate representative price. Since the model performs a factor estimate and is only +30% to -20% accurate in its capital estimate, fluctuations due to considerations such as these are not important. It can be shown, however, that for most equipment the purchase price is strongly dependent upon throughput.

As a result of this relationship, the cost per unit throughput of a piece of manufacturing equipment tends to drop as throughput increases; that is, equipment cost scales with throughput. As a result, in the PECVD example above the plant engineer might find a PECVD system costs \$925 000, \$1.475 million, and \$2.350 million for throughputs of 500, 1000, and 2000 wafers/hr, respectively. If the plant engineer chooses the first unit the capital spent on PECVD systems will be \$3.700 million; for the second unit, \$2.950 million; and for the third unit, \$1.475 million. All three choices provide the same performance, but the third option, which has benefited from economies of scale, provides the lowest cost per unit throughput.

In section 5.3.1, a procedure is outlined for estimating major equipment cost as a function of throughput. Equipment price estimates as a function of throughput are estimated for all major pieces of PV module manufacturing equipment using this procedure in combination with market survey data from *Photon International*. Detailed results of this analysis appear in Appendix C.

As indicated previously in section 5.2.3.1, major equipment is but one element of the total capital cost of the plant. The chemical engineering industry has established guidelines for estimating the total capital cost from the cost of major equipment, but these methods are not directly applicable to PV and tend to overestimate capital requirements. The reason for this is chiefly that chemical processing equipment is typically built on-site from raw materials and minimally prefabricated parts, while PV manufacturing equipment is usually built off-site nearly to completion and shipped with minimal installation work required. As a result, the guidelines contained in the chemical engineering literature make provisions for construction

activities that are not applicable to PV plants.

Section 5.3.1.2 describes the derivation of a Lang-factor-like capital cost factor to estimate the plant's total capital cost as a function of plant size. With the aid of published data used for calibration, it will be shown that this factor decreases as plant capacity grows. As a result, increasing plant capacity provides a double benefit to capital costs: First, the increase in throughput produces a reduction in the per-unit-throughput cost of capital equipment. Second, the increase in plant capacity reduces the capital cost factor κ calculated in equation (5.14). Since the total capital equipment cost C_{me} is multiplied by this factor to determine the total capital cost for the entire plant, a reduction in κ also reduces the amount of capital required for the plant.

5.3.1.1 Capital Equipment Cost as a Function of Throughput

In general, as the throughput of a piece of equipment increases so does its price. However, the increase in price is generally not a linear function of the increase in throughput. Early investigations into the nature of economies of scale noted that a doubling in the throughput of some equipment increased the price by a factor of only 1.5, or $2^{0.6}$. Because of the value of the exponent, this relationship was dubbed the "six-tenths rule." The general form of this relationship is:

$$\frac{P_2}{P_1} = \left(\frac{T_2}{T_1} \right)^b, \quad (5.21)$$

where P_1 and T_1 are the price and throughput, respectively, of one piece of equipment, P_2 and T_2 are the price and throughput, respectively, of the other piece of equipment, and b is the exponent that encapsulates the relationship between price and throughput. While b is nominally equal to 0.6, its actual value varies depending on the type of equipment studied; nonetheless, the name has stuck and the relationship is generally referred to as the six-tenths rule regardless of the actual value of the exponent.

Using the aforementioned *Photon International* market surveys, it is possible to derive this relationship for equipment dedicated to all phases of the PV module manufacturing process. This has two major advantages:

Table 5.7: Nominal throughput and equipment cost for PECVD deposition systems.

Manufacturer	Model	Nominal Throughput (wafers/hr)	Cost (\$)
Centrotherm	E 2000 HT 320-4	710	1810000
	E 2000 HT 410-4	1050	1940000
MVSystems	—	475	756000
OTB	DEPx	960	1690000
	DEPx-plus	1440	1905000
Roth & Rau	SINA XS	345	689000
	SINA XS	430	835000
	SINA S	655	1130000
	SINA M	940	1250000
	SINA L	1170	1570000
	SINA L	1650	1810000
	SINA XL	2250	2180000
Semco	TWYN	450	707500

1. It allows capital equipment costs to be expressed as a representative value for a particular *type* of equipment instead of tying the calculations to a particular *piece* of equipment.
2. Expressing capital cost as a function of throughput inherently provides a means for studying the effects of economies of scale on PV module price.

This relationship is derived here for PECVD systems as an example to illustrate the procedure, which consists of a simple statistical regression analysis, and clarify how capital costs are determined in this manner.

Cost and throughput data from the 2006 market survey on PECVD systems are shown in Table 5.7 [122]. Each system has a range of wafer sizes and thicknesses that it is capable of handling, so which of the systems in the survey is appropriate to include in the analysis is dependent upon wafer dimensions; unless otherwise stated, this thesis always presumes 156-mm wafers approximately 175 μm to 250 μm in thickness. Accordingly, the throughput listed in Table 5.7 is the nominal rate reported by the manufacturer for 156-mm wafers. Where only a maximum rate was reported it was assumed to be equal to the nominal rate.

The equipment cost is plotted as a function of nominal throughput on a log-log scale in Figure 5.2. Consistent with the power relationship anticipated in equation (5.21), the data

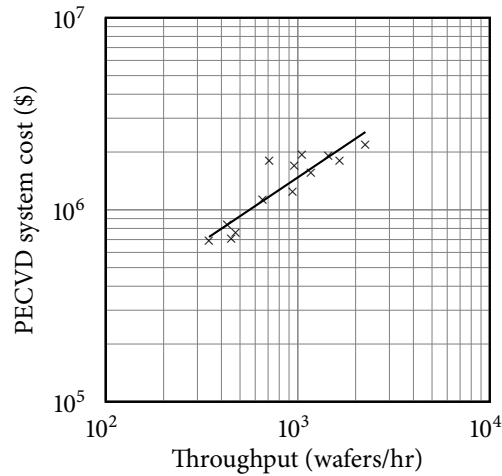


Figure 5.2: Cost of PECVD deposition equipment as a function of nominal throughput for 156-mm wafers.

form a nearly straight line on the graph. Power regression of these data yields:

$$P = 14307T^{0.6711} \quad 345 \leq T \leq 2250, \quad (5.22)$$

where P is the equipment price for throughput T . Equation (5.22) is denoted by the solid line in Figure 5.2.

Note that T is limited to the interval 345 wafers/hr to 2250 wafers/hr, which are the low and high throughput values from Table 5.7. Extrapolating beyond this interval implicitly assumes that larger or smaller machines will have the same economies of scale of existing machines, which may or may not be the case. In many cases, equipment may have a fundamental limitation — difficulty maintaining a uniform temperature over a very large area, for example — that precludes attaining higher throughput rates with the same economies of scale of smaller equipment. While no such examples will be seen in this thesis, practical examples do exist in the chemical engineering literature [118].

Results for all of the equipment types covered in the *Photon International* market surveys of 2006 are summarized in Table 5.8. Details of the derivation for each type of equipment are presented in Appendix C. The capital cost of a piece of equipment is calculated as follows:

Table 5.8: Regression coefficients for computing representative capital equipment costs.

Equipment type	Unit	Throughput		Regression coefficients	
		Min	Max	Intercept	Exponent
Band saw	bricks/hr	2.29	4	597853	0.1395
Wire saw	bricks/hr	0.19	1.33	733652	0.2986
Wet bench (saw damage removal) ^a	wafers/hr	1200	4000	1158600	0
Wet bench (phosphorus glass removal)	wafers/hr	1200	4000	10206	0.5128
Wet bench (surface texturing) ^a	wafers/hr	1200	4000	1175300	0
Tube furnace ^a	wafers/hr	150	2000	766700	0
Inline furnace	wafers/hr	200	2625	15798	0.5234
PECVD deposition system	wafers/hr	345	2250	14307	0.6711
Screen-print line (automated)	wafers/hr	750	2880	5363.1	0.7782
Solar cell tester/sorter	cells/hr	300	3600	468.95	0.916
Combined tabber/stringer	cells/hr	300	1300	611.81	0.9887
Laminator (standard EVA) ^b	m ² /hr	0.44	52.8	44843	0.57
Laminator (fast-cure EVA) ^b	m ² /hr	0.76	73.8	28007	0.6199
Solar simulator ^a	modules/hr	30	720	109000	0

^a The prices of some equipment in the surveys were virtually independent of throughput rate. See Appendix C for details and discussion.

^b Laminator throughput is expressed in units of square meters of module area per hour.

- Determine the required throughput, ensuring that it falls in the range of allowable throughputs.
- Raise the throughput value to the exponent shown in the exponent column.
- Multiply the result by the value shown in the intercept column.

The result is the capital equipment cost for one piece of the selected equipment.

A value of zero for the exponent denotes that the equipment cost is independent of its throughput rate. This indicates that throughput is not a fundamental limiting factor in the cost of the equipment and that the equipment is easily scalable to throughput rates of at least the maximum value shown in Table 5.8. Equipment meeting this description typically consists of fairly simple, relatively low-cost component parts and can be easily scaled at little to no cost either through duplication or expansion of these parts. For example, the throughput of a tube furnace can be increased by using multiple tubes, and the throughput of a wet bench can be increased by using larger or multiple reservoirs.

A value of unity for the exponent denotes that equipment cost is proportional to throughput rate; that is, a doubling in throughput causes a corresponding doubling in price. Alternatively, one can say that the capital cost per unit throughput remains constant regardless of total throughput. Obviously, economies of scale are not available with such equipment. This most commonly occurs with equipment that is complex or built through duplication of high-cost component parts. The combined tabber/stringer shown in Table 5.8 is an example of this, requiring complex robotics to handle, flip, and solder solar cells and strings with minimum breakage. Simplified contacting schemes would minimize or eliminate the need for much of this handling and are thought to be key in reducing tabber/stringer costs.

An exponent between zero and one indicates that the capital cost of the equipment increases with throughput, but not in direct proportion to it (i.e., the capital cost per unit throughput decreases with increasing throughput). As can be seen from Table 5.8, this is the typical case and the usual source of economies of scale in capital equipment. It is also possible for the exponent to be greater than unity, indicating that the capital cost per unit throughput *increases* with increasing throughput. This may occur with complex equipment or when extraordinary measures are required to obtain high throughput rates; however, it can also be a temporary artifact of pricing decisions by equipment manufacturers in competition with one another. Competition can also produce negative exponents, particularly in markets with a lot of new entrants. While at first glance it seems counterproductive to purchase high-throughput equipment for which the exponent exceeds unity, such equipment may make more efficient use of materials, labor, or factory floor space and offset the higher cost per unit throughput compared to a smaller unit.

As an example, consider a PECVD silicon nitride deposition system for which the required throughput is 1500 wafers/hr. This value falls within the allowable throughput range, so using the intercept and exponent values from Table 5.8 the price P of the system is simply:

$$\begin{aligned}
 P &= 14307 \times (1500)^{0.6711} \\
 &= \$1\,936\,526.
 \end{aligned}
 \tag{5.23}$$

Suppose, however, that the plant required a throughput of 4000 wafers/hr at the silicon nitride

deposition step. This exceeds the maximum throughput allowed in Table 5.8, indicating that multiple deposition systems are needed to achieve the required throughput.

When multiple pieces of equipment are required to achieve a desired outcome manufacturers typically opt to use identical pieces of equipment for all duplicates; this is referred to as a “balanced” production line. In this case, balancing the production line means using two deposition systems, each with a throughput of 2000 wafers/hr and each at a cost of:

$$\begin{aligned}
 P &= 14307 \times (2000)^{0.6711} \\
 &= \$2\,348\,929.
 \end{aligned}
 \tag{5.24}$$

Since two systems are required, the total capital cost for PECVD deposition systems is \$4 697 858.

5.3.1.2 Capital Cost Factor for Estimating Total Plant Cost

In section 5.2.3.1 a factor κ was presented by which major equipment cost is multiplied to find the total capital cost of a PV module manufacturing plant. As described there, it is modeled after a similar multiplicative factor called the Lang factor that is sometimes used in chemical plant analysis.

The capital cost factor κ is necessary because, while it is known that a PV module manufacturing plant incurs indirect capital expenses for construction, building acquisition, land acquisition and preparation, installation of equipment and support facilities, and a range of other expenses, it is not clear how great these expenses are and how they are distributed. However, the principle behind the Lang factor is that all of these expenses can be represented by a single multiplier applied to major equipment cost [123]. That is, given a multiplier κ and a capital cost of major equipment C_{me} , the total capital cost of the plant C_{tot} is:

$$C_{tot} = \kappa C_{me}. \tag{5.25}$$

Given this relationship, the indirect capital expense C_{ind} is:

$$\begin{aligned}
 C_{ind} &= C_{tot} - C_{me} \\
 &= (\kappa - 1)C_{me}.
 \end{aligned}
 \tag{5.26}$$

Table 5.9: Capital requirements C_{tot} for multicrystalline silicon PV module manufacturing plants using turnkey production lines from Spire [119].

Plant size (MW_p)	Total cost (million \$)	Cost per W_p (\$)
1	7.0	7.00
5	22.5	4.50
10	25.0	2.50
25	45.0	1.80
50	75.0	1.50
100	130.0	1.30

While this description of indirect capital costs is not as satisfying as a detailed breakdown of which costs are incurred where, insufficient data are available to make the more detailed estimate. However, an appropriate data set for estimating κ exists in the form of a plant capital cost estimate as a function of plant capacity produced by Spire for its multicrystalline silicon turnkey production lines [119]. Spire’s estimates, both in terms of total plant capital cost and capital cost per peak watt of capacity, are shown in Table 5.9. Note the very high cost per W_p for plants smaller than 10 MW_p ; these are a result of poor economies of scale and inefficient use of automation. At production volumes of 1 MW_p , little no automation is possible and factory equipment tends to be underutilized, which in turn pushes capital cost per W_p very high.

To derive an expression for κ , a capital equipment cost for plants comparable to those in Table 5.9 must be computed using the model’s algorithm. For a given plant size, κ is then simply the ratio of Spire’s total capital cost to the capital equipment cost calculated by the model. Regressing these values of κ against plant size produces an expression for κ as a function of plant size.

The Spire calculations assume PV modules containing 36 solar cells, each a 156-mm square with an efficiency of 15%. The description of the manufacturing process indicates that it is a fairly standard process for producing PV modules from multicrystalline silicon solar cells with a single-layer silicon nitride antireflection coating and a co-fired aluminum BSF. No wafer thickness is specified in [119], but 300 μm was common at the time these calculations appear to have been performed; therefore, this is the thickness assumed.

Table 5.10: Capital equipment cost for Spire process with total capital cost estimate and resulting value for κ .

Plant size (MW _p)	Spire total cost (million \$)	Modeled equipment cost (million \$)	κ
1	7.0	6.13	1.14
5	22.5	7.70	2.92
10	25.0	9.33	2.68
25	45.0	17.31	2.60
50	75.0	31.71	2.37
100	130.0	60.16	2.16

The modeled equipment cost for each plant as a function of plant size is shown in Table 5.3.1.2 along with Spire's total capital cost estimate and the resulting κ . Note the relatively low value of κ for the 1-MW_p plant compared to the others. At 5 MW_p, κ spikes sharply upward before declining slowly with increasing plant size. As discussed above, the 1 MW_p plant is too small to automate cost-effectively; however, the equipment choices built into the model assume a normal industry level of automation for significantly large plants. As a result, the model overestimates capital equipment costs for the 1 MW_p case.

To express κ more generally as a function of plant size a power regression of the κ values in Table 5.3.1.2 was performed. While linear regression also provides a good fit to the data, power regression was selected because of its close association with quantitative models of scale economies. From a statistical standpoint, it also fits the data slightly better than a linear regression. The resulting fit, excluding the outlier data point for the 1 MW_p plant, is:

$$\kappa(P) = 3.4P^{-0.095}, \quad (5.27)$$

where P is the plant capacity in MW_p. The data and the regression fit are shown in Figure 5.3.

5.3.2 ESTIMATING MATERIAL COSTS

Material costs are estimated as a function of volume in a manner very similar to that in which equipment costs are estimated as a function of throughput. That is, the cost per unit of any raw material is related to the material volume through a power law relationship. This method of estimating material costs was developed in the late 1960s [124, 125]. An update in the late

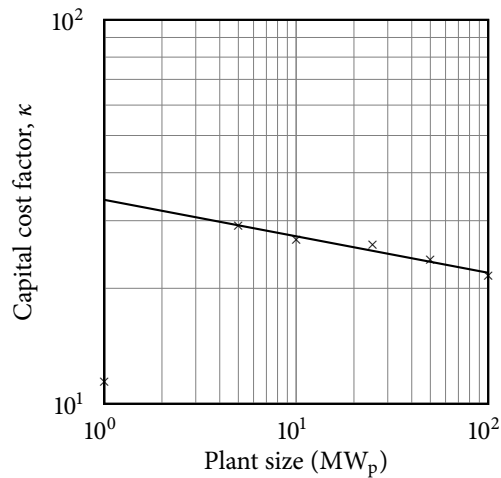


Figure 5.3: Results of power regression analysis for determination of κ .

1990s found that unit prices for specialty chemicals decline with volume at the same rate, almost regardless of the specific chemical [126].

The one exception to the power law relationship is commodity materials. The unit cost of a commodity material is virtually constant regardless of volume. Perhaps the most significant example in the PV industry is silicon feedstock, which currently costs about \$70/kg on contract and upward of \$300/kg on the spot market regardless of how much is purchased. In addition, the prices of certain specialty chemicals that are composed largely of commodity materials tend not to exhibit the great economies of scale seen in other specialty chemicals. The silver and aluminum screen-printing pastes used to form solar cell contacts are an example of this type of specialty chemical.

The derivation of the power law relationship for material prices is nearly identical to that for equipment prices. As an example, see the quantity and price data for phosphorus oxychloride (POCl_3) in Table 5.11. POCl_3 is used in the solar cell fabrication process to diffuse n-type phosphorus emitters into p-type wafers. Note the steep decline in POCl_3 cost per gram as volume increases.

The price per gram is plotted on a log-log scale as a function of volume in Figure 5.4

Table 5.11: Price quotations for phosphorus oxychloride (POCl₃) as a function of volume [127–129].

Volume (g)	Price (\$)	Unit price (\$/g)
10	76.00	7.60
50	257.50	5.15
100	381.50	3.82
250000	245 000.00	0.98

along with a regression fit described by:

$$P = 10.86q_{\text{mat}}^{-0.196}, \quad (5.28)$$

where P is the unit price per gram of POCl₃ and V is the number of grams purchased. Thus, each time the required volume of POCl₃ doubles, the unit price is changed by a factor of $2^{-0.196} = 0.873$ — that is, the unit price is cut by 12.7%.

Scale relationships for other materials used in the model are derived in detail in Appendix C. These are summarized in Table 5.12. The materials with zeroes in the exponent column are commodity materials and materials for which insufficient data were available to establish a cost-volume relationship. Similar to the process outlined for calculating the capital cost of a piece of equipment, the unit cost of a material is computed as follows:

- Determine the required quantity of raw material.
- Raise the quantity to the exponent shown in the exponent column.
- Multiply the result by the value shown in the intercept column.

The result is the cost of one unit of the selected material. To calculate the total cost of the raw material, multiply the unit cost by the quantity required.

5.3.3 ESTIMATING LABOR COSTS

Economies of scale for labor work different than those for capital equipment and raw materials. A company cannot reduce wages simply because it hires more workers, so the unit cost of

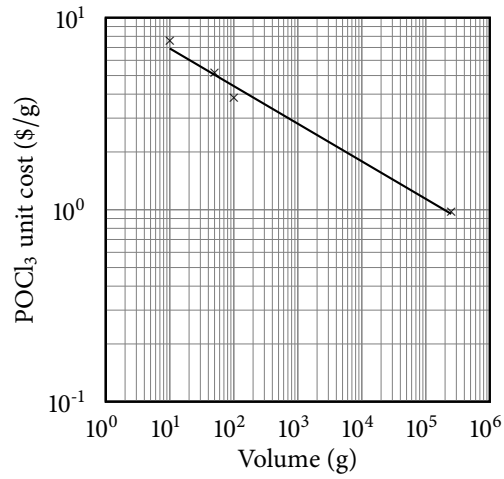


Figure 5.4: Cost of phosphorus oxychloride as a function of purchase volume.

Table 5.12: Regression coefficients for computing unit material prices as a function of required volume.

Material	Unit	Regression coefficients	
		Intercept	Exponent
Ammonia	L	48.075	-0.6253
Argon	L	22.608	-0.5291
Buffered oxide etch	L	129.31	-0.2982
Carbon tetrafluoride	L	70.709	-0.3710
Ethylene glycol	L	84.358	-0.5646
Helium	L	24.748	-0.5287
Hydrochloric acid	L	22.726	-0.2400
Hydrofluoric acid	L	218.62	-0.3829
Nitric acid	L	34.560	-0.4000
Nitrogen	L	28.175	-0.5947
Oxygen	L	18.430	-0.4430
Phosphoric acid	L	0.7379	-0.2774
Phosphorus oxychloride	g	10.859	-0.1959
Potassium hydroxide	kg	22.895	-0.3048
Silane	L	129.43	-0.4221
Silicon carbide	kg	2.7835	-0.5880
Sodium hydroxide	kg	262.83	-0.4379

labor does not decrease with increasing production scale. However, it is often the case that if one worker can handle a particular piece of production equipment, that same worker can handle a larger version of the equipment; indeed, that is the assumption used by the model. Thus, the number of equipment operators required per unit throughput can be expected to decrease when high-throughput equipment is used.

Returning to the example of the number of PECVD systems required to accommodate a throughput of 2000 wafers/hr, if a PECVD system requires one operator per shift then the systems with throughputs of 500, 1000, and 2000 wafers/hr will require four, two, and one operator per shift, respectively, to meet production demands. Thus, high-throughput equipment not only reduces capital cost, it also reduces the cost of direct operating labor. Furthermore, since the costs of supervisory labor and overhead are both proportional to the cost of direct operating labor, the use of high-throughput equipment has a cost-reducing ripple effect.

The number of operators required per workstation per shift are determined on a case-by-case basis for each type of equipment, as some pieces of equipment require more attention than others.

5.4 MODEL CODING AND IMPLEMENTATION

The cost model is written in Matlab as an object-oriented program organized as a set of reusable code modules. This allows the model to be organized much the same as an actual PV plant would be. A code module representing the plant itself contains a chain of code modules representing the individual process steps. These, in turn, contain code modules representing the materials and labor required to complete the process step. The model is executed by loading a plant specification file.

The plant is specified by writing a list of keywords and associated values to a plain text file. Each line of the file begins with a keyword, and the keyword is followed by the value desired for the variable represented by the keyword. For example, the keyword `PLANT_CAPACITY` is followed by a value equal to the number of W_p of the plant's manufacturing capacity. The production sequence is specified by repeated use of the `WORKSTATION` keyword, each time

followed by the name of a file specifying the capital, labor, and material requirements of the production step. A sample plant specification file is shown in Figure 5.5 (the keywords are defined in the program's manual).

As mentioned previously, the program is invoked loading the plant specification file. The sequence of events that occurs upon loading is illustrated in the flowchart in Figure 5.6. The program simply reads each line of the input file and parses it into a keyword and data. It then matches the keyword to a variable within the program, each of which corresponds to one of the variables described in section 5.2. If the keyword is `WORKSTATION` the data receives special handling; instead of being assigned to a plant variable, it is used to load a workstation specification file. Similarly, the `CATALOG` keywords in the plant specification refer to cost catalogs used to look up the costs of material and labor for the plant. When the entire plant specification file has been read, all of the data are processed to produce an estimate of manufacturing cost.

Figure 5.7 shows the contents of a sample workstation specification file. The `BASE_COST` and `EXPONENT` keywords refer to the intercept and exponent, respectively, used in section 5.3.1.1 to estimate the capital cost of equipment as a function of throughput. The `THRU_MIN` and `THRU_MAX` keywords refer to the minimum and maximum throughput rates available in commercial equipment of this type. This information is used later during workstation initialization to determine the actual throughput of the individual machines at this step. From that, the number of machines required is calculated using equation (5.6) and the cost of each machine is calculated using equation (5.21).

The process by which the workstation specification file is read and processed is very similar to that used in reading the plant specification file. The process is illustrated in the flowchart of Figure 5.8. The value following each keyword in the workstation specification file is simply assigned to the corresponding variable within the workstation code module. As with the plant specification, each of these keywords corresponds to a variable described in section 5.2.

Once the plant specification is loaded the plant is initialized. Initialization consists of processing the data from the plant specification to produce a manufacturing cost estimate. This

```

% PLANT DESCRIPTOR FILE
%
DESCRIPTOR          Roadmap H 100 Mwp
PLANT_CAPACITY     100000000    % WATTS

% PRODUCT DATA
%
PRODUCT_CAPACITY   168.2    % AMOUNT OF CAPACITY MET BY ONE ITEM
CELL_THICKNESS     100      % MICROMETERS
CELLS_PER_MODULE   36
BRICKS_PER_INGOT   16

% COST CATALOGS
%
MATERIAL_CATALOG   DEFAULT.MCAT
LABOR_CATALOG      DEFAULT.LCAT

% CAPITAL AND LABOR FACTORS
%
CAPITAL_FACTOR     3.4      -0.095 % BASE AND EXPONENT FOR COMPUTING LANG-LIKE CAPITAL FACTOR
CAPITAL_CONTINGENCY 0.05    % FRACTION OF EQUIPMENT ADDED TO EQUIPMENT COST FOR CONTINGENCY
DIRECT_SALARY      0.18    % FRACTION OF OPERATING LABOR
MAINT_REPAIR       0.06    % FRACTION OF DEPRECIABLE CAPITAL
OP_SUPPLIES        0.15    % FRACTION OF MAINT_REPAIR
LAB_CHARGES        0.15    % FRACTION OF OPERATING LABOR
DEPRECIATION       0.235   % FRACTION OF DEPRECIABLE CAPITAL
TAXES_INS          0.03    % FRACTION OF DEPRECIABLE CAPITAL
OVERHEAD           0.70    % FRACTION OF DIRECT LABOR, SALARIES AND MAINTENANCE
ADMINISTRATION     0.02    % FRACTION OF TOTAL MANUFACTURING COST
SELLING            0.01    % FRACTION OF TOTAL MANUFACTURING COST
RESEARCH           0.00    % FRACTION OF TOTAL MANUFACTURING COST
ROYALTIES          0.00    % FRACTION OF TOTAL MANUFACTURING COST
SHIFTS             3       % SHIFTS PER DAY
HOURS              8       % FISCAL HOURS PER SHIFT
DAYS               7       % FISCAL DAYS PER WEEK
WEEKS              52      % FISCAL WEEKS PER YEAR
HOLIDAYS           10      % HOLIDAYS PER YEAR
WORK_HOURS         8       % WORK HOURS PER WORKER PER SHIFT
WORK_DAYS          5       % WORKING DAYS PER WORKING WEEK
WORK_WEEKS        50      % WORKING WEEKS PER FISCAL YEAR
PAID_HOLIDAYS     10      % AVERAGE PAID HOLIDAYS PER PERSON PER YEAR
PAID_VACATION     12      % AVERAGE PAID VACATION DAYS PER PERSON PER YEAR
PAID_PERSONAL     5       % AVERAGE PAID ABSENTEEISM DAYS PER PERSON PER YEAR

% PRODUCTION LINE
%
WORKSTATION        HEM_FURNACE
WORKSTATION        BAND_SAW
WORKSTATION        WIRE_SAW_160
WORKSTATION        TEXTURE_ETCHER
WORKSTATION        TUBE_FURNACE
WORKSTATION        PSG_ETCHER
WORKSTATION        PECVD_DIRECT
WORKSTATION        PECVD_DIRECT
WORKSTATION        SCREEN_PRINT_LINE_ALPHA1
WORKSTATION        CELL_TESTER
WORKSTATION        CELL_SORTER
WORKSTATION        TABBER_STRINGER
WORKSTATION        LAMINATOR
WORKSTATION        MODULE_TESTER

```

Figure 5.5: Example of plant specification file.

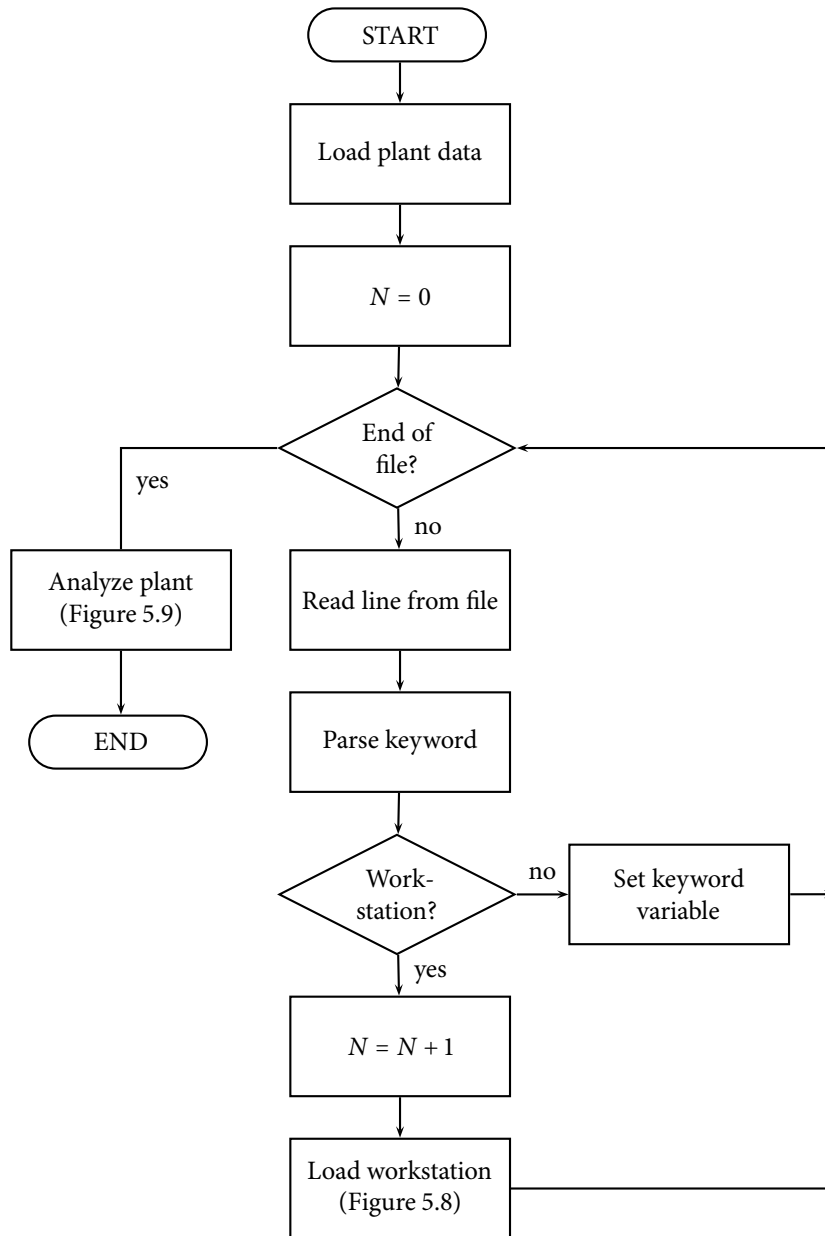


Figure 5.6: Flow diagram showing the operation of the manufacturing cost model.

```

% HF DIP BENCH DESCRIPTOR FILE
%
DESCRIPTOR          Generic HF Dip Bench
INPUT_TYPE          W
OUTPUT_TYPE         W

BASE_COST           10206
EXPONENT            0.5138
THRU_MIN            1200   % CELLS/HR
THRU_MAX            4000   % CELLS/HR

% INPUT/OUTPUT
%
BASE_YIELD          0.99
YIELD_EXPONENT      0
ETCH_THICKNESS      0.04   % MICROMETERS ETCHED

% PROCESS CHARACTERISTICS
%
DUTY_CYCLE          0.90

% DIRECT LABOR REQUIREMENTS PER MACHINE PER SHIFT
%
LABOR               1      % PERSON/SHIFT

% DIRECT REQUIREMENTS PER WAFER
%
MATERIAL            HYDROFLUORIC_ACID  0.002  % L
MATERIAL            WATER                0.500  % L
MATERIAL            ELECTRICITY          0.004  % KWH

```

Figure 5.7: Example of workstation specification file.

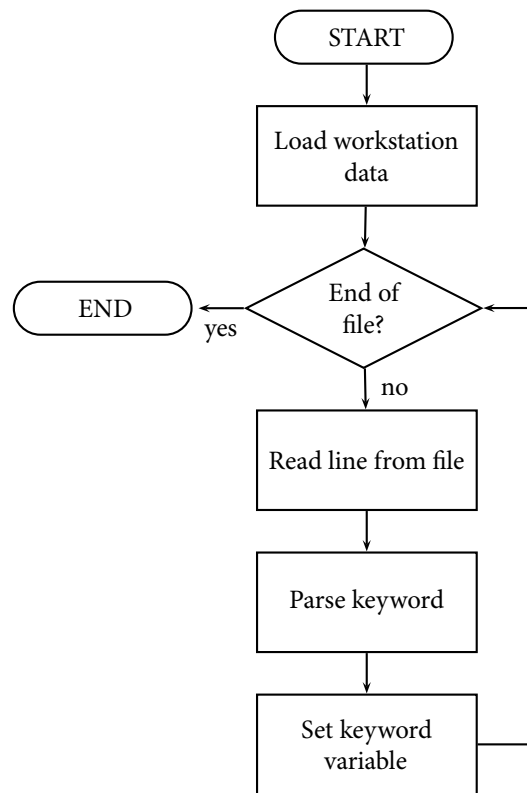


Figure 5.8: Flow diagram showing the workstation loading process.

process is illustrated in Figure 5.9. It consists of stepping backward through the production sequence to initialize each workstation based on the required throughput at each step. After the entire process sequence has been initialized, the capital, labor, and material requirements from each step are summed to produce direct capital, labor, and material requirements for the entire plant. Once these requirements are known, labor and material prices may be determined from the cost catalogs listed in the plant specification. Finally, indirect manufacturing requirements (such as indirect labor, operating supplies, and overhead) are factored from the direct requirements using the factors listed in the plant specification according to the procedure outlined in section 5.2.3.

Workstation initialization is straightforward and is illustrated in Figure 5.10. The throughput required of the workstation is determined from information provided by the plant code module. From this, the throughput and cost of each workstation may be determined using the appropriate data from the workstation specification file (as discussed earlier in this section).

After plant processing is complete, the program prints information on the production sequence (including the number of machines required at each process step) and manufacturing cost to the screen for the user to evaluate. The output for the plant specified in Figure 5.5 is shown in Figure 5.11. This plant produces 100 MW_p of PV modules each year from the output of 19 HEM furnaces casting multicrystalline silicon ingots. The total direct manufacturing cost is \$88.6 million, or about \$0.89/W_p. Fixed manufacturing costs add an additional \$20.6 million, or \$0.21/W_p. Adding direct and fixed manufacturing expenses yields a direct manufacturing cost of \$109.2 million, or \$1.09/W_p, and general expenses an additional \$3.38 million, or \$0.03/W_p. This sums to \$112.7 million in total manufacturing expenses each year, resulting in a total manufacturing cost of \$1.13/W_p (the per W_p figures do not add perfectly because of rounding errors).

Frequently it is desirable to perform a profitability analysis to determine the likelihood that the product is worth investing in. For this purpose, the model includes a utility command that may be run on the plant to generate an income statement on the basis of user-specified criteria. The user may specify a required return on investment or a desired markup over COGS. Sample output based on the cost sheet of Figure 5.11 is shown in Figure 5.12.

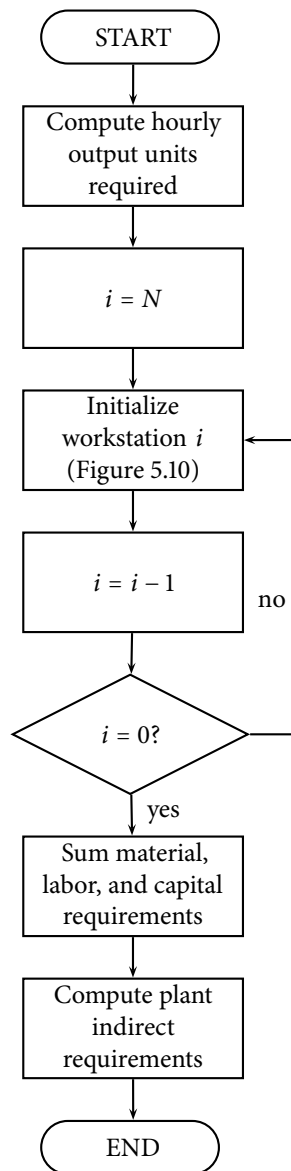


Figure 5.9: Flow diagram showing the plant initialization process.

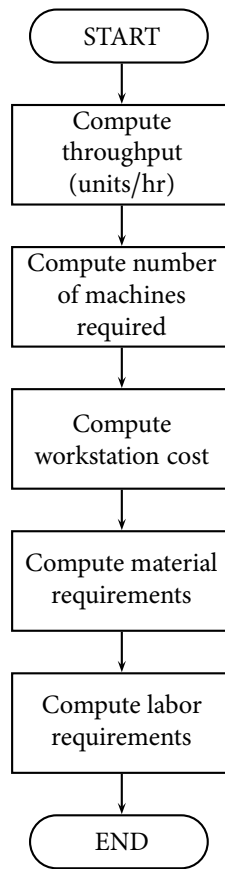


Figure 5.10: Flow diagram showing the workstation initialization process.

```

>> p = plant('tech_roadmap_H_100')

p =

Roadmap H 100 MWp
Capacity: 100.0 MWp
Total capital cost: $ 93592198 ($ 0.94 / Wp)
Capital equipment: $ 42634456 ($ 0.43 / Wp)
Workstation listing:
  19          HEM Furnace $ 12350000
   2          Generic Band Saw $ 1342083
   4          Generic Wire Saw $ 3139333
   1          Generic Texture Etcher $ 1055675
   2          Generic Tube Furnace $ 1525720
   1 Generic Phosphorus Glass Removal Etcher $ 628524
   4          Generic PECVD (Direct) $ 7288785
   4          Generic PECVD (Direct) $ 7195034
   2          Generic Screen-Printing Line $ 3149609
   2          Generic Cell Tester $ 181300
   1          Generic Cell Sorter $ 675975
   3          Generic Tabber/Stringer $ 1447101
   2          Generic Laminator $ 470656
   1          Generic PV Module Tester $ 154450

COST SHEET ($/Wp in parentheses)
Direct Manufacturing Costs
Raw materials: 73608763 (0.74)
Operating labor: 9110226 (0.09)
Direct salaries: 1639841 (0.02)
Maint. & repair: 2558067 (0.03)
Oper. supplies: 383710 (0.00)
Lab charges: 1366534 (0.01)
-----
Total Direct: 88667140 (0.89)

Fixed Manufacturing Costs
Depreciation: 10019097 (0.10)
Taxes/Insurance: 1279034 (0.01)
Overhead: 9315693 (0.09)
-----
Total Fixed: 20613824 (0.21)

General Manufacturing Expenses
Administration: 2253216 (0.02)
Selling Costs: 1126608 (0.01)
R&D: 0 (0.00)
Royalties: 0 (0.00)
-----
Total General: 3379824 (0.03)

TOTAL: 112660788 (1.13)

```

Figure 5.11: Sample output from the manufacturing cost model directly after plant initialization.

```
>> i = income_statement(p, 'roi', 0.2)

i =

Income Statement for Roadmap H 100 MWp
Capacity: 100.0 MWp
Total capital cost: $ 93592198 ($ 0.94 / Wp)

Revenue: $ 136063489 ($ 1.36 / Wp)
COGS:    $ 109280965 ($ 1.09 / Wp)
-----
Gross:   $ 26782524 ($ 0.27 / Wp)
Op Exp:  $ 3379824 ($ 0.03 / Wp)
-----
Op Inc:  $ 23402701 ($ 0.23 / Wp)
Deprec:  $ 10019097 ($ 0.10 / Wp)
Taxable: $ 13383604 ($ 0.13 / Wp)
Tax:     $ 4684261 ($ 0.05 / Wp)
-----
Net:     $ 18718440 ($ 0.19 / Wp)

Markup over COGS: 24.5%
Markup over total: 20.8%

Gross margin:     19.7%
Net margin:       13.8%
ROI:              20.0%
Payout period:   3.3 yr
```

Figure 5.12: Sample income statement generated from the cost sheet of Figure 5.11 on the previous page.

This income statement was generated on the criterion that the plant produce a 20% return on investment. It shows that to achieve this, the plant will require annual revenues of \$136.0 million, or $\$1.36/W_p$. This represents a 24.5% markup over COGS and provides gross and net margins of 19.7% and 13.8%, respectively. If shipping costs represent 5% of wholesale cost and product distributors require a markup of 20% over wholesale, the retail price of the module will be equal to a 25% markup over wholesale, or $\$1.70/W_p$.

5.5 MODEL VALIDATION

Model validation was accomplished by computing PV module manufacturing cost for a 25 MW_p production line and comparing to detailed calculations provided by GT Solar for their turnkey production line [53, 127, 128]. The complete turnkey system for which calculations were provided includes multicrystalline silicon ingot casting using the heat exchanger method (HEM); wafering by means of wire saw; processing into solar cells with a single-layer silicon nitride antireflection coating and cofired aluminum back surface field; testing, tabbing, and stringing of the solar cells; lamination and assembly into completed PV modules; and module testing.

The GT Solar calculations assume a module comprised of 36 multicrystalline silicon solar cells 150 mm in diameter and 325 μm thick with an efficiency of 13.5%. Therefore, the cells and modules are rated at 3.04 W_p and 109.35 W_p, respectively. Because GT Solar's calculations were provided several years ago, they do not reflect current costs for several commodity materials used in the turnkey production process. Therefore, for purposes of validating the model these commodity prices were set equal to those used in GT Solar's original calculations instead of values that would be appropriate today. The values used in the validation process are summarized in Table 5.13. All other values, including capital and material costs as well as associated overhead and support, were computed using model defaults as described in previous sections.

The model calculations are compared to the GT Solar calculations in Table 5.14. The two calculations agree on both direct and total manufacturing cost to within about 3%. Note that the classification of expenses used by the model is more detailed than those used in the

Table 5.13: Input assumptions, including prices for commodity materials, assumed in validating the PV module manufacturing cost model against GT Solar calculations for a 25 MW_p turnkey production line.

Parameter	Value
Module power (W _p)	109.35
Cell power (W _p)	3.04
Cell efficiency (%)	13.5
Cell diameter (mm)	150
Cell thickness (μm)	325
Kerf thickness (μm)	210
Silicon feedstock price (\$/kg)	20
Electricity price (\$/kW·h)	0.10
Silver paste price (\$/g)	0.30
Silver-aluminum paste price (\$/g)	0.25
Aluminum paste price (\$/g)	0.08
Operating labor wages (\$/yr)	20 000
Research & development (% of mfg. cost)	0

GT Solar calculations. The GT Solar classifications correspond to the model calculations in roughly the following manner:

- In the GT Solar calculations, “raw materials” includes both direct material requirements for the PV module itself as well as materials required for maintenance and repair. In the model calculations, maintenance materials are classified under “maintenance & repair.”
- “Direct labor” in the GT Solar calculations includes wages for equipment operators, maintenance personnel, and salaried employees working on the factory floor. Each of these is categorized separately in the model calculations, with “maintenance & repair” including both wages for maintenance personnel and materials required for repairs.
- The GT Solar calculations make no allowance for operating supplies and laboratory charges. While these costs are small, they are significant enough that they should be accounted for; the model does this, including them as direct manufacturing expenses.
- GT Solar assumes a 7-year straight line depreciation on capital equipment, but do not account for other depreciable capital such as the factory building, computers, and

office furniture. As described in section 5.4, the model makes an effort to fully account for depreciable capital and, as a result, computes slightly greater depreciation.

- One hundred percent debt financing for capital equipment is assumed in the GT Solar calculations, so an interest charge is included in the fixed manufacturing expenses. The model assumes 100% equity financing, so includes no interest charges.
- GT Solar calculates sales, general, and administrative expenses (SG&A) as 10% of materials, labor, and overhead, and does not include provisions for research and development. The model follows a different algorithm, as described in section 5.4, and arrives at a slightly different result.

Finally, it is worth noting that both sets of calculations are consistent with the breakdown of actual plant costs published by Margadonna and Ferrazza [50] in 1998, though they do not agree precisely because of differences in plant size and input assumptions.

5.6 GENERATING A MANUFACTURING COST ROADMAP FROM THE TECHNOLOGY ROADMAP TO 20% EFFICIENCY

The manufacturing cost model may now be applied to the technology roadmap developed in section 4.5. The base manufacturing process used for the industrial solar cell in step A of the roadmap is shown in Figure 5.13 on page 166. The screen-print and co-fire step for the front and rear contacts is performed using a screen printing line, which combines screen printing and contact firing into a single turnkey system. This explains why they are listed as a single step in Figure 5.13.

The changes assumed to be made to the production process between steps along the technology roadmap are summarized in Table 5.15 on page 167. A silicon feedstock price of \$70/kg, which is representative of current contract prices, is assumed throughout the roadmap and noted at step A of the table. The physical parameters assumed for the wafers and cells manufactured in this roadmap are found in Table 4.2 on page 112.

The results of manufacturing cost modeling at each step of this roadmap are shown in Figure 5.14 on page 168. Both COGS and estimated retail price are shown. The retail price

Table 5.14: Comparison of GT Solar manufacturing cost calculations to modeled manufacturing cost for the same process.

(a) GT Solar calculations (\$/W _p)	(b) Model calculations (\$/W _p)
<i>Direct manufacturing expenses</i>	
Raw materials	1.12
Direct labor	0.13
Total	1.25
<i>Fixed manufacturing expenses</i>	
Depreciation	0.17
Interest	0.05
Overhead	0.13
Total	0.35
Direct manufacturing cost	1.60
<i>General manufacturing expenses</i>	
SG&A	0.15
Total manufacturing cost	1.75
<i>Direct manufacturing expenses</i>	
Raw materials	1.09
Operating labor	0.12
Direct salaries & overhead	0.02
Maintenance & repair	0.05
Operating supplies	0.01
Laboratory charges	0.02
Total	1.31
<i>Fixed manufacturing expenses</i>	
Depreciation	0.19
Local taxes & insurance	0.02
Overhead	0.13
Total	0.34
Direct manufacturing cost	1.65
<i>General manufacturing expenses</i>	
Administration	0.03
Selling costs	0.02
Research & development	0.00
Royalties	0.00
Total	0.05
Total manufacturing cost	1.70

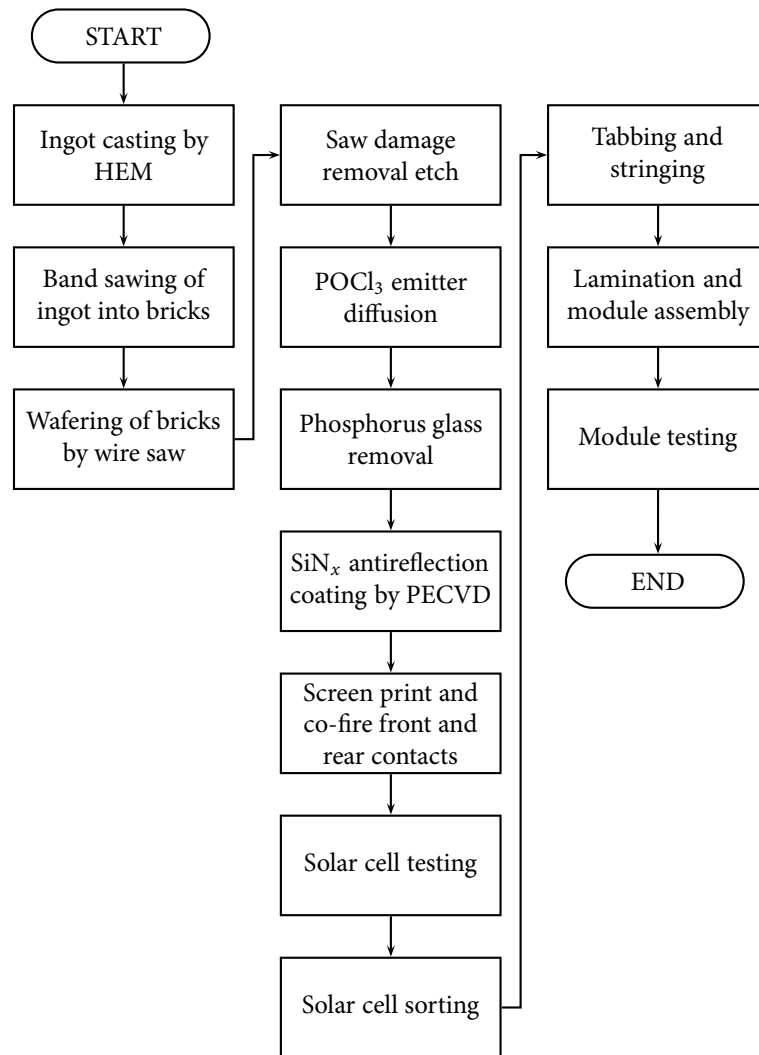


Figure 5.13: Process flow diagram for base industrial solar cell (step A in the technology roadmap).

Table 5.15: Changes to manufacturing process at each step of the technology roadmap described in section 4.5.

	Cell description	Efficiency (%)	Manufacturing process
A.	Industrial solar cell (current)	14.4	Base manufacturing process (see Figure 5.13 on the preceding page). Assumes silicon feedstock price of \$70/kg.
B.	Improved screen printing	15.3	Silver paste consumption reduced from 0.16 g/wafer to 0.10 g/wafer.
C.	Lifetime enhancement	15.7	No change — lifetime enhancement assumed to come from fundamental understanding of gettering processes incurring no significant change in manufacturing process.
D.	Back surface reflector	17.7	Additional PECVD SiN _x deposition step for rear surface passivation.
E.	Reduce cell thickness to 100 μm	17.7	Wafers sliced to 100 μm instead of 250 μm with concurrent kerf thickness reduction from 190 μm to 160 μm.
F.	Selective emitter	18.4	No change — selective emitter dopant assumed incorporated into front contact paste.
G.	Random pyramids on front	19.8	Texture etching step replaces saw damage etching step.
H.	Reduce resistivity to 0.6 Ω·cm	20.0	No change.

is estimated from the wholesale price required to provide 20% return on investment. It is assumed that shipping will cost about 5% of wholesale and that the distributor will require an additional 20% markup over wholesale. Thus, a 25% markup over wholesale is used to determine the retail price. This is consistent with how some analysts see the retail PV market shaping up in the near future [119].

The final step of the roadmap, which produces a solar cell with 20% efficiency, results in an estimated retail cost of \$1.70/W_p. The LCOE of a PV system designed using this module and all of the others in the roadmap is shown in Figure 5.15. The LCOE is calculated using the combined PV system and LCOE model SAM (which was described in detail in section 2.3.3) assuming a residential PV system in Phoenix in 2015. Accordingly, all system cost assumptions aside from the module itself were taken from Table 3.4 on page 56. As Figure 5.15 shows, the final step of the PV cost roadmap only achieves an LCOE of 10.7 ¢/kW·h, which falls just short of the 10 ¢/kW·h goal established by DOE. However, there are multiple paths by which

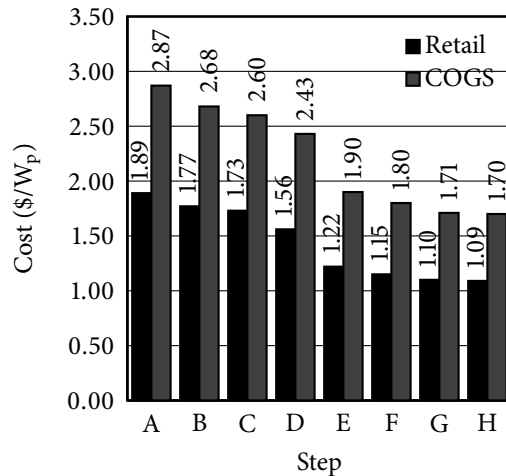


Figure 5.14: Results of manufacturing cost modeling of the solar cell technology roadmap of Figure 4.9 on page 112 for 100 MW_p annual production capacity.

the cost may still be reduced.

One path is for the PV manufacturer to simply accept a smaller return on investment. However, if the markup from wholesale to retail remains 25% then the wholesale cost must be \$1.20/W_p to produce a retail price of \$1.50/W_p. COGS in step H, the final step of the roadmap, is \$1.10/W_p, leaving room for a return on investment of just 7.8%. A larger return can still be realized if distributors can be convinced to reduce their margins, but whether they would do so would depend upon market conditions. A safer path to grid parity is to find a way to further reduce COGS, which would protect profit margins and keep the industry healthy.

Another path is to increase production beyond 100 MW_p/yr to take advantage of economies of scale. Scaling up to 500 MW_p/yr only reduces COGS from \$1.10/W_p to \$1.06/W_p. However, the total capital cost of the plant drops from \$0.94/W_p to \$0.74/W_p. Since return on investment is measured against the total capital cost, this reduction means at 500 MW_p the estimated retail price drops to \$1.59/W_p from \$1.70/W_p at 100 MW_p. This is a significant improvement; furthermore, if return on investment is sacrificed to reach the \$1.50/W_p retail target it need only be reduced to 14.0% instead of to 7.8%. This is a much more acceptable loss.

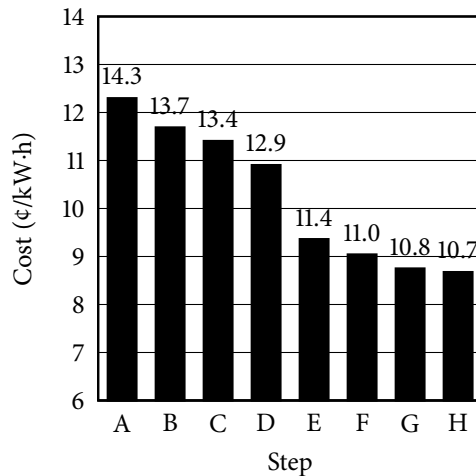


Figure 5.15: Levelized cost roadmap for residential PV systems using the estimated retail prices from the cost roadmap in Figure 5.14 on the preceding page and 2015 BOS costs from the MYPP reference system shown in Table 3.4 on page 56.

In performing this assessment, it must be borne in mind that the model of indirect capital factor developed in section 5.3.1.2 is based on plant sizes only up to 100 MW_p. As a result, when assessing manufacturing costs at higher volumes the indirect capital costs are being extrapolated. The error introduced by this extrapolation is unknown. However, the results appear to be consistent with the scale assessments discussed in Chapter 2.

One more path to achieving the required cost reduction is to simply reduce costs. There are numerous ways in which this might be done, from slashing labor and reducing research and development expenditures to minimizing consumption of the most expensive materials and utilities. By far the most expensive single material in the c-Si production process is silicon feedstock, and since a shortage in purified silicon developed in 2004 the prices of feedstock have been artificially high. Therefore, it is reasonable to assume that feedstock prices will come down in the future as more supply is created to sate demand.

The question then is how far feedstock prices must fall for the roadmap to achieve the \$1.50/W_p target price by 2015. Alternatively, since wafer thickness determines the amount of silicon required to make a solar cell, one might ask what combination of feedstock cost and cell thickness are required to reach the target. These questions are answered in Figure 5.16,

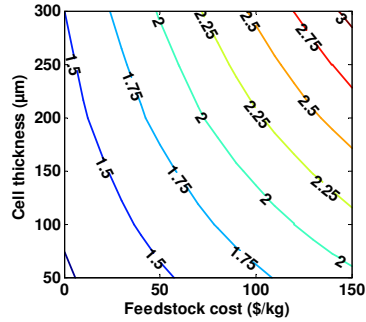


Figure 5.16: Estimated retail price of a PV module (displayed on contour lines in $\$/W_p$) made from 20%-efficient solar cells from the roadmap as a function of feedstock cost and cell thickness.

which shows the results of manufacturing cost modeling for the 20%-efficient roadmap cell as a function of cell thickness and feedstock cost.

Following the line corresponding to a retail module price of $\$1.50/W_p$, it is seen that with a cell thickness of $100\ \mu\text{m}$ a feedstock cost of $\$38/\text{kg}$ is required. This is a profitable selling price even for high-purity microelectronics-grade feedstock, so once the market's current supply and demand issues are resolved this price should be eminently achievable.

5.7 CONCLUSIONS

This chapter detailed the development of a comprehensive and flexible numerical model for estimating the manufacturing cost of photovoltaic cells and modules. The model carefully balances the requirement for detail with the need to be able to quickly evaluate the economic prospects of a solar cell design and its associated manufacturing process. All aspects of the model, including capital costs, material and labor requirements and costs, and indirect costs, are under the direct control of the user, and the model can, in theory, be used to model any PV production process. It is believed that this is only model of its kind currently in existence.

The model was validated against detailed manufacturing cost calculations provided by GT Solar for a $25\ \text{MW}_p$ turnkey multicrystalline silicon production line. Agreement between

GT Solar's calculations and the model's estimate was excellent.

Novel features of the model include statistical representations of the capital costs of major equipment and unit costs of required materials. These features allow the user to quickly customize the fabrication process evaluated by the model without having to painstakingly account for every detail, a problem suffered by the model's long-defunct predecessor SAMICS. They also allow the model to automatically account for economies of scale, adjusting capital and material costs on the basis of production volume.

Use of the model was demonstrated through application to a sequence of solar cell design improvements developed in Chapter 4. It was shown that while the technology roadmap successfully improved solar cell efficiency to 20%, it did so at an estimated retail price of $\$1.70/W_p$. This fell short of the $\$1.50/W_p$ retail module price goal prescribed by DOE for grid parity. However, through further application of the model several paths were developed to close the gap and reach the goal. These included reducing profits, scaling up production, and adjusting wafer thickness based on the actual price of silicon feedstock. Since the current silicon feedstock prices used in the modeling are inflated by supply problems, the outlook is good for the technology roadmap to achieve the prices required for grid parity.

CHAPTER 6

MODELING THE IMPACT OF SYSTEM RELIABILITY ON ENERGY PRODUCTION AND COST

In conventional energy sources, failure-related damages are limited to repair costs and the cost of energy not served. When the unit is idle, no fuel is consumed and production resumes when failure is cleared. In renewable energy systems the fuel is free, and each time the system is non-operational the potential for energy production (and revenues) is lost. The loss of potential revenues is important for renewable distributed generation (DG) systems where the large initial investment is usually compensated by the price paid (or the payment avoided) for electricity during the lifetime of the system. In evaluating the payback time and energy price per kW·h generated by such system, the system is assumed to work without interruptions. Photovoltaic (PV) systems are highly reliable, but as any complex system they occasionally fail; neglecting the effects of those failures may lead to somewhat optimistic performance and life-cycle cost (LCC) predictions. The vast majority of PV system failures are believed to be inverter-related [25, 130, 131]. Since PV systems are highly modular, they can vary in size from tens of watts to over a megawatt. As a result, PV systems use inverters in a wide array of sizes and topologies [132–134], which complicates the evaluation and modeling of inverter failure modes.

The cost of energy produced by a photovoltaic system is dependent upon the amount of energy produced by the system and the amortized cost of the system's components. Clearly, the amount of energy produced by the system over its lifetime is dependent upon how often the system fails and for how long. A number of simulation tools exist for predicting the energy output of a system, fully accounting for system geometry and geography, as described in section 2.3.2. However, these tools either use crude estimators of system reliability or ignore the effects of system downtime altogether. Furthermore, cost calculations implicitly assume that the cost of the system and details of its financing are well known. In reality, the

costs of the system components are often known only approximately until they are actually purchased; this seems to be especially true for installation costs, which may sometimes not be known until after the system is installed. As a result, system planning may be compromised by a lack of certainty over the final energy cost.

This research attempts to address these shortcomings by applying a Monte Carlo model to predict the occurrence and duration of system failures. The results are used to estimate the effects of down time on the energy production of a system over its service life. A similar stochastic approach is used to estimate system cost, reflecting uncertainties in the costs of system components in the final cost of the installed system. The combination of these calculations yields a probabilistic estimate, in the form of a probability density function, of the final cost of energy produced by the system.

The advantages to this approach are manifold. The output distribution yields an *expected* cost per unit energy and a strongly bounded range of *possible* values for the cost. Statistical analysis of the results can provide information about the accuracy of calculation as well as its sensitivity to down time and system component costs — important information that is difficult or impossible to establish using a deterministic model. Furthermore, the distribution makes the probability of meeting or exceeding a given cost target readily apparent. These properties of the stochastic approach give the analyst valuable tools for system planning and analyzing financial risk.

This chapter proceeds by first providing some background in the statistical analysis of reliability. It then presents a stochastic reliability model to be used in conjunction with existing PV system models to assess the impact of system failures on annual energy production. The model uses a single probability distribution to represent all failures of the system, regardless of their reason or source. Next, it proposes a method by which this global failure distribution can be decomposed into its component parts to enable investigations into *why* the system fails and *how* its failure record might be improved. Since, as described above, most PV system failures are thought to originate with the inverter, this latter task focuses on developing a method to better understand and improve inverter reliability.

6.1 FACTORS IN PHOTOVOLTAIC SYSTEM RELIABILITY

A basic photovoltaic (PV) system consists of two blocks connected in series: solar modules and the power conversion unit (PCU), or inverter. While the complete failure of either block leads to the downtime of the entire system, a large number of solar module failures can generally be tolerated without failing the entire system. Furthermore, solar modules are typically backed with warranties of at least 20 years and have demonstrated very high reliability in the field: A mean time between failures (MTBF) of 522 yr has been reported for residential systems and 6666 yr for utility systems [25]. Note that this is not to say that solar modules installed in a residential PV system typically last 522 yr, but that in a given year one would expect one module of every 522 to fail. Similarly, the MTBF for utilities means that about 3 modules of every 20 000 will fail in a given year. Inverter reliability data is less widely available, but by all accounts is substantially lower than for PV modules: MTBF between one and 16 years have been reported using field data [25, 135]. Inverter warranties tend to be in the three- to five-year range, and while some manufacturers have recently introduced warranties as long as 10 years they still fall far short of equaling the reliability of PV modules. Given this disparity in reliability, inverters often must be replaced one or more times in the course of a PV system's service life. The use of multiple inverters to improve both system efficiency and reliability has been investigated [136], but there is doubt about whether this solution is economical [137].

Repair time varies greatly, and can be anywhere from couple of hours for large continuously monitored systems to a couple of months for remote installations and large installations that depend on service by the manufacturer. Typically for residential non-monitored systems it includes a failure identification period of one month (using meter data from the utility bill) followed by one to two weeks for system repair. For large installations (either in size or volume) several monitoring strategies can be utilized ranging from continuous monitoring of system performance and comparison with predicted output obtained using meteorological data, to a less frequent (weekly, bi-weekly) phone-in of inverter diagnostic data to a central computer. Likewise, repair costs vary greatly, depending on the nature of the required repair.

It has been suggested that inverter repair costs should not exceed 1 ¢/kW·h for residential PV systems and 0.5 ¢/kW·h for commercial and utility systems for them to be economical, both values that are ultimately governed by the combination of failure rate and repair cost [25].

Neither the MTBF nor the mean time to repair (MTTR) is usually known in advance. They may be extracted from experimental data, if it is available in sufficient volume, or estimated using a reliability prediction standard. While failure and repair times may be estimated even from very small data sets, doing so leads to great uncertainty in predicting future performance. Several initiatives aimed at collecting performance data for a large number of PV systems are currently underway, notably at Sandia National Laboratories [138] and the Florida Solar Energy Center [139]; however, detailed data on inverter failures from these initiatives is not widely available and future reliability of PV systems must be estimated using the limited available data.

Inverter manufacturers also face pressure to reduce the capital costs of PV inverters. The U.S. Department of Energy estimates that residential inverter costs must decrease by about a factor of three, from \$0.90 / W_p to \$0.30 / W_p , before residential PV systems achieve parity with grid power costs [22]. The required reduction is less severe for larger commercial- and utility-sized inverters, whose prices benefit from economies of scale [137], but even these costs must nonetheless be reduced. Therefore, PV inverter manufacturers must find a way to simultaneously achieve significant increases in reliability and appreciable reductions in price.

The failure modes of greatest concern are those exposed to high thermal and electrical stress, as well as the thermal management system itself. Little information about these failure modes has been published, but PV industry representatives at a U.S. Department of Energy (DOE) workshop agreed that the most urgent problem affecting inverter reliability is the quality of the DC bus capacitors [140]. These capacitors are almost always aluminum electrolytics and have proved too expensive and too unreliable to provide a high level of performance in the difficult operating environment that PV inverters impose. To reduce inverter prices and increase inverter reliability to the levels targeted by DOE and the U.S. PV industry will require capacitors that are twice as reliable and half as costly as the electrolytic capacitors presently used. However, the PV inverter industry requires substantial growth before it will

be large enough to demand the desired characteristics from capacitor manufacturers. These conclusions are independently corroborated in [141].

In this thesis, an approach to PV inverter reliability analysis is proposed based on inverter subsystems and operating environment. It uses estimates of inverter component reliability in combination with Monte Carlo simulation to assess the expected availability of a particular inverter design. Since the inputs to the model are expected to vary widely depending upon inverter design, environment, and purpose, this thesis does not offer specific recommendations; instead, it proposes a generalized model that may be adapted to specific situations and inverter designs. It also uses Monte Carlo simulations based on an existing inverter design to make qualitative assessments of several potential approaches to increasing inverter reliability.

The Monte Carlo approach has been used previously to investigate “green power” pricing initiatives [142] and estimate the impact of inverter failures on PV system energy production and cost [136]. This work builds upon these earlier works by proposing a model that decomposes the inverter into several subsystems to estimate the reliability of each subsystem separately. The reliability of the inverter as a whole is then estimated from the subsystem reliabilities. For purposes of reliability analysis, the subsystems need not correspond to the physical subsystems of the inverter; as illustrated in this study, they correspond to the inverter’s major failure modes.

6.2 MODELING RELIABILITY AND AVAILABILITY

The most widely used index in reliability studies is the mean time between failures (MTBF). It is the mean (average) time period between system failures due to the random failures of one of its component parts, i.e. it tells how long a system is expected to work without failing. Note that this is a system measure that says nothing about an individual component. The overall availability of the system depends also on the repair time; that is, how long after failure a unit will be off-line. This is characterized by the mean time to repair (MTTR). Both MTBF and MTTR may be computed from statistical distributions of failure and repair rates.

The failure of a component, subsystem, or system can be characterized by a probability density function (pdf), denoted $f(t)$. The cumulative density function (cdf), which describes

the probability that a failure will have occurred at or before time t , is then [143]:

$$F(t) = \int_0^t f(\tau) d\tau. \quad (6.1)$$

where $F(\infty) = 1$. The reliability function is defined as:

$$R(t) = 1 - F(t), \quad (6.2)$$

and the failure rate is defined:

$$\lambda(t) = \frac{f(t)}{R(t)}. \quad (6.3)$$

Finally, the mean time to failure (MTTF) is defined:

$$\text{MTTF} = \int_0^{\infty} R(t) dt. \quad (6.4)$$

Once a failure is determined to have occurred, repair times may be calculated in an analogous manner. Given a failure rate λ and a repair rate μ , system availability — the fraction of time that a repairable system is operational — is simply [143]:

$$A = \frac{\text{MTTF}}{\text{MTTF} + \text{MTTR}}. \quad (6.5)$$

Note that $A \rightarrow 1$ when $\mu \gg \lambda$, indicating that availability is maximized when repair rates are high and failure rates are low. In a system composed of N subsystems, availability may be expressed:

$$A = \prod_{i=1}^N A_i, \quad (6.6)$$

where A_1, \dots, A_N are the availabilities of the individual subsystems. By equation (6.6), the availability of the whole system may never be greater than the availability of the weakest subsystem (though it may be substantially lower, depending on the availabilities of the other subsystems). Equation (6.5) can be rewritten for subsystem i as:

$$A_i = (1 + \sigma_i)^{-1}, \quad (6.7)$$

where

$$\sigma_i = \frac{\text{MTTR}_i}{\text{MTBF}_i} \quad (6.8)$$

is the unavailability contribution of subsystem i .

Two of the most important statistical distributions in reliability analysis are the exponential and the Weibull distributions. System reliability generally follows a trend known as the “bathtub curve,” by which the failure rate declines for a short period after the system begins service (the so-called “infant mortality” period), then levels off at some constant value for the bulk of the system’s life. Eventually, a gradual increase in the failure rate is observed, signaling the end of the system’s life. The declining failure rate seen during the infant mortality period and the increasing failure rate observed near the end of life are typically well represented by the Weibull distribution, while the constant failure rate observed in between those periods is accurately represented by the exponential distribution, which is a special case of the Weibull distribution. Weibull distributions are also commonly used to represent repair rates, which frequently are not constant. In all cases, failure and repair rates may be decomposed into parallel distributions distinguished by failure mode.

6.2.1 THE EXPONENTIAL DISTRIBUTION

It may be shown that when the failure rate, defined in equation (6.3), is constant, the PDF $f(t)$ follows the exponential distribution [144]:

$$f(t) = \lambda e^{-\lambda t}. \quad (6.9)$$

By equation (6.1) the CDF is then:

$$F(t) = 1 - e^{-\lambda t}, \quad (6.10)$$

and by equation (6.2) the reliability function is:

$$R(t) = e^{-\lambda t}. \quad (6.11)$$

Finally, by equation (6.4) the mean time to failure is:

$$\begin{aligned} \text{MTTF} &= \int_0^{\infty} e^{-\lambda t} dt \\ &= \frac{1}{\lambda}. \end{aligned} \quad (6.12)$$

A constant repair rate yields a similar set of equations, with the repair rate μ substituted for λ and the MTTF instead written as the mean time to repair (MTTR) [144]:

$$\text{MTTR} = \frac{1}{\mu}. \quad (6.13)$$

6.2.2 THE WEIBULL DISTRIBUTION

The PDF $f(t)$ and CDF $F(t)$ of the two-parameter Weibull distribution are:

$$f(t) = \frac{\beta}{\eta} \left(\frac{t}{\eta} \right)^{\beta-1} e^{-(t/\eta)^\beta} \quad (6.14)$$

$$F(t) = 1 - e^{-(t/\eta)^\beta}. \quad (6.15)$$

In this distribution, η_f is the scale parameter and β_f is the shape parameter. The scale parameter is proportional to MTTF:

$$\text{MTTF} = \eta_f \Gamma \left(\frac{1}{\beta_f} + 1 \right). \quad (6.16)$$

where $\Gamma(\cdot)$ is the gamma function. The failure rate is obtained from equation (6.3):

$$\lambda(t) = \frac{\beta_f}{\eta_f} \left(\frac{t}{\eta_f} \right)^{\beta_f-1}. \quad (6.17)$$

One of the most advantageous characteristics of the Weibull distribution is its ability to provide relatively accurate analysis using a very small data sample [145]. This is extremely important in the case of evaluating the field operation of relatively reliable systems, such as PV systems. The parameters of the Weibull distribution cannot be obtained in closed form, and have to be computed using an iterative procedure. While several other methods are

available, two are most widely used: median rank regression curve fitting using the times to failure as a dependant variable, and maximum likelihood estimation (MLE). It is useful to note that when $\beta_f = 1$ the two-parameter Weibull distribution is identical to the exponential distribution with $\lambda = 1/\eta_f$.

Repair parameters are calculated analogously to failure parameters, appropriately derived from field repair data. Accordingly, the MTTR is:

$$\text{MTTR} = \eta_r \Gamma \left(\frac{1}{\beta_r} + 1 \right), \quad (6.18)$$

and the repair rate is:

$$\mu(t) = \frac{\beta_r}{\eta_r} \left(\frac{t}{\eta_r} \right)^{\beta_r - 1}, \quad (6.19)$$

where η_r and β_r are the scale and shape parameters, respectively, that determine the repair rate distribution. While these are analogous to the parameters η_f and β_f that determine the failure characteristics, the repair parameters should not be confused with the failure parameters.

6.3 DEVELOPMENT OF A STOCHASTIC RELIABILITY MODEL FOR PV SYSTEM SIMULATION

The PV system simulator used in this work was developed at Georgia Tech, but is based on the well established model PVFORM [146]. The Georgia Tech model calculates module temperatures more accurately and contains provisions for simulating a wider range of system geometries. The model has been validated using data from an operating PV system [80].

The system simulated in this example is a hypothetical south-facing, grid-connected 3 kW_p system located in Atlanta, Georgia. The TMY2 database [147] is used as a climate model to determine the power output from the PV modules at one-hour intervals over the course of a full year. An inverter model determines the AC power output of the system at each interval. Finally, a stochastic reliability model developed in this research determines the frequency and duration of system failures. It should be noted that the TMY2 database

consists of well characterized, statistically filtered climate observations; therefore, modeling variations in weather conditions was unnecessary.

System failures are modeled based on five years of operational data from the 340-kW_p PV system atop the Georgia Tech Aquatic Center (GTAC). The reliability model consists of two random functions, one to determine the time to the next failure and another to determine the duration of each failure. The two-parameter Weibull distribution is used to represent both of these functions because of its ability to take on a wide range of characteristics, including mimicking other distributions. The cumulative density function (cdf) of the two-parameter Weibull distribution is

$$F(x|\eta, \beta) = \int_0^x \frac{\beta}{\eta} \left(\frac{t}{\eta}\right)^{\beta-1} e^{-\left(\frac{t}{\eta}\right)^\beta} dt, \quad x \geq 0, \quad (6.20)$$

where $\eta > 0$ and $\beta > 0$ are called the *location* and *shape* parameters, respectively. The values used for these parameters in this simulation were derived from the aforementioned GTAC data by a previous investigator [80]. The time to failure was determined using $\eta_1 = 13\,213$ hr and $\beta_1 = 1.052$, and failure duration was determined using $\eta_2 = 718.4$ hr and $\beta_2 = 1.7397$. (The subscripts 1 and 2 are used to denote time to failure and failure duration, respectively.)

The flowchart of Figure 6.1 illustrates the manner in which these values were used to determine the frequency and duration of failures. The system was modeled in one-hour increments, tracked by the counter t , over its entire service life T . A second counter, t_1 , was used when the system was operating properly to track the amount of time since the previous failure (or since the start of the simulation if no failures had yet occurred). A third counter, t_2 , was used during failures to indicate the time elapsed since the start of the failure. A boolean flag, FAIL, was used to indicate whether the system was in a failure state (FAIL = true) or not (FAIL = false). At the start of the simulation, all counters were set to 0 hr and the FAIL flag was set to false.

Prior to executing the reliability model, the PV system simulator was run as if there were no failures. This produced a matrix of data indicating the system's ideal energy output over each hour of its service life, $E(t)$. The reliability module was then executed using these data. At the start of each loop through the model, t was checked to see if it exceeded T ,

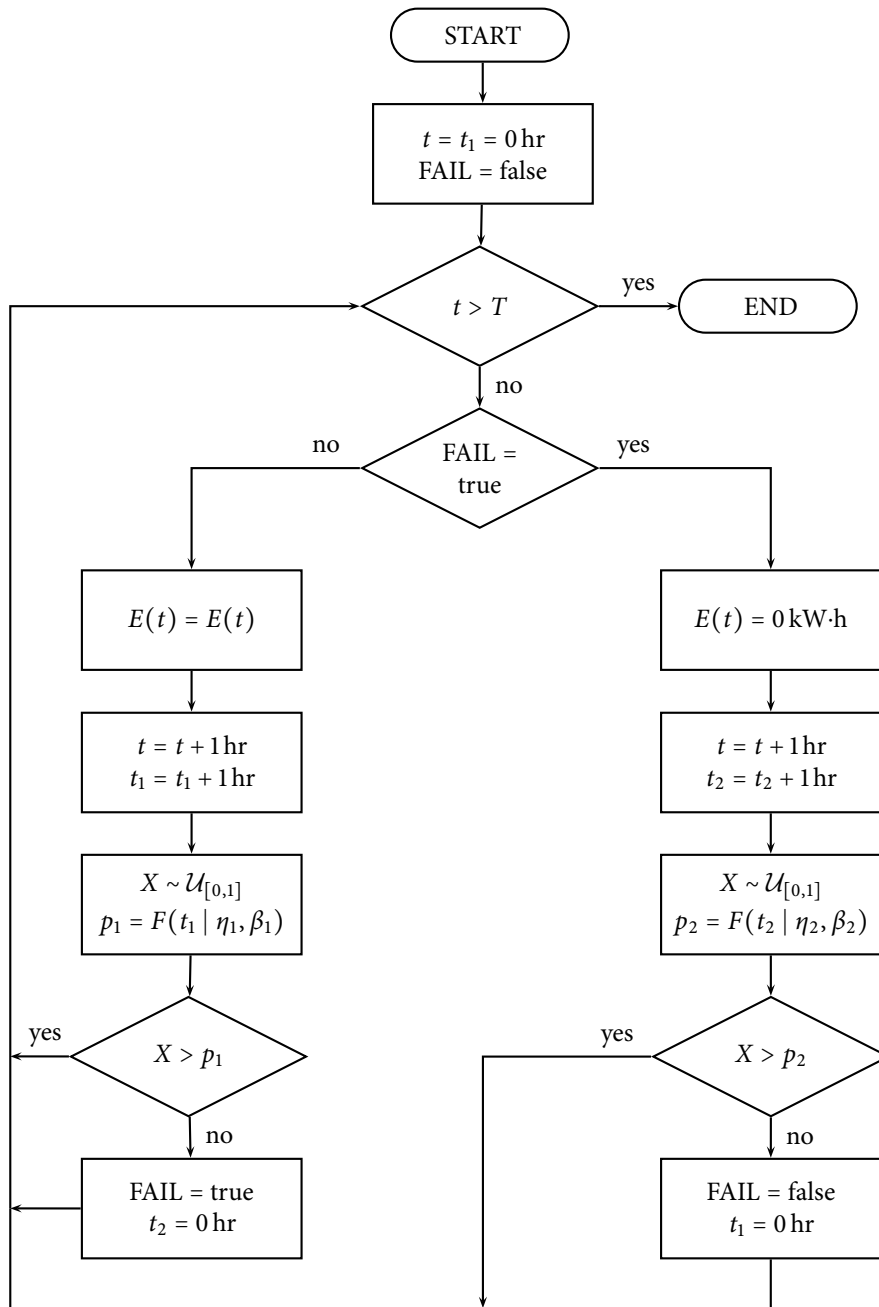


Figure 6.1: Flow diagram of reliability model for a PV system with a service life of T hours.

the system's service life. If it did, the simulation halted. If it did not, FAIL was checked to determine whether the system was in a failure state. If it was not, the system was assumed to run perfectly for the entire hour t and $E(t)$ was left at its ideal value. Next, both t and t_1 were incremented and $p_1 = F(t_1 | \eta_1, \beta_1)$ was calculated, p_1 being the probability that a failure would occur at time t_1 since recovery from the last failure. Then X was sampled from the uniform distribution between zero and unity ($\mathcal{U}_{[0,1]}$) and compared to p_1 . If $X > p_1$, no failure occurred and the program returned to the beginning of the loop. If, however, $X \leq p_1$, a failure occurred. In that case, FAIL was set to true and t_2 was set to 0 hr before returning to the start of the loop.

If the check of the FAIL flag at the start of the loop indicated the system was already in a failure state, the system was assumed not run at all for the entire hour t and $E(t)$ was reset to 0 kW·h. Next, t and t_2 were incremented and $p_2 = F(t_2 | \eta_1, \beta_1)$ was calculated, p_2 being the probability that the system would recover at time t_2 since onset of the failure. Then X was sampled from $\mathcal{U}_{[0,1]}$ and compared to p_2 . If $X > p_2$, the system did not recover and the program returned to the beginning of the loop. If $X \leq p_2$, the system recovered; then, FAIL was set to false and t_1 was set to 0 hr before returning to the start of the loop.

The loop was executed repeatedly until it covered the entire lifetime of the system (i.e., until $t > T$). The main loop and its sub-loops were implemented in part using code specific to Matlab in order to accelerate program execution. The program's output was a modified matrix $E(t)$ whose elements were reset to 0 kW·h for each hour t during which the system had failed.

6.3.1 SIMULATION RESULTS

Figure 6.2 shows the annual energy output of the system over a 30-year service life for a typical simulation using the algorithm outlined above. The total energy produced by the system over its life is simply the sum of the energy production in each of the system's 30 years. In order to obtain an adequate number of samples for analysis, the simulation must be repeated a sufficient number of times to ensure stability of the statistical moments of the output quantities. The required number of samples is a function of model complexity and

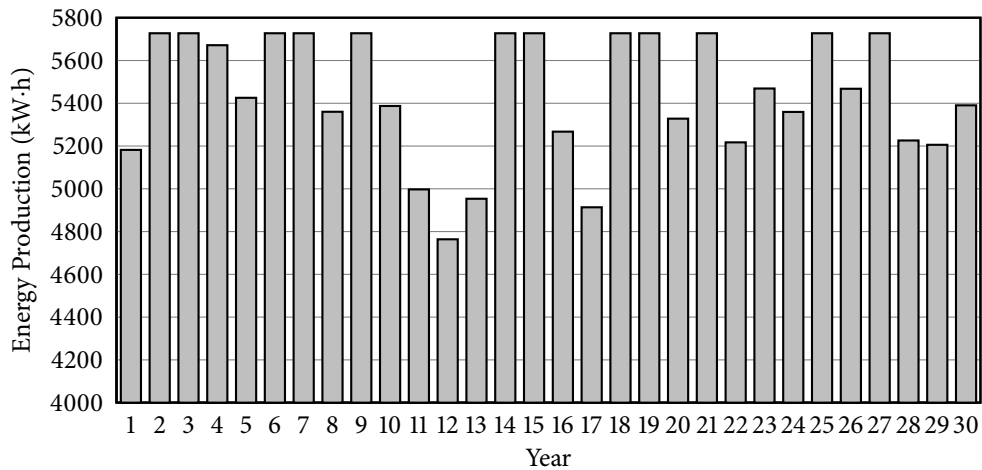
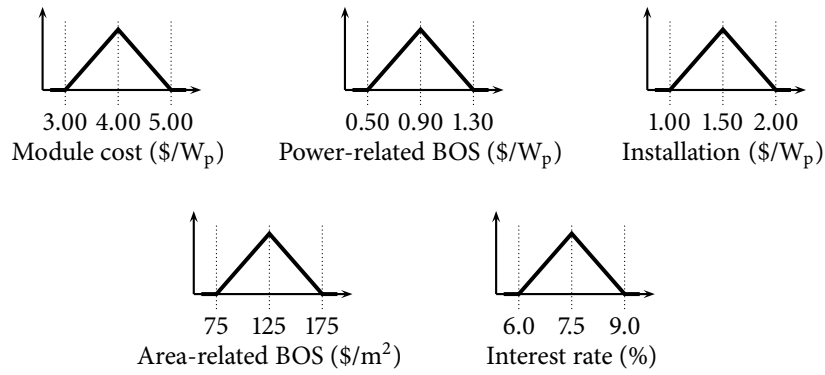


Figure 6.2: Typical modeled annual energy output for the sample PV system over its 30-year life span.

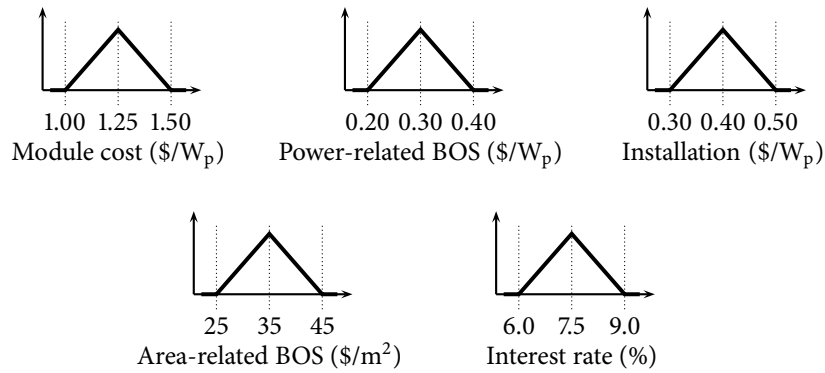
input variable specifications.

The cost of the system is modeled using standard equations for amortizing a loan [148], with simple adjustments for U.S. federal tax credits on interest payments. Its inputs are module cost, power- and area-related BOS costs, installation cost, interest rate, and marginal tax rate. It also requires the system's lifetime, rated power, and area. If only the minimum and maximum possible values for each variable were known, the uniform distributions could be assumed and the system cost could be computed using simple interval arithmetic instead of stochastic methods. However, Monte Carlo simulation is required when the values in the range are not equally probable. Two different cases were investigated in these simulations, one a base case corresponding to current PV system prices and the other a low-cost case corresponding to the *U.S. Photovoltaic Industry Roadmap* goals for 2020. Each case assumed triangular probability distributions for five cost-related input parameters as shown in Figure 6.3. Both cases use the same energy production estimates. For each sample in the simulations, the calculated system cost is divided by the energy produced to yield an estimate of the energy cost per kWh. The aggregate of the samples was used to produce the probability distribution functions for the cost of energy shown in Figure 6.4.

In the absence of inverter failures, the simulated system produces 5727.5 kWh per year.



(a) Base case.



(b) Low-cost case.

Figure 6.3: Input distributions for system component costs and financial parameters.

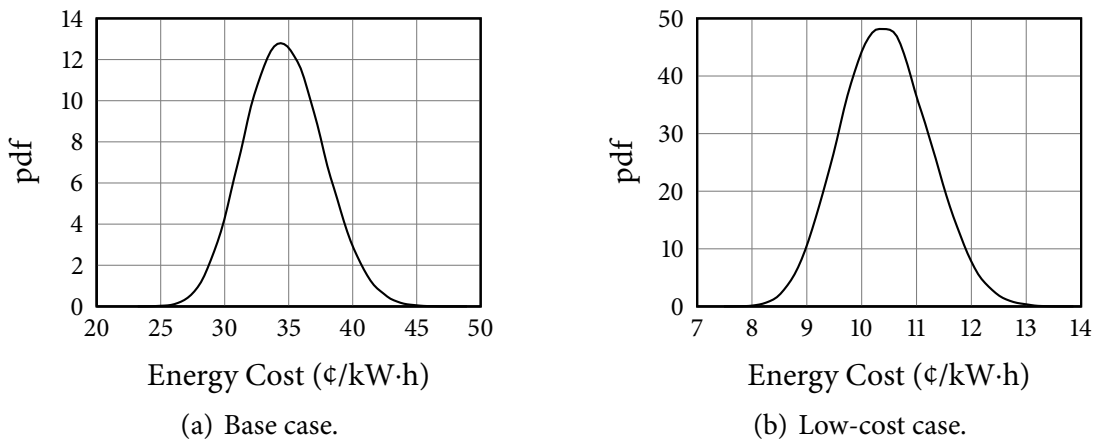


Figure 6.4: Probability density function for the cost of energy produced by the system over its 30-year lifetime. (a) Mean 34.7 ¢/kW·h, 90% confidence interval 29.8 ¢/kW·h to 39.8 ¢/kW·h. (b) Mean 10.4 ¢/kW·h, 90% confidence interval 9.2 ¢/kW·h to 11.8 ¢/kW·h.

Using this energy output level and the median values of the input distributions shown in Figure 6.3 to calculate the total cost of the system yields an estimated energy cost of \$0.330/kW·h for the base case and \$0.099/kW·h for the low-cost case. These are the results that would be obtained if only deterministic estimates of the cost parameters were used. The probability density function for the energy cost resulting from Monte Carlo simulations of this system is shown in Figure 6.4. The mean cost of the electricity produced by the system the base case is \$0.347/kW·h, with a 90% confidence interval of \$0.298/kW·h to \$0.398/kW·h. Thus, while the system is expected to produce electricity at a cost of \$0.347/kW·h, the actual cost can lie anywhere within the confidence interval. In the low-cost case, the mean energy cost is \$0.104/kW·h and the 90% confidence interval is \$0.092/kW·h to \$0.118/kW·h. The true cost of each system will depend on the actual cost of the system components, the actual interest rate paid, and the actual incidence of system failures and their durations.

If failures are neglected, the mean cost of energy obtained in this simulation is \$0.330/kW·h for the base case and \$0.099/kW·h for the low-cost case, both the same as for the deterministic estimates. Thus, the mean cost of the system failures is \$0.017/kW·h in the base and \$0.005/kW·h in the low-cost case. Thus, in both cases the economic cost of the system failures is about 5% of cost of electricity without failures. That it should be the same fraction of the cost in each system is unsurprising considering that the electricity cost is directly proportional to the installed cost of the system. Therefore, an inverter with the reliability characteristics of the one modeled in these simulations would be expected to add, on average, 5% to the cost of electricity produced by the system as a result of random failures.

6.3.2 SENSITIVITY ANALYSIS

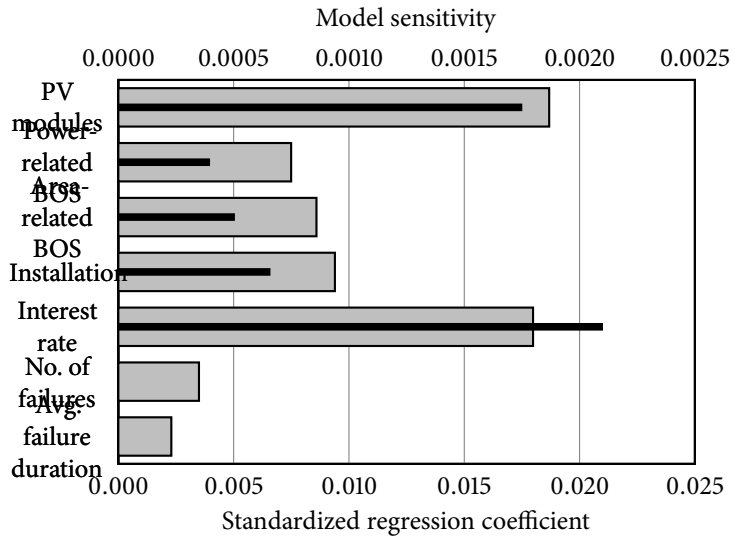
Sensitivity analysis was performed using two different methods. The first method calculated model sensitivity by calculating the change in energy cost produced by a 1% change in each of the input parameters, using the median values of the distributions shown in Figure 6.3 as bases. The results are represented by the black bars in Figure 6.5. Each input was varied independently in this calculation, and the result indicates which parameters have the greatest influence over energy cost when considered independently. One of the weaknesses of this

method is that it cannot be used with parameters that are inherently stochastic. Since there is no way to accurately represent the impact of system failures on energy cost in a deterministic manner, it is not possible to determine model sensitivity to these parameters and they have no black bars in Figure 6.5.

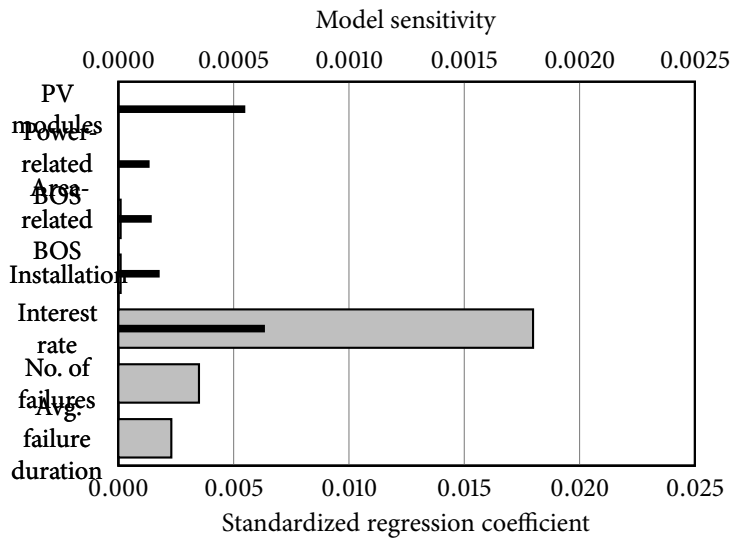
The second method used the statistical data generated by the Monte Carlo simulation to calculate standardized regression coefficients for each of the inputs [149], represented by the gray bars in Figure 6.5. The number of failures over the system's life and the average duration of each failure were both included in the regression. These coefficients indicate the change in energy cost resulting from a change of one standard deviation in the associated input. For example, a one-standard-deviation increase in module cost in the base case (about $\$0.41/W_p$, given the distribution of Figure 6.3) will increase the energy cost by $\$0.019/kW\cdot h$. Calculating sensitivity in this manner simultaneously accounts for the effects of model sensitivity and input uncertainty, both of which contribute to uncertainty in the energy cost. Thus, while model sensitivity indicates that the model is most sensitive to the interest rate, the uncertainty in module cost during the Monte Carlo simulation had the greatest impact on energy cost given the simulation's assumptions. Another advantage of this method of sensitivity analysis is that it can be used when correlations exist between input parameters, while the method above assumes independent inputs.

The model sensitivity results for the base case, shown in Figure 6.5(a), indicate that the most expedient way to reduce the cost of energy produced by the PV system would be to reduce the PV module cost or to find a mortgage with a lower interest rate. The standardized regression coefficients indicate that the uncertainties in these same two input parameters are most responsible for the uncertainty in the energy cost. As noted, the first method could not be applied to system reliability; however, the second method indicates that the two measures of system reliability, while not insignificant, are the least significant of the investigated parameters.

In the low-cost case, shown in Figure 6.5(b), model sensitivity is qualitatively the same as it was in the base case, though quantitatively it is smaller in magnitude for all inputs. This indicates that a 1% change in any of the parameters will produce a smaller change in



(a) Base case.



(b) Low-cost case.

Figure 6.5: Sensitivity of energy cost to the input parameters. Black bars show model sensitivity, the change in energy cost per 1% change in the input parameter. Gray bars show the standardized regression coefficient, the change in energy cost resulting from a change of one standard deviation in a given input.

energy cost than the same 1% change would in the base case. This is not surprising since the magnitudes of both the inputs (with the exception of interest rate) and the energy cost are smaller than in the base case. As in the base case, model sensitivity for the low-cost case indicates that reducing the module cost or the interest rate would be the most expedient way to reduce energy cost. While the model sensitivity of the low-cost case was qualitatively similar to that of the base case, the standardized regression coefficients differ substantially. In the low-cost case, they indicate that nearly all of the uncertainty in energy cost comes from the uncertainties in the interest rate and system failure characteristics. These mask the effects of uncertainty in the other parameters, even despite the high model sensitivity to module cost. Thus, while reducing uncertainty in module cost would significantly reduce the uncertainty in energy cost in the base case, it would not reduce it noticeably in the low-cost case (though the high model sensitivity indicates that reducing module cost itself — as opposed to uncertainty in module cost — would still be expected to have a significant effect on energy cost in both cases).

It should be noted that both methods of sensitivity analysis linearize the model to produce a local approximation of the relationships between the inputs and the energy cost. Therefore, the results shown in Figure 6.5 are not global and, as shown, can change substantially when the input assumptions change.

It should also be stressed that the values and distributions used in these simulations, while intended to be realistic, are hypothetical examples used to illustrate the application of Monte Carlo simulation to this model. In order to apply this approach to real systems and obtain meaningful data, appropriate input distributions must be identified for real PV system components.

These preliminary results demonstrate the successful development of a stochastic treatment for the problem of estimating PV system energy output in the face of random system failures. The method has been further developed to incorporate a stochastic method for estimating the uncertainty in the cost of energy generated by the PV system. By using a stochastic model, a greater range of information can be incorporated into the model than in traditional simulations. Furthermore, the statistical tools that can be brought to bear on the

output data provide powerful methods for gaining insight into system design and behavior. The approach demonstrated here provides a flexible, multifaceted tool for investigating PV system cost components and behavior.

6.4 CHARACTERISTICS OF INVERTERS FOR PHOTOVOLTAIC SYSTEMS

PV inverters all share a set of common characteristics. In nearly all cases, they convert DC power from a PV system to AC at one of the standard utility voltages. The AC may be single- or three-phase, and may be 50 or 60 Hz. They often incorporate maximum power point trackers (MPPTs) to ensure the maximum available energy is extracted from the PV modules. Off-grid PV systems often use on-site energy storage such as batteries, and inverters meant for these systems will sometimes incorporate circuitry to manage battery charging and discharging. Grid-connected PV systems, which have become the most common systems in recent years, require circuitry to synchronize their output with that of the power grid.

For purposes of reliability analysis, PV inverters may be broadly classified in three categories: easily accessible, remote, and unserviceable:

- *Easily accessible* inverters are located in a house, place of business, or utility site. They are monitored regularly, if not continuously, and may be reached easily for repair. These make up the majority of the PV inverter market.
- *Remote* inverters are located at an isolated site that requires AC power, such as a remote telecommunications installation. They may be monitored remotely, but are difficult for repair crews to reach.
- *Unserviceable* inverters cannot be serviced once put into service. An example is an inverter in a PV-powered satellite, which cannot be reached once in orbit. Because these inverters are specialized and often one-of-a-kind designs, they are the most likely to have unusual features (e.g., to produce AC at 400 Hz instead of standard utility frequencies [150]).

The first two classes are treated as repairable systems. While unserviceable inverters are repairable in theory, they cannot be repaired in practice and are therefore considered non-repairable. Inverter topologies can vary considerably within each class, depending in part upon inverter size, grid-tie requirements, and anticipated operating environment. Excellent reviews of modern inverter topologies may be found in [132, 151, 152].

The relative importance of reliability for each class of inverter can be described by the costs associated with failure. In general, the cost of a failure is equal to the value of the energy that would have been generated while the system was down (cost of energy not served) plus the cost of repair and replacement parts, which may require a premium if repair crews are dispatched at unusual times, and any penalties perceived by the end-user. In a grid-connected PV system, a perceived penalty would be the cost of the energy purchased to replace the energy not generated, while in an off-grid system one would include any physical losses incurred as a result of the down time. The character and value of these physical losses can run a wide gamut: In a remote cabin they might come in the form of spoiled food, while in a satellite they would be equal to all of the construction and launch costs, minus any economic benefit derived prior to the failure. Some systems may also incur contractual penalties when failures occur.

The cost of failure is, in general, lowest for easily accessible inverters. Their failures are the easiest to detect and repair, minimizing downtime and repair costs. However, if failures are frequent the costs of service can add up over time and the inconvenience caused by downtime can grow into a more serious issue. Failures in remote inverters can take longer to notice, longer to repair, and require more time “on the clock” for repair crews, making individual failures in these inverters more expensive than those of easily accessible inverters. Finally, failures of unserviceable inverters are the most costly, since the entire unit powered by the inverter is permanently lost.

In the following sections, a method is developed to estimate inverter reliability and evaluate designs for maximum availability. To illustrate the method, sample calculations are made based on the topology of the inverter employed in the 342 kW_p PV system installed on the roof of the Georgia Tech Aquatic Center (GTAC), though the method is general enough

to apply to other designs. The advantages of the approach are discussed and a call is made to establish a repository of failure data to facilitate further study and validation of PV inverter reliability investigations.

The goal of the proposed approach is to establish a means of estimating inverter reliability on the basis of subsystem, rather than component, failure data. A subsystem may consist of multiple components, each making its own contribution to the subsystem failure rate, and different subsystems can have different component counts. As a result, failure rates for individual components can result in misleading conclusions about which sections of the inverter are most likely to fail. The proposed method, by considering reliability at the subsystem level, aims to simplify inverter reliability assessment and focus inverter design efforts on the most unreliable subsystems; these, in turn, can be dissected and analyzed at the component level. Inverter availability is also considered within the context of repairable systems. This offers inverter designers two paths to improving uptime, reducing the number of failures and minimizing failure duration, providing a broader range of design options.

6.5 DETERMINATION OF INVERTER FAILURE AND REPAIR RATES

Failure rates are best determined from field data on failure times and modes, but may also be determined from accelerated life testing. However, such data is not widely available. Sandia National Laboratories and the Florida Solar Energy Center both have ongoing programs to monitor inverters in the field and collect reliability data, but thus far the information they have collected has not been made publicly available. Similarly, inverter manufacturers conduct accelerated life tests and may collect field data on the failure rates of their products, but they are reluctant to share this information. Finally, failures may be estimated using models of component aging based on operating environment, temperature, voltage stress, and other relevant factors [153, 154], though these so-called physics-of-failure methods tend to be complex and unsuitable for estimation of field reliability [155]. For purposes of the present study, this leaves two sources available for estimating failure rates: field failure data from the GTAC inverter and published standards for failure rate prediction.

6.5.1 GTAC INVERTER EXPERIENCE

In advance of the 1996 Olympic Games in Atlanta, a 342 kW_p PV system was installed on the GTAC roof. At the time of its installation it was the largest roof-mounted PV array in the world. The system consists of 2856 120 W_p multicrystalline Si modules wired in 238 series strings of 12 modules each, installed directly on the roof with an approximate standoff height of 9 cm. The power from the roof is fed to an electrical room, located underneath the diving pool, via seven circuits through a single 315 kW (DC) power conditioning unit (PCU), which performs the inversion and injects the power into the local utility grid through a Δ -Y isolation transformer. The system is described in detail in [156, 157], and an extensive review of its performance over its first decade of operation appears in [158].

The overall availability of the system since its commissioning in June 1996, which includes all downtimes due to failures and scheduled experiments, is 87%, as shown in Figure 6.6. This relatively low value is explained by two factors. First, while failures have generally been detected within a couple of days, periods of downtime were prolonged by delays in obtaining replacement parts. Second, the GTAC building that houses the PV system on its roof underwent an 18-month renovation during 2002 and 2003, resulting in a number of planned and unplanned disconnections to accommodate construction.

The power conditioning system is the least reliable part of a PV system. Although the PCU accounts for less than 7% of the complete cost of the GTAC PV system, it is responsible for almost all system downtime. The PCU installed at GTAC was one of the first PV PCUs of that size installed in the US, which may explain a somewhat high number of outages early in its service life. The dates when failures occurred, times between failures (TBF), times to repair (TTR), and causes of failure are summarized in Table 6.1.

The power conditioning system used in the GTAC PV system originally had two ventilation fans, supplied by three-phase AC voltage source, installed on top of the cabinet in the horizontal position. These malfunctioned on several occasions. When a fan fails, the temperature inside the PCU cabinet rises above the designed safe value and an overtemperature sensor temporarily disables the PCU. This results in series of on/off periods during the

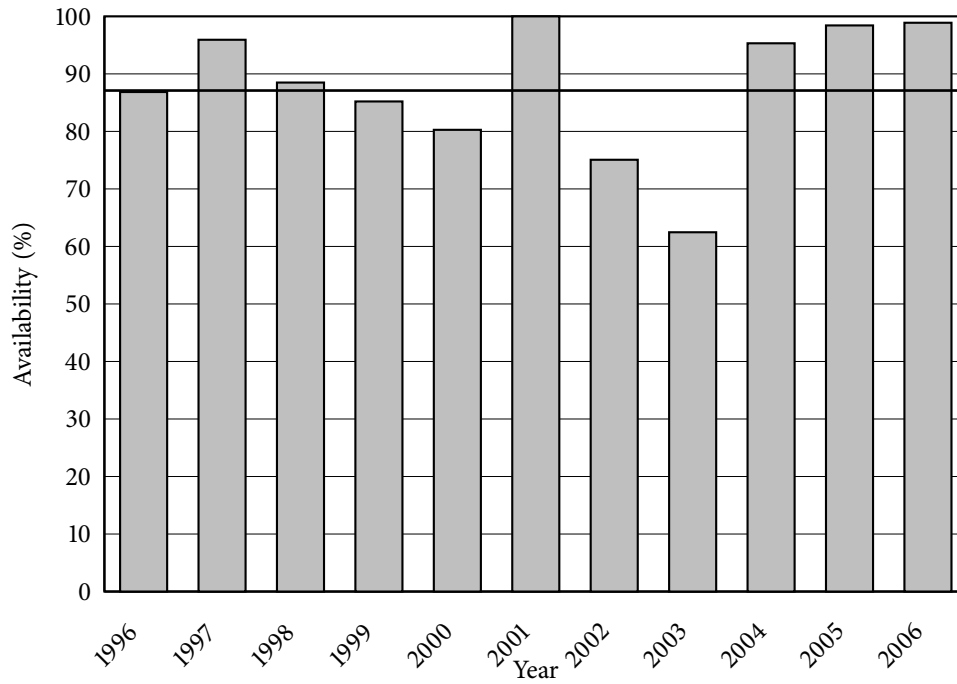


Figure 6.6: GTAC PV system availability (through March 2006). The solid black line represents average system availability since system activation in July 1996.

Table 6.1: Failure history of the GTAC PV system.

Fault #	Fault date	TBF (days)	TTR (days)	Failure description
Start	07/01/96			
1	07/15/96	14	15	Lightning strike
2	10/08/96	85	9	Plumbing failure
3	05/01/98	570	18	Current transducer
4	06/02/98	32	31	PCU fan
5	09/28/99	483	66	PCU fan
6	02/27/00	152	32	PCU fan
7	06/06/00	100	24	DC matrix IGBT
8	07/07/00	31	17	PCU fan
9	10/28/03	1208	7	Ground fault

day, depending on the ambient temperature. If failure occurs during winter, the system may work for the whole day without interruptions, while a failure during summer may produce more than five off/on sequences. This type of behavior causes difficulties in diagnosing the fault, since operation may appear almost normal. After several fan replacements and system inspection, the fans were redesigned to remove the cause of recurrent fan failures. The three-phase fans were replaced with single-phase versions in July 2000, and aside from a major ground fault the system has been operating without interruption since that time.

There were also several non-recurring faults. The current transducer in the PCU failed in May 1998 and had to be replaced. One of the IGBTs in the DC switching matrix broke down in June 2000, and the whole matrix had to be rebuilt. However, the IGBT failure is suspected to be the result of an overtemperature situation with the PCU fans as the root cause. Finally, the data acquisition system (DAS) was recalibrated in 1998; however, that did not interfere with the system's operation.

Because the redesign of the PCU fans has nearly eliminated failures from the system, the GTAC failure history cannot be considered representative of the inverter in its current form. Indeed, the only system failure that has occurred since that time was a ground fault that was unrelated to the inverter itself. As a result, the failures incurred by the GTAC inverter must be considered infant mortality failures. This conclusion is further supported by the fact that the GTAC inverter was, at the time it was constructed, a new model that the vendor had not yet deployed in the field. Unfortunately, no other failure histories for similar inverters are available for analysis. As a result, failure rates must be estimated using a reliability prediction standard.

This experience with the GTAC inverter emphasizes the need to collect data from a large number of identical or similar systems to improve the accuracy of failure estimates. While a small quantity of input data can be analyzed using techniques like Weibull analysis, a lack of data increases uncertainty in the estimated failure rates. Reliability prediction standards are available to assist in forecasting failure rates, but PV inverters often operate in inhospitable environments where they are exposed to extreme temperatures and frequent thermal cycling and load stress. Accurate assessment of inverter reliability requires a larger

amount of information from a larger number of identical or similar systems, or a smaller number of systems observed over a longer period of time.

6.5.2 ESTIMATING FAILURE RATES FROM A PREDICTION STANDARD

Alternatively, failure rates for individual components may be estimated from a failure rate prediction standard, then aggregated to produce subsystem failure rates. While at first glance this seems at odds with the previously stated intention to investigate subsystem failure rates so the failure rates of individual components does not *need* to be addressed, this exercise fulfills several functions. First, it provides component failure rates that will be used later to show that attention may be focused on the wrong subsystem when only component, and not subsystem, failure rates are considered. Second, it permits the construction of an illustrative example of the proposed method in the absence of sufficient field data. Finally, it illustrates how subsystems may be defined and decomposed for further analysis.

Reliability standards are helpful, but since reasonable inverter designs frequently contain a large number of components reliability calculations can be complicated and time-consuming to implement. Furthermore, standards frequently lag behind advancing technology and many of the components in use today cannot be found in some of the most widely used standards. The absence of these components from the standards requires that information be found about their operation at extreme temperatures and a determination made about whether this information is accurate. It is possible to account for this by thermal modeling, but then the validity of the thermal model must be proven.

The oldest and most widely used standard is MIL-HDBK-217F [159], which was developed in 1962 by the U.S. Department of Defense to provide a common basis for comparison of reliability predictions for competing electronic equipment designs [155]. It provides reliability models for numerous part types used in electronic systems. These models are based on a combination of field data, statistical analysis, and simplifying assumptions for the part types it covers. It is often criticized for being “pessimistic,” that is, producing reliability computations that indicate lower reliability than experienced in the field [155, 160]. In recent years a number of alternatives to MIL-HDBK-217F have been developed, notably [161], which was

originally developed by Bellcore specifically for consumer, as opposed to military, electronic hardware [155], and IEEE 493 [162], which was developed to address issues of power system reliability. However, the goal of the present work is to describe a novel approach to PV inverter reliability analysis; as such, qualitative results are more important than quantitative ones. Furthermore, quantitative results based on the GTAC PCU cannot be applied to other inverter designs. Therefore, for illustrative purposes failure rates are based primarily on MIL-HDBK-217F and IEEE 493. The methods outlined here are, however, flexible enough to accommodate failure probabilities calculated by other methods.

The failure rates modeled in [159] are constant in time and take on the form:

$$\lambda = \lambda_b \prod_{i=1}^n \pi_i, \quad (6.21)$$

where λ_b is the base failure rate and the π_i are modifiers that account for operating environment and other factors affecting reliability (the number of modifiers n depends on the component type).

As previously noted, the major subsystems in the GTAC inverter are the PCU cooling fans, the IGBTs that drive the inverter stage, and the energy-storage capacitors in the inverter stage. Therefore, failure rates must be estimated for each of these subsystems. Performing these estimates using a failure rate catalog requires the subsystem failure rate to be estimated from aggregated failure rates for the individual components that comprise the subsystem. To estimate failure rates for the GTAC inverter, specifications for the components from each of the major subsystems were used to estimate component failure rates. Then, part counts were used to aggregate these into failure rates for the entire subsystem.

The calculations used to estimate the failure rates for individual components are detailed in the following sections. Data collected from the GTAC inverter indicates that its typical operating temperature is in a fairly narrow band around 40 °C; this is the operating temperature for which the following failure rates were estimated.

6.5.2.1 Storage Capacitor Subsystem

The failure rate model for capacitors prescribed by MIL-HDBK-217F is:

$$\lambda_C = \lambda_b \pi_{CV} \pi_Q \pi_E, \quad (6.22)$$

where π_{CV} is the capacitance factor, π_Q is the quality factor, and π_E is the environment factor.

The base failure rate λ_b for a capacitor with a rated operating temperature of 105 °C is:

$$\lambda_b = 0.00254 \left[\left(\frac{S}{0.5} \right)^3 + 1 \right] \exp \left[5.09 \left(\frac{T + 273}{378} \right)^5 \right], \quad (6.23)$$

where the stress factor S is the ratio of operating voltage to maximum rated voltage and T is the operating temperature in °C.

The capacitance factor π_{CV} is:

$$\pi_{CV} = 0.34C^{0.18}, \quad (6.24)$$

where C is the rated capacitance. Values for π_Q and π_E are tabulated in MIL-HDBK-217F for various quality and environment specifications, respectively.

The GTAC inverter has 32 capacitors rated at 3300 μ F, 450 V, 105 °C, non-mil-spec. The peak voltage applied to the capacitors is 375 V. Because the capacitors are non-mil-spec, $\pi_Q = 10$, and their relatively benign indoor operating environment yields $\pi_E = 1.0$. These figures yield a failure rate $\lambda_C = 3.03$ per million hours per capacitor.

6.5.2.2 Power Stage Driver Subsystem

Because MIL-HDBK-217F was last updated in 1991 it does not make provision for estimating IGBT failure rates. Previous investigators have coped with this by basing their IGBT failure rates on power MOSFETs [160], bipolar power transistors [163], or by turning to an alternative failure rate catalog such as RDF 2000 [164]. For purposes of this work, the authors elected to use the method described in [160], which sets the IGBT failure rate equal to half that of an equivalent power MOSFET. Thus, the IGBT failure rate was calculated according to:

$$\lambda_{IGBT} = 0.5\lambda_b \pi_T \pi_Q \pi_E, \quad (6.25)$$

where π_T is the temperature factor and π_Q and π_E are the quality and environment factors, respectively.

For MOSFETs, $\lambda_b = 0.060$. The temperature factor π_Q is computed from:

$$\pi_T = \exp \left[-1925 \left(\frac{1}{T_j + 273} \cdot \frac{1}{298} \right) \right], \quad (6.26)$$

where T_j is the junction operating temperature of the device, assumed here to be equal to the ambient temperature of 40 °C. As for capacitors, the quality and environment factors are tabulated in MIL-HDBK-217F; for non-mil-spec MOSFETs, $\pi_Q = 5.0$, and $\pi_E = 1.0$ for conditions corresponding to the inverter's operating environment.

Following this procedure for the eight 1200 V non-mil-spec IGBTs in the GTAC inverter yields a failure rate of $\lambda_{IGBT} = 0.90$ per million hours.

6.5.2.3 Cooling Subsystem

MIL-HDBK-217F does not directly address cooling fans such as the ones used in the GTAC inverter PCU, and addressing them as motors according to that standard yields extremely high rates of failure that are quite at odds with operating experience since the single-phase fans were installed seven years ago. IEEE 493, which contains failure data collected from power electronic equipment in the field, suggests a failure rate for propeller fans of the type used in the GTAC inverter PCU of 0.01041 per year. This translates to $\lambda_F = 1.36$ per million hours.

6.5.2.4 Isolation Transformer

Again, MIL-HDBK-217F does not directly address isolation transformers. However, IEEE 493 gives a failure rate of 0.00284 per year for Δ -Y isolation transformers smaller than 600 V. This annual failure rate corresponds to an hourly failure rate of 0.37 per million hours. Thus, the failure rate assumed for the 480 V isolation transformer in the GTAC inverter is $\lambda_T = 0.37$ per million hours.

6.5.3 ESTIMATING REPAIR RATES

As a repairable system, when the inverter fails during its service life the cause of the failure will be diagnosed and repaired. The amount of time required to complete the repair will be the sum of the times required to detect the failure, summon maintenance personnel to the site, diagnose the problem, obtain and install spare parts, test the repair, and reactivate the inverter. All of these times will be influenced by the inverter classification (as described in section 6.4), the proximity and availability of maintenance personnel, the complexity of the diagnosis and repair, and the availability of spare parts. As noted in section 6.5.1, much of the downtime experienced by the GTAC inverter has been spent waiting for spare parts.

Because the time to repair is largely a function of factors that cannot be scientifically quantified, it is not possible to estimate it from a prediction standard (except in specific circumstances — IEEE 493, for example, includes MTTR data that a utility might find useful, but that is not applicable to independently operating PV systems). Instead, it must be estimated from field data, operating experience, or, in the worst case, informed opinion based on the factors likely to contribute to repair time in a particular situation. When the sample of chronological repair data is small, the uncertainty in the predicted repair rate is large. As with failure data, the more information available the more accurate the repair time estimate. In the present case, the best available repair data comes from the GTAC failure record; therefore, this is what will be used to estimate repair rates for the inverter subsystems.

The GTAC inverter has experienced replacement of an IGBT and two capacitors. All three of were replaced simultaneously after the DC matrix IGBT failure in 2000. This leaves only one data point for the repair rate estimates for IGBTs and capacitors. While it is possible — even likely — that independent failures of these components would produce different repair rates for each, there is presently no way to know for certain. As a result, the repair rates are assumed constant for IGBTs and capacitors with a mean time to repair (MTTR) equal to 24 days, or 576 hours, as indicated by Table 6.1. This implies an exponential distribution for the repair time with repair rates μ_{IGBT} and μ_C for IGBTs and capacitors, respectively, equal to 0.0017 per hour. No failures of the isolation transformer have been experienced, but it will be seen in

Table 6.2: Weibull parameters and sample repair times for GTAC inverter repair distributions.

Subsystem	η (hr)	β	Repair times (hr)		
			10%ile	MTTR	90%ile
Cooling	995	2.18	355	881	1458
Power Stage Driver	576	1	61	576	1376
Storage Capacitors	576	1	61	576	1376

the next section that its predicted failure rate is small enough to be neglected in simulations; therefore, its repair rate is not estimated.

The PCU fans failed four times before they were replaced in 2000. While the current single-phase fans are not identical to the original three-phase fans, diagnosis and replacement of the new fans in the event of a future failure can be reasonably expected to take roughly the same amount of time as for the originals. Therefore, the repair times shown in Table 6.1 may be used to estimate the repair rates for the current PCU fans. As previously stated, the Weibull distribution is well suited to describing probability distributions using only a small amount of field data [145]. Accordingly, the PCU fan repair times from Table 6.1 were fit to the two-parameter Weibull distribution using MLE, yielding $\eta_F = 995$ hr and $\beta_F = 2.18$. Substituting these into equation (6.16) yields a MTTR equal to 881 hr. By equation (6.17), this corresponds to a non-constant repair rate $\mu_F = (6.18 \times 10^{-7})t^{1.18}$ per hour.

Recalling that the Weibull distribution with $\beta = 1$ is identical to the exponential distribution, all three repair distributions are summarized in Table 6.2 as Weibull distributions, along with the corresponding 10th and 90th percentile repair times. The table suggests that maximum repair times are similar for all three systems, but that on average, IGBT and capacitor failures will be repaired more quickly than fan failures. This is consistent with the fact that $\beta_F > 1$, which indicates short repair times are unlikely. While it must be borne in mind that these values are derived from a small sample of field data, no qualitative difference may be asserted between these estimates and those that would be produced by informed opinion, the only other repair time estimation method available for the given data set. Clearly, the quality of these estimates would improve with a larger data set.

6.6 MODELING INVERTER RELIABILITY AND AVAILABILITY

The inverter may be modeled as a chain of functional blocks connected in series, each corresponding to a subsystem of the inverter circuit fulfilling a particular function. For example, one block may represent to the inverter's temperature control circuitry, another the IGBTs in the switching stage, and another the DC bus capacitors. Note that these blocks do not necessarily share a one-to-one correspondence with inverter topology, but since the inverter cannot function without any of them they are considered to be series-connected for purposes of reliability analysis. As a result, the failure of any one block constitutes a failure of the inverter as a whole. It is important to note that the level of detail may be increased here in nested decompositions, all the way down to individual components. However, here it is presented only as a viable approach to reliability analysis and to motivate further work to determine the level of decomposition necessary to provide a sufficient model of inverter reliability and failure modes.

6.6.1 SIMULATING INVERTER FAILURES

Inverter failures were modeled by representing the inverter as three series-connected blocks representing the cooling system, power stage driver, storage capacitors, and isolation transformer. Since the blocks were series-connected, a failure in any one block resulted in a failure of the entire inverter. The failure rates computed for individual components were multiplied by the quantity of the component in the PCU and the product used as the total failure rate in the simulation. These values are summarized in Table 6.3. Since the subsystem failure rate for the isolation transformer is more than an order of magnitude lower than those of the other subsystems, it is neglected for purposes of the simulation.

These failure rates were used in a 10,000-sample Monte Carlo simulation to estimate the numbers of each type of failure the inverter would be expected to encounter over its rated 30-year service life. The mean number of failures of any type over the 30-year simulation period was 25.2, distributed according to the histogram in Figure 6.7(a). The distributions of fan, IGBT, and capacitor failures are shown in Figures 6.7(b), 6.7(c) and 6.7(d), respectively. Clearly, capacitor failures dominate.

Table 6.3: Failure rates (per million hours) used for Monte Carlo simulation of GTAC inverter.

Subsystem	Component fail rate	Component quantity	Subsystem fail rate
Storage Capacitors	3.03	32	97.0
Power Stage Driver	0.90	8	7.2
Cooling	1.36	2	2.4
Isolation Transformer	0.37	1	0.37

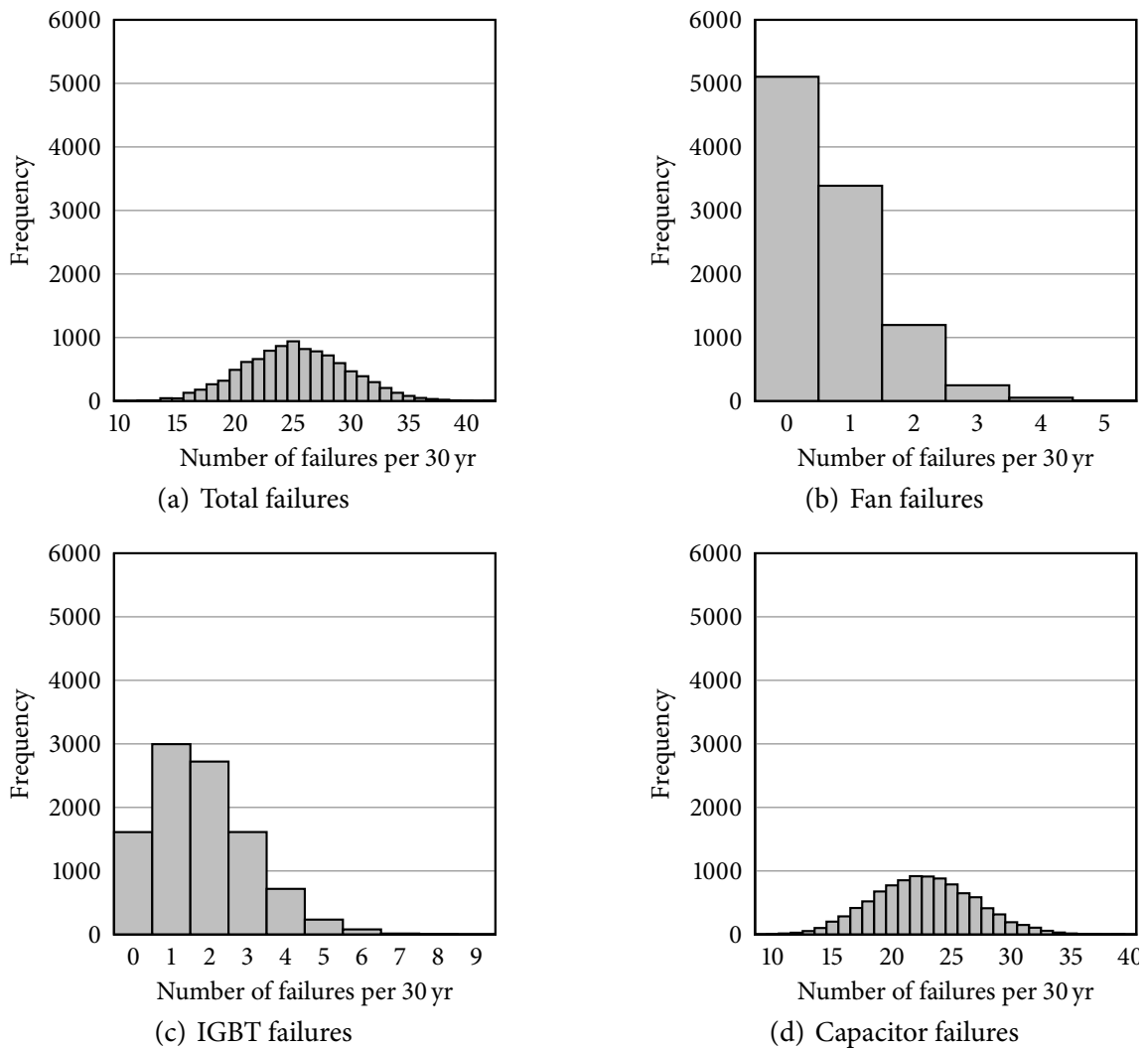


Figure 6.7: Histograms showing distributions of failures per inverter subsystem modeled over 30-year service life using failure rates from Table 6.3 and 10 000 samples.

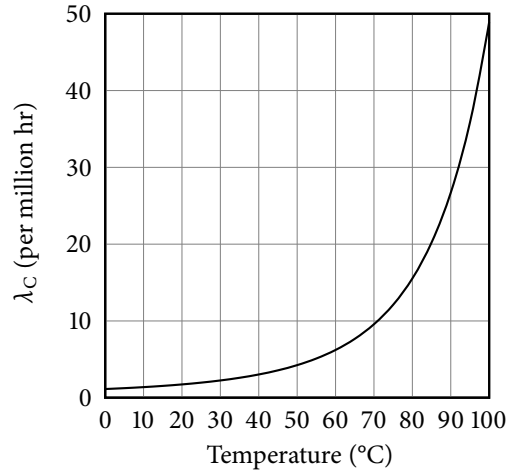


Figure 6.8: Capacitor failure rate modeled as a function of temperature.

It should be noted that many inverters are exposed to much harsher operating environments than the GTAC inverter, particularly small consumer inverters of the type used in residential PV systems. It is not uncommon for PV inverters to be exposed to operating temperatures as high as 70 °C [165]. The capacitor failure rate for the type of capacitor used in the GTAC inverter is illustrated as a function of temperature in Figure 6.8.

From the histograms in Figure 6.7 it is clear that the simulation predicts much more frequent failures than Table 6.1 indicates have actually been observed in the GTAC inverter. This is a result of the pessimistic assumptions of the MIL-HDBK-217F prediction standard and once again underscores the need for a greater volume of inverter reliability data.

6.6.2 IMPROVING INVERTER AVAILABILITY

Several methods have been proposed to increase the availability of PV inverters. In principle, the simplest and most desirable method is simply to increase the reliability of the most vulnerable components; specifically, the DC bus capacitors. In practice, however, this involves a substantial increase in component costs, as the only commercially available high-reliability capacitors are expensive military-grade capacitors. Availability may also be increased without improving reliability by reducing repair times. This may be accomplished through the use of user-serviceable parts that can easily be changed in much the same manner as a fuse or a light

bulb. The viability of this approach relies on sufficient built-in diagnostic methods to alert the user that a serviceable part needs replacement, and would also need to be accomplished in a manner that protects the user's safety and does not compromise UL listing [141]. The requirements for each of these methods to improve availability are explored in the following sections.

6.6.2.1 *Increasing Reliability*

To reduce the number of capacitor failures, the simulation was repeated using failure rates for capacitors of higher quality. Military specification capacitors were assumed, corresponding to type "M" in MIL-HDBK-217F with $\pi_Q = 1.0$. Using this value with equation (6.22) produces a failure rate estimate of $\lambda_C = 0.30$ failures per million hours. This was multiplied by 32 to account for the quantity of capacitors in the inverter and the Monte Carlo simulation repeated using 10,000 samples. The results are shown in Figure 6.9. The reduced capacitor failure rate results in a much narrower distribution of both total failures and capacitor failures, as shown in Figures 6.9(a) and 6.9(d), respectively.

With the high-reliability capacitors, the mean number of failures over the 30-year inverter life drops from 25.2 to 5.1. The number of each type of failure for the two simulations is summarized in Table 6.4. As expected, the decline in the total failure rate is due exclusively to the greater reliability of the capacitors, and the reduction in the standard deviation of the number of capacitor failures also reduced the standard deviation of the total number of failures. The increased reliability offered by the military-grade capacitors brings the number of storage capacitor subsystem failures over the inverter's life into line with that of the other failure modes.

6.6.3 INCREASING REPAIR RATES

Another way to increase the availability of a repairable system is to increase the rate at which failures are repaired when they occur. A number of methods exist for allocating failure rates to achieve a desired system availability goal [166]. Typically, the goal in using these is to calculate the desired failure rate on the basis of a known repair rate. However, they may also

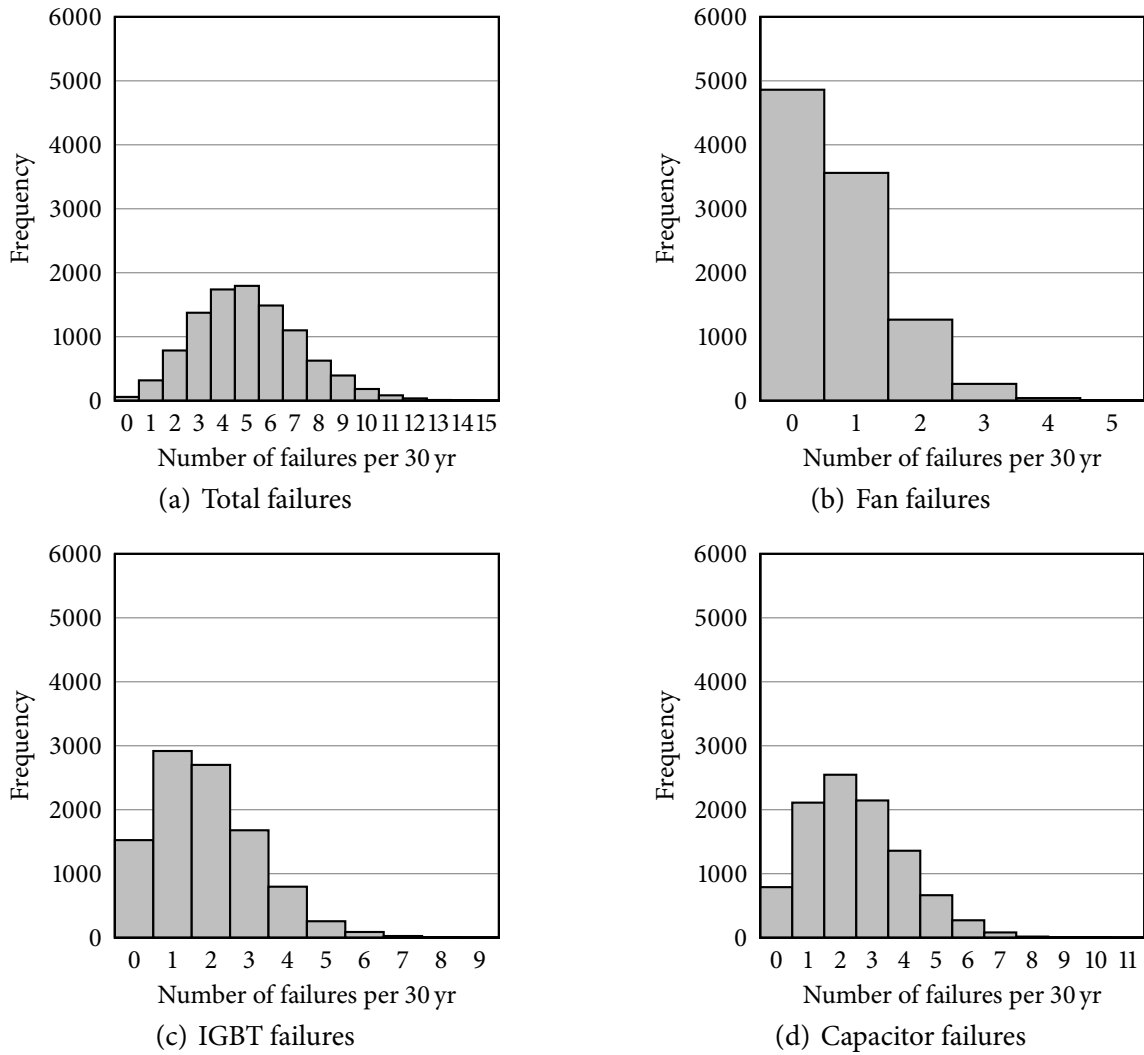


Figure 6.9: Histograms showing Distribution of failures per inverter subsystem modeled over 30-year service life using failure rate for military-grade capacitors (0.30 per million hours) with rates for other components from Table 6.3 and 10 000 samples.

Table 6.4: Mean (standard deviation) number of failures and overall mean availability in 30-year inverter life for 10,000 simulations.

	Standard	Mil-spec
Cooling	0.7 (0.8)	0.7 (0.8)
Power Stage Driver	1.8 (1.3)	1.9 (1.4)
Storage Capacitors	22.7 (4.3)	2.5 (1.6)
Total	25.2 (4.5)	5.1 (2.2)
Mean Availability (%)	94.4	98.9

be used to determine the required repair rate to achieve a given level of availability on the basis of known failure rates.

In section 6.6.2.1, availability was increased from 94.4% to 98.9% by using high-reliability military-grade capacitors instead of standard consumer-grade capacitors. However, military-grade components are cost-prohibitive, particularly considering that PV inverter manufacturers would like to see capacitor costs cut in half. Using failure allocation methods, repair rates may be calculated that will provide the same level of availability as using military-grade capacitors.

Recall from equation (6.6) that system availability is the product of the availabilities of each subsystem. If the system is required to have 98.9% availability, and each subsystem is required to have the same availability as every other subsystem, then each subsystem i must have availability A_i equal to 99.6%. Since the failure rates are all constant, equation (6.8) may be rewritten:

$$\sigma_i = \frac{\lambda_i}{\mu_i}, \quad (6.27)$$

where λ_i and μ_i are the failure and repair rates, respectively, for subsystem i . Solving equation (6.27) for μ_i yields:

$$\mu_i = \frac{\lambda_i}{\sigma_i}, \quad (6.28)$$

where

$$\begin{aligned} \sigma_i &= \frac{1}{A_i} - 1 \\ &= 0.0037. \end{aligned} \quad (6.29)$$

Substituting λ for each of the subsystems from Table 6.3 yields the required repair rate for each subsystem, displayed with its corresponding MTTR in Table 6.5.

Comparing the results with the MTTRs derived from the GTAC repair data in Table 6.2 indicates that the repair rates for the PCU fans and IGBTs at GTAC are sufficient to achieve the desired availability. However, capacitor repair rates must improve by an order of magnitude.

Table 6.5: Required repair rates to achieve 98.9% availability with consumer-grade components.

Subsystem	Required μ (per million hr)	MTTR (hr)
PCU fans	736	1358
IGBTs	1948	513
Capacitors	26,264	38.1

The capacitor MTTR of 38.1 hours — just over a day and half — suggests that achieving such high reliability with consumer-quality components will require the capacitors to be user-serviceable, and that replacement capacitors be widely available.

6.7 DISCUSSION

Cheaper, more reliable inverters are required if PV systems are to become a widely accepted means of generating electric power. Industry consensus is that the single largest roadblock preventing this goal from being achieved is the quality of the capacitors currently available [167]. Unserviceable inverters, which are usually found only in projects with enormous budgets, are able to overcome this issue by using much more reliable military-grade capacitors and other high quality components in order to maximize the reliability and minimize the chance failure of the mission-critical subsystem. However, this is not an option for the vast majority of inverters sold.

It must be stressed that the decomposition of the inverter subsystems illustrated here is not the only decomposition possible, nor is it necessarily the most appropriate one. The most effective and realistic decomposition will be based on field failure data and tied closely to inverter topology. Since topology and failure rates can vary from inverter to inverter, and component counts and sizes are largely dependent upon the amount of power the inverter is designed to handle, the ideal decomposition will vary from inverter to inverter. For example, a detailed decomposition of a three-level inverter might follow the wind converter model of [168], with an emphasis on component reliability. However, determination of the optimal model should be based both on inverter design information and experimental data from

which such identification would be made possible.

Furthermore, this study does not address failure modes that do not completely shut down the inverter. These may occur when parts wear out and operate with reduced effectiveness without failing catastrophically, as can happen near the end of a capacitor's service life [153, 169]. They may also occur in fault-tolerant inverter designs [170–173] and in inverters that use fault-tolerant components such as self-healing capacitor arrays [172]. These add a layer of complexity to modeling efforts in that the inverter may continue to operate at reduced (or even full) effectiveness despite the presence of a fault. However, they may offer opportunities for fault detection and repair that minimize failure costs by allowing repairs to be delayed until a scheduled shutdown period.

Detailed component failure data is required to enable deeper decompositions of inverter subsystems and more in-depth study of failure modes. Further study of other reliability-related effects, such as component aging in the harsh PV operating environment, are highly compatible with the modeling framework presented here and may provide deeper insight into the failure mechanisms of PV inverters and their components. However, regardless of the models employed, accurate forecasting of inverter reliability requires a reasonably large amount of failure data that reflects the components, subsystem designs, and operating conditions typically found in PV inverters.

The estimated component failure rates used here are sufficient for purposes of developing this analysis method, but application and validation require additional field data. Partial validation of the model should be possible through the use of synthesized statistical data sets, but the present work is limited in scope to analysis of inverter reliability given the subsystem failure rates. These rates are calculated in an ideal case from large databases of chronological failure records in the absence of which partial data sets can be used to reconstruct such information. However, the purpose of this paper is to propose a subsystem-based methodology to simplify the analysis of inverter reliability and availability. The absence of large database of failure information prevents a thorough validation, which the authors look forward to doing in the future.

Efforts to study, understand, and improve inverter reliability would benefit greatly from

the establishment of an international database of failure data from which to draw meaningful and accurate forecasting inputs. This is because the information available in failure prediction standards might not provide accurate data for components as they are used in PV inverters, particularly where high-temperature operation is concerned, and some of the standards do not contain all of the components currently used in PV inverters. Several efforts to collect inverter and PV system reliability data have already been started [138, 139, 174], but these initiatives are limited in scope and do not make detailed data on inverter failures widely available. Therefore, the authors promote the idea of a more organized and collaborative effort, perhaps resulting in an international repository of data available to a large group of people who can use it for reliability assessment.

6.8 CONCLUSIONS

In this study, a model was developed for the stochastic simulation of PV system failures. The model uses probability distributions to simulate the random intervals between failures and the length of time required to repair a failed system. Using Monte Carlo simulation techniques, the model was applied to the deterministic output from a PV system model to estimate the effect of random system failures on energy production. For the failure and repair distributions assumed in the sample calculation it was found that system failures increase the cost of electricity from PV by about 5%. This figure will be different for different failure distributions, so this result is not and cannot be universal. However, the model may be applied to any PV system provided appropriate failure distributions are available.

A methodology was also developed for estimating failure distributions for inverters, the most often failed components in PV systems, on the basis of their topology. This methodology is based on well established reliability assessment techniques, but is simplified to accommodate the rapid pace of PV inverter development. The methodology divides the inverter into subsystems based loosely upon the inverter's topology. Next, the components in each subsystem are evaluated to determine their individual failure rates. The failure rates for all of the components within each subsystem are summed to give an aggregate failure rate for the subsystem. Using this information, inverter failures may be simulated and the subsystem

causing them noted. In this manner, the least reliable subsystems may be identified and targeted for improvement. In the case of an inverter matching the topology of the GTAC inverter, capacitors are by far the most troublesome component. This is consistent with PV industry experience [167].

The failure rate calculation was repeated assuming the use of military-grade capacitors. While these are cost-prohibitive for use in consumer and industrial inverters, applying the methodology to them provides a best-case scenario. The use of these capacitors was shown to provide much better results and significantly higher system availability than when consumer-grade capacitors were assumed. The possibility of equaling the availability attained with the military grade capacitors by accelerating repair times was investigated. It was determined that the capacitors would require an MTTR of about 38 hr to achieve this, implying that the capacitors would have to be user-serviceable. While this option is currently being explored, it is still in its early stages of development.

CHAPTER 7

GUIDELINES FOR FUTURE WORK

In this thesis, a series of models were linked to assess the cost and performance of all aspects of photovoltaics across the entire value chain. In some cases, this involved nothing more than novel applications using existing models, such as establishing low-cost solar cell design guidelines on the basis of first principles and simulations performed with the device simulator PCID. In other cases, however, it involved the derivation and development of complex original models. In the end, a process was demonstrated to model the value chain from silicon to solar cell to working PV system. However, because of the breadth and generality of this topic, which encompasses nearly the entire field of photovoltaics, an enormous number of possibilities exist for future research.

In this chapter, several applications for the manufacturing cost model developed in Chapter 5 are suggested for which the results would be particularly notable. Further improvements to the model itself are also suggested, and a development path is suggested to more tightly integrate all of the models across the value chain into a single inter-operable suite.

7.1 IMPROVE SCALE ESTIMATES IN MANUFACTURING COST MODEL

The easiest and most immediate improvement that could be made to the manufacturing cost model is to improve the capital and material cost data used to model the effects of economies of scale. In many cases, enough data exists to make a very good estimate of capital cost as a function of throughput, and of material unit cost as a function of material volume purchased. However, in some cases the data are somewhat lacking. In these cases, as described in section 5.3 and Appendix C, the scale estimates were based on guidelines from the literature.

This situation, while acceptable, is not ideal and can be rectified by additional data collection. This is a straightforward task, though the lacking data are not available from

published sources and must therefore be collected directly from equipment and material vendors. This is a time-consuming task and, while it *will* improve the accuracy of the estimate, the manufacturing cost is relatively insensitive to small errors in the costs of most materials. However, it *can* be sensitive to the exponent that relates cost to throughput and volume, which is the primary reason to desire more complete cost data.

It is also important to note that all cost data must be revisited periodically to ensure up-to-date accuracy. This is a function of prices changing over time, both because of inflation and for other reasons (e.g., supply problems, advances in manufacturing methods, or changes in material quality requirements) and cannot be avoided.

Finally, some PV manufacturing processes exist or have been proposed that use equipment not surveyed by the editors of *Photon International*. Silicon ingot production equipment, such as Cz pullers and multicrystalline ingot furnaces, are the most important example of such equipment. While all of the manufacturing cost modeling presented in this thesis was based on HEM multicrystalline wafers, to extend the model to other types of wafers will require information on the capital, material, and labor requirements of those methods.

7.2 MONTE CARLO SIMULATION TO ASSESS UNCERTAINTY IN MANUFACTURING COST

It is often the case in assessing manufacturing cost that some parameters are not known with a great deal of certainty. Even for the most mature technologies, certain things about the manufacturing process simply cannot be known accurately without spending a great deal of time and money on pilot production lines and plant design. By analyzing uncertainties in the process specification it is possible to better understand the accuracy of the manufacturing cost estimate and how to improve it. Monte Carlo simulation is well suited to this task.

Monte Carlo simulation was discussed in Chapter 4, where it was used to model the effects of variability in material parameters on solar cell efficiency. It was used again in Chapter 6 to model the reliability of PV systems. Its application to the manufacturing cost model described in Chapter 5 would work in much the same manner as in these other applications: The values of one or more parameters in the model would be assigned a probability distribution that

reflects the degree of certainty the modeler has about the parameters. These distributions would then be sampled and the manufacturing cost calculated for each sample to produce a statistical distribution on the manufacturing cost estimate.

Constructing these distributions differs from constructing those representing material variability, which should be based on measured physical data, and PV system reliability, which should be based on system failure data collected in the field or estimated using a reliability handbook such as MIL-HDBK-217F [159]. In the case of manufacturing cost estimation, uncertainty arises from capital costs and labor and material requirements and cannot be characterized by physical measurements or tabulated data. In general, uncertainty in the cost model parameters must be estimated on the basis of expert opinion.

This does not diminish its importance or significance. For example, during the development of a specialized piece of equipment one might only know that it will cost between \$300 000 and \$1 million. Using this as a measure of uncertainty in the equipment's capital cost, the developers of the equipment can use the cost model in conjunction with Monte Carlo simulation to understand the impact of the machine's capital cost on the manufacturing cost of the solar cells or modules it will be used to make.

This idea can be extended to other aspects of the equipment's operation: material requirements, labor requirements, and throughput, for example. By using Monte Carlo simulation to model the uncertainty in these factors simultaneously, a complete picture of the impact on manufacturing cost can be developed. This includes a strongly bounded estimate of the error in the calculated manufacturing cost; furthermore, through additional statistical analysis, the sensitivity of the manufacturing cost to these parameters can be estimated. Among other things, this can allow one to assess which of the uncertain parameters are the most important to address [175].

Having Monte Carlo simulation at one's disposal would be helpful not just for assessing process steps using new equipment, but also for accounting for uncertainty during the early stages of process development. For example, even though screen-printing of metal pastes for contact formation is well understood, during process development it might be difficult to know how much paste each solar cell will require with great precision (particularly if the

paste formulation to be used during production is not yet established, in which case the price of the paste may also be uncertain). Monte Carlo simulation can translate this uncertainty into the associated uncertainty in manufacturing cost.

While Monte Carlo simulation is not the only method available for assessing uncertainty and sensitivity of manufacturing cost to its input parameters, it is the only one that can simultaneously evaluate a large number of uncertain parameters. Simultaneous evaluation captures the effects of interactions between parameters and can also account for correlations between variables. This power comes at the cost of increased evaluation time, as thousands or even millions of samples may be required to perform an effective simulation, and increased complexity in setup and analysis. However, variance reduction techniques and modern statistical analysis software can mitigate these disadvantages considerably.

7.3 MODELING THE MANUFACTURING COST OF ORGANIC AND OTHER “NEXT GENERATION” SOLAR CELLS

Several solar cell technologies that are still in relatively early stages of development have been designed specifically with low manufacturing costs in mind. However, because the manufacturing processes proposed for these designs are, in most cases, incomplete or highly speculative, it is difficult to quantify how much these technologies might cost while they are still under development. The cost model developed in this thesis, in combination with the Monte Carlo simulation techniques described in section 7.2, might be applied to help assess not just how much these technologies might cost to manufacture, but to help direct research by assessing which manufacturing processes hold the most promise.

As explained in Chapter 5, a complete manufacturing cost estimate requires a manufacturing process specification and estimates of capital, material, and labor requirements. Clearly, these are difficult requirements to meet for a speculative process, and modeling manufacturing cost in a deterministic manner is unlikely to produce meaningful results. However, by explicitly accounting for the uncertainty in these speculative processes using probability distributions on input parameters and contingency costs to cover unforeseeable expenses, the utility of the results can be greatly enhanced.

Obviously, the more speculative the process, the greater the uncertainty, and by the time all uncertainties are accounted for the error bound on the manufacturing cost is likely to be very wide. However, a statistically based sensitivity analysis can help determine which parts of the process contribute most to the uncertainty, guiding researchers to the parts of the process most in need of refinement.

One very promising example of an ostensibly low-cost technology whose manufacturing processes are still speculative is organic solar cells. These are made from electrically conductive plastics that, in theory, can be manufactured using processes akin to those used to print newspapers and magazines. These manufacturing processes are expected by many to make large-scale production of organic cells rapid and inexpensive.

Currently, however, organic solar cells are relatively undeveloped; as a result, efficiencies are quite low and the service life of an organic cell is thought to be very short in comparison to crystalline silicon. While the past several years have seen rapid progress on both of these issues and laboratory research continues, there are still no rigorous estimates of what the manufacturing costs might ultimately be. This would be an ideal application for a Monte-Carlo-enabled manufacturing cost model.

7.4 DEVELOP AN INTER-OPERABLE SUITE OF MODELS TO SIMULATE THE ENTIRE PHOTOVOLTAIC VALUE CHAIN

Anytime one attempts to bring together several disparate models, such as was done in this thesis with device, system, manufacturing cost, and energy cost models, difficulties will be encountered in transferring data between them so the results from one model may be used within another. The data transfer issue is very important — whenever data is manipulated directly by the user there is a possibility that the user will introduce errors.

This can be avoided by ensuring that each of the models produces data in format that the others can parse. Such a suite of inter-operable models would not only minimize user error during data transfer, it would eliminate errors due to having to specify the same parameters to multiple models. For example, in the current arrangement the module power output must be specified to the system model and to the manufacturing cost model; if a user erroneously

supplies different values to each of the models, the simulation is ruined and must be repeated. If all models use the same set of inputs, this problem is avoided.

Producing such a suite of models appears to be a daunting task, particularly since some of the models used in this thesis are commercial products with proprietary restrictions and some are original models developed as part of this research. However, the amount of work required to accomplish this is not as great as it might seem:

- The University of New South Wales recently released the source code to the simple one-dimensional device model PC1D. As a result, it can now be customized to provide and transfer data in any manner required.
- Multidimensional device models such as DESSIS_{ISE} frequently use plain text files and other non-proprietary file formats to store and transfer data. Simple “helper” applications could be developed to parse these files and automate the transfer between models should this type of device model be used.
- The manufacturing cost model, as an original model developed in this research, can be freely modified to perform whatever tasks and conversions required.
- The system and energy cost modeling in this thesis relied on SAM, for which the source code is not publicly available. However, its algorithms are well known and many of them have already been incorporated into an original model developed in previous research at Georgia Tech [80]. This model could easily replace SAM in the system and energy cost modeling role with minimal additional development.

APPENDIX A

ECONOMIC CALCULATIONS FOR PHOTOVOLTAIC SYSTEMS

Photovoltaic systems are long-lived projects that produce electric power, a commodity with economic value, over an extended period of time. Since they require no fuel for operation, most of the expenses associated with a PV system occur during design and construction. It is tempting to suggest that the unit cost (e.g., ¢/kW·h) of generating electricity from photovoltaics is simply the installed cost of the system divided by the amount of energy produced over the course of its service life. This, however, is incorrect.

Even in the idealized case that the PV system never incurs any additional expenses beyond the initial purchase and installation cost, the time value of money affects the economic value of energy generated after the installation date — in other words, the cost of producing energy depends not just on how much energy is produced, but *when* it is produced. In reality, small maintenance expenditures occur over the course of the system's time in operation, and some components of the system may wear out and require replacement at irregular intervals. Clearly, these additional expenses must be factored into the cost calculation. Finally, costs associated with obtaining the capital required to finance construction of the PV system must be taken into account.

Taking all of these expenses into consideration to calculate a single value representing the unit cost of a unit of electricity generated by a PV system is relatively straightforward. It is accomplished by modeling all expenditures associated with the system as a series of annual cash flows over time. These cash flows need not be equal from year to year, and they can be analyzed to determine the cost of electricity produced by the system.

The analysis that follows is intended only as a primer and is based largely upon the work of Short et al. [26]. Deviations from this are noted in the text. Section A.1 introduces important terminology and mathematics from the field of finance. It describes what is meant

by terms like *cash flow* and *time value of money*. Section A.2 explains how to apply these concepts to the analysis of PV systems and calculate the levelized cost of electricity.

A.1 CONCEPTS IN FINANCIAL ANALYSIS

Analyzing the cost of generating electricity from PV consists of determining the annual expenditures associated with the system, adjusting them to account for inflation and the time value of money, and summing them to produce a meaningful assessment of their aggregate value. While simple in principle, a number of methods exist for making this assessment, though which are most appropriate depends on the intended purpose of the assessment.

The metric focused upon in this appendix is levelized cost of electricity. As described in Chapter 1, this has become the *de facto* metric upon which PV system economics are judged because it is easily comparable to utility electricity rates. This is not to say that other valuation measures are not useful, but in most situations LCOE is a sufficient figure of merit, if not the preferred one. For a complete discussion of other metrics, the interested reader is referred to [26].

The following sections describe the major concepts required to assess LCOE. Many of these concepts are exploited elsewhere in this thesis, particularly in Chapters 3 and 6. This appendix is intended to supplement those chapters and provide deeper insight into the economics of PV systems.

A.1.1 CASH FLOW

Simply put, cash flow is a measure of money received or spent. By convention, receipts are generally represented by positive values and expenditures by negative values. Net cash flow is the difference between receipts and expenditures. When expenditures are greater than receipts the net cash flow is negative, and vice versa. A chronological sequence of transactions is a *series* of cash flows.

A series of cash flows can be represented using a *cash flow diagram*, which presents a graphical view of expenditures in successive time periods. A cash flow diagram may show gross cash flows, in which case each time period may include more than one receipt or

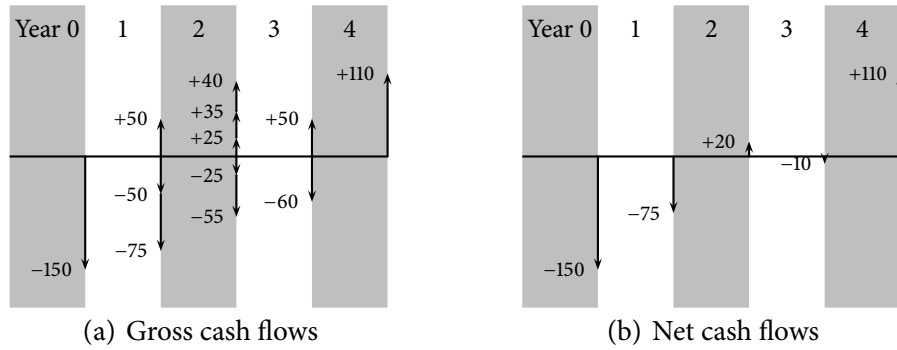


Figure A.1: Sample cash flow diagrams representing (a) gross and (b) the equivalent net cash flows (arbitrary units).

expenditure, or it may show net cash flows. Figure A.1(a) shows a series of positive and negative cash flows over a five-year period; Figure A.1(b) shows the same series expressed as net cash flows.

Since PV systems operate over a span of decades, financial parameters such as finance rate, inflation, and the time value of money are critical factors in determining the levelized cost of electricity. The actual expenditures on the PV system are represented as negative cash flows, while the monetary value of annual electricity production is represented as a series of positive cash flows. The unit cost of electricity for which the positive cash flows cancel the negative cash flows determines LCOE. This is discussed in greater detail in section A.2.

A.1.2 INFLATION

When discussing cash flows and the time value of money, it is important to recognize the difference between value and purchasing power. Suppose prices increase by 3% in the coming year. In that case, a year from now \$1.03 will be required to purchase an item that costs \$1.00 today. However, \$1.00 invested today at an annual rate of 10% will grow to \$1.10 in a year's time. The former describes the change in purchasing power over time, while the latter reflects the change in value. One can purchase an item for \$1.00 today, or invest \$1.00 for a year's time, purchase the same item then for \$1.03, and have \$0.07 left over. This introduces the idea of *nominal* and *real* cash flows. A nominal cash flow is not adjusted for inflation and describes

an expenditure or receipt in terms of the actual amount of a transaction. A real cash flow is simply a nominal cash flow adjusted for inflation to some base year. In the example above, \$1.00 invested today represents a nominal cash flow of $-\$1.00$ in the base year resulting in a nominal cash flow of $+\$1.00$ one year from now.

Inflation describes the change in buying power of a dollar over time. It is typically expressed as a percentage over a period of time. An annual inflation rate of 3% indicates that goods available for a dollar today will cost \$1.03 in a year's time. More generally, P_0 dollars worth of goods will cost P_n dollars in n years time, where

$$P_n = P_0(1 + e)^n \quad (\text{A.1})$$

and e is the annual inflation rate. Conversely, P_n dollars in year n has the buying power of P_0 dollars in the base year where

$$P_0 = \frac{P_n}{(1 + e)^n}. \quad (\text{A.2})$$

Base-year dollars are often called *constant* or *real* dollars, while n -year dollars are called *current* or *nominal* dollars. Real dollars measure buying power and should always be used when comparing cash flows from different years. However, transactions are always conducted in nominal dollars (except those occurring during the base year, when real and nominal dollars are equivalent). Hence, equation (A.2) must be used to convert nominal dollars to real dollars before comparing cash flows from different years.

A.1.3 DISCOUNT RATE

The discount rate describes the change in value of a dollar over time. It is superficially quite similar to the inflation rate, but the distinction between buying power (described by inflation) and value (described by the discount rate) is important. While a dollar today has less buying power than a dollar tomorrow, that dollar may be invested in an interest-bearing account and earn a return that outpaces inflation. The value, in real dollars, of an amount P invested for n years at an annual interest rate d is

$$P_n = P \left(\frac{1 + d_n}{1 + e} \right)^n. \quad (\text{A.3})$$

Discount rates are often expressed as *nominal* and *real* discount rates. The rate d_n in equation (A.3) is the nominal discount rate. The real discount rate d_r is simply d_n adjusted for inflation:

$$d_r = \frac{1 + d_n}{1 + e} - 1, \quad (\text{A.4})$$

and equation (A.3) can be equivalently written:

$$P_n = P(1 + d_r)^n. \quad (\text{A.5})$$

In practice the discount rate represents the rate of return required from an investment. This requirement is not the same for all investors. As a result, the discount rate is generally determined on a project-by-project basis and may be adjusted by the investor to account for the perceived risk in the investment. Determining the appropriate discount rate for energy projects is a vast subject about which entire volumes have been written [176]. In the United States, the National Institute of Standards and Technology (NIST) annually publishes discount rates for use in life-cycle cost evaluations of renewable energy projects in federally owned and leased buildings [177]. For 2006 it specifies a real discount rate of 3.0% and a nominal discount rate of 4.6%. By way of comparison, the U.S. Department of Energy's Solar America Initiative requires applicants for its Technology Pathway Partnerships to use a real discount rate of 5.5% in evaluating their proposals [178]. However, private investors may use higher discount rates than these if they perceive a particular energy project to be risky or simply require a higher return on investment. For example, the cost of capital to electric power utilities is typically higher than the discount rates for federal projects, requiring utilities to use higher discount rates in order to maintain profitability [179].

A.1.4 NET PRESENT VALUE

Net present value (NPV) is the value, in real dollars, of a series of cash flows. It is most commonly used to determine whether a project is economical, or to compare two competing projects to assess which will be more profitable. It is generally applied to after-tax cash flows.

The formula for computing NPV is:

$$C_{\text{NPV}} = \sum_{i=0}^N \frac{F_i}{(1 + d_r)^i}. \quad (\text{A.6})$$

If the NPV is positive, the project will be profitable and is considered economical. If it is negative, the project will lose money and is considered uneconomical. When comparing two or more projects, the one with the highest NPV is the most economical.

It is important to note the dependence of NPV on discount rate, which appears in the denominator of equation (A.6). When the discount rate is high, compounding effectively reduces future cash flows and gives greater weight to those occurring early in the analysis period. The cost-effectiveness of a project, then, depends heavily on both the discount rate and the distribution of positive and negative cash flows over the life of the project. An increase in discount rate can change NPV from positive to negative; similarly, when comparing two projects it can change the conclusion about which is more economical.

A.2 CALCULATING THE LEVELIZED COST OF ELECTRICITY

The levelized cost of electricity (LCOE) — also known as the levelized bus bar cost — for an energy-producing facility is computed from the net present value of the cash flows throughout the facility's life cycle. This includes initial expenses, operating and maintenance expenses, taxes, and decommissioning expenses [180]. The levelized cost allows the costs of competing energy technologies to be compared even when they operate on different scales, require different levels of investment, or operate over different time periods [26].

The total life cycle cost (TLCC) is [26]

$$C_{\text{TLCC}} = I + C_{\text{O\&M}}, \quad (\text{A.7})$$

where I is the initial investment required and $C_{\text{O\&M}}$ is the present value of all operating and maintenance costs. If the system has a service of N years, $C_{\text{O\&M}}$ is

$$C_{\text{O\&M}} = \sum_{i=1}^N \frac{C_i}{(1 + \delta)^i}, \quad (\text{A.8})$$

where C_i is the operating and maintenance cost in year i and δ is the annual discount rate.

LCOE is the cost per unit energy produced by the system over the analysis period that equals the TLCC when discounted back to the base year. The LCOE is

$$C_{\text{LCOE}} = \frac{C_{\text{TLCC}}}{\sum_{i=1}^N \frac{Q_i}{(1+\delta)^i}} \quad (\text{A.9})$$

where Q_i is the energy produced in year i .

APPENDIX B

EXAMPLES USING THE ANALYTICAL COST MODEL

This chapter contains additional examples showing how to use and interpret the analytical model presented in Chapter 3 for calculating efficiency premium and module cost for grid parity.

B.1 EXAMPLE EFFICIENCY PREMIUM CALCULATION: CRYSTALLINE SILICON AND CADMIUM TELLURIDE

This calculation compares the current best commercially available c-Si and CdTe PV modules in a residential system on the basis of efficiency premium using the 2005 MYPP benchmarks to determine BOS costs. System one uses the c-Si module, which is assumed to be a Sunpower module with 17.0% efficiency and -0.36% /celsius temperature coefficient. System two uses the CdTe module, represented by a First Solar module with 11.1% efficiency and a temperature coefficient of $-0.25\%/^{\circ}\text{C}$. The results of this calculation were presented in Table 3.13 on page 89.

The comparison proceeds as follows:

1. Using equation (3.1), the area-related cost of each module is computed. BOS costs are determined using module efficiency and the function derived for residential systems in 2005 as shown in Table 3.5. Finally, the values for AWOCT are taken from Table 3.3 for glass/cell/polymer module architecture tilted at 22.6° . The data gathered are displayed in Table B.1.
2. Compute r from equation (3.42) using these values:

$$\begin{aligned} r &= \frac{0.111 \times [1 - 0.0025 \times (45.1^{\circ}\text{C} - 25^{\circ}\text{C})]}{0.170 \times [1 - 0.0036 \times (47.3^{\circ}\text{C} - 25^{\circ}\text{C})]} \\ &= 0.67. \end{aligned} \tag{B.1}$$

Table B.1: Input data for efficiency premium calculation comparing Sunpower c-Si module with 17% efficiency to First Solar CdTe module with 11.1% efficiency.

Parameter	System 1 Sunpower	System 2 First Solar
Module efficiency, η	0.170	0.111
Module cost, A_m (\$/m ²)	638	194
Module temperature coefficient, α_T (%/°C)	-0.36	-0.25
Expected AWOCT, \bar{T} (°C)	47.3	45.1
BOS cost, A_{bos} (\$/m ²)	527	450
Expected system life, N (yr)	30	30

3. From the values in Table B.1, the BOS parameters ν and ω are:

$$\begin{aligned}\nu &= \frac{\$527/\text{m}^2}{\$638/\text{m}^2} \\ &= 0.83\end{aligned}\tag{B.2}$$

$$\begin{aligned}\omega &= \frac{\$450/\text{m}^2}{\$527/\text{m}^2} \\ &= 0.85.\end{aligned}\tag{B.3}$$

4. Since $N_1 = N_2$, let $\lambda_F = \lambda_D = 1$ and skip to step 9.

9. Compute $(A_{m,2}/A_{m,1})_{eq}$:

$$\begin{aligned}\left(\frac{A_{m,2}}{A_{m,1}}\right)_{eq} &= 0.67 + (0.67 - 0.85) \times 0.83 \\ &= 0.53.\end{aligned}\tag{B.4}$$

10. Compute the efficiency premium:

$$\begin{aligned}\Delta C_m &= \left(0.53 \times \frac{0.170}{0.111} - 1\right) \times \$3.75/W_p \\ &= -\$0.73/W_p,\end{aligned}\tag{B.5}$$

yields a $\$0.73/W_p$ premium that the negative sign indicates favors system one.

This efficiency premium suggests that the maximum economical cost for the CdTe modules is $\$3.02/W_p$. Since they cost only $\$1.75/W_p$, they are more economical than the c-Si modules by a large margin. See section 3.4.2 for further discussion of this calculation.

Table B.2: Input data for efficiency premium calculation comparing Sunpower c-Si module with 17% efficiency to First Solar CdTe module with 11.1% efficiency.

Parameter	System 1	System 2
Module efficiency, η	0.200	0.165
Module cost, A_m (\$/m ²)	300	
Module temperature coefficient, α_T (%/°C)	-0.50	-0.25
Expected AWOCT, \bar{T} (°C)	47.3	45.1
BOS cost, A_{bos} (\$/m ²)	350	315
Expected system life, N (yr)	30	20

B.2 EXAMPLE EFFICIENCY PREMIUM CALCULATION: CRYSTALLINE SILICON AND CADMIUM TELLURIDE WITH UNEQUAL SERVICE LIVES

This calculation compares the 20%-efficient c-Si module targeted for grid parity in 2015 to a hypothetical CdTe module with 16.5% efficiency (the current record for a CdTe module). Like the previous section, it compares them on the basis of efficiency premium; however, it assumes the c-Si module has achieved a retail cost of \$1.50/W_p and that the CdTe module has a service life of only 20 yr. The results of this calculation were presented in Table 3.14 on page 90.

The comparison proceeds as follows:

1. Using equation (3.1), the area-related cost of each module is computed. BOS costs are determined using module efficiency and the function derived for residential systems in 2005 as shown in Table 3.5. Finally, the values for AWOCT are taken from Table 3.3 for glass/cell/polymer module architecture tilted at 22.6°. The data gathered are displayed in Table B.2.
2. Compute r from equation (3.42) using these values:

$$\begin{aligned}
 r &= \frac{0.165 \times [1 - 0.0025 \times (45.1^\circ\text{C} - 25^\circ\text{C})]}{0.200 \times [1 - 0.0050 \times (47.3^\circ\text{C} - 25^\circ\text{C})]} \\
 &= 0.88.
 \end{aligned}
 \tag{B.6}$$

3. From the values in Table B.1, the BOS parameters ν and ω are:

$$\begin{aligned}\nu &= \frac{\$350/\text{m}^2}{\$300/\text{m}^2} \\ &= 1.17\end{aligned}\tag{B.7}$$

$$\begin{aligned}\omega &= \frac{\$315/\text{m}^2}{\$350/\text{m}^2} \\ &= 0.90.\end{aligned}\tag{B.8}$$

4. First, compute F_1 and F_2 :

$$\begin{aligned}F_1 &= \frac{0.08(1 + 0.08)^{30}}{(1 + 0.08)^{30} - 1} \\ &= 0.089\end{aligned}\tag{B.9}$$

$$\begin{aligned}F_2 &= \frac{0.08(1 + 0.08)^{20}}{(1 + 0.08)^{20} - 1} \\ &= 0.102.\end{aligned}\tag{B.10}$$

5. Compute λ_F :

$$\begin{aligned}\lambda_F &= \frac{0.102}{0.089} \\ &= 1.15.\end{aligned}\tag{B.11}$$

6. Compute the uniform nominal discount factors $D_{n,1}$ and $D_{n,2}$ for each system:

$$\begin{aligned}D_{n,1} &= \frac{0.12(1 + 0.12)^{30}}{(1 + 0.12)^{30} - 1} \\ &= 0.124\end{aligned}\tag{B.12}$$

$$\begin{aligned}D_{n,2} &= \frac{0.12(1 + 0.12)^{20}}{(1 + 0.12)^{20} - 1} \\ &= 0.134.\end{aligned}\tag{B.13}$$

7. Compute the uniform real discount factors $D_{r,1}$ and $D_{r,2}$ for each system:

$$D_r = \frac{0.093(1 + 0.093)^{30}}{(1 + 0.093)^{30} - 1}$$

$$= 0.100 \quad (\text{B.14})$$

$$D_r = \frac{0.093(1 + 0.093)^{20}}{(1 + 0.093)^{20} - 1}$$

$$= 0.112. \quad (\text{B.15})$$

8. Compute λ_D :

$$\lambda_D = \frac{0.104 \times 0.124}{0.100 \times 0.127}$$

$$= 1.04. \quad (\text{B.16})$$

9. Compute $(A_{m,2}/A_{m,1})_{\text{eq}}$:

$$\left(\frac{A_{m,2}}{A_{m,1}} \right)_{\text{eq}} = \frac{0.88}{1.15 \times 1.04} + \left(\frac{0.88}{1.15 \times 1.04} - 0.90 \right) \times 1.17$$

$$= 0.55. \quad (\text{B.17})$$

10. Compute the efficiency premium:

$$\Delta C_m = \left(0.55 \times \frac{0.200}{0.165} - 1 \right) \times \$1.50/W_p$$

$$= -\$0.49/W_p, \quad (\text{B.18})$$

yields a $\$0.49/W_p$ premium that the negative sign indicates favors system one.

This efficiency premium suggests that the maximum economical cost for CdTe modules in 2015 will be $\$1.01/W_p$ if 20%-efficient c-Si modules are available for $\$1.50/W_p$. Thus, the shorter-lived CdTe modules must cost about a third less than the c-Si modules. See section 3.4.2 for further discussion of this calculation.

APPENDIX C

SCALE PARAMETERS FOR MODELING PHOTOVOLTAIC MODULE MANUFACTURING COSTS

C.1 CAPITAL EQUIPMENT

Capital equipment costs are estimated according to the six-tenths rule from regression analysis of market survey data published periodically in the PV industry trade publication *Photon International*. The market data are fit to power regressions of the form:

$$P = AT^b, \quad (C.1)$$

where P is the capital cost of the equipment, A and b are the regression parameters, and T is a value indicating the throughput rate of the type of equipment analyzed. The exponent b is an indicator of the power of production scale to affect the capital cost of the equipment in question. When $b = 0$, scale has no effect on the cost of the equipment and A is equal to the equipment's capital cost regardless of its throughput. When $b = 1$, the cost of the equipment is directly proportional to throughput and A is equal to the cost of the equipment per unit throughput. However, the typical case is that $0 < b < 1$, indicating that equipment cost per unit throughput decreases with increasing production scale.

The following sections apply power regression analysis to market survey data for each of the major types of production equipment used in PV module manufacturing. The results of these analyses are summarized in Table 5.8 and were used in computing the capital cost of PV module manufacturing plants in the model described in Chapter 5.

The survey data presented in these sections is applicable to producing solar cells from multicrystalline silicon wafers 156 mm in diameter with a thickness in the range of 175 μm to 250 μm ; these dimensions correspond to the wafers most commonly used in the PV industry today. The same survey data may be used to compute appropriate regression parameters for wafers of other sizes, but the choice of wafer size affects the throughput value used in the

Table C.1: Nominal throughput and equipment cost for band saws.

Manufacturer	Model	Nominal Throughput (bricks/hr)	Cost (\$)
Logomatic	LS 212 S / C / Q ^a	4	740220
Meyer + Burger	BS 801	2.29	630230
	BS 805	2.29	753200
Sermas Industrie	HPSS	2.67	637180

^a Logomatic's system is comprised of three separate saws, each of which performs a part of the brick-cutting process and is listed separately in the published market survey. All three saws are combined into a single entry here.

analysis. The choice of wafer size can also affect which equipment models are included in the analysis, as some equipment is incompatible with unusually large, small, thick, or thin wafers.

In general, the survey data specify one price for a particular equipment model. However, in many cases they specify a price *range*. In these cases, the price assumed is the midpoint of the range. In some cases, a range of throughputs is specified in addition to the range of prices. In these cases, the low price is ascribed to the lower throughput value and the high price to the higher throughput value. In any case, the price presented in the tabulated data in the following sections is the price used in the analysis. Equipment for which either a price or a throughput value was missing was excluded from the analysis.

C.1.1 BAND SAWS

After the casting of a silicon ingot, band saws are used to cut the ingot into bricks of the proper size and shape for slicing wafers of the required dimensions. Market survey data applicable to cutting multicrystalline silicon ingots into 156-mm bricks 250 mm long is presented in Table C.1 [181]. One of the saws included in the survey, an unnamed model produced by Themis, is not included in this analysis because it is incapable of processing multicrystalline silicon ingots.

The data from Table C.1 are plotted in Figure C.1. Power regression of these data yields:

$$P = 597853T^{0.1395} \quad 2.29 \leq T \leq 4, \quad (\text{C.2})$$

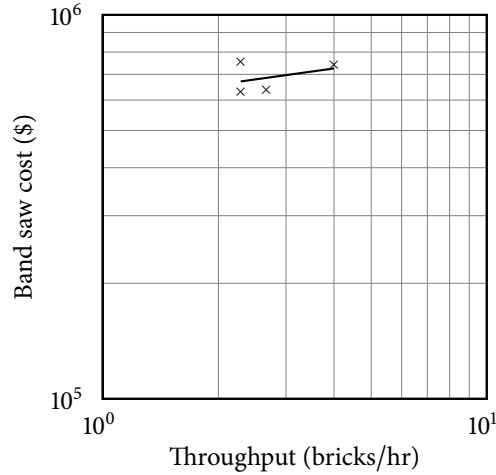


Figure C.1: Band saw cost as a function of nominal throughput for 156-mm bricks.

where P is the equipment price for throughput T . Equation (C.2) is denoted by the solid line in Figure C.1. Note that $b = 0.1395$, which is approaching zero. This indicates that increasing band saw throughput does not have a sizable impact on equipment cost: Since $2^{0.1395} = 1.10$, a doubling of throughput increases band saw cost by only about 10%.

C.1.2 WIRE SAWS

Once the ingot has been cut into bricks, the bricks are sliced into wafers of the desired thickness using a wire saw. Market survey data applicable to wafering 156-mm multicrystalline bricks 250 mm long is presented in Table C.2 [181]. Throughput for all saws is estimated based on a cutting rate of 0.4 mm/min, which is fairly typical [127].

The data from Table C.2 are plotted in Figure C.2. Power regression of these data yields:

$$P = 733652T^{0.2986} \quad 0.19 \leq T \leq 1.33, \quad (\text{C.3})$$

where P is the equipment price for throughput T . Equation (C.3) is denoted by the solid line in Figure C.2. Since $2^{0.2986} = 1.23$, a doubling in wire saw throughput increases the cost of the saw by 23%.

Table C.2: Nominal throughput and equipment cost for wire saws.

Manufacturer	Model	Nominal Throughput (bricks/hr)	Cost (\$)
HCT Shaping Systems	E500SD-B	1.28	910250
	E500SD-B/5	1.28	634450
Meyer + Burger	DS 265 Slurry & Diamond Wire	0.19	415025
	DS 264	0.52	730140
	DS 262/C	1.33	1821575
Nippei Toyama	MWM442D Series	0.38	2977875
	PV500	0.77	595562.5
	MWM6500SS	1.28	701912.5
Themis	AWSM 3800.3 (3800.3S)	1.02	605625
	AWSM 3800.4S	1.03	642025
	AWSM 3800.5	1.03	726975
Toyo Advanced Tech.	HCT-Toyo E500SD-L	1.28	680625
Takatori	MWS-3525D	0.32	600000
	MWS-812SD	0.19	650000

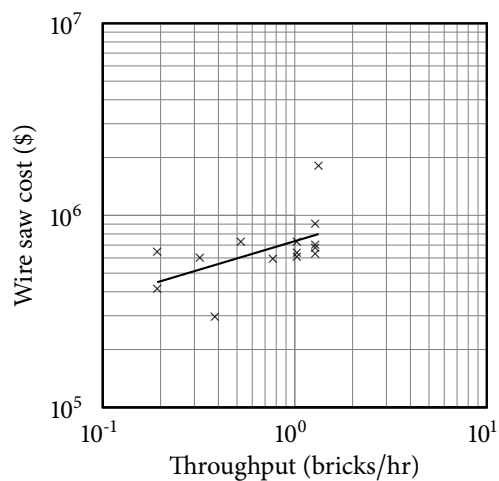


Figure C.2: Wire saw cost as a function of nominal throughput for 156-mm bricks.

Table C.3: Nominal throughput and equipment cost for saw-damage removal equipment.

Manufacturer	Model	Nominal Throughput (wafers/hr)	Cost (\$)
Gebr. Schmid	Acid Texture	4000	1079435
Rena	Astec Alkali + Acidic Batch System	2400	1750000
	InTex	2000	826910
	InTex HT	3000	1000000
Stangl	SDR 100	1200	1095260
	SDR 200	2400	1200000

C.1.3 WET ETCHING EQUIPMENT

Wet etching of wafers is necessary at various points in the solar cell fabrication process for removing saw damage, surface texturing, and phosphorus glass removal. While all three of these tasks are closely related, slight differences in controls and chemical handling functions mean that wet etching equipment is typically designed for a specific one of these tasks. This is usually of little consequence, as different pieces of equipment are typically used for different wet etching tasks. However, a small number of combination units that can perform more than one wet etching task are available. These machines cannot be considered in the same analysis as their single-function counterparts, since they might skew the results. Since they are also not popular [182] they are not analyzed at all.

C.1.3.1 Saw Damage Removal

The wire sawing process introduces microcracks into the wafer surface that can propagate and increase the likelihood of breakage if not removed. The damage is typically removed via chemical etching. Market survey data applicable to wet etching equipment for saw-damage removal (SDR) on 156-mm multicrystalline wafers is presented in Table C.3 [182].

The data from Table C.3 are plotted in Figure C.3. Power regression of these data yields:

$$P = 868608T^{0.0336} \quad 1200 \leq T \leq 4000, \quad (\text{C.4})$$

where P is the equipment price for throughput T . Equation (C.4) is denoted by the solid line in Figure C.3. Note that the exponent is approximately equal to zero, indicating that

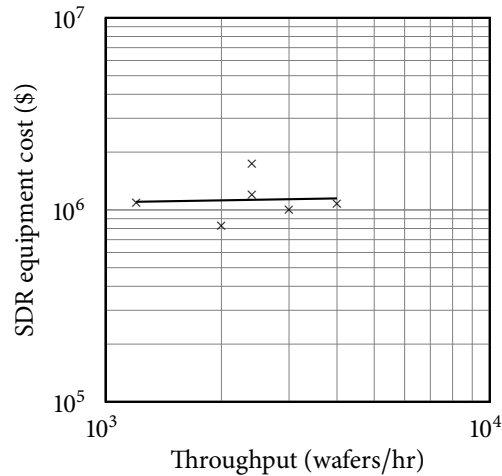


Figure C.3: Saw-damage removal equipment cost as a function of nominal throughput for 156-mm wafers.

equipment cost is largely independent of throughput. Because its value is so small, for cost modeling purposes SDR equipment costs are assumed to be \$1 158 600 regardless of throughput (though the throughput of a single machine is still restricted to values between 1200 and 4000 wafers/hr). The independence of equipment cost with respect to throughput is most likely because the size of the reservoirs in which the wafers are etched and rinsed has little effect on the cost of the equipment.

C.1.3.2 Phosphorus Glass Removal

Emitter diffusion typically leaves a phosphorus oxide glass (PSG) on the surface of the wafer that can cause problems during subsequent processing. This glass is generally removed by acid etching. Market survey data applicable to wet etching equipment for PSG removal on 156-mm multicrystalline wafers is presented in Table C.4 [182].

The data from Table C.4 are plotted in Figure C.4. Power regression of these data yields:

$$P = 10206T^{0.5128} \quad 1200 \leq T \leq 4000, \quad (\text{C.5})$$

where P is the equipment price for throughput T . Equation (C.5) is denoted by the solid line in Figure C.4. Unlike for the SDR equipment, the exponent is significantly larger than zero.

Table C.4: Nominal throughput and equipment cost for phosphorus glass removal equipment.

Manufacturer	Model	Nominal Throughput (wafers/hr)	Cost (\$)
EnviroEtch Corporation	EnviroEtch 10	2500	360000
Gebr. Schmid	PSG Etch	4000	627215
Rena	Astec HF/O3 SM	2400	445260
	InOx	2000	483425
	InOx HT	3000	636090
	InOxSide	2000	826910
	InOxSide HT	3000	1000000
Stangl	PSG 100	1200	356210
	PSG 200	2400	508870

The reason for this is unclear, but since $2^{0.5128} = 1.43$, a doubling in PSG removal throughput increases the cost of the equipment by 43%.

C.1.3.3 Texture Etching

The wire sawing process introduces microcracks into the wafer surface that can propagate and increase the likelihood of breakage if not removed. The damage is typically removed via chemical etching. Market survey data applicable to wet etching equipment for saw-damage removal (SDR) on 156-mm multicrystalline wafers is presented in Table C.5 [182].

The data from Table C.5 are plotted in Figure C.5. Power regression of these data yields:

$$P = 1175300T^{-0.0016} \quad 1200 \leq T \leq 4000, \quad (\text{C.6})$$

where P is the equipment price for throughput T . Equation (C.6) is denoted by the solid line in Figure C.5. As for the SDR equipment, the exponent is approximately zero. Because

Table C.5: Nominal throughput and equipment cost for texture etching equipment.

Manufacturer	Model	Nominal Throughput (wafers/hr)	Cost (\$)
Gebr. Schmid	Acid Texture	4000	1079435
Rena	Astec Alkali + Acidic Batch System	2400	1750000
	InTex	2000	826910
	InTex HT	3000	1000000
Stangl	T 100	1200	1145260
	T 200	2400	1250000

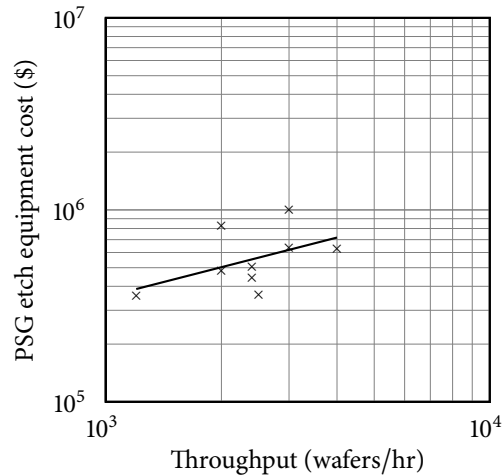


Figure C.4: Phosphorus glass removal equipment cost as a function of nominal throughput for 156-mm wafers.

its value is so small, for cost modeling purposes PSG removal equipment costs are assumed to be \$1 175 300 regardless of throughput (though the throughput of a single machine is still restricted to values between 1200 and 4000 wafers/hr). As with SDR equipment, the independence of equipment cost with respect to throughput is most likely because the size of the reservoirs in which the wafers are etched and rinsed has little effect on the cost of the equipment.

C.1.4 FURNACES

In a PV production line, furnaces serve two major functions: emitter diffusion and contact firing. Traditional tube furnaces of the same type commonly used in the microelectronics industry are the most popular units for emitter diffusions, while inline furnaces are commonly used for contact firing [183]. Inline furnaces are, however, gaining popularity for emitter diffusions. Each furnace type is characterized in the following sections.

C.1.4.1 Tube Furnaces

Tube furnaces generally consist of a stack of one or more quartz tubes and are popular for emitter diffusions because they are easy to control and produce highly uniform emitters.

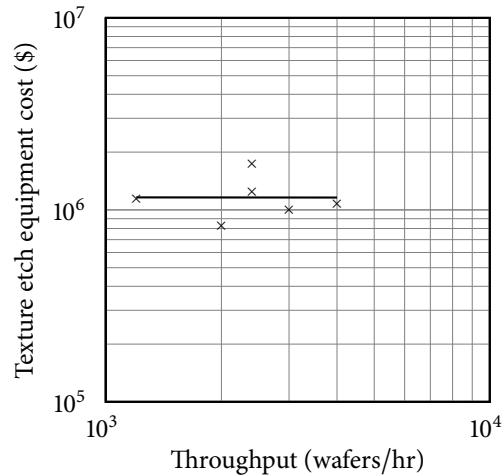


Figure C.5: Texture-etching equipment cost as a function of nominal throughput for 156-mm wafers.

Market survey data applicable to tube furnaces for diffusions on 156-mm multicrystalline wafers is presented in Table C.6 [183].

The data from Table C.6 are plotted in Figure C.6. Power regression of these data yields:

$$P = 839598 T^{-0.0171} \quad 150 \leq T \leq 2000, \quad (\text{C.7})$$

where P is the equipment price for throughput T . Equation (C.7) is denoted by the solid line in Figure C.6. Note that the exponent is approximately zero. Because its value is so small, for cost modeling purposes tube furnace costs are assumed to be \$766 700 regardless of throughput (though the throughput of a single machine is still restricted to values between 150 and 2000 wafers/hr). The independence of furnace cost with respect to throughput is most likely because throughput can be dramatically increased by simply adding an additional, relatively inexpensive furnace tube to an existing furnace design.

C.1.4.2 *Inline Furnaces*

Tube furnaces generally consist of a stack of one or more quartz tubes and are popular for emitter diffusions because they are easy to control and produce highly uniform emitters. Market survey data applicable to tube furnaces for diffusions on 156-mm multicrystalline wafers is presented in Table C.7 [183].

Table C.6: Nominal throughput and equipment cost for tube-type diffusion furnaces.

Manufacturer	Model	Nominal Throughput (wafers/hr)	Cost (\$)
Centrotherm	E1200	150	667785
	E1550	330	763182.5
	E 2000	600	826780
	E 2000 XL	600	1100000
MRL	1148	1250	550000
Semco	DF5200 LYDOP	1600	825795
	DF6000 LYDOP	2000	955795
SVCS	SVSOL	1600	575000
Tempress	TS61004 / TS121003-4	1600	635985

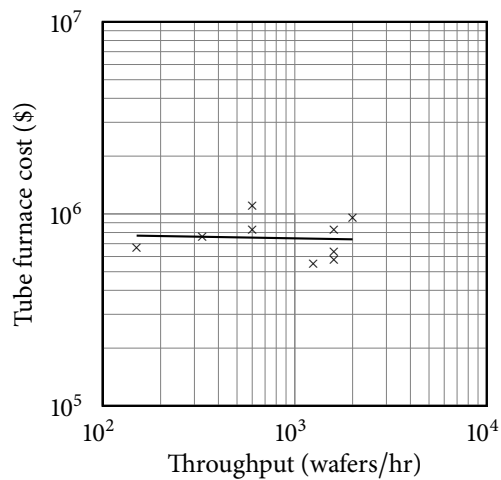


Figure C.6: Tube furnace cost as a function of nominal throughput for 156-mm wafers.

Table C.7: Nominal throughput and equipment cost for inline furnaces.

Manufacturer	Model	Nominal Throughput (wafers/hr)	Cost (\$)
Centrotherm	DO 16000-600-DIFF-CANtrol	1000	952995
	DO 16000-900-DIFF-CANtrol	1600	1016590
	WBS 2500	1600	1800000
Despatch	PD 108-14	200	275000
	PD 342-36	1000	650000
	PD 414-36	1250	725000
Koyo	47-IR	1500	174295
Sierratherm	7K28	1450	300000
	7K38	2250	400000
	XR750	750	500000
	XRI500	1500	800000
Tecnofimes	TCF15	1135	953980
	TCF680	1900	1250000
	TCF920	2210	1270000
	TCF2500	2625	1900000
TPS	TPS-F850-90	1250	300000

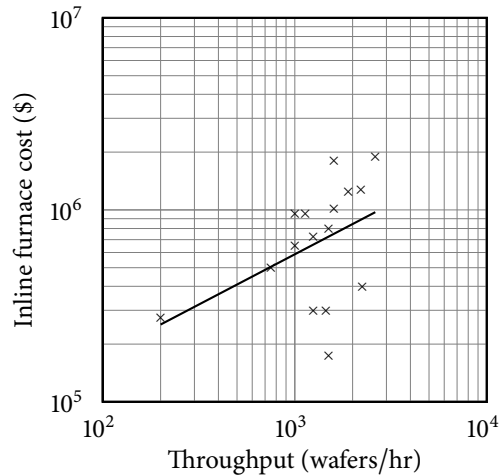


Figure C.7: Inline furnace cost as a function of nominal throughput for 156-mm wafers.

The data from Table C.7 are plotted in Figure C.7. Power regression of these data yields:

$$P = 15798T^{0.5234} \quad 200 \leq T \leq 2625, \quad (\text{C.8})$$

where P is the equipment price for throughput T . Equation (C.8) is denoted by the solid line in Figure C.7. Note that the data points are more scattered than in the corresponding charts for other types of equipment. This appears to be the result of a large number of new product introductions in recent years. For purposes of cost modeling in this thesis, the relationship expressed in equation (C.8) is used for estimating the capital cost of inline furnaces. Since $2^{0.5234} = 1.44$, a doubling in inline furnace throughput increases the cost of the equipment by 44%.

C.1.5 PECVD SILICON NITRIDE DEPOSITION SYSTEMS

Silicon nitride is typically applied to the front surface of silicon wafers to act as an antireflection coating and surface passivation layer. It can also be used to passivate the rear surface in lieu of a back-surface field. Economies of scale for PECVD deposition equipment was discussed in detail in section 5.3.1.1, but the analysis is summarized here. Market survey data applicable to PECVD deposition systems compatible with 156-mm multicrystalline wafers is presented in Table C.8 [122].

Table C.8: Nominal throughput and equipment cost for PECVD deposition systems.

Manufacturer	Model	Nominal Throughput (wafers/hr)	Cost (\$)
Centrotherm	E 2000 HT 320-4	710	1810000
	E 2000 HT 410-4	1050	1940000
MVSystems	—	475	756000
OTB	DEPx	960	1690000
	DEPx-plus	1440	1905000
Roth & Rau	SINA XS	345	689000
	SINA XS	430	835000
	SINA S	655	1130000
	SINA M	940	1250000
	SINA L	1170	1570000
	SINA L	1650	1810000
	SINA XL	2250	2180000
Semco	TWYN	450	707500

The data from Table C.8 are plotted in Figure C.8. Power regression of these data yields:

$$P = 14307T^{0.6711} \quad 345 \leq T \leq 2250, \quad (\text{C.9})$$

where P is the equipment price for throughput T . Equation (C.9) is denoted by the solid line in Figure C.8.

C.1.6 FULLY AUTOMATED SCREEN-PRINTING LINES

In nearly all high-volume, low-cost solar cell applications, screen-printed metal pastes are used to form the front and rear contacts to the device. Screen-printed aluminum is also commonly used in the formation of p-type back surface fields. Screen-printing is generally a three-step process: Silver is used to form an ohmic contact to the n-type emitter, aluminum is used to form a BSF or ohmic contact to the p-type base, and silver solder pads are printed over the aluminum layer to facilitate soldering of the metal interconnect tabs that form the electrical connection between solar cells in the finished module.

Screen printers may be purchased as separate units or as a fully automated line, which includes all of the required printing equipment along with handling equipment to flip and rotate wafers into the proper positions for printing. For simplicity, the cost modeling performed in this thesis all assumes a fully automated line for contact printing. Market survey data

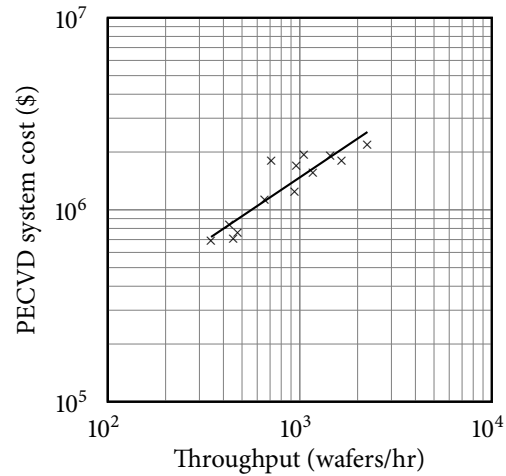


Figure C.8: Cost of PECVD deposition equipment as a function of nominal throughput for 156-mm wafers.

applicable to fully automated screen-printing lines compatible with 156-mm multicrystalline wafers is presented in Table C.9 [184].

The data from Table C.9 are plotted in Figure C.9. Power regression of these data yields:

$$P = 5048.3T^{0.7859} \quad 1200 \leq T \leq 2880, \quad (\text{C.10})$$

where P is the equipment price for throughput T . Equation (C.10) is denoted by the solid line in Figure C.9. Since $2^{0.7859} = 1.72$, a doubling in screen-printing throughput increases the cost of the equipment by 72%. The value of the exponent is higher for this equipment than for most of the equipment discussed here primarily because the complexity of a fully automated screen print line makes it more expensive to increase throughput.

C.1.7 SOLAR CELL TESTERS AND SORTERS

Once solar cell fabrication is complete the cells are tested under a solar simulator and sorted into bins based on measured short-circuit current. Sorting the cells ensures that only cells with similar I-V characteristics will be interconnected later, a precaution that minimizes losses in power output due to electrical mismatches. Market survey data on cell testers and sorters for 156-mm multicrystalline silicon solar cells is presented in Table C.10 [185].

Table C.9: Nominal throughput and equipment cost for fully automated screen-printing lines.

Manufacturer	Model	Nominal Throughput (wafers/hr)	Cost (\$)
AMI Presco	Conveyor Solar Print Line	750	600000
	Servo Solar Print Line	750	900000
	Walking Beam High Speed Solar Line	1200	1300000
ASYS	Metallization Line (dual con)	1200	1600000
Aurel	VS1520MM	1200	1300000
Baccini	Rotary Table Printer Line	1440	1210000
	Rotary Table Printer Line in Y-configuration	2880	2400000
	Twin Table Printer Line	1200	1500000
	Dual Head Twin Table Printer Line	2400	2800000
Machines Dubuit	238	1500	1500000
Seishin	SS-150-2-PVX-line	1200	1200000

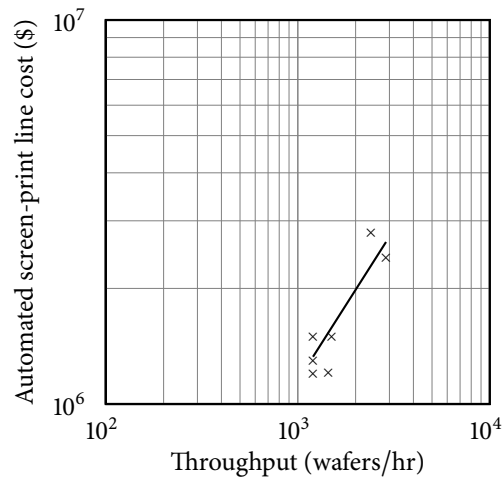


Figure C.9: Fully automated screen-printing line cost as a function of nominal throughput for 156-mm wafers.

Table C.10: Nominal throughput and equipment cost for solar cell tester/sorters.

Manufacturer	Model	Nominal Throughput (cells/hr)	Cost (\$)
Aurel	Wafer - Cell Sorter	900	200000
Baccini	High Speed T & S	1440	320750
	Very High Speed T & S	2400	692820
	Very High Speed T & S Vers. II	2400	724895
Belval	Pasan CS 1100	900	219760
	Pasan CS 900	900	205110
	Pasan CS 1200	1200	227900
	Pasan CS 1800	1800	260450
Gorosabel	CL 604	1100	263010
	CL 800	2300	384900
GT Solar	GT-CTX 2400	2400	565000
Manz	MCT-1800	1800	538860
	MCT-2700	2700	756970
	MCT-3600	3600	1000000
NPC	NCT-180AA-S	1200	494700
	NCT-180AA-T	1000	257580
P.Energy	P.Energy C 300 A	300	130860
	P.Energy C 750 A	750	198860
	P.Energy C 900 A	900	229660
	P.Energy C 1200 A	1200	255320
Schmid	C-SORT 3000	3000	1034900
Spectra-Nova	S-N CTA(B) 100 series	600	175000
Spire - Nisshinbo	SPI-CELL SORTER	1000	350000
Sunlight	Claces A1	1000	192450

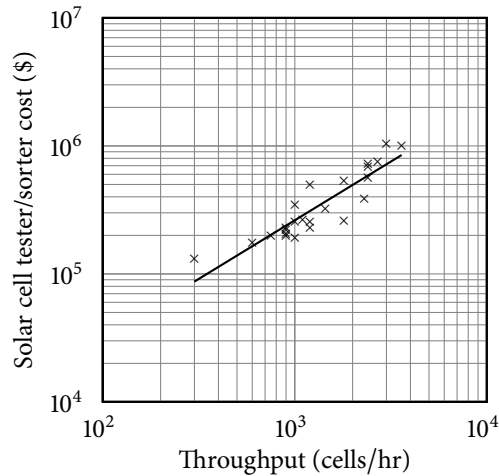


Figure C.10: Solar cell tester/sorter cost as a function of nominal throughput for 156-mm wafers.

The data from Table C.10 are plotted in Figure C.10. Power regression of these data yields:

$$P = 468.95T^{0.9160} \quad 300 \leq T \leq 3600, \quad (\text{C.11})$$

where P is the equipment price for throughput T . Equation (C.11) is denoted by the solid line in Figure C.10. Since $2^{0.9160} = 1.87$, a doubling in screen-printing throughput increases the cost of the equipment by 87%. As with the fully automated screen-printing line, the complexity of the equipment makes it expensive to increase throughput. If the statistical distributions of solar cell output characteristics could be narrowed as described in Chapter 4 it is possible the need for sorting would be reduced, potentially leading to a commensurate reduction in the capital cost of testing and sorting equipment.

C.1.8 COMBINED TABBER/STRINGERS

After testing and sorting, solar cells must be electrically interconnected to create PV modules. The interconnection process nominally consists of two steps. The first is tabbing, in which a metal tab is soldered to the contacts on one side of the solar cell. The length of the tab is such that it can significantly overlap a neighboring cell when two cells are placed side-by-side. The second step is stringing, in which the cells are flipped over and interleaved such that the tab

Table C.11: Nominal throughput and equipment cost for combined tabber/stringers.

Manufacturer	Model	Nominal Throughput (cells/hr)	Cost (\$)
Ecoprogetti	ET5MW/3000	300	144700
	ET20MW/3000	1200	382900
GT Solar	GT-Atlas	600	670000
Komax Systems	Xcell 2500	630	350000
	Xcell 2500 D	1260	675000
NPC	NTS-150-S-H(L)	600	292600
	NTS-150-D-H(L)	600	292600
	NTS-210-S-H(L)	600	327500
	NTS-150-S-H-3K	600	358000
P.Energy	NTS-210-S-H-3K	600	393000
	P.Energy TS 300 IRA	300	142900
	P.Energy TS 450 IRA	450	183800
Seishin	P.Energy TS 600 IRA	600	222100
	SS-TSM Series	900	349400
	Solarwatt AG	SLA 400	420
SLA 500		720	536000
Somont	Somont D6	1100	574300
	Somont D8	1100	701900
	Somont Rapid	1300	1008200
Spire-Nisshinbo	SPI-ASSEMBLER 6000	500	492500
Strela	MLS 500	550	382900
teamtechnik	TT 700	700	459450
	TT 900	900	548750

soldered to one side of one cell can be soldered to the appropriate contact on the other side of another cell. In this way, the positive contact of one cell is electrically connected to the negative contact of another, increasing the voltage of the series-connected pair. Typically, enough cells are soldered in series to produce a V_{OC} of 20 V to 45 V.

Tabbers and stringers may be purchased as separate units or as combined units that perform both tasks. However, the 2006 market survey in *Photon International* included only two stringers, both produced by the same manufacturer and both having the same throughput. Therefore, only combined tabber/stringers (CTS) were considered for analysis. Market survey data on combined tabber/stringers for 156-mm multicrystalline silicon solar cells is presented in Table C.11 [186]. Note that in subsequent analysis, the CTS20 from Solar Automation proved to be a statistical outlier and was therefore not included in the analysis.

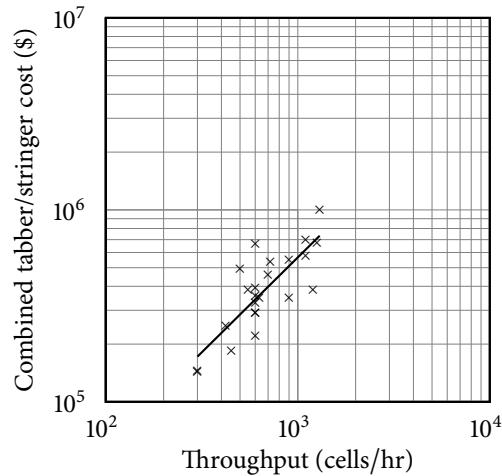


Figure C.11: Combined tabber/stringer cost as a function of nominal throughput for 156-mm wafers.

The data from Table C.11 are plotted in Figure C.11. Power regression of these data yields:

$$P = 611.81T^{0.9887} \quad 300 \leq T \leq 1300, \quad (\text{C.12})$$

where P is the equipment price for throughput T . Equation (C.12) is denoted by the solid line in Figure C.10. Since $2^{0.9887} = 1.98$, a doubling in CTS throughput increases the cost of the equipment by 98%, a number that is not surprising considering that the exponent is very nearly unity. Because it is so close to one, the intercept parameter is approximately equal to the equipment cost per unit throughput, which can be said to be approximately \$612/cell/hr. CTS equipment is among the most complex and handling-intensive equipment in the PV module production process, so this conclusion is not unexpected. It is possible that rear-contacted solar cell designs would require less handling and reduce the cost of this equipment.

C.1.9 LAMINATORS

Once cells have been tabbed and stringed they are laminated between sheets of ethyl vinyl acetate (EVA) sandwiched between a sheet of glass, which forms the front of the module, and a polymer backing material. The laminator applies heat and pressure to melt the EVA and

cause it to flow around the cells to protect them from the elements and provide mechanical stability. Laminating equipment typically consists of a flat bed with a clamshell top that closes over the sandwich to facilitate application of the required heat and pressure. A single piece of equipment can simultaneously laminate as many modules as will fit on the flat bed.

Market survey data on laminators is presented in Table C.12 [187]. Throughput values are expressed in units of m^2/hr , referring to module area, and are calculated on the basis of the specified heating area and curing time for each laminator. Complicating matters is the availability of both standard and fast-cure EVAs; throughputs and regression analyses are provided for both types.

The data from Table C.12 are plotted in Figure C.12. Power regression of these data yields:

$$P = 44843T^{0.5700} \quad 0.4 \leq T \leq 52.8 \quad (\text{C.13})$$

for standard-cure EVA and:

$$P = 28007T^{0.6199} \quad 0.8 \leq T \leq 73.8 \quad (\text{C.14})$$

for fast-cure EVA, where P is the equipment price for throughput T . Equation (C.13) is denoted by the solid line and equation (C.14) is denoted by the dashed line in Figure C.12. In both cases the exponent is approximately 0.6, and since $2^{0.6} \approx 1.5$, a doubling in CTS throughput increases the cost of the equipment by about 50%.

C.1.10 SOLAR SIMULATORS

The final step in PV module manufacturing is testing the finished PV module with a solar simulator. These systems consist of a lamp that simulates solar irradiance, a load to absorb the output of the PV module, and metering equipment to measure output current and voltage. Market survey data on solar simulators is presented in Table C.13 [188].

The data from Table C.13 are plotted in Figure C.13. Power regression of these data yields:

$$P = 276806T^{-0.1585} \quad 30 \leq T \leq 720, \quad (\text{C.15})$$

Table C.12: Nominal throughput and equipment cost for PV module laminators.

Manufacturer	Model	Nominal Throughput (m ² /hr)		Cost (\$)
		Std. EVA	Fast EVA	
Ecoprogetti	Ecolam01	4.5	8.0	89000
	Ecolam03	11.4	20.4	193700
	Ecolam 05	11.4	20.4	220400
	Ecolam MAXI	13.5	24.0	230500
EETS	PVLAM0300	2.4	—	45800
	PVLAM1200	6.5	—	86200
	PVLAM3000	20.2	—	361700
Hindhivac	VL – 1	2.9	7.2	49000
	VL – 2	3.6	9.0	57000
	VL – 2A	4.3	10.8	70000
	VL – 3	4.5	11.2	78500
	VL – 4	5.2	13.0	87500
	VL – 5	9.0	22.5	160000
Meier	10/08	1.6	4.0	63000
	15/10	3.0	7.5	101100
	18/11	4.0	9.9	126600
	20/12	4.8	12.0	152000
	25/15	7.5	18.8	292300
	28/18	10.1	25.2	311500
	36/21	15.1	37.8	432000
	38/22	16.7	41.8	483000
	46/21	19.3	48.3	622000
NPC	LM-50×50-S	1.4	2.0	47000
	LM-110×160-S	10.8	15.9	86300
	LM-140×200-S	16.8	24.6	127300
	LM-140×240-S	20.0	29.4	133400
	LM-155×240-S	22.0	32.3	139500
	LM-170×255-S	25.5	37.5	158600
	LM-A-140×200-S	16.8	24.6	168200
	LM-A-140×240-S	20.0	29.4	174300
	LM-A-170×255-S	25.5	37.5	203000
	LM-SA-140×330	27.7	40.6	279000
	LM-SA-155×240	22.0	32.3	258900
	LM-SA-170×260	24.9	36.4	266700
	LM-SA-170×370-S	39.8	58.4	322500
	LM-SA-170×400-S	39.8	58.4	349000
	LM-SA-215×320-S	40.3	59.0	349000
LM-SA-215×400-S	50.3	73.8	436000	
P.Energy	L A3 A	0.4	0.8	31800
	L 036 A	1.3	2.2	44500
	L 094 A	1.9	3.2	62300
	L 150 A	5.1	8.7	71200
	L 200 A	8.9	11.4	95400
	L 400 A	17.8	22.9	159000
	L 600 A	26.7	34.3	197000

Table C.12: Continued.

Manufacturer	Model	Nominal Throughput (m ² /hr)		Cost (\$)
		Std. EVA	Fast EVA	
Spire-Nisshinbo	SPI-350	4.4	7.3	147500
	SPI-480	7.9	13.2	197500
	SPI-580	9.4	15.7	257500
	SPI 580N	7.0	12.0	245000
	SPI 680N	7.9	13.5	272500
	SPI 1734N	12.4	21.3	370000
	SPI 1834N	13.1	22.5	397500
Wemhöner	SolarLam Basic 1000	52.8	—	401000
3S	S1713	6.9	13.8	170200
	S2821	17.6	35.3	216600
	S2926	22.6	45.2	275400
	S3621	22.7	45.4	265500

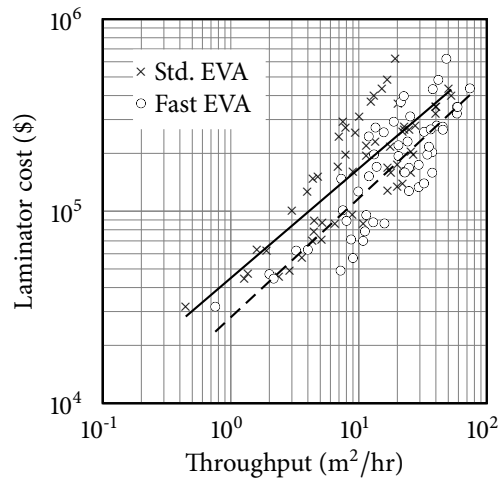


Figure C.12: Laminator cost as a function of nominal throughput for standard-cure and fast-cure EVAs.

Table C.13: Nominal throughput and equipment cost for solar simulators.

Manufacturer	Model	Nominal Throughput (modules/hr)	Cost (\$)
Aescusoft	ModFlash2004	120	76305
Belval	Pasan MMT 302	180	88500
	Pasan SS IIIa	60	88500
	Pasan SS IIIb	120	139000
	Pasan SS IIIc	120	113700
	PSS 8	40	98600
Berger Lichttechnik	PSS 30	30	124900
	PSS 32	30	124900
	PSS 40	60	333700
	Ecosun01	120	116300
Ecoprogetti	Ecosun02	120	65700
	MT2250	50	84000
EETS	PVMT 8000-A	30	84000
	SUN S4000	30	120500
	QuickSun 540LA	180	123200
Endeas	QuickSun 700A	60	82100
	QuickSun 700A	120	98600
	PV-SuSi	200	120700
Mencke & Tegtmeier	NMS-140x200	60	219700
	NMS-90x600	60	465800
	NMS-300R	90	202100
NPC	Sol 7×15 inverted	720	139000
	Sol 20×20	720	91000
	Sol 33×33	720	164300
	Sol 13×17	720	78400
Optosolar	S-N MTA-100	100	110250
	S-N MTB-100	100	95250
Spectra-Nova	N/A	250	50600
Shanghai Jiao Tong University	SPI-SUN 3500i	60	155000
	Module QA 4600	60	330000
	SPI-SUN 4600i	60	192500
	SPI-SUN 480i	60	180000
	SPI-SUN 660	60	220000
Spire-Nisshinbo	WPPS-1.5×1.2U-50×4	60	270000
	WPPS-1.6×1.4-50×6	60	390000
Wacom			

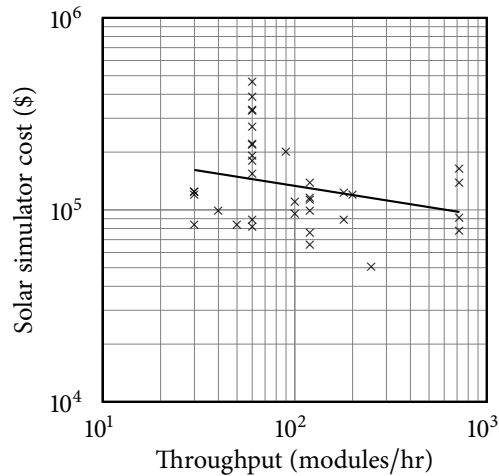


Figure C.13: Solar simulator cost as a function of nominal throughput.

where P is the equipment price for throughput T . Equation (C.15) is denoted by the solid line in Figure C.13. Note the negative exponent indicating that simulator cost drops with increasing throughput. This result is a statistical artifact resulting from a large number of unusually expensive simulator models with a throughput of 60 modules/hr; for purposes of modeling in this thesis, simulator cost is assumed to be \$109 000 regardless of throughput.

C.2 RAW MATERIALS

As with capital equipment costs, the unit price of a raw material may be estimated as a function of volume using a power law relationship. This follows the equation [124, 125]:

$$P = AV^b, \quad (\text{C.16})$$

where P is the price of the material per unit, V is the number of units required, and A and b are regression coefficients. While A and b generally must be empirically determined on a case-by-case basis, specialty chemicals, for which pricing information in large quantities can be difficult to find, tend to have $b \approx -0.75$ [126]. Thus, when necessary the large-volume prices of these materials may be estimated from laboratory-scale chemical prices.

The prices of commodity materials are independent of purchase volume and instead depend primarily upon supply and demand. They also tend to have the most volatile prices. In

Table C.14: Price quotations for ammonia as a function of volume [127–129].

Volume (L)	Price (\$)	Unit price (\$/L)
236	372.50	1.58
1 750 000	10 500.00	0.006

the context of PV manufacturing, these materials tend to be those containing large amounts of purified metal: silicon feedstock, metal screen-printing pastes, aluminum module frames, etc. They can be represented by equation (C.16) with A set equal to the unit price of the commodity and $b = 0$.

The following sections apply power regression analysis to chemical price data for the major chemicals required in PV module manufacturing. The cost data for small quantities of chemicals are obtained primarily from Aldrich [129], and those for large quantities primarily from Matthei [127, 128]. In some cases the number of data points available for regression was smaller than desirable; these cases are noted in the following sections, along with any assumptions made about the material price.

C.2.1 AMMONIA

Silane is used during PECVD processes as a reactant in the deposition of hydrogenated SiN_x films used for surface and bulk passivation and antireflection coatings. The amount of ammonia required during the deposition process depends both on the equipment used and on the desired composition and properties (optical and electrical) of the film. In the market survey by *Photon International* a range of ammonia consumption rates is specified for most PECVD units [122]; using the average of this range, one arrives at the conclusion that direct PECVD systems require about 0.39 L/wafer of silane while indirect PECVD systems require only about 0.096 L/wafer. The price of silane is displayed as a function of volume in Table C.14. Unfortunately, only two data points are available; however, ammonia constitutes a very small expense in PV manufacturing, and errors here are unlikely to have any significant impact on modeling results.

Since there are only two data points, a regression analysis is unnecessary. The intercept

Table C.15: Price quotations for argon as a function of volume [127–129].

Volume (L)	Price (\$)	Unit price (\$/L)
56	150.50	2.69
5 150 000	96 820.00	0.002

and exponent can be calculated directly from the two data points:

$$P = 48.07V^{-0.625}, \quad (\text{C.17})$$

where P is the unit price per liter of ammonia and V is the number of liters purchased. Thus, each time the required quantity of ammonia doubles, the unit price drops to a factor of $2^{-0.625} = 0.648$ times the original price — that is, the unit price is cut by 35.2%.

C.2.2 ARGON

Argon is used during the ingot casting process to provide an inert atmosphere and control the solidification process. Only two data points were available for this analysis, but since argon is not a major manufacturing expense any error introduced by the lack of data should be insignificant. The price of argon is displayed as a function of volume in Table C.15.

Since there are only two data points, a regression analysis is unnecessary. The intercept and exponent can be calculated directly from the two data points:

$$P = 22.61V^{-0.53}, \quad (\text{C.18})$$

where P is the unit price per liter of argon and V is the number of liters purchased. Thus, each time the required quantity of argon doubles, the unit price drops to a factor of $2^{-0.53} = 0.693$ times the original price — that is, the unit price is cut by 30.7%.

C.2.3 CARBON TETRAFLUORIDE

Carbon tetrafluoride (CF_4) is frequently used as a cleaning for PECVD processing equipment. The price of CF_4 is displayed as a function of volume in Table C.16. Unfortunately, only

Table C.16: Price quotations for carbon tetrafluoride as a function of volume [127–129].

Volume (L)	Price (\$)	Unit price (\$/L)
7.258	246.00	33.89
404 200	940 000.00	0.43

two data points are available; however, CF_4 is used infrequently — only during PECVD cleaning cycles — and in small amounts. Therefore, it constitutes a very small expense in PV manufacturing and errors here are unlikely to be significant.

Since there are only two data points, a regression analysis is unnecessary. The intercept and exponent can be calculated directly from the two data points:

$$P = 70.71V^{-0.3710}, \quad (\text{C.19})$$

where P is the unit price per liter of CF_4 and V is the number of liters purchased. Thus, each time the required quantity of CF_4 doubles, the unit price drops to a factor of $2^{-0.3710} = 0.773$ times the original price — that is, the unit price is cut by 22.7%.

C.2.4 ETHYLENE GLYCOL

Ethylene glycol is mixed with silicon carbide particles to form a slurry used in wire sawing of silicon wafers [189]. Slurries may also be oil-based, but ethylene glycol is often considered more environmentally friendly in part because it is water-based [190]. The amount of ethylene glycol required during the sawing process varies, but 60 mL/wafer is typical. The price of ethylene glycol is displayed as a function of volume in Table C.17.

Table C.17: Price quotations for ethylene glycol as a function of volume [127–129].

Volume (L)	Price (\$)	Unit price (\$/L)
0.1	25.40	254.00
1	49.90	49.90
2	71.00	35.50
200	715.00	3.58

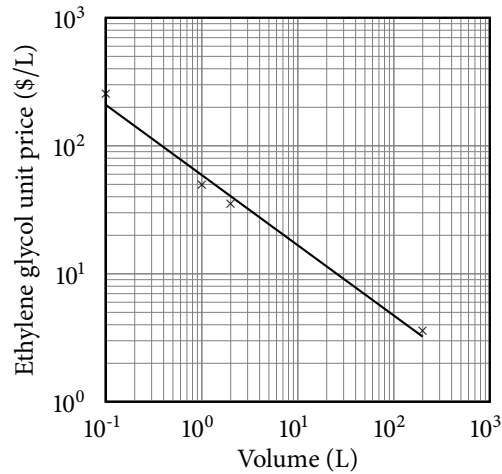


Figure C.14: Price of ethylene glycol as a function of purchase volume.

The price per liter is plotted on a log-log scale as a function of volume in Figure C.14 along with a regression fit described by:

$$P = 59.06 V^{-0.5486}, \quad (\text{C.20})$$

where P is the unit price per liter of ethylene glycol and V is the number of liters purchased. Thus, each time the required $2^{-0.5486} = 0.684$ — that is, the unit price is cut by 31.6%.

C.2.5 HELIUM

Helium is used during the ingot casting process to provide an inert atmosphere and control the solidification process. Only two data points were available for this analysis, but since helium is not a major manufacturing expense any error introduced by the lack of data should be insignificant. The price of helium is displayed as a function of volume in Table C.18.

Table C.18: Price quotations for helium as a function of volume [127–129].

Volume (L)	Price (\$)	Unit price (\$/L)
56	165.00	2.95
5 150 000	36 050.00	0.007

Table C.19: Price quotations for hydrochloric acid as a function of volume [127–129].

Volume (L)	Price (\$)	Unit price (\$/L)
2.5	45.60	18.24
25 000	50 000.00	2.00

Since there are only two data points, a regression analysis is unnecessary. The intercept and exponent can be calculated directly from the two data points:

$$P = 24.75V^{-0.53}, \quad (\text{C.21})$$

where P is the unit price per liter of helium and V is the number of liters purchased. Thus, each time the required quantity of helium doubles, the unit price drops to a factor of $2^{-0.53} = 0.693$ times the original price — that is, the unit price is cut by 30.7%.

C.2.6 HYDROCHLORIC ACID

Hydrochloric acid (HCl) is frequently used in wafer cleaning processes. Only two data points were available for this analysis, but HCl is used in such small amounts that errors in the price estimate should not significantly affect the manufacturing cost estimate. The price of HCl is displayed as a function of volume in Table C.19.

Since there are only two data points, a regression analysis is unnecessary. The intercept and exponent can be calculated directly from the two data points:

$$P = 22.73V^{-0.2400}, \quad (\text{C.22})$$

where P is the unit price per liter of HCl and V is the number of liters purchased. Thus, each time the required quantity of HCl doubles, the unit price drops to a factor of $2^{-0.2400} = 0.847$ times the original price — that is, the unit price is cut by 15.3%.

C.2.7 HYDROFLUORIC ACID

Hydrofluoric acid (HF) is frequently used in wafer cleaning processes to remove silicon dioxide glass from wafer surfaces. Only two data points were available for this analysis,

Table C.20: Price quotations for hydrofluoric acid as a function of volume [129].

Volume (L)	Price (\$)	Unit price (\$/L)
0.1	52.80	528.00
0.8	190.50	238.13

neither of them for high volumes of HF. As a result, all HF prices estimated for high-volume manufacturing processes in this thesis use extrapolated price estimates. The error introduced in doing this should be small, however, since HF is not a major manufacturing expense. The price of HF is displayed as a function of volume in Table C.20.

Since there are only two data points, a regression analysis is unnecessary. The intercept and exponent can be calculated directly from the two data points:

$$P = 218.62V^{-0.38}, \quad (\text{C.23})$$

where P is the unit price per liter of HF and V is the number of liters purchased. Thus, each time the required quantity of HF doubles, the unit price drops to a factor of $2^{-0.38} = 0.767$ times the original price — that is, the unit price is cut by 23.3%.

C.2.8 NITRIC ACID

Nitric acid (HNO_3) is sometimes used in wafer cleaning and etching processes. The only readily available data on HNO_3 prices were for laboratory quantities. Since HNO_3 expenditures make up a small amount of the total manufacturing cost, quotes for larger quantities were not aggressively pursued. Instead, the unit price of HNO_3 was estimated according to:

$$P = 34.56V^{-0.40}, \quad (\text{C.24})$$

where P is the unit price per liter of HNO_3 and V is the number of liters purchased. The parameters in equation (C.24) were estimated from the actual price of a laboratory quantity of semiconductor-grade HNO_3 [129] and a rule-of-thumb exponent for commodity chemicals [126]. According to equation (C.24), each time the required quantity of HNO_3 doubles, the unit price drops to a factor of $2^{-0.40} = 0.758$ times the original price — that is, the unit price is cut by 24.2%.

Table C.21: Price quotations for nitrogen as a function of volume [127–129].

Volume (L)	Price (\$)	Unit price (\$/L)
56	144.00	2.57
815 616 000	115 200.00	0.00014

C.2.9 NITROGEN

As an inexpensive inert gas, nitrogen is used in many high-temperature processes that require a non-reactive ambient gas. It is used, for example, as a carrier gas for phosphorus oxychloride (POCl_3) during emitter diffusion, and to provide an inert atmosphere during some steps of PECVD processing. The price of nitrogen is displayed as a function of volume in Table C.21. Unfortunately, only two data points are available; however, nitrogen constitutes a very small expense in PV manufacturing, and errors here are unlikely to have any significant impact on modeling results.

Since there are only two data points, a regression analysis is unnecessary. The intercept and exponent can be calculated directly from the two data points:

$$P = 28.18V^{-0.5947}, \quad (\text{C.25})$$

where P is the unit price per liter of nitrogen and V is the number of liters purchased. Thus, each time the required quantity of nitrogen doubles, the unit price drops to a factor of $2^{-0.5947} = 0.662$ times the original price — that is, the unit price is cut by 33.8%.

C.2.10 OXYGEN

Oxygen is used during wafer diffusion and oxidation steps to form passivating silicon dioxide layers or diffusion barriers. It is sometimes also used in other parts of the manufacturing process. Only two data points were available for this analysis, but oxygen is used in small enough quantities that errors in the price estimate should not significantly affect the manufacturing cost estimate. The price of oxygen is displayed as a function of volume in Table C.22.

Table C.22: Price quotations for oxygen as a function of volume [127–129].

Volume (L)	Price (\$)	Unit price (\$/L)
56	173.50	3.10
2 500 000	67 500.00	0.03

Since there are only two data points, a regression analysis is unnecessary. The intercept and exponent can be calculated directly from the two data points:

$$P = 18.43V^{-0.4430}, \quad (\text{C.26})$$

where P is the unit price per liter of oxygen and V is the number of liters purchased. Thus, each time the required quantity of oxygen doubles, the unit price drops to a factor of $2^{-0.4430} = 0.736$ times the original price — that is, the unit price is cut by 26.4%.

C.2.11 PHOSPHORUS OXYCHLORIDE

Phosphorus oxychloride is a liquid dopant used in the formation of n-type emitters via high-temperature diffusion. It is typically used with a bubbler in a tube furnace, where a gas is forced through a container of liquid POCl_3 to form a vapor. When the vapors come in contact with the silicon surface their phosphorus diffuses into the wafer. Consumption of POCl_3 during the diffusion process is typically about 0.03 g/wafer. The price of POCl_3 was displayed as a function of volume in Table 5.11 on page 149, but for convenience it is displayed here again in Table C.23.

Table C.23: Price quotations for phosphorus oxychloride (POCl_3) as a function of volume [127–129].

Volume (g)	Price (\$)	Unit price (\$/g)
10	76.00	7.60
50	257.50	5.15
100	381.50	3.82
250000	245 000.00	0.98

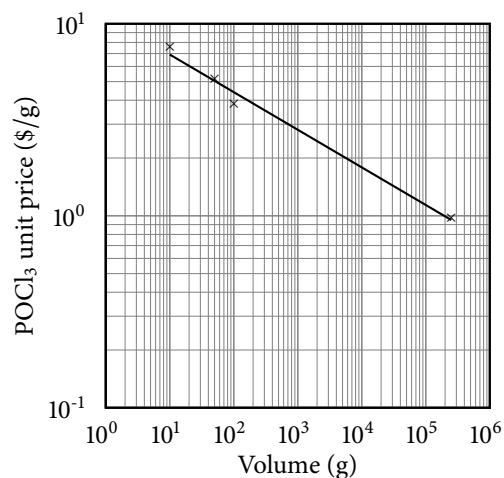


Figure C.15: Price of phosphorus oxychloride as a function of purchase volume.

The price per gram is plotted on a log-log scale as a function of volume in Figure C.15 along with a regression fit described by:

$$P = 10.86 V^{-0.196}, \quad (\text{C.27})$$

where P is the unit price per gram of POCl_3 and V is the number of grams purchased. Thus, each time the required volume of POCl_3 doubles, the unit price is changed by a factor of $2^{-0.196} = 0.873$ — that is, the unit price is cut by 12.7%.

C.2.12 SILANE

Silane is used during PECVD processes as a reactant in the deposition of thin films of silicon-based compounds such as SiN_x and a-Si. In c-Si PV manufacturing, it is used to deposit SiN_x layers used for antireflection and surface passivation. The amount of silane required during the deposition process depends both on the equipment used and on the desired composition and properties (optical and electrical) of the film. In the market survey by *Photon International* a range of silane consumption rates is specified for most PECVD units [122]; using the average of this range, one arrives at the conclusion that direct PECVD systems require about 0.05 L/wafer of silane.

Table C.24: Price quotations for silane as a function of volume [127–129].

Volume (L)	Price (\$)	Unit price (\$/L)
7.4	75.60	560.00
37	725.00	19.58
228000	171 000	0.75

Indirect PECVD systems, on the other hand, consume silane at a rate that decreases with increasing machine throughput. Using power law estimates similar to those used for estimating capital and material requirements throughout this chapter in combination with the consumption rates from the market surveys, one arrives at a silane requirement of:

$$\dot{q}_{\text{mat}} = 0.205 T^{-0.26}, \quad (\text{C.28})$$

where \dot{q}_{mat} is the silane requirement in L/wafer and T is the throughput of the PECVD system in wafers/hr. Using the range of throughput rates for remote PECVD systems given in section C.1.5, which is 345 wafers/hr to 2250 wafers/hr, equation (C.28) calculates a range of 0.028 L/wafer for the highest-throughput systems to 0.045 L/wafer for those with the lowest throughput. The derivation of equation (C.28) is not shown in this thesis.

The price of silane is displayed as a function of volume in Table C.24.

The price per liter is plotted on a log-log scale as a function of volume in Figure C.16 along with a regression fit described by:

$$P = 129.43 V^{-0.4221}, \quad (\text{C.29})$$

where P is the unit price per liter of silane and V is the number of liters purchased. Thus, each time the required $2^{-0.5486} = 0.746$ — that is, the unit price is cut by 25.4%.

C.2.13 SILICON CARBIDE

Silicon carbide (SiC), mixed into a slurry with an oil- or water-based liquid, is used as an abrasive during wire sawing of silicon wafers [189]. To minimize kerf loss, the smallest particle sizes that still provide efficient and consistent wafering are desired. Consumption of

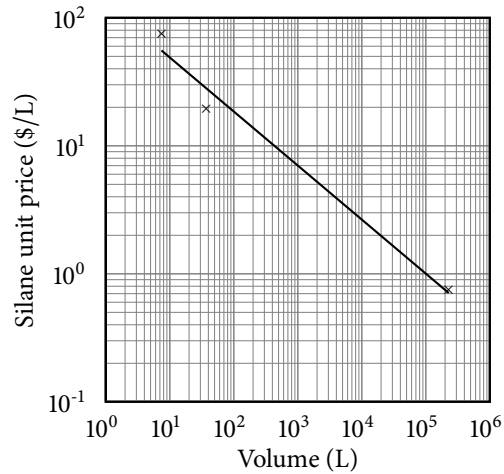


Figure C.16: Price of silane as a function of purchase volume.

SiC during wafering varies, but is typically around 60 g/wafer. The price of 400– mesh SiC is displayed as a function of volume in Table C.25.

The price per gram is plotted on a log-log scale as a function of volume in Figure C.17 along with a regression fit described by:

$$P = 2.784V^{-0.588}, \quad (\text{C.30})$$

where P is the unit price per gram of SiC and V is the number of grams purchased. Thus, each time the required $2^{-0.588} = 0.665$ — that is, the unit price is cut by 33.5%.

C.2.14 SODIUM HYDROXIDE

Sodium hydroxide (NaOH) is an alkaline etching agent frequently used to remove saw damage from the surface of freshly sawed silicon wafers. It can also be used as a texture

Table C.25: Price quotations for 400– mesh silicon carbide as a function of volume [127–129].

Volume (g)	Price (\$)	Unit price (\$/g)
250	22.50	0.090
1000	61.60	0.062
50 000	225.00	0.005

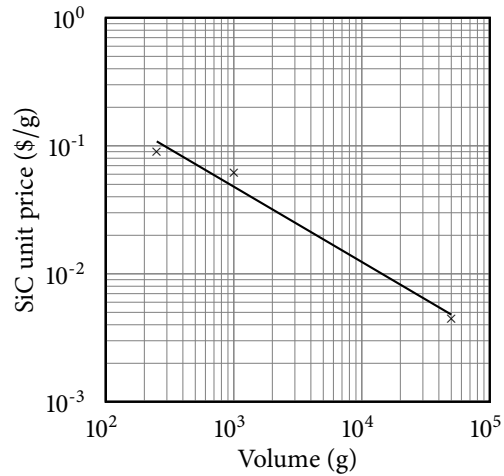


Figure C.17: Price of 400– mesh silicon carbide as a function of purchase volume.

etching agent. Consumption of NaOH during the saw damage etching process is typically about 18 g/wafer. The price of NaOH is displayed as a function of volume in Table C.26.

The price per kilogram is plotted on a log-log scale as a function of volume in Figure C.18 along with a regression fit described by:

$$P = 262.83V^{-0.4379}, \quad (\text{C.31})$$

where P is the unit price per gram of NaOH and V is the number of grams purchased. Thus, each time the required volume of NaOH doubles, the unit price is changed by a factor of $2^{-0.4379} = 0.738$ — that is, the unit price is cut by 26.2%.

Table C.26: Price quotations for sodium hydroxide (NaOH) as a function of volume [127–129].

Volume (kg)	Price (\$)	Unit price (\$/kg)
0.025	30.10	1204.00
0.1	62.90	629.00
0.5	233.50	467.00
62600	125 200.00	2.00

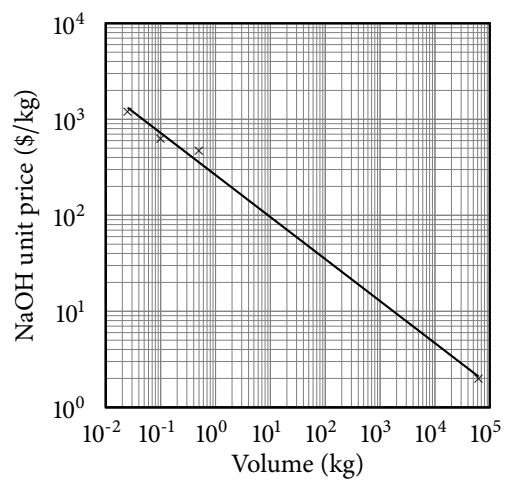


Figure C.18: Price of sodium hydroxide as a function of purchase volume.

REFERENCES

- [1] DR. SEUSS, *The Lorax*. New York: Random House Books for Young Readers, 1971.
- [2] INTERNATIONAL ENERGY AGENCY, *Key World Energy Statistics*. Paris: OECD/IEA, 2007.
- [3] INTERNATIONAL ENERGY AGENCY, *World Energy Outlook 2006*. Paris: OECD/IEA, 2006.
- [4] J. V. D. SAUNDERS and G. R. REINHART, “Demographic and economic correlates of development as measured by energy consumption,” *Demography*, vol. 4, no. 2, pp. 773–779, 1967.
- [5] A. MAZUR and E. ROSA, “Energy and life-style,” *Science*, vol. 186, no. 4164, pp. 607–610, 15 Nov. 1974.
- [6] M. S. ALAM, B. K. BALA, A. M. Z. HUQ, and M. A. MATIN, “A model for the quality of life as a function of electrical energy consumption,” *Energy*, vol. 16, no. 4, pp. 739–745, Apr. 1991.
- [7] J. GOLDEMBERG, “Energy needs in developing countries and sustainability,” *Science*, vol. 269, no. 5227, pp. 1058–1059, 25 Aug. 1995.
- [8] J. H. SEINFELD and S. N. PANDIS, *Atmospheric Chemistry and Physics: From Air Pollution to Climate Change*. New York: John Wiley & Sons, Inc., 1998.
- [9] S. HOLGATE, H. KOREN, J. SAMET, and R. MAYNARD, Eds., *Air Pollution and Health*. San Diego: Academic Press, 1999.
- [10] D. M. CHAPIN, C. S. FULLER, and G. L. PEARSON, “A new silicon p-n junction photocell for converting solar radiation into electrical power,” *Journal of Applied Physics*, vol. 25, no. 5, pp. 676–677, May 1954.
- [11] J. PERLIN, *From Space to Earth: The Story of Solar Electricity*. Ann Arbor, Michigan: aatec publications, 1999.
- [12] T. BRADFORD, *Solar Revolution*. Cambridge, Massachusetts: The MIT Press, 2006.
- [13] A. RICHMAN, “The polls: Public attitudes toward the energy crisis,” *Public Opinion Quarterly*, vol. 43, no. 4, pp. 576–585, Winter 1979.
- [14] P. D. MAYCOCK, *The World Photovoltaic Market 1975–2001*. Warrenton, Virginia: PV Energy Systems, Inc., 2001.
- [15] PROMETHEUS INSTITUTE, “23rd annual data collection — final,” *PV News*, vol. 26, no. 4, pp. 8–10, Apr. 2007.

- [16] R. HULSTROM, R. BIRD, and C. RIORDAN, “Solar spectral irradiance data sets for selected terrestrial conditions,” *Solar Cells*, vol. 15, no. 4, pp. 365–391, Dec. 1985.
- [17] INTERNATIONAL ENERGY AGENCY. (2007, 30 Oct.) IEA energy statistics — electricity for United States. [Online]. Available: http://www.iea.org/Textbase/stats/electricitydata.asp?COUNTRY_CODE=US&Submit=Submit
- [18] INTERNATIONAL ENERGY AGENCY. (2007, 30 Oct.) IEA energy statistics — electricity for world. [Online]. Available: http://www.iea.org/Textbase/stats/electricitydata.asp?COUNTRY_CODE=29&Submit=Submit
- [19] P. D. MAYCOCK, “Changes in the 2003 PV market data,” *PV News*, vol. 22, no. 4, pp. 2–3, Apr. 2003.
- [20] P. D. MAYCOCK, *PV News*, vol. 24, no. 4, pp. 1–4, Apr. 2005.
- [21] PROMETHEUS INSTITUTE, “24th annual data collection — preliminary,” *PV News*, vol. 27, no. 3, pp. 8–9, Mar. 2008.
- [22] OFFICE OF ENERGY EFFICIENCY AND RENEWABLE ENERGY. (2007) Solar energy technologies program: Multi-year program plan 2007–2011 and beyond. United States Department of Energy. Washington, DC. [Online]. Available: http://www1.eere.energy.gov/solar/pdfs/set_myp_2007-2011_proof_2.pdf
- [23] J. NELSON, *The Physics of Solar Cells*. London: Imperial College Press, 2003.
- [24] J. ZHAO, A. WANG, and M. A. GREEN, “24.5% efficiency silicon PERT cells on MCZ substrates and 24.7% efficiency PERL cells on FZ substrates,” *Progress in Photovoltaics: Research and Applications*, vol. 7, no. 6, pp. 471–474, 1999.
- [25] A. MAISH, “Defining requirements for improved photovoltaic system reliability,” *Progress in Photovoltaics: Research and Applications*, vol. 7, pp. 165–173, 1999.
- [26] W. SHORT, D. J. PACKEY, and T. HOLT, “A manual for the economic evaluation of energy efficiency and renewable energy technologies,” National Renewable Energy Laboratory, Golden, Colorado, Tech. Rep. NREL/TP-462-5173, Mar. 1995.
- [27] P. A. BASORE and D. A. CLUGSTON, “PCID version 4 for Windows: from analysis to design,” in *Proceedings of the 25th IEEE Photovoltaic Specialists Conference*, Washington, DC, 13–17 May 1996, pp. 377–381.
- [28] H. DE MOOR, I. HAGEMANN, J. HERRERO, P. MALBRANCHE, S. SIEBENTRITT, T. SCHEDEL-NIEDRIG, T. RIEDLE, J. POORTMANS, J. NIJS, J. SZLUFCHIK, A. JÄGER-WALDAU, F. KARG, E. ÖZSAN, S. PIETRUSZKO, S. HAYWOOD, M. TOPIC, R. SCHROPP, J. RATH, J. LÖFFLER, B. DIMMLER, M. POWALLA, and J. SPRINGER, *PVNET European Roadmap for PV R&D*, A. JÄGER-WALDAU, Ed. Luxembourg: Office for Official Publications of the European Communities, 2004, no. EUR 21087 EN.
- [29] P. D. MAYCOCK, *PV News*, vol. 22, no. 3, pp. 1–5, Mar. 2003.

- [30] P. D. MAYCOCK, *PV News*, vol. 22, no. 5, pp. 1–4, May 2003.
- [31] ENERGY INFORMATION ADMINISTRATION, “Annual energy review 2002,” United States Department of Energy, Washington, DC, Report DOE/EIA-0384(2002), Oct. 2003.
- [32] INTERNATIONAL ENERGY AGENCY, *Experience Curves for Energy Technology Policy*. Paris: OECD/IEA, 2000.
- [33] R. M. MARGOLIS, “Photovoltaic technology experience curves and markets,” in *Proceedings of the NCPV and Solar Program Review Meeting*, Denver, Colorado, 24–26 Mar. 2003, in press.
- [34] M. A. GREEN, “Green energy visions: Personal views on the future of photovoltaics,” in *Proceedings of the 3rd World Conference on Photovoltaic Energy Conversion*, Osaka, Japan, 11–18 May 2003, pp. O-1–O-5.
- [35] R. M. SWANSON, “A vision for crystalline silicon solar cells,” in *Proceedings of the 19th European Photovoltaic Solar Energy Conference*, Paris, France, 7–11 Jun. 2004, pp. 1078–1081.
- [36] PROMETHEUS INSTITUTE, “Supply and demand — mid-year update,” *PV News*, vol. 27, no. 4, pp. 6–8, Apr. 2008.
- [37] U.S. CONGRESS, OFFICE OF TECHNOLOGY ASSESSMENT, “Renewing our energy future,” U.S. Government Printing Office, Washington, DC, Report OTA-ETI-614, Sep. 1995.
- [38] C. HARMON, “Experience curves of photovoltaic technology,” International Institute for Applied Systems Analysis, Laxenburg, Austria, Interim Report IR-00-014, 2000.
- [39] B. G. CARBAJAL, “A 1982 low cost photovoltaic module factory study,” in *Proceedings of the 13th IEEE Photovoltaic Specialists Conference*, Washington, DC, 5–8 Jun. 1978, pp. 252–256.
- [40] L. A. GRENON and M. G. COLEMAN, “Silicon solar cells, a manufacturing cost analysis,” in *Proceedings of the 13th IEEE Photovoltaic Specialists Conference*, Washington, DC, 5–8 Jun. 1978, pp. 246–251.
- [41] L. A. GRENON and M. G. COLEMAN, “Flat plate vs. concentrator solar photovoltaic cells: A manufacturing cost analysis,” in *Proceedings of the 14th IEEE Photovoltaic Specialists Conference*, San Diego, California, 7–10 Jan. 1980, pp. 488–493.
- [42] J. H. WOHLGEMUTH, S. NARAYANAN, and R. BRENNEMAN, “Cost effectiveness of high efficiency cell processes as applied to cast polycrystalline silicon,” in *Proceedings of the 21st IEEE Photovoltaic Specialists Conference*, Kissimmee, Florida, 21–25 May 1990, pp. 221–226.
- [43] G. DARKAZALLI, S. HOGAN, and M. NOWLAN, “Sensitivity analysis and evaluation of manufacturing cost of crystalline silicon PV modules,” in *Proceedings of the 22nd IEEE Photovoltaic Specialists Conference*, Las Vegas, Nevada, 7–11 Oct. 1991, pp. 818–821.

- [44] R. HILL, "Prospects for photovoltaics," *Energy World*, no. 208, pp. 8–10, 1993.
- [45] J. ALONSO, U. UGALDE, and A. LUQUE, "Module price reduction by high production volume PV factories," in *Proceedings of the 13th European Photovoltaic Solar Energy Conference*, Nice, France, 23–27 Oct. 1995, pp. 855–858.
- [46] U. UGALDE, J. ALONSO, T. BRUTON, J. M. WOODCOCK, K. ROY, and K. DE CLERQ, "A general procedure for cost evaluations: Application to the MUSIC FM project," in *Proceedings of the 14th European Photovoltaic Solar Energy Conference*, Barcelona, Spain, 30 Jun.–4 Jul. 1997, pp. 897–900.
- [47] T. M. BRUTON, J. M. WOODCOCK, K. ROY, B. GARRARD, J. ALONSO, J. NIJS, A. RÄUBER, A. VALLÈRA, H. SCHADE, E. ALSEMA, R. HILL, and B. DIMMLER, "Multi-megawatt upscaling of silicon and thin film solar cell and module manufacturing 'MUSIC FM,'" European Commission, Final Report APAS RENA CT94 0008, 1997.
- [48] T. M. BRUTON, G. LUTHARDT, K.-D. RASCH, K. ROY, I. A. DORRITY, B. GARRARD, L. TEALE, J. ALONSO, U. UGALDE, K. DECLERQ, J. NIJS, J. SZLUFCHIK, A. RÄUBER, W. WETTLING, and A. VALLÈRA, "A study of the manufacture at 500 MW_p p.a. of crystalline silicon photovoltaic modules," in *Proceedings of the 14th European Photovoltaic Solar Energy Conference*, Barcelona, Spain, 30 Jun.–4 Jul. 1997, pp. 11–16.
- [49] R. G. LITTLE and M. J. NOWLAN, "Crystalline silicon photovoltaics: The hurdle for thin films," *Progress in Photovoltaics: Research and Applications*, vol. 5, no. 5, pp. 309–315, Sep.–Oct. 1997.
- [50] D. MARGADONNA and F. FERRAZZA, "The status of crystalline Si modules," *Renewable Energy*, vol. 15, pp. 83–88, 1998.
- [51] L. FRANTZIS, E. JONES, C. LEE, M. WOOD, and P. WORMSER, "Opportunities for cost reductions in photovoltaic modules," in *Proceedings of the 16th European Photovoltaic Solar Energy Conference*, Glasgow, UK, 1–5 May 2000, pp. 2100–2103.
- [52] N. M. PEARSALL and R. HILL, "Photovoltaic modules, systems and applications," in *Clean Electricity from Photovoltaics*, ser. Series on Photoconversion of Solar Energy, M. D. ARCHER and R. HILL, Eds. London: Imperial College Press, 2001, vol. 1, ch. 15, pp. 671–712.
- [53] P. D. MAYCOCK, *Photovoltaic Technology, Performance, and Cost 1995–2010: 2001 Update (with 2000 Market Data)*. Warrenton, Virginia: PV Energy Systems, Inc., 2002.
- [54] T. M. BRUTON, "MUSIC FM — five years on fantasy or reality?" in *PV in Europe*, Rome, Italy, 7–11 Oct. 2002, 921–923.
- [55] A. ROHATGI, "Road to cost-effective crystalline silicon photovoltaics," in *Proceedings of the 3rd World Conference on Photovoltaic Energy Conversion*, Osaka, Japan, 11–18 May 2003, pp. A29–A34.

- [56] K. A. MÜNZER, K. T. HOLDERMANN, R. E. SCHLOSSER, and S. STERK, "Thin monocrystalline silicon solar cells," *IEEE Transactions on Electron Devices*, vol. ED-46, no. 10, pp. 2055–2061, Oct. 1999.
- [57] T. M. BRUTON, S. R. ROBERTS, R. W. RUSSELL, W. WARTA, S. GLUNZ, W. KOCH, A. LUQUE, R. LAGO, L. J. CABALLERO, C. DEL CAÑIZO, A. MARTI, L. FRISSON, and A. VALLERA, "A production route to high efficiency solar cells made with ultra thin silicon wafers," in *Proceedings of the 17th European Photovoltaic Solar Energy Conference*, Munich, Germany, 22–26 Oct. 2001, pp. 1282–1286.
- [58] J. WOHLGEMUTH, "Cast polycrystalline silicon photovoltaic module manufacturing technology improvements," National Renewable Energy Laboratory, Golden, CO, Final Subcontractor Report NREL/SR-520-26071, Jun. 1999. [Online]. Available: <http://www.nrel.gov/docs/fy99osti/26071.pdf>
- [59] H. K. GUMMEL, "A self-consistent iterative scheme for one-dimensional steady state transistor calculations," *IEEE Transactions on Electron Devices*, vol. ED-11, pp. 455–465, Oct. 1964.
- [60] W. V. VAN ROOSBROECK, "Theory of flow of electrons and holes in germanium and other semiconductors," *Bell System Technical Journal*, vol. 29, pp. 560–607, 1950.
- [61] H. W. LOEB, R. ANDREW, and W. LOVE, "Application of 2-dimensional solutions of the Shockley-Poisson equation to inversion-layer M.O.S.T. devices," *Electronics Letters*, vol. 4, no. 17, pp. 352–354, Aug. 1968.
- [62] J. E. SCHROEDER and R. S. MULLER, "IGFET analysis through numerical solution of Poisson's equation," *IEEE Transactions on Electron Devices*, vol. ED-15, no. 12, pp. 954–961, Dec. 1968.
- [63] J. W. SLOTBOOM, "Iterative scheme for 1- and 2-dimensional D.C.-transistor simulation," *Electronics Letters*, vol. 5, no. 26, pp. 677–678, Dec. 1969.
- [64] E. M. BUTURLA, P. E. COTTRELL, B. M. GROSSMAN, K. A. SALSBURG, M. B. LAWLOR, and C. T. McMULLEN, "Three-dimensional finite element simulation of semiconductor devices," in *International Solid State Circuits Conference*. Institute of Electrical and Electronics Engineers, 1980, pp. 76–77.
- [65] A. YOSHII, S. HORIGUCHI, and T. SUDO, "A numerical analysis for very small semiconductor devices," in *International Solid State Circuits Conference*. Institute of Electrical and Electronics Engineers, 1980, pp. 80–81.
- [66] G. HEISER, "Design and implementation of a three-dimensional, general purpose semiconductor device simulator," Ph.D. dissertation, Institute for Computer Science, ETH Zürich, 1991.
- [67] J. G. FOSSUM, "Computer-aided numerical analysis of silicon solar cells," *Solid-State Electronics*, vol. 19, pp. 269–277, 1976.

- [68] R. J. SCHWARTZ and G. B. TURNER, “Numerical cell performance modeling and predictions for the future,” in *Proceedings of the 19th IEEE Photovoltaic Specialists Conference*, New Orleans, Louisiana, 1–4 May 1987, pp. 19–24.
- [69] J. L. GRAY, R. J. SCHWARTZ, and R. D. NASBY, “Two dimensional effects in conventional solar cells operated at high intensities,” in *Technical Digest — International Electron Devices Meeting*. Institute of Electrical and Electronics Engineers, 1982, pp. 510–513.
- [70] P. D. DEMOULIN and M. S. LUNDSTROM, “Theoretical comparison of conventional and unconventional GaAs cell design,” in *Proceedings of the 19th IEEE Photovoltaic Specialists Conference*, New Orleans, Louisiana, 1–4 May 1987, pp. 925–930.
- [71] M. WOLF, “Designing practical silicon solar cells approaching the ‘limit conversion efficiency,’” in *Proceedings of the 14th IEEE Photovoltaic Specialists Conference*, San Diego, California, 7–10 Jan. 1980, pp. 563–568.
- [72] P. A. BASORE, D. T. ROVER, and A. W. SMITH, “PC-1D version 2: Enhanced numerical solar cell modeling,” in *Proceedings of the 20th IEEE Photovoltaic Specialists Conference*, Las Vegas, Nevada, 26–30 Sep. 1988, pp. 389–396.
- [73] D. T. ROVER, P. A. BASORE, and G. M. THORSON, “Solar cell modeling on personal computers,” in *Proceedings of the 18th IEEE Photovoltaic Specialists Conference*, Las Vegas, Nevada, 21–25 Oct. 1985, pp. 703–709.
- [74] A. ROHATGI, A. W. SMITH, S. A. RINGEL, and G. AUGUSTINE, “High efficiency crystalline solar cell research,” Georgia Institute of Technology, Annual Report to Solar Energy Research Institute XB 7-06070-1, 1987.
- [75] J. L. GRAY, “ADEPT: A general purpose numerical device simulator for modeling solar cells in one-, two-, and three-dimensions,” in *Proceedings of the 22nd IEEE Photovoltaic Specialists Conference*, Las Vegas, Nevada, 7–11 Oct. 1991, pp. 436–438.
- [76] ISE INTEGRATED SYSTEMS ENGINEERING AG, *ISE TCAD Manuals Release 5*, ISE Integrated Systems Engineering AG, Zürich, Switzerland, 1998.
- [77] *ISE TCAD Release 10*, ISE Integrated Systems Engineering AG, Zürich, Switzerland, 2004.
- [78] S. A. KLEIN, J. A. DUFFIE, and W. A. BECKMAN, “TRNSYS — a transient simulation program,” *ASHRAE Transactions*, vol. 82, pp. 623–633, 1976.
- [79] M. PELOSI, *PV-DesignPro Photovoltaic Simulation Program*, Maui Solar Energy Software Corporation, Haiku, Hawaii, 2002.
- [80] A. PREGELJ, “Impact of distributed generation on power network operation,” Ph.D. dissertation, Georgia Institute of Technology, Atlanta, Georgia, 2003.
- [81] *Solar Advisor Model: User Guide (Version 1.0)*, National Renewable Energy Laboratory, Golden, Colorado, 15 May 2007, accessed 4 June 2007. [Online]. Available: http://www.nrel.gov/analysis/sam/downloads/sam_userguide.pdf

- [82] S. A. KLEIN and W. A. BECKMAN, *PV F-CHART User's Manual: Windows Version 3.01W*, F-Chart Software, Madison, Wisconsin, 2001.
- [83] NATIONAL RENEWABLE ENERGY LABORATORY. (2007, 5 Nov.) HOMER — analysis of micropower system options. [Online]. Available: <http://analysis.nrel.gov/homer/>
- [84] OFFICE OF ENERGY EFFICIENCY AND RENEWABLE ENERGY. (2007, 5 Nov.) Building technologies program: Building energy software tools directory. [Online]. Available: http://www.eere.energy.gov/buildings/tools_directory/
- [85] NATURAL RESOURCES CANADA. (2007, 5 Nov.) RETScreen international home multilingue. [Online]. Available: <http://www.retscreen.net/ang/home.php>
- [86] A. BLACK, "A new solar financial analysis calculator," in *Solar 2006*. Denver, Colorado: American Solar Energy Society, 9–13 Jul. 2006.
- [87] D. REDFIELD, "Procedure for minimizing the cost per watt of photovoltaic systems," *RCA Review*, vol. 38, no. 4, pp. 463–474, Dec. 1977.
- [88] D. REDFIELD, "Cost criterion for low efficiency solar cells to make system power cost competitive with that of high efficiency cells," in *Proceedings of the 13th IEEE Photovoltaic Specialists Conference*, Washington, DC, 5–8 Jun. 1978, pp. 911–913.
- [89] B. N. POST and D. G. SCHUELER, "Array subsystem development for photovoltaic array fields," in *Proceedings of the 15th IEEE Photovoltaic Specialists Conference*, Kissimmee, Florida, 12–15 May 1981, pp. 718–724.
- [90] G. J. JONES and H. N. POST, "The impact of photovoltaic device conversion efficiency on system energy cost," in *Extended Abstracts, The Electrochemical Society Spring Meeting*, vol. 82-1, Montreal, Canada, 9–14 May 1982, pp. 75–76.
- [91] H. KIESS, "The economic relevance of the efficiency of photovoltaic energy conversion," in *Proceedings of the 14th European Photovoltaic Solar Energy Conference*, Barcelona, Spain, 30 Jun.–4 Jul. 1997, pp. 904–907.
- [92] C. WHITAKER and M. REAL, "The impact of efficiency on area-related system costs," *Progress in Photovoltaics: Research and Applications*, vol. 7, no. 3, pp. 199–207, 1999.
- [93] J. C. C. FAN, "Theoretical temperature dependence of solar cell parameters," *Solar Cells*, vol. 17, no. 2–3, pp. 309–315, 1986.
- [94] X. DENG and E. A. SCHIFF, "Amorphous silicon-based solar cells," in *Handbook of Photovoltaic Science and Engineering*, A. LUQUE and S. HEGEDUS, Eds. Chichester: John Wiley & Sons, Ltd., 2003, ch. 12, pp. 505–565.
- [95] W. N. SHAFARMAN and L. STOLT, "Cu(InGa)Se₂ solar cells," in *Handbook of Photovoltaic Science and Engineering*, A. LUQUE and S. HEGEDUS, Eds. Chichester: John Wiley & Sons, Ltd., 2003, ch. 13, pp. 567–616.

- [96] K. EMERY, “Measurement and characterization of solar cells and modules,” in *Handbook of Photovoltaic Science and Engineering*, A. LUQUE and S. HEGEDUS, Eds. Chichester: John Wiley & Sons, Ltd., 2003, ch. 16, pp. 701–752.
- [97] D. L. KING, W. E. BOYSON, and J. A. KRATOCHVIL, “Photovoltaic array performance model,” Sandia National Laboratories, Albuquerque, New Mexico, Tech. Rep. SAND2004-3535, Aug. 2004.
- [98] K. BÜCHER, G. KLEISS, and D. BÄTZNER, “Photovoltaic modules in buildings: Performance and safety,” *Renewable Energy*, vol. 15, no. 1–4, pp. 545–551, Sep.–Dec. 1998.
- [99] OFFICE OF ENERGY EFFICIENCY AND RENEWABLE ENERGY, “Solar energy technologies program: Multi-year program plan 2007–2011 and beyond,” http://www1.eere.energy.gov/solar/pdfs/set_myp_2007-2011_proof_2.pdf, Washington, DC, 2007, accessed 25 May 2007.
- [100] J. MAZER and C. CORNELIUS, “Solar America Initiative (SAI) — overview,” in *Extended Abstracts and Papers, 16th Workshop on Crystalline Silicon Solar Cell Materials and Processes*, Denver, Colorado, 6–9 Aug. 2006, pp. 38–41.
- [101] C. CORNELIUS, Private communication, 19 May 2007.
- [102] M. A. GREEN, K. EMERY, Y. HISHIKAWA, and W. WARTA, “Solar cell efficiency tables (version 31),” *Progress in Photovoltaics: Research and Applications*, vol. 16, no. 1, pp. 61–67, Jan. 2008.
- [103] B. YAN, G. YUE, J. M. OWENS, J. YANG, and S. GUHA, “Over 15% efficient hydrogenated amorphous silicon based triple-junction solar cells incorporating nanocrystalline silicon,” in *Proceedings of the 4th World Conference on Photovoltaic Energy Conversion*, Waikoloa, Hawaii, 7–12 May 2006, pp. 1477–1480.
- [104] S. HEGEDUS, “Thin film solar modules: The low cost, high throughput and versatile alternative to Si wafers,” *Progress in Photovoltaics: Research and Applications*, vol. 14, no. 5, pp. 393–411, Aug. 2006.
- [105] C. A. GUEYMARD, “Spectral effects on latitude-tilt and vertical PV modules as affected by latitude, air mass, and climate,” in *Optical Modeling and Measurements for Solar Energy Systems*, ser. Proceedings of the SPIE, vol. 6657, San Diego, California, Aug. 2007, pp. 66520C-1–66520C-9.
- [106] FIRST SOLAR, INC., “Form 10-K to Securities and Exchange Commission for fiscal year 2006,” 16 Mar. 2007.
- [107] U.S. BUREAU OF LABOR STATISTICS. (2007, 15 May) Consumer price index, all urban consumers (CPI-U). [Online]. Available: <ftp://ftp.bls.gov/pub/special.requests/cpi/cpiiai.txt>

- [108] A. RISTOW, M. HILALI, A. EBONG, and A. ROHATGI, “Screen-printed back surface reflector for light trapping in crystalline silicon solar cells,” in *Proceedings of the 17th European Photovoltaic Solar Energy Conference*, Munich, Germany, 22–26 Oct. 2001, pp. 1335–1338.
- [109] M. J. KERR and A. CUEVAS, “Very low bulk and surface recombination in oxidized silicon wafers,” *Semiconductor Science and Technology*, vol. 17, no. 1, pp. 35–38, 7 Jan. 2002.
- [110] S. DAUWE, J. SCHMIDT, and R. HEZEL, “Very low surface recombination velocities on p- and n-type silicon wafers passivated with hydrogenated amorphous silicon films,” in *Proceedings of the 29th IEEE Photovoltaic Specialists Conference*, New Orleans, Louisiana, 20–24 May 2002, pp. 1246–1249.
- [111] M. A. GREEN, *Solar Cells*. Kensington, NSW: University of New South Wales, 1992.
- [112] A. W. WEEBER, H. TATHGAR, F. HUSTER, M. J. A. A. GORIS, L. J. GEERLIGS, . GJERSTAD, B. TERHEIDEN, M. McCANN, and P. FATH, “High-quality mc-Si wafers for high-efficiency solar cells,” in *Proceedings of the 19th European Photovoltaic Solar Energy Conference*, Paris, France, 7–11 Jun. 2004, pp. 1009–1012.
- [113] R. TURTON, R. C. BAILIE, W. B. WHITING, and J. A. SHAEIWITZ, *Analysis, Synthesis, and Design of Chemical Processes*, ser. Prentice Hall International Series in the Physical and Chemical Engineering Sciences. Upper Saddle River, New Jersey: Prentice Hall PTR, 1998.
- [114] S. C. WOOD, “Factory modeling,” in *Handbook of Semiconductor Manufacturing Technology*, Y. NISHI and R. DOERING, Eds. New York: Marcel Dekker, Inc., 2000, ch. 36, pp. 1103–1122.
- [115] K. K. HUMPHREYS and P. WELLMAN, *Basic Cost Engineering*, 3rd ed. New York: Marcel Dekker, 1996.
- [116] J. P. TANNER, *Practical Cost Estimating for Manufacturing*, ser. Manufacturing Engineering and Materials Processing. New York: Marcel Dekker, Inc., 1996, vol. 48, ch. 7, pp. 341–430.
- [117] R. G. CHAMBERLAIN, “A normative price for a manufactured product: The SAMICS methodology. Volume II: Analysis,” Jet Propulsion Laboratory, Pasadena, California, Report DOE/JPL-1012-79/5, 15 Jan. 1979.
- [118] K. M. GUTHRIE, *Process Plant Estimating, Evaluation, and Control*. Solana Beach, California: Craftsman Book Company of America, 1974.
- [119] P. MAYCOCK and T. BRADFORD, “PV technology, performance, and manufacturing cost — 2006,” Prometheus Institute, Cambridge, Massachusetts, Report, 2006.
- [120] INTERNAL REVENUE SERVICE, “How to depreciate property,” United States Department of the Treasury, Washington, DC, Publication 946, 2007.

- [121] BUREAU OF LABOR STATISTICS, “Occupational employment and wages, 2006,” United States Department of Labor, Washington, DC, News Release USDL 07-0712, May 2007.
- [122] B. BRAND, “True blue: Market survey on SiNx deposition systems,” *Photon International*, pp. 90–99, Mar. 2006.
- [123] H. J. LANG, “Simplified approach to preliminary cost estimates,” *Chemical Engineering*, vol. 55, no. 6, pp. 112–113, 1948.
- [124] D. J. MASSEY and J. H. BLACK, “Predicting chemical prices,” *Chemical Engineering*, vol. 76, no. 23, pp. 150–154, 20 Oct. 1969.
- [125] J. T. SOMMERFELD and C. T. LENK, “Thermodynamics helps you predict selling price,” *Chemical Engineering*, vol. 77, no. 10, pp. 136–138, 4 May 1970.
- [126] P. W. HART and J. T. SOMMERFELD, “Cost estimation of specialty chemicals from laboratory-scale prices,” *Cost Engineering*, vol. 39, no. 3, pp. 31–35, Mar. 1997.
- [127] K. MATTHEI, Private communication, 20 Jun. 2003.
- [128] K. MATTHEI, Private communication, 19 Mar. 2003.
- [129] ALDRICH, *Handbook of Fine Chemicals 2007–2008*. Milwaukee, Wisconsin: Sigma-Aldrich Company, 2006.
- [130] W. BOWER, “Inverters — critical photovoltaic balance-of-system components: Status, issues, and new-millennium opportunities,” *Progress in Photovoltaics: Research and Applications*, vol. 8, no. 1, pp. 113–126, 2000.
- [131] T. ERGE, V. U. HOFFMANN, and K. KIEFER, “The German experience with grid-connected PV-systems,” *Solar Energy*, vol. 70, no. 6, pp. 479–487, 2001.
- [132] J. M. CARRASCO, L. G. FRANQUELO, J. T. BIALASIEWICZ, E. GALVÁN, R. C. P. GUIADO, M. A. M. PRATS, J. I. LEÓN, and N. MORENO-ALFONSO, “Power-electronic systems for the grid integration of renewable energy sources: A survey,” *IEEE Transactions on Industrial Electronics*, vol. 53, no. 4, pp. 1002–1016, Aug. 2006.
- [133] F. BLAABJERG, R. TEODORESCU, M. LISERRE, and A. V. TIMBUS, “Overview of control and grid synchronization for distributed power generation systems,” *IEEE Transactions on Industrial Electronics*, vol. 53, no. 5, pp. 1398–1409, Oct. 2006.
- [134] S. ALEPUZ, S. BUSQUETS-MONGE, J. BORDONAU, J. GAGO, D. GONZALEZ, and J. BALCELLS, “Interfacing renewable energy sources to the utility grid using a three-level inverter,” *IEEE Transactions on Industrial Electronics*, vol. 53, no. 5, pp. 1504–1511, Oct. 2006.
- [135] A. B. MAISH, C. ATCITY, S. HESTER, D. GREENBERG, D. OSBORN, and D. COLLIER, “Photovoltaic system reliability,” in *Proceedings of the 26th IEEE Photovoltaic Specialists Conference*, Anaheim, California, 29 Sep.–3 Oct. 1997, pp. 1049–1054.

- [136] A. PREGELJ, M. BEGOVIĆ, and A. ROHATGI, “Impact of inverter configuration on PV system reliability and energy production,” in *Proceedings of the 29th IEEE Photovoltaic Specialists Conference*, New Orleans, Louisiana, 20–24 May 2002, pp. 1388–1391.
- [137] P. A. B. JAMES, A. S. BAHAJ, and R. M. BRAID, “PV array <5 kWp + single inverter = grid connected PV system: Are multiple inverter alternatives economic?” *Solar Energy*, vol. 80, no. 9, pp. 1179–1188, Sep. 2006.
- [138] L. M. MOORE, “Sandia’s PV reliability database: Helping business do business,” *Quarterly Highlights of Sandia’s Solar Programs*, 2001.
- [139] N. G. DHERE, “Reliability of PV modules and balance-of-system components,” in *Proceedings of the 31st IEEE Photovoltaic Specialists Conference*, Orlando, Florida, 3–7 Jan. 2005, pp. 1570–1576.
- [140] D. TON and W. BOWER. (2005, Jan.) Summary report on the DOE high-tech inverter workshop. U.S. Department of Energy. [Online]. Available: http://www1.eere.energy.gov/solar/pdfs/inverter_II_workshop.pdf
- [141] NAVIGANT CONSULTING, INC., “A review of PV inverter technology cost and performance projections,” National Renewable Energy Laboratory, Golden, Colorado, Subcontract Report NREL/SR-620-38771, Jan. 2006.
- [142] M. BEGOVIĆ, A. PREGELJ, A. ROHATGI, and C. HONSBURG, “Green power: Status and perspectives,” *Proceedings of the IEEE*, vol. 89, no. 12, pp. 1734–1743, Dec. 2001.
- [143] B. GNEDENKO, I. PAVLOV, and I. USHAKOV, *Statistical Reliability Engineering*, S. CHAKRAVARTY, Ed. New York: John Wiley & Sons, Inc., 1999.
- [144] J. ENDRENYI, *Reliability Modeling in Electric Power Systems*. Chichester: John Wiley & Sons, 1978.
- [145] B. DODSON, *Weibull Analysis*. Milwaukee, Wisconsin: ASQ Quality Press, 1994.
- [146] D. F. MENICUCCI and J. P. FERNANDEZ, “User’s manual for PVFORM: Photovoltaic system simulation program for stand-alone and grid-interactive applications,” Sandia National Laboratories, Final Report SAND85-0376, 1989.
- [147] W. MARION and K. URBAN, *User’s Manual for TMY2s*, National Renewable Energy Laboratory, Golden, Colorado, Jun. 1995.
- [148] S. A. ROSS, R. W. WESTERFIELD, and B. D. JORDAN, *Essentials of Corporate Finance*. Chicago: Richard D. Irwin, 1996.
- [149] R. L. IMAN and J. C. HELTON, “An investigation of uncertainty and sensitivity analysis techniques for computer models,” *Risk Analysis*, vol. 8, no. 1, pp. 71–90, 1988.
- [150] M. R. PATEL, *Spacecraft Power Systems*. Boca Raton, Florida: CRC Press, 2005.

- [151] H. RUDNICK, J. DIXON, and L. MORÁN, “Delivering clean and pure power,” *IEEE Power & Energy Magazine*, vol. 1, no. 5, pp. 32–40, Sep.–Oct. 2003.
- [152] J. RODRÍGUEZ, S. BERNET, B. WU, J. O. PONETT, and S. KOURO, “Multilevel voltage-source-converter topologies for industrial medium-voltage drives,” *IEEE Transactions on Industrial Electronics*, vol. 54, no. 6, pp. 2930–2945, Dec. 2007.
- [153] W. J. SARJEANT, F. W. MACDOUGALL, D. W. LARSON, and I. KOHLBERG, “Energy storage capacitors: Aging, and diagnostic approaches for life validation,” *IEEE Transactions on Magnetics*, vol. 33, no. 1, pp. 501–506, Jan. 1997.
- [154] J. J. NELSON, G. VENKATARAMANAN, and A. M. EL-REFAIE, “Fast thermal profiling of power semiconductor devices using fourier techniques,” *IEEE Transactions on Industrial Electronics*, vol. 53, no. 2, pp. 521–529, Apr. 2006.
- [155] A. GOEL and R. J. GRAVES, “Electronic system reliability: Collating prediction models,” *IEEE Transactions on Device and Materials Reliability*, vol. 6, no. 2, pp. 258–265, Jun. 2006.
- [156] M. E. ROPP, M. BEGOVIĆ, A. ROHATGI, and R. LONG, “Design considerations for large roof-integrated photovoltaic arrays,” *Progress in Photovoltaics: Research and Applications*, vol. 5, no. 1, pp. 55–67, 1997.
- [157] A. ROHATGI, M. BEGOVIĆ, M. ROPP, and A. PREGELJ, “Design and performance of the Georgia Tech Aquatic Center photovoltaic system,” Georgia Institute of Technology, Atlanta, Georgia, Technical Report DOE/GO/10019--T1-Vol.2, 1996.
- [158] M. BEGOVIĆ, S. R. GHOSH, and A. ROHATGI, “Decade performance of a roof-mounted photovoltaic array,” in *Proceedings of the 4th World Conference on Photovoltaic Energy Conversion*, Waikoloa, Hawaii, 7–12 May 2006, pp. 2383–2386.
- [159] “Reliability prediction of electronic equipment,” United States Department of Defense, Washington, DC, Military Handbook MIL-HDBK-217F, 2 Dec. 1991.
- [160] M. ATEN, G. TOWERS, C. WHITLEY, P. WHEELER, J. CLARE, and K. BRADLEY, “Reliability comparison of matrix and other converter topologies,” *IEEE Transactions on Aerospace and Electronic Systems*, vol. 42, no. 3, pp. 867–875, Jul. 2006.
- [161] NAVESINK RESEARCH & ENGINEERING CENTER, “Reliability prediction procedure for electronic equipment,” Telcordia Technologies, Inc., Red Bank, New Jersey, Special Report SR-332, Issue 2, Sep. 2006.
- [162] “Design of reliable industrial and commercial power systems,” Institute of Electrical and Electronics Engineers, Inc., New York, IEEE Std 493-2007, 2007.
- [163] G. CHEN, R. BURGOS, Z. LIANG, F. LACAUX, F. WANG, J. D. VAN WYK, W. G. ODENDAAL, and D. BOROYEVICH, “Reliability-oriented design considerations for high-power converter modules,” in *Proceedings of the 35th IEEE Power Electronics Specialists Conference*, Aachen, Germany, 2004, pp. 419–425.

- [164] D. HIRSCHMANN, D. TISSEN, S. SCHRÖDER, and R. W. DE DONCKER, “Reliability prediction for inverters in hybrid electrical vehicles,” *IEEE Transactions on Power Electronics*, vol. 22, no. 6, pp. 2511–2517, Nov. 2007.
- [165] P. M. ROOIJ, J. EIKELBOOM, and P. HESKES, “Reliability testing of grid connected PV inverters,” in *Proceedings of the 16th European Photovoltaic Solar Energy Conference*, Glasgow, UK, 1–5 May 2000, pp. 2221–2224.
- [166] S. V. AMARI and V. HEGDE, “New allocation methods for repairable systems,” in *Reliability and Maintainability Symposium 2006*, 23–26 Jan. 2006, pp. 290–295.
- [167] D. TON and W. BOWER, “Summary report on the DOE high-tech inverter workshop,” U.S. Department of Energy, Jan. 2005.
- [168] R. C. PORTILLO, M. M. PRATS, J. I. LEÓN, J. A. SÁNCHEZ, J. M. CARRASCO, E. GALVÁN, and L. G. FRANQUELO, “Modeling strategy for back-to-back three-level converters applied to high-power wind turbines,” *IEEE Transactions on Industrial Electronics*, vol. 53, no. 5, pp. 1483–1491, Oct. 2006.
- [169] A. LAHYANI, P. VENET, G. GRELLET, and P.-J. VIVERGE, “Failure prediction of electrolytic capacitors during operation of a switchmode power supply,” *IEEE Transactions on Power Electronics*, vol. 13, no. 6, pp. 1199–1207, Nov. 1998.
- [170] F. RICARDEAU, P. BAUDESSON, T. MEYNARD, and C. TURPIN, “Fail-safe capability of a high voltage IGBT inverter source,” *The European Physical Journal: Applied Physics*, vol. 15, pp. 189–198, 2001.
- [171] F. RICARDEAU, P. BAUDESSON, and T. MEYNARD, “Failures-tolerance and remedial strategies of a PWM multicell inverter,” *IEEE Transactions on Power Electronics*, vol. 17, no. 6, pp. 905–912, Nov. 2002.
- [172] C. TURPIN, P. BAUDESSON, F. RICARDEAU, F. FOREST, and T. A. MEYNARD, “Fault management of multicell converters,” *IEEE Transactions on Industrial Electronics*, vol. 49, no. 5, pp. 988–997, Oct. 2002.
- [173] M. MA, L. HU, A. CHEN, and X. HE, “Reconfiguration of carrier-based modulation strategy for fault tolerant multilevel inverters,” *IEEE Transactions on Power Electronics*, vol. 22, no. 5, pp. 2050–2060, Sep. 2007.
- [174] H. LAUKAMP, “Reliability study of grid connected pv systems: Field experience and recommended design practice,” IEA Photovoltaic Systems Programme, Task 7 Report IEA-PVPS T7-08:2002, Mar. 2002.
- [175] A. SALTELLI, K. CHAN, and E. M. SCOTT, Eds., *Sensitivity Analysis*. Chichester, England: John Wiley & Sons, Ltd., 2000.
- [176] R. C. LIND, K. J. ARROW, G. R. COREY, P. DASGUPTA, A. K. SEN, T. STAUFFER, J. E. STIGLITZ, J. A. STOCKFISCH, and R. WILSON, *Discounting for Time and Risk in Energy Policy*. Washington, DC: Resources for the Future, Inc., 1982.

- [177] A. S. RUSHING and S. K. FULLER, “Energy price indices and discount factors for life-cycle cost analysis — April 2006,” National Institute of Standards and Technology, Washington, DC, Report NISTIR85-3273-21, Apr. 2006.
- [178] SOLAR AMERICA INITIATIVE, “Technology pathway partnerships reference document,” U.S. Department of Energy, Opportunity DE-PS36-06GO96034, 2006.
- [179] P. HERMAN, T. WEAVER, J. CHAMBERLIN, D. TOULSON, and P. HANSER, “End-use technical assessment guide (end-use TAG) volume 4: Fundamentals and methods,” Electric Power Research Institute, Palo Alto, CA, Final Report CU-7222, Apr. 1991.
- [180] D. M. KAMMEN and S. PACCA, “Assessing the costs of electricity,” *Annual Review of Environment and Resources*, vol. 29, pp. 301–344, Nov. 2004.
- [181] M. SCHMELA, “Thin is beautiful: Market survey on band and wire saws,” *Photon International*, pp. 118–126, May 2006.
- [182] M. SCHMELA, “Bath time for wafers: Market survey on wet etching equipment,” *Photon International*, pp. 96–103, Dec. 2006.
- [183] M. SCHMELA, “Small steps: Market survey on diffusion furnaces,” *Photon International*, pp. 82–89, Aug. 2006.
- [184] B. BRAND, “The artistic side of solar cells: Market survey on screen printers,” *Photon International*, pp. 96–111, Jul. 2006.
- [185] M. SCHMELA, “High speed testing: Market survey on cell testers and cell sorters,” *Photon International*, pp. 122–139, Oct. 2006.
- [186] B. BRAND, “Mastering electrical connection of thin cells: Market survey on tabbers, stringers, combined tabbers and stringers (CTS) and ribbons,” *Photon International*, pp. 170–183, Sep. 2006.
- [187] B. BRAND, “Squeezing down the costs: Market survey on laminators and encapsulation material,” *Photon International*, pp. 90–111, Aug. 2006.
- [188] B. BRAND, “Sun on demand: Market survey on solar simulators for PV modules,” *Photon International*, pp. 112–125, Jun. 2006.
- [189] H. J. MÖLLER, “Basic mechanisms and models of multi-wire sawing,” *Advanced Engineering Materials*, vol. 6, no. 7, pp. 501–513, Jun. 2004.
- [190] Y. S. TSUO, J. M. GEE, P. MENNA, D. S. STREBKOV, A. PINOV, and V. ZADDE, “Environmentally benign silicon solar cell manufacturing,” in *Proceedings of the 2nd World Conference on Photovoltaic Energy Conversion*, Vienna, Austria, 6–10 Jul. 1998, pp. 1199–1204.

VITA

Alan Ristow was born in Ann Arbor, Michigan in 1971. He earned his B.S.E. in aerospace engineering from the University of Michigan in 1993. While pursuing his undergraduate degree he was a member of the University of Michigan Solar Car Team and led the solar array design for the team's top-placing entry in the 1993 GM Sunrayce USA, a cross-country solar car race from Florida to Michigan. At Yazaki EDS Engineering, he performed design and testing of automotive body control modules for Chrysler vehicles. In 1999 he earned his M.S. in electrical and computer engineering from the Georgia Institute of Technology. Since joining the University Center of Excellence for Photovoltaics Research and Education, he has pursued a range of interests from solar cell fabrication and characterization to modeling the performance and economics of solar cells and systems.